CRANFIELD UNIVERSITY

Olusola Oloruntoba

Steady State and Transient Liquid Gas Pipe Flow Models

School of Water, Energy and Environment

PhD
Academic Year: 2015 - 2016

Supervisor: Dr Fuat Kara, Co-Supervisor: Prof John Oakey

October 2016

CRANFIELD UNIVERSITY

School of Water, Energy and Environment

PhD

Academic Year: 2015 - 2016

Olusola Oloruntoba

Steady State and Transient Liquid Gas Pipe Flow Models

Supervisor: Dr Fuat Kara, Co-Supervisor: Prof John Oakey)

October 2016

This thesis is submitted in partial fulfilment of the requirements for the degree of Doctor of Philosophy

Abstract

Two-phase flow analyses are critical to successful design and operations of liquid-gas pipe flow applications found in major industrial fields, such as petroleum, nuclear, chemical, geothermal and space industries. Due to difficulties in obtaining analytical solutions, approximate solutions have been applied to two-phase flows. However, several limitations still exist, and categorised into three prediction models, namely: flow regime, pressure gradient, and transient models.

Previous studies show that existing flow regime models and maps for horizontal flows under-predicts transition from stratified to annular flow. Furthermore, there is requirement to include criteria for identifying mist and plug flows in unified flow regime model. In order to improve under-prediction in stratified to annular prediction, nondimensional liquid film height in original criterion is replaced with nondimensional liquid holdup. This shifts stratified to annular transition line towards higher gas superficial velocity thus improving prediction. Using experimental data available in literature, a simple flow rate dependent criterion is proposed for identifying the existence of mist flow. Two criteria are proposed for identifying plug flow in horizontal and inclined flows. The first criterion is the exact criterion for identifying bubble flow in vertical flows. The second criterion is also based on bubble flow criterion but fitted to experimental data. Transition criterion for the existence of dispersed-bubble flow is also proposed, based on stability of gas bubble in liquid flow. These flow regime criteria are combined in a solution algorithm to obtain a unified flow regime model, which has been verified using existing unified flow regime models and map, and validated using experimental data.

Mechanistic or phenomenal methods are generally applied in predicting pressure gradient in two-phase liquid-gas pipe flow. These methods relies on prior knowledge of prevalent flow regime, and subsequent application of flow regime specific pressure gradient model. This approach is susceptible to error should wrong flow regime be selected. In order to overcome this problem, a Single Equation Two-Phase Mechanistic (SETM) model is proposed. SETM is obtained by combining: liquid-gas momentum equations, existing and modified flow regime criteria, and new flow

regime boundaries at the initiation and completion of transition to annular flow. Thus, SETM implicitly determines pressure gradient and flow regime in liquid-gas pipe flow, and also captures liquid-gas interface transition from flat to curved interface. SETM is applicable to all pipe inclination, and has been validated using experimental data available in literature. Further, prediction of flow characteristic features per flow regime, such as identified flow regime, liquid holdup in slug film region, ratio of slug regions, and apparent liquid heights, have been verified against theoretical limits for different flow regimes. Alternative to SETM, modified homogeneous pressure gradient model is also proposed for liquid-gas pipe flow. Existing homogeneous models are applicable to dispersed bubble flow, and slug flow with low or negligible liquid-gas slip. The modified homogeneous model is obtained by correcting mixture fanny friction factor using error between experimental pressure gradient and unmodified homogeneous pressure gradient; observed error is particularly large at high liquid-gas slip values. The modified homogeneous model is therefore applicable to all flow regimes, including stratified, annular, and mist flows. The modified model has been verified against existing homogeneous model, and validated using published experimental data.

Transient analysis is critical to liquid-gas pipe flow design. Rigorous analytical solution is generally not available. Alternative solution method is full numerical solution approach, which is subject to high demand on computational resources and time, especially for long pipelines. Hence simplified transient methods are sort. Existing simplified transient liquid-gas pipe flow models assume quasi-steady state conditions for liquid-gas momentum equations, thus neglecting convective terms in the momentum equations. The simplified transient liquid-gas pipe flow model proposed in this study include: (a) transient liquid-gas continuity equations, (b) transient convective terms of liquid-gas momentum equations, and (c) steady state pressure gradient terms of liquid-gas momentum equations. The proposed transient model captures gas and/or liquid flow variations at coarse pipe discretisation, and has been validated against published experimental data and verified with a proprietary program (OLGA).

Dedication

To Yeshua Hamashiach (Jesus Christ) and my family.

"I can do all things through Christ Who strengthens me"
– Philippians 4:13

Barukh atah Adonai, Eloheinu, melekh ha'olam.
Blessed are You, Lord, our God, Sovereign of the universe.

Hodu l'Adonai ki tov, ki lay'olam khas doe.
O give thanks unto the Lord for He is good, for His mercy endures forever.

Acknowledgements

First and foremost, I would like to express my deep and sincere appreciation to the Lord Jesus Christ, the Creator of the Heaven and the Earth (Genesis 1:1), the Giver of wisdom and understanding (James 3:17), who died for the sins of the whole world, whom God raised from the dead on the third day, ascended to heaven and seated at the right hand of God, and will come back to judge this world in righteousness.

My appreciation also goes to my sponsors PTDF Nigeria for the full scholarship awarded to me to pursue a doctorate degree at Cranfield University.

I would also like to extend special thanks to my supervisors: Dr Fuat Kara and Prof John Oakey. I appreciate their immense contributions to the success of my PhD research.

I am indebted to my family for the support and encouragement I received from them during the course of my PhD research.

Contents

List of Figures

List of Tables

Nomenclature

$-\frac{dP}{dL}$ pressure gradient, $[Pa/m]$

$-\left(\frac{dP}{dL}\right)_C$ computed pressure gradient or annular-core pressure gradient, $[Pa/m]$

$-\left(\frac{dP}{dL}\right)_G$ pressure gradient in gas, $[Pa/m]$

$-\left(\frac{dP}{dL}\right)_L$ pressure gradient in liquid, $[Pa/m]$

$-\left(\frac{dP}{dL}\right)_M$ measured pressure gradient, $[Pa/m]$

α no-slip void fraction, $[-]$

α_c critical void fraction, $[-]$

α_G liquid fraction, $[-]$

α_L gas fraction, $[-]$

$\bar{X}$, $\bar{K}$, $\bar{F}$, $\bar{T}$, $\bar{Y}$ parameters of Taitel and Dukler (1976a) to find flow regime, $[-]$

β length ratio of slug unit's film zone to slug body ($= L_F/L_U$), $[-]$

δ_L liquid film thickness, $[m]$

ϵ_R average error, $[-]$

λ characteristic value, $[-]$

μ_G dynamic viscosity of gas, $[Ns/m^2]$

μ_L dynamic viscosity of liquid, $[Ns/m^2]$

π mathematical constant, $[\approx 3.142]$

ρ_C density of annular gas-core, $[Kg/m^3]$

ρ_F density of film region (gas and liquid), $[Kg/m^3]$

ρ_G density of gas, $[kg/m^3]$

ρ_L density of liquid, $[kg/m^3]$

ρ_M mixture density, $[Kg/m^3]$

ρ_S density of slug body (gas and liquid), $[Kg/m^3]$

$\rho_{L,0}$ density of liquid at standard conditions ($P = 1\ atm,\ T = 15^0C$), $[Kg/m^3]$

σ surface tension, $[N/m]$

τ_R Reynold's stress, $[Ns/m^2]$

τ_W wall shear stress, $[Ns/m^2]$

$\mathbf{I}$ identity matrix

$\mathbf{M}^{det}$ determinant of matrix $\mathbf{M}$

$\mathbf{M}_1$,$\mathbf{M}_2$ non-singular square matrix

$\mathbf{S}$ vector of source terms

$\mathbf{U}$ vector of conservative variables

θ inclination of pipe, $[radians]$

ε pipe roughness, $[m]$

ε_{abs} absolute average percentage error, $[\%]$

ε_{ave} average percentage error, $[\%]$

$\widetilde{h}_L$ non-dimensional liquid film height, $[-]$

A,A_P pipe cross-sectional area, $[m^2]$

A_C cross-sectional area of annular gas core, $[m^2]$

A_F liquid film cross-sectional area, $[m^2]$

A_G cross-sectional area of gas pocket or flow, $[m^2]$

A_L cross-sectional area of liquid flow, $[m^2]$

A_P cross-section area of pipe, $[m^2]$

$A_{F,f}$ liquid cross-sectional area corresponding to $S_{I,f}$, $[m^2]$

c geometric term in the stratified/nostratified transition model of Taitel and Dukler (1976b), $[-]$

C_0 flow distribution coefficient, $[-]$

C_D drag coefficient, $[-]$

c_G speed of sound in gas, $[m/s]$

c_L speed of sound in liquid, $[m/s]$

CFL Courant-Friedrichs-Levy, $[-]$

D internal diameter of pipe, $[m]$

d_C hydraulic diameter of annular gas-core, $[m]$

d_D bubble diameter, $[m]$

d_F hydraulic diameter of liquid film, $[m]$

d_G hydraulic diameter of gas, $[m]$

f^a Calibration factor for U^a_{SG}, $[-]$

f^b Calibration factor for U^b_{SG}, $[-]$

F^H_B buoyancy force per unit length, $[N/m]$

F^V_B buoyancy force in vertical flow, $[N]$

F^V_D drag force in vertical flow, $[N]$

f_F film-wall friction factor, $[-]$

f_G gas-wall friction factor, $[-]$

f_L liquid-wall friction factor, $[-]$

f_M mixture friction factor, $[-]$

f_S slug-wall friction factor, $[-]$

F^H_T turbulent force per unit length, $[N/m]$

g acceleration due to gravity, $[m/s^2]$

H_L liquid holdup, $[-]$

h_L liquid film height, $[m]$

H_{LLS} liquid holdup in slug body, $[-]$

H^{min}_{LLS} minimum liquid holdup in slug body, $[-]$

H_{LTB} liquid holdup in film region of slug unit, $[-]$

H^*_{LTB} calculated H_{LTB} for slug model of Taitel and Barnea (1990), $[-]$

HM general homogeneous two-phase pressure gradient model

$HM1$ modified homogeneous two-phase pressure gradient model: model 1

$HM2$ modified homogeneous two-phase pressure gradient model: model 2

L_F length of slug unit's film region, $[m]$

L_S length of slug unit's slug body region, $[m]$

L_U length of slug unit, $[m]$

N number of elements in computational domain, $[-]$

N_{eq} number of equations to solve in computational domain, $[-]$

$P_{L,0}$ pressure of liquid at standard conditions ($P = 1\ atm,\ T = 15^0C$), $[Pa]$

R correlation coefficient, $[-]$

Re_F Reynolds number of film

Re_G Reynolds number of gas flow, $[-]$

Re_L Reynolds number of liquid flow, $[-]$

Re_M Reynolds number of mixture flow, $[-]$

s arbitrary constant in dispersed-bubble transition criterion of Taitel and Dukler (1976b), $[-]$

S_F liquid film perimeter, $[m]$

S_G perimeter of gas-wall interface, $[m]$

S_I gas-liquid interface perimeter, $[m]$

S_I perimeter of gas-liquid interface, $[m]$

S_L perimeter of liquid-wall interface, $[m]$

$S_{I,f}$ horizontal interface between gas and liquid, $[m]$

SD standard deviation, $[\%]$

t time, $[s]$

t_{N+1} simulation time at (N+1) discretisation, $[s]$

t_{ratio} ratio of computational time, $[-]$

U' turbulent non-radial velocity, $[m/s]$

U_C velocity of annular gas-core, $[m/s]$

U_D drift velocity, $[m/s]$

U_F film velocity, $[m/s]$

U_{GLS} gas bubble velocity in slug body, $[m/s]$

U_{GTB} velocity of gas-pocket in slug unit, $[m/s]$

U_{LLS} liquid velocity in slug body, $[m/s]$

U_{LTB} velocity of liquid film in slug unit, $[m/s]$

U_{SG}^1 gas superficial velocity at *initiation* of transition to annular flow, $[m/s]$

U_{SG}^2 gas superficial velocity at *completion* of transition to annular flow, $[m/s]$

U_{TB} terminal velocity of Taylor Bubble, $[m/s]$

V^* root-mean-square of V', $[m/s]$

V' turbulent radial velocity, $[m/s]$

V_L^H horizontal component of liquid velocity, $[m/s]$

V_L^V vertical component of liquid velocity, $[m/s]$

$V_{0\infty}$ terminal velocity of a single bubble in an infinite stagnant liquid medium

V_G gas velocity, $[m/s]$

V_{SG} superficial gas velocity, $[m/s]$

V_{SL} superficial liquid velocity, $[m/s]$

We Weber number, $[-]$

X apparent liquid height to SETM, $[m]$

x, L length, $[m]$

y U_{SG} required to estimate X, $[m/s]$

λ_{max}^n largest wave speed in computational domain, $[m/s]$

λ_L no-slip liquid holdup, $[-]$

μ_M, μ_S mixture dynamic viscosity, $[Ns/m^2]$

μ_S dynamic viscosity of slug body, $[Ns/m^2]$

τ_G, τ_{WG} gas-wall shear stress, $[Ns/m^2]$

τ_I, τ_{LG} gas-liquid interface shear stress, $[Ns/m^2]$

τ_L, τ_{WL} liquid wall shear stress, $[Ns/m^2]$

τ_{WM} mixture-wall shear stress, $[Ns/m^2]$

τ_F shear stress of film region, $[N/m^2]$

τ_S shear stress of slug, $[N/m^2]$

$\widetilde{h}_L^1$ non-dimensional height of liquid at *initiation* of transition to annular, $[-]$

$\widetilde{h}_L^2$ non-dimensional height of liquid at *completion* of transition to annular, $[-]$

C_F, C_L, n liquid friction factor coefficients for laminar and turbulent flows, $[-]$

C_G, m gas friction factor coefficients for laminar and turbulent flows, $[-]$

$F_G^{\dagger}$ Kelvin-Helmholtz gravity force per unit area, $[Ns/m^2]$

f_M^{mod} modified friction factor of mixture flow, $[-]$

$F_S^{\dagger}$ Kelvin-Helmholtz suction force per unit area, $[Ns/m^2]$

h'_G gas height associated with wave peak, $[m]$

h_G equilibrium gas height, $[m]$

H_{GLS} void fraction in slug body, $[-]$

H_{GTB} void fraction in slug film region, $[-]$

H^*_{LLS} intermediate value of H_{LLS}, $[-]$

$H_{LLS}{}^H$ horizontal component of H_{LLS}, $[-]$

$H_{LLS}{}^V$ vertical component of H_{LLS}, $[-]$

H_L^e liquid holdup corresponding to U_{SG}^e, $[-]$

H_L^f liquid holdup corresponding to U_{SG}^f, $[-]$

H_L^C liquid holdup of Choi et al. (2012), $[-]$

H_L^{exp} experimental liquid holdup, $[-]$

P' pressure of perturbed system, $[Pascal, Pa]$

P_G gas pressure, $[Pascal, Pa]$

P_L liquid pressure, $[Pascal, Pa]$

P pressure, $[Pascal, Pa]$

Re_S slug body Reynolds number, $[-]$

Re Reynolds number, $[-]$

T temperature, $[Kelvin, K]$

U_M, U_S, V_M mixture velocity, $[m/s]$

U_G^a gas velocity corresponding to U_{SG}^a, $[m/s]$

U_G^b gas velocity corresponding to U_{SG}^b, $[m/s]$

U_G velocity of gas $(= V_G)$, $[m/s]$

U_L velocity of liquid $(= V_L)$, $[m/s]$

$U_{SG}^a, U_{SG}^d, U_{SG}^e$ possible values of gas superficial velocity at *completion* of transition to annular flow, $[m/s]$

$U_{SG}^b, U_{SG}^c, U_{SG}^f$ possible values of gas superficial velocity at *initiation* of transition to annular flow, $[m/s]$

U_{SG}^{E} U_{SG} at End of flow regime transition to annular, $[m/s]$

U_{SG}^{S} U_{SG} at Start of flow regime transition to annular, $[m/s]$

U_{SG} superficial velocity of gas $(= V_{SG})$, $[m/s]$

U_{SL} superficial velocity of liquid $(= V_{SL})$, $[m/s]$

V_{L}^{H} liquid velocity in horizontal flow, $[m/s]$

V_{L}^{V} liquid velocity in vertical flow, $[m/s]$

$\triangle t$ temporal increment, $[s]$

$\triangle x$ spatial increment, $[m]$

AGA American Gas Association

API American Petroleum Institute

LEDA Advanced Transient Multiphase Flow Simulator

OLGA Dynamic Multiphase Flow Simulator

Chapter 1

Introduction

Multiphase flow is a general flow occurrence in several major industrial fields, such as petroleum, nuclear, chemical, geothermal and space industries. Multiphase flow also exists in domestic appliances, and the natural environment, such as the sea and atmosphere. From industrial fields' perspective, multiphase flow spans several engineering applications. Examples of these engineering applications include: production and transportation of oil-water-gas mixtures, liquid-gas separator, distillation plant, boilers, condensers, nuclear reactors, among others. The design of these engineering applications are generally challenging, largely due to the complex nature of multiphase flows. In the light of this problem, several research activities have been carried out on multiphase flow, since the 1950s, to provide design tools for predicting multiphase-flow-dependent engineering applications. The scope of this study is liquid-gas pipe flow in the petroleum industry.

1.1 Background

Majority of multiphase liquid-gas pipe flow research studies aim at providing methods for predicting pressure profile, phase fraction, heat and mass transfer. Unfortunately, rigorous solution to conservations equations governing multiphase flow is not available (Shoham, 2005; Prosperetti and Tryggvason, 2007; Jerez-Carrizales et al., 2015). However, from practical engineering design considerations, approximate multiphase analysis and solutions are usually acceptable. Therefore, approximate multiphase solutions are sort in many research activities.

One of the major approximations to multiphase flow is the two-phase analysis approach. This approach assumes phases with similar physical properties as a single or combined phase. Typical example is approximating multicomponent (or multiphase) petroleum productions from wells, as liquid and gas (i.e. liquid-gas two-phase) products. Mathematical representation of liquid-gas pipe flow conservation equations is

referred to as **Two-Fluid conservation** model. Further simplification, with the assumption of homogeneous flow, gives **Drift-Flux conservation** model (Matovu et al., 2014). In the absence of rigorous analytical solution for simple to complex flow configurations, numerical solution of Two-Fluid and Drift-Flux conservation models generally gives accurate results at very fine discretisation schemes, but requires high computational resources and time. This limitation has favoured the application of experimentally determined **Empirical** models which are generally solved analytically.

Earlier empirical models for predicting liquid-gas pipe flow include: Homogeneous No-Slip model, Separated model, Similarity model, and Drift-Flux model. Other empirical models, which are widely used in the petroleum industry, include those by: Beggs and Brill, Hagedorn and Brown, Duns and Ros, Flanigan, Dukler et al., Eaton et al., Orkiszewski, Aziz et al., Hasan and Kabir, among others. In general, liquid-gas pipe flow empirical models require low computational resources and time. However, they generally give accurate predictions for system domains (i.e. liquid-gas flow rates, physical properties of liquid and gas, and pipe configurations) for which they were derived (Shoham, 2005; Jerez-Carrizales et al., 2015).

Requirements for improved liquid-gas pipe flow prediction models, applicable to a wide range of system domain, led to the development of mechanistic or phenomenological prediction models. Liquid-gas pipe flow mechanistic models have been demonstrated to give good predictions for pressure gradient and/or liquid holdup (Govier and Aziz, 1972; Brill, 1987; Shoham, 2005; Jerez-Carrizales et al., 2015). A major disadvantage to mechanistic methods is the requirement to: (a) first know the prevalent flow regime or flow pattern (defined as physical configuration of flow), (b) then apply flow-regime-dependent mechanistic model to find pressure gradient and/or liquid holdup.

Furthermore, considerations for the design of liquid-gas flow in pipes, require transient analysis. Examples of transient scenarios include: imposed variation of input gas and/or liquid flow rates, and outlet pressure. Transient liquid-gas flow analysis is particularly important for designing liquid-gas separators, slug catchers, pipeline fatigue design, among others (Shoham, 2005; Jerez-Carrizales et al., 2015).

1.2 Motivation

1.2.1 Flow regime model

Accurate determination of prevalent flow regime is essential to application of appropriate pressure gradient mechanistic model. Existing flow regime mechanistic models have been shown to be limited in prediction accuracy. In order to overcome this limitation, a new unified flow regime model is proposed in this study. This new unified flow regime model is a combination of new flow regime transition criteria, it is applicable to horizontal through upward vertical flow, and provides improvements to existing unified flow regime methods and maps.

1.2.2 Mechanistic model

The major requirement, to first determine flow regime before selecting appropriate pressure gradient mechanistic model, is subjective as it depends on accurate determination of the prevalent flow regime (Shoham, 2005; Cheng et al., 2008; Jerez-Carrizales et al., 2015). This problem is further complicated by the fact that flow regime determination is also not an exact science. In order to overcome the need to first find the prevalent flow regime, a new mechanistic model is developed in this study. This new mechanistic model is referred to as: Single Equation Two-Phase Mechanistic Model (SETM). SETM is capable of predicting simultaneously, prevalent flow regime and pressure gradient in a two-phase pipe flow. Furthermore, general homogeneous two-phase pressure gradient model is modified to improve prediction accuracy. The modified homogeneous model is obtained by correcting mixture fanny friction factor, using error between experimental pressure gradient and unmodified homogeneous pressure gradient; observed error is particularly large at high liquid-gas slip values. Hence the modified homogeneous model is applicable to all flow regimes, including stratified, annular, and mist flows. The modified friction factor affects only the frictional component, and not gravitational component, of total pressure gradient. Therefore, the modified homogeneous pressure gradient is applicable to all pipe inclination angles. Finally, the liquid holdup model of Choi et al. (2012) is modified, using a correction factor, for improved prediction accuracy. The correction factor is obtained from error between experimental liquid holdup and original Choi et al. liquid holdup predictions. In particular, the modified liquid holdup model gives improved prediction for low-liquid liquid-gas pipe flows, including: annular and mist flows. The modified Choi et al. liquid holdup model is only applicable to horizontal flows, since only horizontal liquid holdup data are used in obtaining the correction factor.

1.2.3 Transient model

Requirements for transient analysis of liquid-gas pipe flow, further complicates the solution of liquid-gas conservation equations encountered under steady-state conditions. Since rigorous solution of the conservation equations do not exist, numerical and simplified solutions are generally applied. Numerical solutions are generally computationally intensive, thus, simplified solutions are favoured wherever applicable. Existing simplified transient liquid-gas two-phase models assume complete quasi-steady state condition for momentum equations of the phases. An alternative simplified transient liquid-gas two-phase model is developed in this study; by considering convective terms in momentum equations, as well as continuity equations in transient state.

1.3 Aim and objectives

Aim

The aim of this study is to develop steady-state and transient models for accurate prediction of liquid-gas two-phase pipe flow.

Objectives

The objectives of this study include:

- to improve flow regime transition models, propose a unified flow regime model, and validate using published experimental data. Thus achieve: (a) improved transition criteria for stratified-annular flows by reducing under-predictions by existing prediction models, (b) proposition of mist flow identification criteria, and (c) extension of bubble flow criteria, in vertical flow, to predict plug flow regime in horizontal flow. Therefore, an improved unified flow regime prediction model would be achieved.

- to develop Single Equation Two-Phase Mechanistic (SETM) model and validate using published experimental data. Thus SETM would provide implicit prediction of flow regime and pressure gradient in liquid-gas pipe flow. Therefore, potential pressure gradient prediction error in existing mechanistic or phenomenological methods, owing to explicit prediction of flow regime and pressure gradient, can be avoided.

- to improve (a) pressure gradient prediction accuracy of homogeneous liquid-gas two-phase pipe flow model, and extend prediction capability to low-liquid (such as annular and mist flows) liquid-gas pipe flow, which is limited in original

homogeneous liquid-gas pipe flow model, (b) prediction accuracy of liquid holdup model of Choi et al. (2012), thus extending prediction capability of existing model to include annular and mist flows (i.e. low-liquid liquid-gas pipe flow), and validate the improved models using published experimental data

- to develop simplified transient model and validate using published experimental data. Thus achieve: (a) simplified liquid-gas pipe flow model with low demand on computational resources and time, (b) preserve convective terms in liquid-gas momentum equations, this capability is generally ignored by existing simplified liquid-gas pipe flow models, and capture flow variations due to changes in liquid and/or gas flow.

1.4 Overview of chapters

- Chapter (2) reviews pertinent literature on flow regime, pressure gradient, and transient models for predicting multiphase/two-phase flow in flowlines.
- Chapter (3) presents the flow regime theory proposed in this study, solution algorithm employed, results of validation exercise, and discussion of results.
- Chapter (4) provides theory behind the Single Equation Two-Phase Mechanistic (SETM) model developed in this study, solution algorithm employed, validation method for SETM, improved homogeneous two-phase pressure gradient for pipe flow, improved liquid holdup prediction for low-liquid two-phase pipe flow, results of validation exercise and flow regime predictions, and discussion of results.
- Chapter (5) outlines the theory for the simplified transient two-phase model proposed in this study, solution algorithm of the simplified transient model, results of validation exercise of the proposed simplified transient model, and discussion of results
- Chapter (6) gives conclusion to this study.

Chapter 2

Literature review

This chapter reviews literature on two-phase gas-liquid flow in pipes. The first section (2.1) of this chapter covers flow regime classification, maps, and prediction models. The second section (2.2), reviews methods for calculating pressure gradient. The last section (2.3) of this chapter reviews transient models for predicting two-phase gas-liquid flow in pipes.

2.1 Flow regime

Two-phase gas-liquid pipe flow exhibits flow distributions with distinct physical configurations, generally referred to as flow regime or flow pattern. Several studies have been carried out to classify two-phase/multiphase flow, develop flow regime identification maps, and develop mathematical methods or models for determining flow regimes. Detailed review on flow regime has been carried out by Govier and Aziz (1972), Delhaye et al. (1981), Hewitt (1982), and Collier and Thome (1994). However, a critical review of flow regime is provided in this section.

2.1.1 Classification of flow regimes

The classification of flow regimes can be subjective. Nevertheless, various studies on two-phase gas-liquid flow regimes agree on the existence of certain flow regimes under horizontal, vertical, and inclined flow conditions in pipes.

Flow regimes in vertical flow

Typical flow regimes of two-phase gas-liquid vertical pipe flow can be classified as: dispersed bubble flow, slug/bubble flow, churn flow, annular flow, and annular mist flow (Hewitt, 1982; Collier and Thome, 1994; Shoham, 2005). Figure (2.1) illustrates two-phase gas-liquid flow regimes in vertical flow.

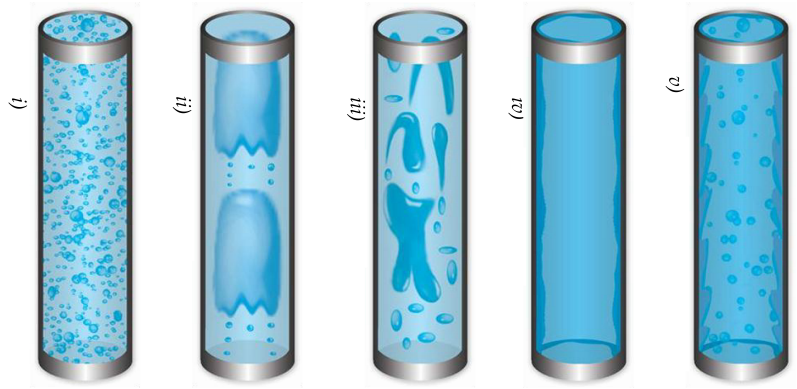

Figure 2.1 – Two-phase gas-liquid flow regimes in vertical flow; adapted from Bratland (2010). (i) dispersed bubble flow, (ii) slug/bubble flow, (iii) churn flow, (iv) annular flow, (v) annular mist flow.

- **Dispersed bubble flow** is characterised by a continuous liquid phase with dispersed gas phase. Liquid flow rate is usually high compared with gas flow rate.
- **Slug/bubble flow** is an intermittent flow of liquid and gas pockets (also referred to as Taylor bubbles). Taylor bubbles are concentrically located in pipe cros-sectoin, with thin liquid film layer on pipe wall.
- **Churn flow** is a chaotic flow and occurs at transition from slug to annular flow.
- **Annular flow** occurs at high gas flow rate. This type of flow is generally classified as separated flow with gas core flow, and liquid film flow on pipe wall.
- **Annular mist flow** is a transition from annular flow. At sufficiently high gas flow rate, liquid film on pipe is entrained into the fast moving gas core to form mist flow.

Flow regimes in horizontal flow

Flow regimes of two-phase gas-liquid horizontal pipe flow can be classified as: dispersed bubble flow, annular/annular mist flow, elongated bubble/plug flow, slug flow, stratified flow, and stratified wavy flow (Hewitt, 1982; Collier and Thome, 1994; Shoham, 2005). Figure (2.2) shows typical two-phase gas-liquid flow regimes in horizontal flow.

- **Dispersed bubble flow** is similar for both vertical and horizontal flow. In horizontal flow, however, dispersed gas flows closer to the upper pipe wall due buoyancy.

- **Annular/annular mist flow** in horizontal flow is similar as for vertical flow. Due to gravity, liquid film thickness is thinner on upper pipe wall compared with lower pipe wall.
- **Plug flow** occurs as dispersed bubble flow experiences increase in gas flow rates. The dispersed gas bubbles accumulate into large and long bubbles at the top of the pipe.
- **Slug flow** in horizontal flow exhibits similar characteristic as for vertical flow. However, gas pockets flows at the upper part of the pipe and liquid film at the lower part.
- **Stratified flow** occurs at sufficiently low liquid flow rate. The flow is characterised by separation of gas-liquid flow into smooth liquid flow at the lower path of the pipe, and gas flowing at the upper part. There exist a smooth gas-liquid interface.
- **Stratified wavy flow** is similar to stratified flow but with wavy gas-liquid interface. The wavy gas-liquid interface is due to increased gas flow rates.

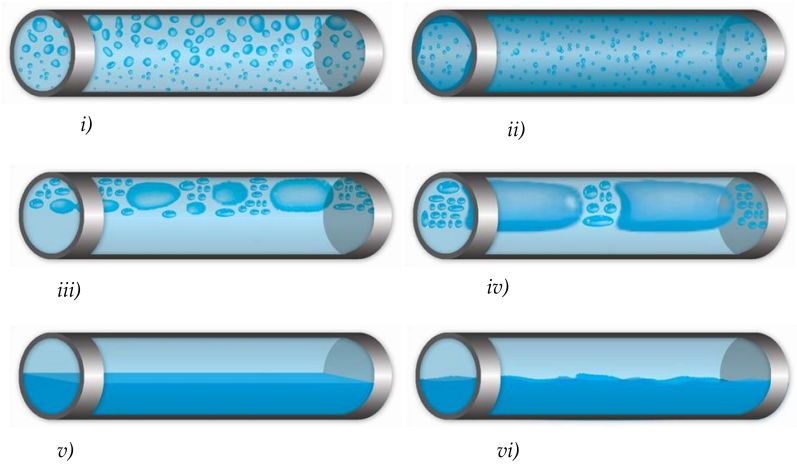

Figure 2.2 – Two-phase gas-liquid flow regimes in horizontal flow; adapted from Bratland (2010). (i) dispersed bubble flow, (ii) annular/annular mist flow, (iii) plug flow, (iv) slug flow, (v) stratified flow, (vi) stratified wavy flow.

Flow regimes for inclined flow

Flow regimes of two-phase gas-liquid in inclined pipe flow is a combination of flow characteristics observed for both the horizontal and vertical flows (Bratland, 2010). Singh and Griffith (1970) carried out experiments using air-water in a shallow upward inclined flow; Singh and Griffith used five pipes (with diameters 1.7 to 3.8 cm).

Gould (1974) and Gould et al. (1974) also carried out experiments and published flow regime maps for horizontal, 45^0 upward inclined, and vertical flow.; coordinate system of Duns and Ros (1963) are applied. Their studies identified four flow pattern, namely: continuous gas phase, continuous liquid phase, continuous gas and liquid phase, alternating phases. Further studies have been conducted by Spedding and Nguyen (1976), Weisman and Kang (1981), and Mukherjee and Brill (1985).

2.1.2 Flow regime maps and prediction models

Previous methods to determine flow-regime were based on experimentally determined correlations relating to specific system variable domains such as, flow conditions, fluid properties, and pipe geometry. Bergelin and Gazley (1949) developed a flow regime map using air, water, and 2.5 cm tube. Bergelin and Gazley specified the axes of the map as mass flow rates of air and water. This meant that, Bergelin and Gazley's map applies only to air-water system. Baker (1954) later published a map developed from several fluids and small diameter. Baker's map axes are combination of mass flux, density, and surface tension of the fluids. Later, Hoogendoorn (1959) conducted experiments using three different liquids (water, spindle oil, and gas oil) and gas (air at pressure 1 to 3 atmosphere). Hoogendoorn showed that the flow regime map of Bergelin and Gazley are inaccurate, and also suggested input gas percentage and superficial mixture velocity as map coordinates. Govier and Omer (1962) carried out an experiment using 2.5 cm cellulose acetane butyrate tube, with air-water two-phase fluid system. Govier and Omer suggested mass velocities of air and water as the axes of their map.

Based on the AGA-API flow regime data bank which contained about 4,475 data points, AI-Sheikh et al. (1970) developed series of graphs, which consists of 12 figures with 10 coordinate systems. Later, a major flow regime map for horizontal flow was developed by Mandhane et al. (1974), which became widely used in the oil and gas industry. Figure 2.3 shows the flow regime of Mandhane et al.. The map of Mandhane et al. was also based on AGA-API flow regime data bank, which now contained 5,935 data points.

These flow regime maps, however, find limited applications beyond system variable domains for which they were derived. Thus the necessity to develop a better flow regime prediction method: mechanistic flow regime models.

Mechanistic flow regime models rely on physical science and are therefore applicable to a wide variety of system variable domains (Barnea, 1987; Kelessidis and

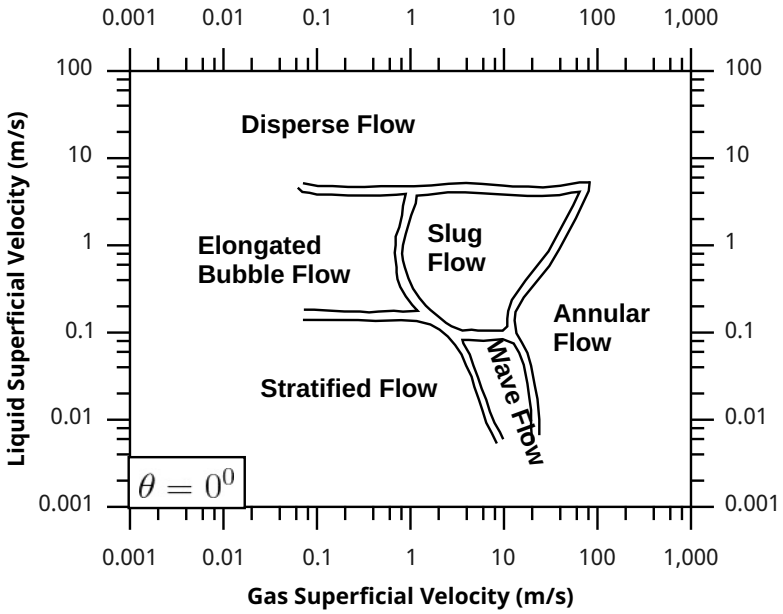

Figure 2.3 – Map of Mandhane et al. (1974)

Dukler, 1989). Mechanistic flow regime models comprise a wide variety of mechanisms broadly classified as horizontal and vertical models. Horizontal flow regime models are applicable to horizontal and slightly inclined flows (Taitel and Dukler, 1976a; Kadambi, 1982; Lin and Hanratty, 1986), while vertical flow regime models apply to vertical and near vertical flows (Taitel et al., 1980; McQuillan and Whalley, 1985; Kaichiro and Ishii, 1984).

Taitel and Dukler pioneered mechanistic flow regime model for two-phase gas-liquid flow (Taitel and Dukler, 1976a; Ahn et al., 2015). Although their work focused on horizontal and lightly inclined flow, they however laid the foundations for the developments of inclined and vertical flow mechanistic models. Taitel and Dukler categorised their flow regime map into 5 regions, namely: stratified smooth, stratified wavy, intermittent (i.e. slug and plug), annular, and dispersed bubble; figure (2.4) illustrates the different flow regimes identified. Taitel and Dukler provided flow regime transition and/or identification criteria, equations (2.1 - 2.4) define parameters (i.e. $\bar{X}$, $\bar{K}$, $\bar{F}$, and $\bar{T}$) employed in figure (2.4). Transition from stratified to intermittent flow occurs when waves in liquid layer grow high enough to bridge the pipe cross-section. Transition from stratified to annular flow occurs when gas flow rate is high enough to cause liquid film form round the pipe inner perimeter. Transition from intermittent to annular occurs when liquid flow is not large enough to sustain intermittent flow, thus collapsing and forming liquid layer around pipe inner

perimeter, resulting in annular flow. Transition from stratified smooth to stratified wavy occurs when gas flow is increased to form liquid waves which are not high enough to form intermittent flow. Transition from intermittent to dispersed bubble occurs when liquid flow rate is high enough to shatter intermittent gas pockets into small bubble, and dispersed in the liquid phase. Other studies have been carried out to provide new or improve existing horizontal flow regime mechanistic models (Ali, 2009).

$$\bar{X} = \left[\frac{-\left(\frac{dP}{dL}\right)_{SL}}{-\left(\frac{dP}{dL}\right)_{SG}} \right]^{\frac{1}{2}} \tag{2.1}$$

$$\bar{K} = F \times (Re_{SL})^{\frac{1}{2}} \tag{2.2}$$

where Reynolds number corresponding to superficial liquid velocity is defined as: $Re_{SL} = (\rho_L U_{SL} D/\mu_L)$.

$$\bar{F} = \left(\frac{\rho_L}{\rho_L - \rho_G} \right)^{\frac{1}{2}} \frac{U_{SG}}{(Dgcos\theta)^{\frac{1}{2}}} \tag{2.3}$$

$$\bar{T} = \left[\frac{-\left(\frac{dP}{dL}\right)_{SL}}{(\rho_L - \rho_G) g cos\theta} \right]^{\frac{1}{2}} \tag{2.4}$$

where, Y (shown in equation (2.5)) accounts for effect of angular inclination of flow.

$$\bar{Y} = \frac{(\rho_L - \rho_G) g sin\theta}{-\left(\frac{dP}{dL}\right)_{SG}} \tag{2.5}$$

The original criteria of Taitel and Dukler for transition from stratified to annular flow has been demonstrated to under-predict experimental observations (França and Lahey, 1992; Asante, 2000). Examination of the original transition criteria in dimensional terms, given in equation (2.6), shows that dimensionless term c (which relates to speed and propagation of wave) can be modified to adjust transition line to match experimental observations. In the original model of Taitel and Dukler, $c = 1 - h_L/D$.

$$U_G \geq c \left[\frac{g(\rho_L - \rho_G) \cos\theta A_G}{\rho_G S_I} \right]^{0.5} \tag{2.6}$$

Taitel et al. (1980) developed a flow regime mechanistic model for two-phase gas-liquid flow in vertical pipe; their flow regime map was divided into five regions, namely: bubble, slug churn, annular, and dispersed bubble. Transition from bubble

to slug occurs at critical void fration ($\alpha_c = 0.25$), where bubbles agglomerate and coalescence to form slug flow. Transition from bubble/slug to dispersed bubble flow is based on the work of Hinze (1955), leading to the development of an expression that predicts the occurrence of turbulent dispersion of gas pockets. Transition to annular is based on force balance between droplet drag and gravity, thus specifying the minimum gas velocity to suspend droplet in annular flow. Transition to churn is identified to occur at vertical pipe entrance; thus an entrance length exists for churn flow to stabilise into slug flow. Methods for calculating this entrance length has been reviewed by Shoham (2005). Similar to horizontal flow, other studies have been carried out to provide new or improve existing vertical flow regime mechanistic models (Ali, 2009).

Limited applicability of these two categories (i.e. horizontal and vertical) of tran-

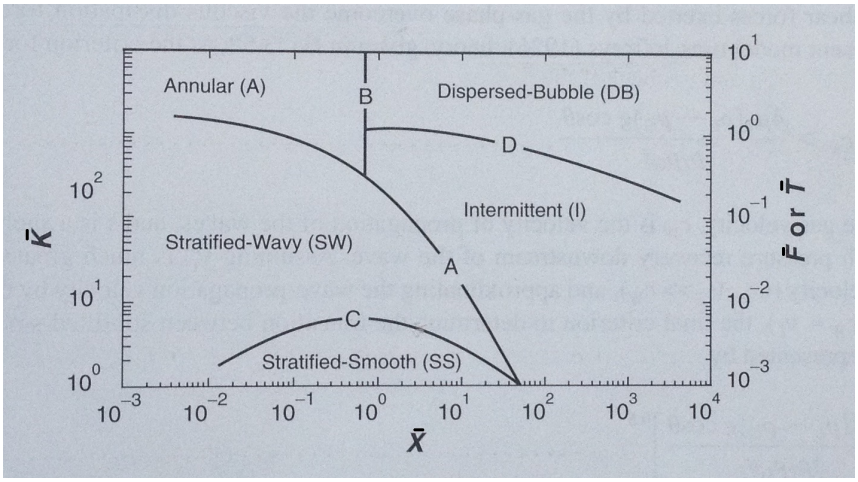

Figure 2.4 – Generalised flow regime map for horizontal flow (Taitel and Dukler, 1976a)

sition models to inclined flows motivated the development of inclined flow regime models (Barnea et al., 1980, 1985). A unified model applicable to all inclination angle was later provided by Barnea (1987) through the combination of different flow regime transition mechanisms, including the methods of Taitel and Dukler (1976a), Taitel et al. (1980), and criteria for the existence of annular and slug flow regimes. Zhang et al. (2003) later provided a unified model for predicting flow regime at all inclination angles, based on slug flow dynamics.

Majority of existing flow regime transition models only determine selected flow regimes, such as slug, dispersed-bubble, annular, stratified/wavy, and bubble. However, mechanism for transition to/from Plug and Mist flow regimes have not been considered. Experimental data show that existing flow regime transition models under predict transition from stratified to annular flow, where some stratified data are

identified as annular. (França and Lahey, 1992; Jepson and Taylor, 1993; Asante, 2000). An improvement to stratified/annular transition model is therefore required.

2.2 Pressure gradient model

Accurate prediction of operational pressure profile is required in the design of multiphase flow transportation in pipelines, flowlines, and risers. However, rigorous analytical solution of pressure profile for multiphase system is not available (Shoham, 2005). Multiphase flow analysis can be simplified as two-phase flow of gas and liquid (Bratland, 2010; Shoham, 2005). Two categories of solution methods are generally employed for practical two-phase or multiphase system design, namely: empirical, and mechanistic pressure gradient models (Lyons et al., 2015; Shoham, 2005).

2.2.1 Empirical pressure gradient models

Empirical pressure gradient models are derived from experiments and are only valid within the boundaries of operational parameters (flow rates of phases), geometrical variables (diameter and pipe inclination angle), and physical properties (densities, viscosities, and surface tension of phases) of the experiments from which they are derived. Several empirical correlations have been developed for calculating pressure gradient in two-phase gas-liquid pipe flow. These include: Beggs and Brill (1973), Hagedorn and Brown (1965), Duns and Ros (1963), Flanigan (1958), Dukler et al. (1964), Eaton et al. (1967), Orkiszewski (1967), Aziz et al. (1972), Hasan and Kabir (1988), among others. Most of these pressure gradient correlations are limited in prediction accuracy (i.e. ability to predict experimental and/field data, with negligible or minimal error) and application areas, since they are only accurate within system domain (includes: fluids flow rates, fluids physical properties, and pipe configuration) for which they are derived (Shoham, 2005; Zhao, 2005). However, the most commonly used correlations and their limitations are provided presently.

The pressure gradient correlation of Dukler et al. was originally developed for horizontal flow due to its inability to accurately predict gravitational pressure loss in inclined and vertical flow, and this model generally underpredicts liquid holdup. These limitations are usually removed by implementing the method of Flanigan to account for gravitational pressure losses in inclined flow, and correlation of Eaton et al.. for calculating liquid holdup. Hagedorn and Brown gives best performance in calculating pressure gradient and liquid holdup for vertical well flow, but not applicable to horizontal and inclined flows. Beggs and Brill (1973) developed correlations

for calculating pressure gradient and liquid holdup, applicable to all pipe inclinations, namely: horizontal, vertical, and inclined pipe flow. Beggs and Brill identified four flow patterns, namely: segregated, intermittent, distributed, and transition. Calculation of pressure gradient and liquid holdup is then based on identified flow pattern. It has been observed that the flow patterns of Beggs and Brill are only valid for horizontal flow, nevertheless, they are valid for calculating pressure gradient and liquid holdup (Shoham, 2005). The model of Beggs and Brill, however, underpredicts pressure loss for vertical flow. Increase in either pipe diameter or gas/liquid ratio generally result in over prediction of pressure gradient. Despite desirable performance of selected pressure gradient correlations, however, these correlations are only applicable within the boundaries of operational parameters, geometrical variables, and physical properties of the experiments from which they were developed. This limitation led to the development of mechanistic models for the prediction of pressure gradient in multiphase/two-phase pipe flow.

2.2.2 Mechanistic pressure gradient models

Mechanistic pressure gradient models are derived based on physical configuration and behaviour of multiphase/two-phase pipe flow (Jerez-Carrizales et al., 2015). Therefore, mechanistic pressure gradient models for multiphase/two-phase pipe flow require identification of prevalent flow regime, followed by solution of flow regime dependent momentum equations of phases. General classification of flow regimes relevant to mechanistic pressure gradient include: stratified, annular, slug, and dispersed-bubble.

Stratified mechanistic modelling was pioneered by Taitel and Dukler (1976a), with modifications made by other contributors, e.g. Zhao (2005). Stratified mechanistic model of Taitel and Dukler employed the concept of separated flow, with gas phase flowing at the upper pipe region and liquid flowing at the lower region (Azevedo et al., 2017). Schematic representation of stratified liquid-gas two-phase pipe flow model is given in figure (2.5). Each phase is modelled as a single phase, but linked by gas-liquid interface interaction. Solution procedure involves solving combined momentum equation of gas and liquid for liquid height. Thereafter, momentum equations of either liquid and gas and can be solved to obtained pressure gradient. Liquid holdup is directly calculated from liquid film height. Taitel and Dukler pressure gradient model for liquid-gas pipe flow is expressed as liquid-gas momentum equations given in equations (2.7) and (2.8).

$$-A_L\left(\frac{dP}{dL}\right)_L - \tau_{WL}S_L + \tau_I S_I - \rho_L A_L g\sin\theta = 0 \tag{2.7}$$

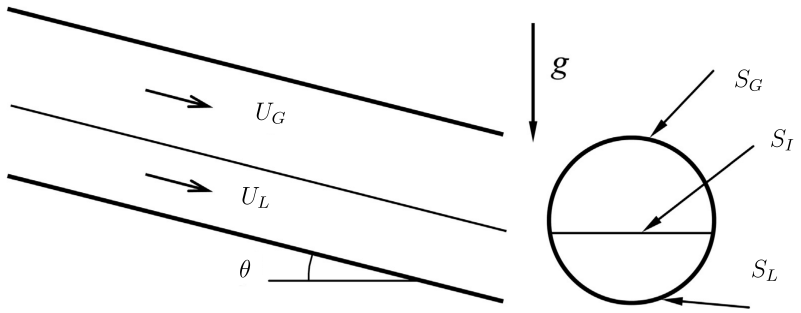

Figure 2.5 – Generalised stratified model for liquid-gas pipe flow (adapted from Azevedo et al. (2017))

$$- A_G \left(\frac{dP}{dL}\right)_G - \tau_{WG} S_G - \tau_I S_I - \rho_G A_G g \sin\theta = 0 \tag{2.8}$$

Equations (2.7) and (2.8) are combined to give equation (2.9), which is subsequently solved for liquid film height (h_L). Thereafter, pressure gradient is determined from either equations (2.7) or (2.8).

$$\tau_{WG}\frac{S_G}{A_G} - \tau_{WL}\frac{S_L}{A_L} + \tau_I S_I\left(\frac{1}{A_L} + \frac{1}{A_G}\right) - (\rho_L - \rho_G) g \sin\theta = 0 \tag{2.9}$$

Geometric terms are defined as:

$$A_L = \frac{1}{4}D^2\left\{\pi - \cos^{-1}\left(2\frac{h_L}{D} - 1\right) + \left(2\frac{h_L}{D} - 1\right)\sqrt{1 - \left(2\frac{h_L}{D} - 1\right)^2}\right\} \tag{2.10}$$

$$A_G = \frac{1}{4}D^2\left\{\cos^{-1}\left(2\frac{h_L}{D} - 1\right) - \left(2\frac{h_L}{D} - 1\right)\sqrt{1 - \left(2\frac{h_L}{D} - 1\right)^2}\right\} \tag{2.11}$$

$$S_L = D\left\{\pi - \cos^{-1}\left(2\frac{h_L}{D} - 1\right)\right\} \tag{2.12}$$

$$S_G = \pi D - S_L \tag{2.13}$$

$$S_I = D\sqrt{1 - \left(2\frac{h_L}{D} - 1\right)^2} \tag{2.14}$$

$$d_L = \frac{4A_L}{S_L} \tag{2.15}$$

$$d_G = \frac{4A_G}{(S_G + S_I)} \tag{2.16}$$

Additional terms are defined as:

$$\tau_{WL} = f_L \frac{\rho_L {U_L}^2}{2} \tag{2.17}$$

$$\tau_{WG} = f_G \frac{\rho_G {U_G}^2}{2} \tag{2.18}$$

$$\tau_I = f_I \frac{\rho_G (U_G - U_L)^2}{2} \tag{2.19}$$

Gas-liquid interface interaction has received several studies (Shoham, 2005). However, Shoham (2005) showed that stratified model of Taitel gives satisfactory results over a wide range of operational conditions. Better stratified flow prediction models were provided for low liquid stratified flow by Hart et al. (1989) and Chen et al. (1997). The methods of Hart et al. and Chen et al. consider gas-liquid interaction as curved interface. Detailed assessment of the models of Hart et al. and Chen et al. has been carried out by Badie et al. (2000). Curved two-phase interface stratified model are also provided or studied by Ullmann and Brauner (2006), Rovinsky et al. (1997), Asante (2000), Gorelik and Brauner (1999), Brauner et al. (1998), Ng et al. (2001), and Hamersma and Hart (1987). As observed earlier, all stratified models for predicting pressure gradient in multiphase/two-phase pipe flow are based on prior knowledge of flow regime

Pioneering work made at modelling annular flow was carried out by Dukler (1960). The work of Dukler was later applied to vertical upward flow by Hewitt (1961). Further developments have been provided towards modelling annular flow. These include the studies of Wallis (1969), Oliemans et al. (1986), Yao and Sylvester (1987), Hasan and Kabir (1988), Alves et al. (1991), among others. Out of these studies, the works of Oliemans et al. and Alves et al. are the most important and widely used. These two methods are developed using the two-phase gas-liquid (or two-fluid) method, with closure correlations applied for friction factors of gas, liquid, and interface, as well as liquid entrainment. Schematic representation of annular liquid-gas two-phase pipe flow model is given in figure (2.6). Solution of annular mechanistic pressure gradient model involves solution of combined momentum of liquid film and gas core for film thickness. Pressure gradient is, thereafter, calculated from either momentum equation of liquid film or gas core. Annular liquid-gas pipe flow pressure gradient model, proposed by Alves et al., is given by momentum equations of liquid and gas-core, expressed as equations (2.20) and (2.21) respectively. The gas-core in annular flow consists of gas flow with liquid entrainment.

$$-A_F \left(\frac{dP}{dL}\right)_L - \tau_{WL} S_L + \tau_I S_I - \rho_L A_F g \sin\theta = 0 \tag{2.20}$$

$$-A_C \left(\frac{dP}{dL}\right)_C - \tau_I S_I - \rho_C A_C g \sin\theta = 0 \tag{2.21}$$

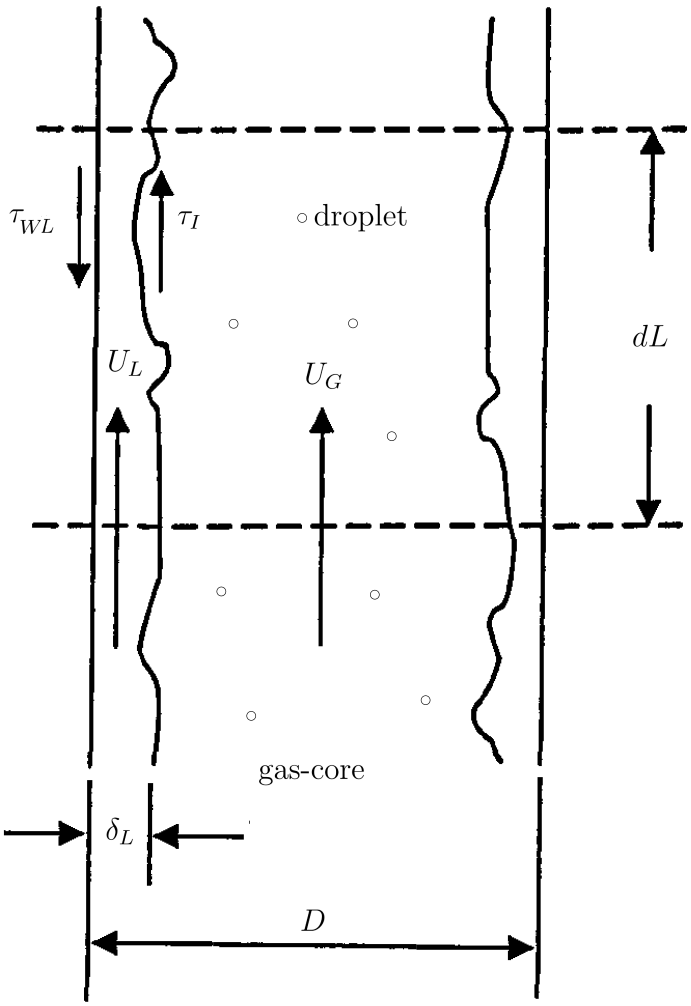

Figure 2.6 – Generalised annular model for liquid-gas pipe flow (adapted from Zangana (2011))

Equations (2.20) and (2.21) are combined to give equation (2.22), which is subsequently solved for liquid film thickness (δ_L). Thereafter, pressure gradient is determined from either equations (2.20) or (2.21).

$$-\tau_{WL}\frac{S_L}{A_F}+\tau_I S_I\left(\frac{1}{A_F}+\frac{1}{A_C}\right)-(\rho_L-\rho_C)g\sin\theta=0 \tag{2.22}$$

Geometric terms are defined as:

$$A_F=\pi\delta_L(D-\delta_L) \tag{2.23}$$

$$A_C=\pi\frac{(D-2\delta_L)^2}{4} \tag{2.24}$$

$$S_L=D\pi \tag{2.25}$$

$$S_I=\pi(D-2\delta_L) \tag{2.26}$$

$$d_L = \frac{4\delta_L(D-\delta_L)}{D} \tag{2.27}$$

$$d_C = (D-2\delta_L) \tag{2.28}$$

Additional terms are defined as:

$$\tau_{WL} = f_F \frac{\rho_L {U_F}^2}{2} \tag{2.29}$$

$$\tau_I = f_I \frac{\rho_C (U_C - U_F)^2}{2} \tag{2.30}$$

Detailed methods for calculating liquid entrainment, friction factor, and liquid holdup have been provided by previous studies (Brill, 1987; Shoham, 2005). Similar to the limitations of stratified mechanistic models, annular mechanistic model for predicting pressure gradient in multiphase/two-phase is only applicable once prevalent flow regime has been identified; in this case, annular flow.

Despite the complex nature of slug flow, slug mechanistic model for predicting two-phase gas-liquid has experienced significant development. Earlier developments include the studies of Dukler and Hubbard (1975) and Nicholson et al. (1978) for predicting slug flow in horizontal pipe; Fernandes et al. (1983), Sylvester (1987), and Vo and Shoham (1989) developed slug models for vertical pipes; and slug flow models in inclined pipe has been developed by Bonnecaze et al. (1971), Hasan and Kabir (1988), Crowley and Rothe (1986), Stanislav et al. (1986). Slug model in vertical flow is shown in figure (2.7).

Sylvester (1987) simplified the original slug model of Fernandes et al. (1983) into eight equations (2.31 - 2.38) which are solved simultaneously for: β, H_{LTB}, U_{LLS}, U_{GTB}, U_{TB}, U_{GLS}, U_{LTB}, and H_{GLS}. Pressure gradient is subsequently calculated using equation (2.39).

$$U_{SG} = \beta U_{GTB}(1-H_{LTB}) + (1-\beta)U_{GLS}(1-H_{LLS}) \tag{2.31}$$

$$U_{SG} = (1-\beta)U_{LLS}H_{LLS} - \beta U_{LTB}H_{LTB} \tag{2.32}$$

$$(U_{TB}-U_{LLS})H_{LLS} = [U_{TB} - (-U_{LTB})]H_{LTB} \tag{2.33}$$

$$(U_{TB}-U_{GLS})(1-H_{LLS}) = (U_{TB}-U_{GTB})(1-H_{LTB}) \tag{2.34}$$

$$U_{TB} = 1.2U_M + 0.35\left[\frac{gD(\rho_L-\rho_G)}{\rho_L}\right]^{\frac{1}{2}} \tag{2.35}$$

$$U_{GLS} = 1.2U_M + 1.53\left[\frac{gD(\rho_L-\rho_G)}{\rho_L^2}\right]^{\frac{1}{4}} H_{LLS}^{0.5} \tag{2.36}$$

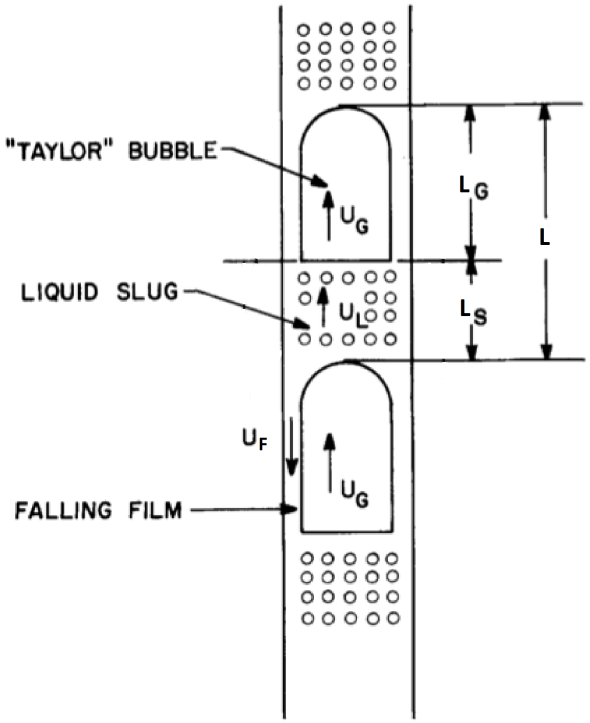

Figure 2.7 – Generalised slug model for liquid-gas pipe flow in vertical direction (adapted from Pompilio (2013))

$$U_{LTB} = 9.916\left[gD\left(1-\sqrt{H_{GTB}}\right)\right]^{\frac{1}{2}} \tag{2.37}$$

$$H_{GLS} = \frac{U_{SG}}{0.425 + 2.65U_M} \tag{2.38}$$

$$-\frac{dP}{dL} = \left(\rho_S g \sin\theta + \frac{\tau_S \pi D}{A}\right)(1-\beta) + \left(\rho_G g \sin\theta + \frac{\tau_F S_F}{A} + \frac{\tau_G S_G}{A}\right)\beta \tag{2.39}$$

Later, Bonnecaze et al. reduced the eight equations in the simplified Sylvester (1987) to a sinlge equation with H_{LTB} as the unknown. Taitel and Barnea provided a major contribution to slug mechanistic modelling of two-phase for all pipe inclination (Taitel and Barnea, 1990; Bassani et al., 2017). Momentum equations of gas and liquid were analysed for slug flow to obtain three different expressions for solving slug model. Two of these expressions or equations require numerical solution. The third equation is generally employed since it can be solved directly to obtain slug film height. Then, pressure gradient is obtained from equation. The equation of Taitel and Barnea was later followed by the simplified slug model of Felizola and Shoham (1995). Extensive studies have been carried out on slug length, frequency, liquid holdup, metering, among other characteristics (Shoham, 2005). Similar to stratified and annular flow mechanistic models, slug mechanistic model rely on prior knowledge of prevalent flow regime.

For dispersed-bubble flow, homogeneous model is generally applicable (Shoham, 2005). Homogeneous model is based on the work of Wallis (1969). Homogeneous model approximates the physical properties of the various phases present as a pseudo-single phase, by using no-slip liquid holdup (λ_L) or actual liquid holdup (H_L) as approximation factor. λ_L and $H_L(=1-\alpha)$ are given in equations (2.40) and (2.41) respectively.

$$\lambda_L = \frac{U_{SL}}{U_{SG}+U_{SL}} \tag{2.40}$$

$$1.53\left[\frac{g(\rho_L-\rho_G)\sigma}{\rho_L^2}\right]^{0.25}(1-\alpha)^{0.5}sin\theta = \frac{U_{SG}}{\alpha} - 1.2\,(U_{SG}+U_{SL}) \tag{2.41}$$

$$-\frac{dP}{dL} = \rho_M g \sin\theta + \frac{\pi D}{A}\tau_{WM} \tag{2.42}$$

Using H_L as approximation term, homogeneous mixture density and viscosity are calculated as linear estimates from values of gas and liquid phases. Pressure gradient model for homogeneous model is then calculated (2.42) for liquid-gas mixture pipe flow using established method employed for single-phase flows (mixture terms are defined as shown in appendix (C.1.4)). In earlier studies, homogeneous model has been applied to all flow regimes but has been shown to give invalid predictions for other flow regimes, including: stratified, annular, and mist flows. (Shoham, 2005). Similar to previously considered mechanistic models, knowledge of prevalent flow regime is required.

The problem associated with pre-knowledge of flow regime in order to choose appropriate pressure gradient mechanistic models, necessitated the need for a new mechanistic model that determines flow regime and pressure gradient simultaneously. A model (SETM) is developed in this work to achieve this requirement.

2.3 Transient model

Transient simulation of multiphase/two-phase has been pioneered by the nuclear industry. This is primarily due to the requirement for fast transient prediction during Loss of Local Accident (LOCA), a prerequisite for licencing nuclear reactors. This requirement led to the development of a number of transient simulators, including: RELAP, COBRA, CATHARE, and TRACE (Prosperetti and Tryggvason, 2007; Talley et al., 2011). These codes were developed based on rigorous solution of continuity, momentum, and energy equations of different phases present in flow (Morales-Ruiz et al., 2012; Brooks et al., 2012). Despite the stringent requirement for fast transient simulation of two-phase flow, these codes are uncomplicated since

water constitute the two-fluid system (i.e. steam-water system), with well-defined physical and chemical characteristics. Further, the geometries of two-phase flow paths in nuclear reactors are relatively simple and well defined. These codes are developed for the nuclear industry, therefore, applying same codes to liquid-gas pipe flow in petroleum industry is subject to prediction error, due to different fluid properties. Furthermore, application of multiphase/two-phase to liquid-gas pipe flow in petroleum industry typically consists long and complex pipe geometries, thus requires numerical solution at fine discretisation schemes; resulting in high demand on computational resources and time.

Development in the petroleum industry led to the requirement for transient multiphase or two-phase flow analysis. Contrary to transient observations in the nuclear industry, transient flow changes in the petroleum industry are usually slow, thus elaborate solution of conservation equations may not be required (Shoham, 2005; Choi et al., 2013). However, fluid compositions and properties, as well as flowlines are usually complex. These limitations of transient simulation in the petroleum industry also motivated the application of simplified transient simulator.

The following two sub-sections review two transient simulation methods generally applied in the petroleum industry. The first transient simulation method is referred to as: "two-fluid and drift flux models." The second transient simulation method is termed: "simplified transient models."

2.3.1 Two-fluid and drift flux transient models

Scoggins (1977) developed a pioneering transient model for the petroleum industry. Scoggins employed the homogeneous slip flow model (which can be termed as drift flux model), coupled with closure relations for estimating liquid holdup. Kohda et al. (1987) later developed a simulator for two-phase pipe flow, based on the drift flux model. The transient model of Kohda et al. was validated using the data of Cunliffe (1978) and additional experimental data. Further studies on the application of drift flux model to transient two-phase modelling has been carried out by other researchers (Pauchon et al., 1993, 1994; Masella et al., 1998; Shoham, 2005; Choi et al., 2013). Multidimensionally capable transient multiphase simulators include Horizon and LEDA (Li, 2011).

Two-fluid model describes separated flow liquid and gas in pipe flow, and detailed mathematical expressions are given in three-dimensional spatial-domain (Pompilio, 2013; Di Salvo, 2014). Three-dimensional two-fluid pipe flow model are typically

solved using detailed computational fluid dynamics solution methods (Prosperetti and Tryggvason, 2007), but demand high computational resources and time (Shoham, 2005; Prosperetti and Tryggvason, 2007; Liu et al., 2011). Therefore, two-fluid pipe flow model is simplified by approximating three-dimensional two-fluid model to one-dimensional two-fluid model. This is achieved by cross-sectional area averaging, and taking pipe length as one-dimensional direction (Pompilio, 2013). Mass transfer between liquid-gas interface is zero for negligible thermal energy variation in flow (Cazarez-Candia et al., 2011; Ma et al., 2011; Shirdel and Sepehrnoori, 2012). One-dimensional two-fluid model is given in equations (2.43 - 2.46):

Gas continuity equation:

$$\frac{\partial}{\partial t}(\alpha_G \rho_G) + \frac{\partial}{\partial x}(\alpha_G \rho_G U_G) = 0 \tag{2.43}$$

Liquid continuity equation:

$$\frac{\partial}{\partial t}(\alpha_L \rho_L) + \frac{\partial}{\partial x}(\alpha_L \rho_L U_L) = 0 \tag{2.44}$$

Gas Momentum equation:

$$\frac{\partial}{\partial t}(\alpha_G \rho_G U_G) + \frac{\partial}{\partial x}\left(\alpha_G \rho_G U_G^2\right) = -\frac{\partial}{\partial x}(\alpha_G P_G) + P_{IG}\frac{\partial}{\partial x}(\alpha_G) - \alpha_G \rho_G g \sin\theta - \tau_{WG} - \tau_{LG} \tag{2.45}$$

Liquid Momentum equation:

$$\frac{\partial}{\partial t}(\alpha_L \rho_L U_L) + \frac{\partial}{\partial x}\left(\alpha_L \rho_L U_L^2\right) = -\frac{\partial}{\partial x}(\alpha_L P_L) + P_{IL}\frac{\partial}{\partial x}(\alpha_L) - \alpha_L \rho_L g \sin\theta - \tau_{WL} + \tau_{LG} \tag{2.46}$$

Different modifications have been developed, which can be broadly classified into three groups. The first group refer to pressure-free two-fluid models Watson (1990); Masella et al. (1998), where pressure is excluded from momentum equations. The second group consists of single-pressure two-fluid models (Stuhmiller, 1977; Bendiksen et al., 1986, 1991), where same pressure is assumed for the two phases. The last group refer to two-fluid models where different pressure is considered for all phases (Pauchon and Banerjee, 1986; Saurel and Abgrall, 1999; Ransom and Hicks, 1984), and generally implemeted by applying closure relation to account for the pressure difference resulting for interfacial and transient effects. The most popular multiphase flow transient simulator in the petroleum industry was developed by Bendiksen et al. (1986) and Bendiksen et al. (1991); this model is referred to as OLGA. OLGA is a dynamic multiphase flow simulator. The name OLGA is an acronym for 'OiL and GAs'. OLGA is based on the concept of "extended two-fluid

model," where three different phases are assumed to exist, namely: liquid phase, gas phase, and droplet phase. OLGA has been jointly developed by IFE and SINTEF, and validated against a large field and experimental datasets (Ali, 2009; Belt et al., 2011). The simulator is widely applied in the petroleum industry for design purposes as well as prediction of various scenarious during production (Bratland, 2010). Black et al. (1990) also developed a two-phase transient simulator based on the two-fluid model. Ishii and Mishima (1984) studied closure relations applied in two-fluid models.

Drift flux and two-fluid models are prone to computational problems, due to ill-posed nature of the conversation equations, as well as solution instability. Comprehensive review of transient simulation methods and their limitations have been carried out by (Dinh et al., 2003; Mao and Harvey, 2011; Ishii and Hibiki, 2014; Jerez-Carrizales et al., 2015). Attempts to overcome high computational resources and solution time associated with rigorous solution of the full conservation equations of liquid-gas two-phase pipe flow equations, motivated the development of simplified transient simulator for two-phase pipe flow.

2.3.2 Simplified transient models

Taitel et al. (1989) proposed a simplified transient two-phase model, by treating liquid continuity as the only transient equation; momentum equations of gas and liquid, and gas continuity equation were treated in a quasi-steady state. These assumptions are valid for slow transient flow variations (Shoham, 2005).

The model of Taitel et al. was modified by Minami and Shoham (1994), using an implicit scheme instead of explicit scheme implemented in the original model. Minami and Shoham also developed an new flow regime transition model for transient flow. The modified model of Taitel et al. was tested against experimental data collected in a 420 m long and 7.79 cm diameter pipe, and air-kerosene two-fluid system. The validation results showed good agreement between model and experimental data, with the exception of liquid blowdown test. During liquid blowdown test when liquid flow rate is set to zero with gas flow rate sustained, complete liquid removal is not achieved.

Li (2011) developed a simplified two-phase transient model by treating continuity equations as transient, but momentum equations in a quasi-steady state. Li validated this model using the data of Vigneron et al. (1995). Later, Choi et al. (2013) developed a simplified transient two-phase model to solve modified continuity equa-

tions, but treated momentum equations as quasi-steady extended drift flux equation.

Existing simplified transient models assume complete quasi-steady state condition for momentum equations. Consequently, an alternative simplified transient two-phase model can be developed; by considering convective terms in momentum equations, as well as continuity equations in transient state. This alternative simplified transient model is developed in this study.

Chapter 3

Flow regime

Flow regime model development and improvement, carried out in this study, is presented in this chapter. The first section (3.1), detailed the theory and model development. The second section (3.3), outlined algorithm for the flow regime. The third section (3.4), presents validation and other results. The last section (3.5), presents discussion.

3.1 Theory: Flow regime

The unified flow regime model proposed in this study is a combination of the development of new flow regime transition criteria, and improvements to existing flow regime transition criteria. Developments of new flow regime transition criteria are described for: transition from intermittent to dispersed bubble flow (subsection (3.1.3)), and transition from mist to annular/stratified (subsection (3.1.5)).

3.1.1 Transition from stratified to non-stratified flow

In this study, criterion for transition from stratified to non-stratified flow is based on the analysis of Taitel and Dukler (1976b). In the original model of Taitel and Dukler, a simplified Kelvin-Helmholtz stability analysis is applied to a laminar flow of gas and liquid layers, to determine transition from stratified to non-stratified flow (refer to figure (3.1)). Taitel and Dukler considered instability of a finite amplitude wave experiencing growth due to suction force per unit area ($F_S^{\dagger}; \dagger$ = Kelvin-Helmholtz) as well as wave decay resulting from gravity force per unit area ($F_G^{\dagger}; \dagger$ = Kelvin-Helmholtz) acting on the wave; refer to equations (3.1) and (3.2) for definitions of these forces in respective order.

$$F_S^{\dagger} = P - P' = \frac{1}{2}\rho_G \left(V_G^2 - V_G'^2\right) \tag{3.1}$$

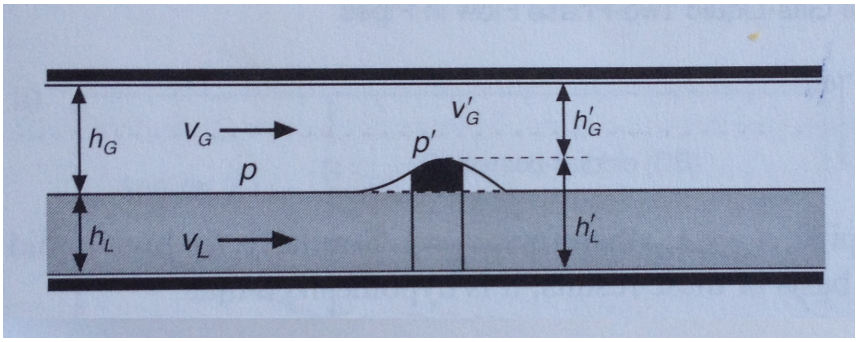

Figure 3.1 – Schematic illustration of simplified Kelvin-Helmholtz stability analysis (Shoham, 2005)

$$F_G^{\dagger} = \left(h_G - h_G^{'}\right)(\rho_L - \rho_G)\, g \tag{3.2}$$

Equating $F_S^{\dagger}$ and $F_G^{\dagger}$ through stability analysis, extending analysis to inclined flow and simplifying gives the final expression (refer to equation 3.3) derived by Taitel and Dukler.

$$V_G \geq c\left[\frac{g(\rho_L - \rho_G)\cos\theta A_G}{\rho_G S_I}\right]^{0.5},\ c = (1 - \widetilde{h}_L) = 1 - h_L/D \tag{3.3}$$

where, V_G = Velocity of gas (m/s), ρ_G = density of gas (kg/m^3), ρ_L = density of liquid (kg/m^3), A_G = cross sectional area of gas phase (m^2), S_I = gas-liquid interface length (m), and , θ = pipe inclination angle $(radian)$. c is a geometric term defined by Taitel and Dukler as $(1-\widetilde{h}_L)$ and relates to effect of wave propagation; where non-dimensional film height is defined as $\widetilde{h}_L(= h_L/D)$, with D = internal pipe diameter (m). In order to improve under prediction in the transition from stratified to annular flow, modification to the expression for coefficient c in the original Taitel and Dukler model, is proposed as $c = 1 - H_L$. The modified c gives lower values at transition from stratified to annular flow, since $\widetilde{h}_L < H_L$. This modification increases the value of V_G provided $0.0 < \widetilde{h}_L < 0.5$. The final expression for transition from stratified to non-stratified flow is defined as:

$$V_G \geq (1 - H_L)\left[\frac{g(\rho_L - \rho_G)\cos\theta A_G}{\rho_G S_I}\right]^{0.5} \tag{3.4}$$

The effect of H_L on c is illustrated in Figure 3.2. It should however be noted that lower values of V_G are obtained for $0.5 < \widetilde{h}_L < 1.0$, when compared with the original model of Taitel and Dukler. If $(1 - \widetilde{h}_L)$ is required for transition to intermittent flow, c can be defined as $c = max[(1 - \widetilde{h}_L), (1 - H_L)]$. Theoretically, the points of intersection of $(1 - \widetilde{h}_L)$ and $(1 - H_L)$ occur at $\widetilde{h}_L = H_L$, $\widetilde{h}_L = 0.0$, $\widetilde{h}_L = 1.0$.

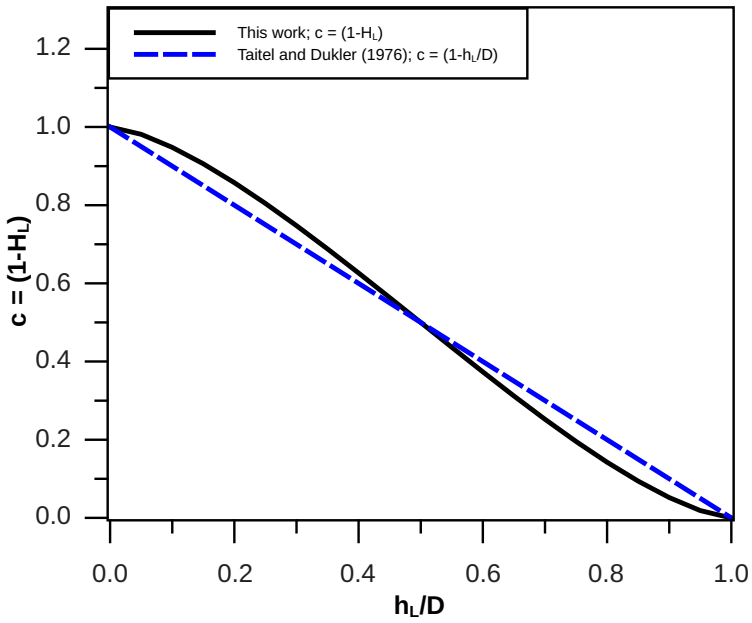

Figure 3.2 – Comparison of present model's $c\ (= 1 - H_L)$ with $c\ (= 1 - \widetilde{h}_L)$ in the original Taitel and Dukler (1976b) model

3.1.2 Transition from annular to intermittent flow

Transition from annular to intermittent flow is based on spontaneous blockage owing to wave-growth criterion (Barnea, 1987; Shoham, 2005). Instability of annular film can occur when liquid film flow at relatively higher rates, and results in wave growth which may lead to spontaneous blockage of the gas core or formation of intermittent flow. Barnea showed that the condition for the stability slug is

$$\frac{A_L}{A_P \cdot H_{LLS}^{min}} = \frac{H_L}{H_{LLS}^{min}} \geq 0.5 \tag{3.5}$$

Minimum liquid holdup in slug body is given as $H_{LLS}^{min} = 0.48$, this corresponds approximately to the maximum bubble volumetric packing in liquid slug (Thome, 2015). Therefore, the final expression for transition from intermittent to annular is

$$H_L < 0.24 \tag{3.6}$$

3.1.3 Transition from intermittent to dispersed-bubble flow

In this study, transition from intermittent to dispersed-bubble flow is based on angular combination of horizontal and vertical criteria. The horizontal criterion employed is the Taitel and Dukler (1976b) criterion for transition from intermittent to dispersed-bubble flow. The vertical criterion employed is a new criterion derived

in this study, following analysis similar to the derivation of Kutateladze criterion for transition to vertical annular flow (Shoham, 2005).

Horizontal criterion

Taitel and Dukler considered transition from intermittent to dispersed-bubble, in horizontal flow, to occur at high liquid flow rates. These flow conditions result in high equilibrium liquid level in pipe, approaching upper pipe wall. Gas phase exits in the form of gas-pocket, which moves to the upper wall of the pipe owing to buoyancy (refer to figure (3.3)). At sufficiently high liquid flow rate, turbulent force

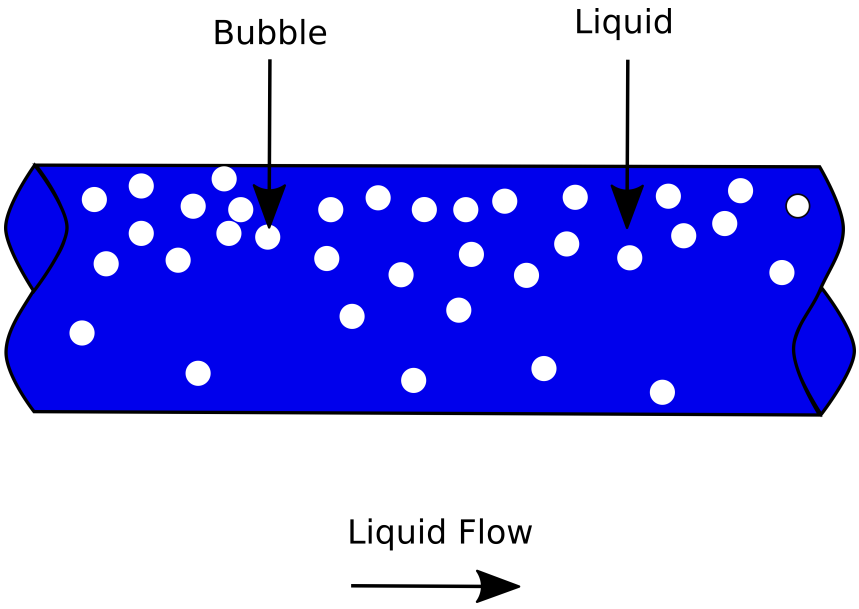

Figure 3.3 – Dispersed-bubble flow in horizontal pipe

per unit length (F_T^H) in the liquid phase overcome the net buoyancy force per unit length (F_B^H) which sustains the gas pocket at the top of the pipe; refer to equations (3.7) and (3.8) for definitions of these forces in respective order.

$$F_T^H = \frac{1}{2}\rho_L \overline{V'^2} S_I \tag{3.7}$$

$$F_B^H = A_G(\rho_L - \rho_G) g \cos\theta \tag{3.8}$$

where, A_G = cross-sectional area of gas pocket, S_I = gas-liquid interface length, and $V^{'}$ = turbulent radial velocity (fluctuating component of liquid phase). The turbulent radial velocity is determined from approximation of Reynold's stress:

$$\tau_R = \rho_L \overline{U'V'} \approx \rho_L \overline{V'^2} \tag{3.9}$$

The wall shear stress is determined from wall friction as:

$$\tau_W = \frac{1}{2} f_L \rho_L V_L^H 2 = \rho_L V^{*2} \tag{3.10}$$

Taitel and Dukler assumed that $\tau_R \approx \tau_W$, therefore, the root-mean-square of V' becomes approximately equal to V^*,

$$\overline{(V'^2)}^{0.5} \approx V^* = V_L^H \left(\frac{f_L}{2} \right)^{0.5} \tag{3.11}$$

Therefore, transition to dispersed-bubble flow will be achieved when $F_T^H \geq F_B^H$. Combining equations (3.7), (3.8), and (3.11), and simplifying gives the final criterion for transition to dispersed bubble in horizontal flow,

$$V_L^H = \left[\frac{4A_G}{S_I} \frac{g \cos\theta}{f_L} \left(1 - \frac{\rho_G}{\rho_L} \right) \right]^{0.5} \tag{3.12}$$

Vertical criterion

For vertical flow, a new criterion is derived, following analysis similar to the derivation of Kutateladze criterion for transition to vertical annular flow (Shoham, 2005). It is assumed that disperse bubbles exist and each bubble is subjected to both buoyancy force (F_B^V) and drag force (F_D^V); refer to figure (3.4) for schematic illustration. Definitions of F_B^V and F_D^V are given in equations (3.13) and (3.14) respectively.

$$F_B^V = \frac{\pi {d_D}^3}{6} g(\rho_L - \rho_G) \tag{3.13}$$

$$F_D^V = C_D \frac{\pi {d_D}^2}{4} \frac{\rho_L \left(V_L^V\right)^2}{2} \tag{3.14}$$

For flow conditions where the buoyancy force is greater than the drag force, $F_B^V > F_D^V$, the dispersed bubbles rise and collide with other bubbles to form gas pockets, and thus, intermittent flow is obtained. However, if $F_D^V \geq F_B^V$, the dispersed bubbles do not rise but flow with the liquid phase. Thus, the criterion for transition from intermittent to dispersed-bubble flow in vertical flow is $F_D^V \geq F_B^V$, and solving for V_L^V gives:

$$V_L^V = \frac{2}{\sqrt{3}} \left[\frac{g d_D \sin\theta (\rho_L - \rho_G)}{\rho_L C_D} \right]^{0.5} \tag{3.15}$$

Bubble diameter can be related to Weber number as (Shoham, 2005),

$$We = \frac{\rho_L \left(V_L^V\right)^2 D}{\sigma}, \; d_D = \frac{\sigma We}{\rho_L \left(V_L^V\right)^2} \tag{3.16}$$

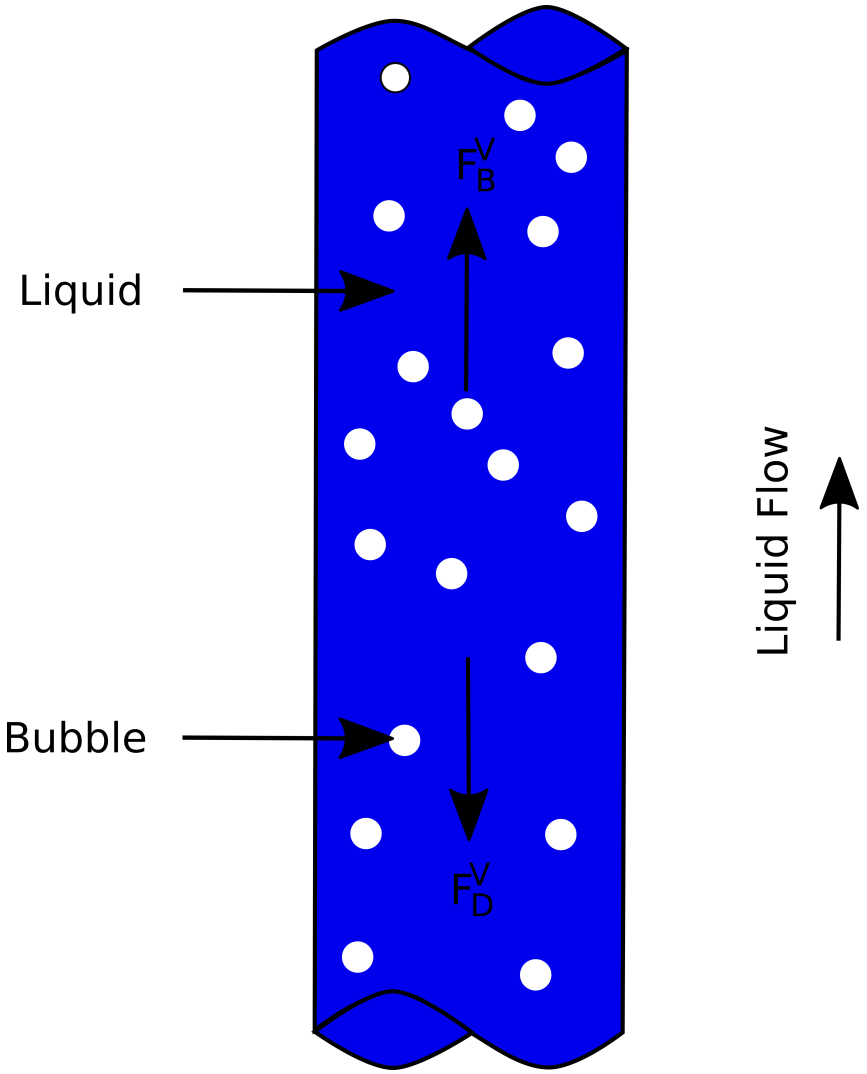

Figure 3.4 – Dispersed-bubble flow in vertical pipe

Substituting equation (3.16) in equation (3.15) gives the final expression for V_L^V as:

$$V_L^V = \left(\frac{4We}{3C_D}\right)^{0.25}\left[\frac{g\sigma\,\sin\theta(\rho_L-\rho_G)}{\rho_L^2}\right]^{0.25} \tag{3.17}$$

For small and evenly distributed bubbles, Turner et al. defined $We = 8$ (Shoham, 2005), while C_D is taken as 0.42 (Loilier, 2006). Therefore, the coefficient in equation (3.17) is approximately equal to 3.1 as shown in equation (3.18).

$$\left(\frac{4We}{3C_D}\right)^{0.25} \approx 3.1 \tag{3.18}$$

Therefore, the final criterion for transition from intermittent to dispersed bubbles in vertical flow is given by

$$V_L^V \geq 3.1\left[\frac{g\sigma\,\sin\theta(\rho_L-\rho_G)}{\rho_L^2}\right]^{0.25} \tag{3.19}$$

Unified criterion for transition from intermittent to dispersed-bubble flow

Therefore, the unified criterion, proposed in this study, for transition from intermittent to dispersed bubble flow is given by angular combination of equations (3.12) and (3.19), as shown in equation (3.20)

$$V_L \geq V_L^H \cos\theta + V_L^V \sin\theta \tag{3.20}$$

This criterion is however valid only for void fraction range: $0 \leq \alpha \leq 0.52$ (Barnea, 1987). Beyond this range, intermittent flow exists irrespective of turbulence forces. α is defined as

$$\alpha = \frac{V_{SG}}{V_{SG} + V_{SL}} \tag{3.21}$$

α is related to no-slip liquid holdup (λ_L), and symbolically expressed in equation (3.22).

$$\lambda_L = \frac{V_{SL}}{V_{SG} + V_{SL}} = 1 - \alpha \tag{3.22}$$

Previous study by Mandhane et al. (1974) shows that transition boundary from intermittent to dispersed bubble flow varies with pipe diameter, since transition occurs at higher liquid superficial velocities for larger pipe diameter. This phenomenon has not been included in this study.

3.1.4 Transition from slug to plug or bubble flow

Two models are proposed for identifying plug flow. The first plug model is based on the work of Barnea (1987). The second plug model is derived from the experimental data of França and Lahey (1992).

First plug model is based on Barnea's presentation of Taitel et al. (1980) criterion (refer to equation (3.23)), for transition from bubble to slug flow, at low liquid flow rates and with negligible turbulence forces.

$$\alpha \leq 0.25 \tag{3.23}$$

The criterion in equation (3.23) is combined with superficial velocities of gas and liquid (defined by equations (3.24) and (3.25) respectively), and bubble-rise velocity is given as terminal velocity of a single bubble in an infinite stagnant liquid medium (Shoham, 2005) (defined as shown in equation (3.26)).

$$V_G = \frac{V_{SG}}{\alpha} \tag{3.24}$$

$$V_L = \frac{V_{SL}}{1-\alpha} \tag{3.25}$$

$$V_{0\infty} = V_G - V_L \tag{3.26}$$

The definition of bubble-rise velocity as presented by Harmathy (1960) is applied (refer to equation (3.27)).

$$V_{0\infty} = 1.53\left[\frac{g\sigma(\rho_L - \rho_G)}{\rho_L^2}\right]^{0.25} \tag{3.27}$$

The resulting equation, after accounting for pipe inclination, is:

$$V_{SL} = 3V_{SG} - 1.15\left[\frac{g\sigma(\rho_L - \rho_G)}{{\rho_L}^2}\right]^{0.25} \sin\theta \tag{3.28}$$

The first plug model determines the existence plug or bubble flow based on pipe inclination angle. At inclinations angle above 70^0, bubbles rise and tend to flow in symmetric bubble flow pattern; thus forming a bubble flow regime. However, for pipe inclinations below 70^0, bubbles rise and tend to accumulate at the upper part of pipe cross-section; resulting in the formation of plug flow regime.

Second plug model The second plug flow model is also based on the method of Barnea (1987). A major modification is, however, made by using ($\alpha \leq 0.5$) instead of ($\alpha \leq 0.25$), thus fitting the second plug model (refer to figure (3.5) and equation (3.29)) to the data of França and Lahey (1992).

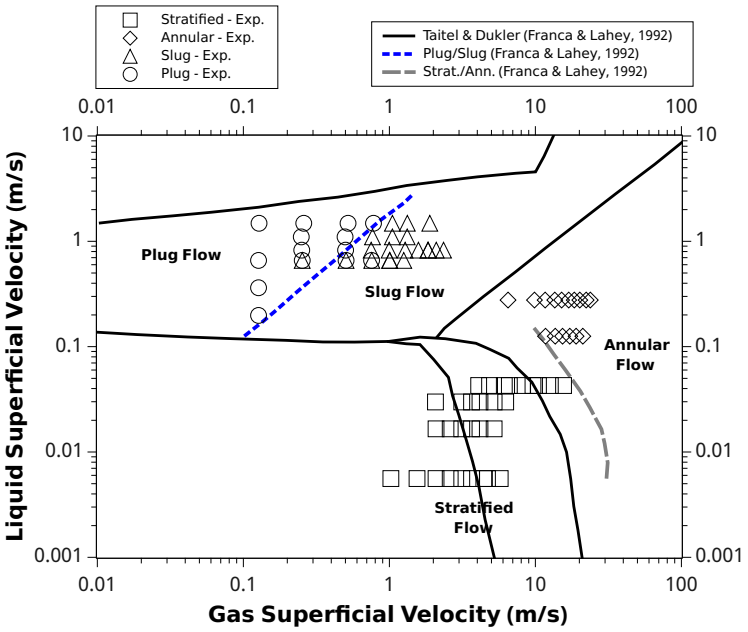

Figure 3.5 – Experimental data of França and Lahey (1992) showing transition from slug to plug, and stratified to annular in horizontal pipe flow

$$V_{SL} = V_{SG} - 0.765 \left[\frac{g\sigma(\rho_L - \rho_G)}{{\rho_L}^2} \right]^{0.25} \sin\theta \tag{3.29}$$

3.1.5 Transition from mist to annular/stratified flow

At very high gas flow rates, annular or stratified film thins out under the shear forces of the gas phase, until it becomes unstable and entrained in the continuous gas phase. In this study, transition criterion from annular/stratified to mist flow is a new criterion (fitted to no-slip void fraction, α) based on the data of Asante (2000). Figure (3.6) shows the data of Asante (2000), while equation (3.30) shows resulting mist transition model.

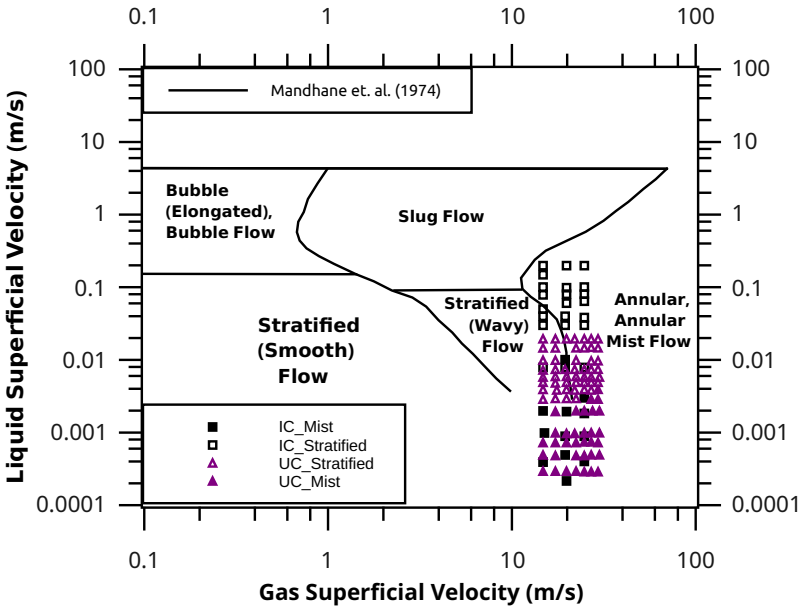

Figure 3.6 – Experimental data of Asante (2000) showing transition from annular/stratified to mist flow

$$(1 - \alpha) \leq 0.0001 \tag{3.30}$$

It should be noted that the proposed transition model (equation (3.30)) only depends on no-slip void fraction.

3.2 Validation Data

França and Lahey (1992) conducted an experiment (summarised in table (3.1)). França and Lahey collected flow regime data, including: plug, slug, stratified, and annular. The authour observed that slug and plug data can be separated on a $log(U_{SL})\ Vs.\ log(U_{SG})$ plot. Further, the author also observed that data from the

experimental data was under-predicted by stratified to annular transition criterion of Taitel and Dukler (1976a). Experimental data of Asante (2000), summarised in table (3.1), also show similar under-prediction by stratified to annular transition criterion of Taitel and Dukler. Furthermore, the two datasets are compared with existing published flow regime map (Mandhane et al. (1974), refer to figure (3.15)) and flow regime model (Taitel and Dukler (1976a), refer to figure (3.14)), with prediction accuracies: Mandhane et al. (1974) – 92% (stratified), Taitel and Dukler (1976a) – 36%, 50% (stratified). Therefore, the two flow regime datasets are predicted by the flow regime map and model. The discrepancies are likely due to model under-predictions identified previously.

Table 3.1 – Range of experimental data for validating unified flow regime model

Source	# data [−]	Flow regime [−]	θ $[deg]$	D $[m]$
Asante (2000) Pressure: 101,325 Pa Temperature: 15 ^0C Fluid: oil/water/air U_{SG}: $5-30\ m{\cdot}s^{-1}$ U_{SL}: $0.02-20\ m{\cdot}s^{-1}$ ρ_G: $1.2\ m{\cdot}s^{-1}$ ρ_L: $oil = 860\ Kg{\cdot}m^{-3}$ ρ_L: $water = 999\ Kg{\cdot}m^{-3}$ μ_G: $1.8e-5\ Pa{\cdot}s$ μ_L: $oil = 0.001\ Pa{\cdot}s$ μ_L: $water = 0.0065\ Pa{\cdot}s$	84	Stratified/ Annular/ Mist	0	$0.0254-0.0762$
França and Lahey (1992) Pressure: $0-14,415.4\ Pa$ Temperature: atmospheric Fluid: water/air U_{SG}: $0.127-23.76\ m{\cdot}s^{-1}$ U_{SL}: $0.0056-1.4853\ m{\cdot}s^{-1}$ ρ_G: $1.17\ m{\cdot}s^{-1}$ ρ_L: $997\ Kg{\cdot}m^{-3}$ μ_G: $1.845e-5\ Pa{\cdot}s$ μ_L: $0.00089\ Pa{\cdot}s$	99	Annular/ Stratified/ Plug/ Slug	0	0.019
Total	183			

3.3 Unified flow regime algorithm

Algorithm for proposed unified flow regime model is presented in this section (refer to figure (3.7)). For a given set of input data, the flow regime algorithm implements the previously described flow regime criteria (subsections (3.1.1) to (3.1.5)) to obtain

a single flow regime output. Input data include: gas and liquid superficial velocities, physical properties (i.e. densities, viscosities, and surface tension) of the two fluids, and pipe geometric variables (i.e. pipe diameter and inclination). Possible flow regime output include: stratified, annular, slug, dispersed-bubble, plug, bubble, and mist.

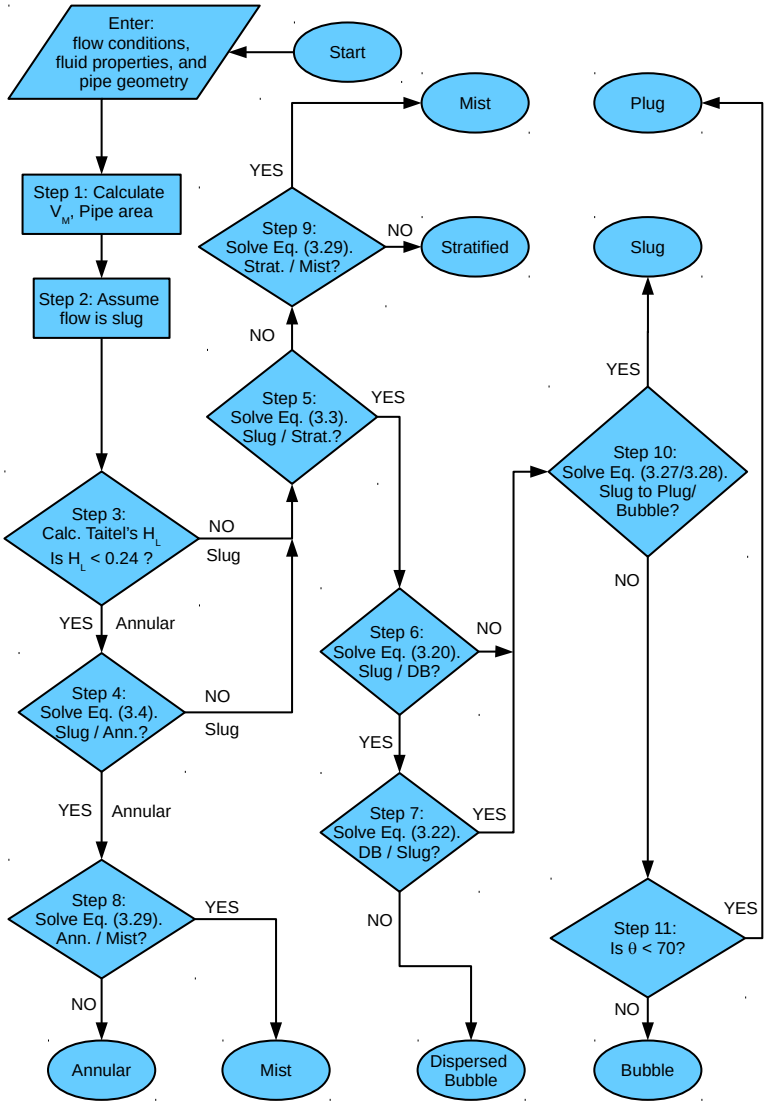

Figure 3.7 – Algorithm for present unified flow regime model

3.4 Results

Results, obtained from the implementation of proposed unified flow regime model, are presented in this section. The results are presented as log-log maps. Subsection (3.4.1) presents results for flow regime map in horizontal two-phase flow. Subsection

(3.4.2) gives results obtained for flow regime map in inclined two-phase flow. Subsection (3.4.3) outlines results for flow regime map in vertical two-phase flow. The last subsection (3.4.4) presents comparison of proposed unified flow regime model with experimental data.

3.4.1 Flow regime map for horizontal two-phase flow

In figures (3.8) and (3.9), predictions of present unified flow regime model is compared with existing horizontal flow regime maps of Taitel and Dukler (1976b) and Mandhane et al. (1974) respectively.

Comparison of present unified flow regime with the model of Taitel and Dukler (1976b)

Figure (3.8) represents flow regime map for air-water two-phase flow in a 78-mm diameter horizontal pipe, at standard temperature and pressure (i.e. 288.15 $[K]$ and $P = 101325$ $[Pa]$ respectively).

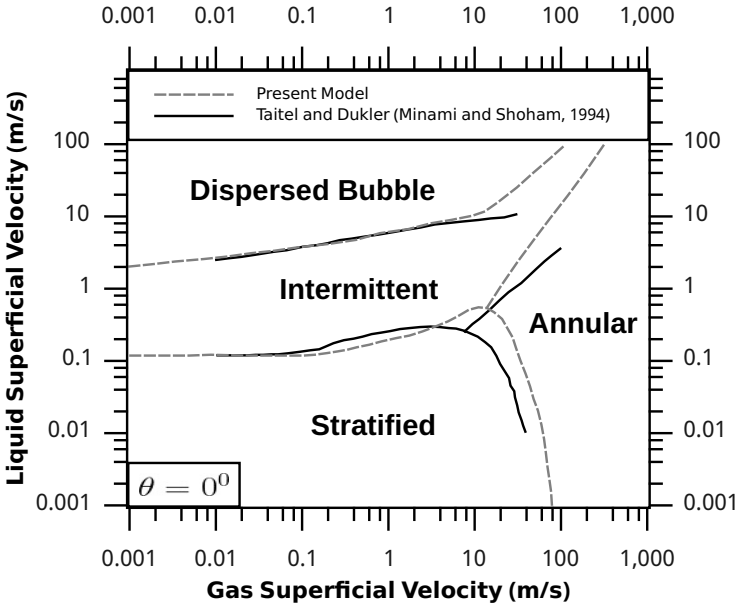

Figure 3.8 – Comparison of present model with Taitel and Dukler (1976b) model for air-water horizontal flow at standard temperature and pressure

At $V_{SG} \leq 10$ $[m/s]$, present model's transition from intermittent to dispersed-bubble flow match Taitel and Dukler's prediction. For $V_{SG} > 10$ $[m/s]$, transition to dispersed-bubble flow regime occur at much lower gas flow rate when compared with Taitel and Dukler (1976b); for instance, at $V_{SG} = 31.0$ $[m/s]$ present flow regime model predicts transition to dispersed-bubble at $V_{SL} = 24.12$ $[m/s]$, while the model of

Taitel and Dukler predicts a lower value at $V_{SL} = 11.07$ $[m/s]$.

Transition from stratified to annular flow regime occurs at higher gas superficial velocities for present model when compared with Taitel and Dukler model (Minami and Shoham, 1994). Transition from stratified to annular flow is examined for liquid superficial velocity range: $0.011 \leq V_{SL} \leq 0.267$ $[m/s]$. The results illustrated in figure (3.8) showed that transition to annular flow in the case of Taitel and Dukler model occurs at gas velocity from 7.96 $[m/s]$ to 39.59 $[m/s]$. Corresponding comparison shows that transition for present model occurs at higher gas velocities from 26.26 $[m/s]$ to 62.38 $[m/s]$.

Transition from stratified to slug flow regime occurs at higher gas superficial velocities for present model when compared with Taitel and Dukler model (Minami and Shoham, 1994).

Comparison of present unified flow regime with the flow regime map of Mandhane et al. (1974)

Figure (3.9) compares present model with flow regime map of Mandhane et al. (1974) for air-water two-phase flow in a 25-mm diameter horizontal pipe, at standard temperature and pressure. In this comparison, elongated bubble and slug

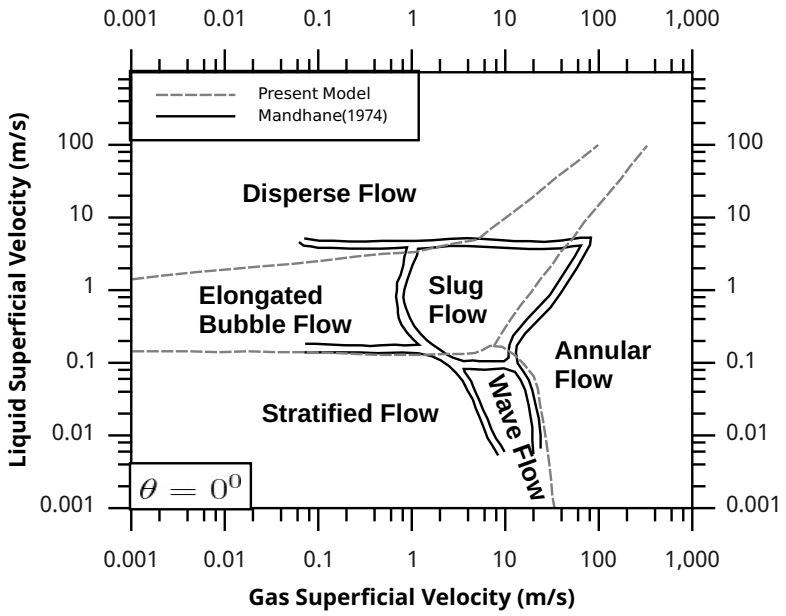

Figure 3.9 – Comparison of present model with Mandhane et al. (1974) horizontal flow regime map

flows in Mandhane et al. (1974) map are categorised as intermittent flow. The prediction of present model's transition from stratified to elongated bubble flow occurs at $V_{SL} \approx 0.130$ $[m/s]$, a value that approximately matches the lower band of Mandhane's transition zone from stratified to elongated bubble flow. Present model predicts transition from wavy (stratified) to slug (intermittent) between $V_{SL} \approx 0.130$ $[m/s]$ and $V_{SL} \approx 0.173$ $[m/s]$. On the other hand, Mandhane's map shows that transition from wavy to slug flow occurs at lower liquid superficial velocities; the upper and lower bands of Mandhane's transition from wavy to slug flow are $V_{SL} \approx 0.082$ $[m/s]$ and $V_{SL} \approx 0.106$ $[m/s]$ respectively.

Figure (3.9) also compares present unified flow regime with flow regime map of Mandhane, for transition from stratified to annular flow. Transition from stratified to annular flow for two-phase flow is examined for liquid superficial velocity within range: $0.007 \leq V_{SL} \leq 0.087$ $[m/s]$. The results show that transition to annular flow in the case of Mandhane map occurs at gas velocity from 14.362 m/s to 23.801 m/s. Corresponding comparison shows that transition for present model occurs at higher gas velocities from 17.140 m/s to 27.696 $[m/s]$.

3.4.2 Flow regime map for inclined two-phase flow

Next, present model's predictions are compared with existing inclined flow regime maps (Barnea (1987)). Figures (3.10) and (3.11) present flow regime maps for air-water two-phase flow in a 51-mm diameter at pipe inclinations $\theta = 30^0$ and $\theta = 80^0$ respectively, with fluid properties determined at standard temperature and pressure.

Comparison of present unified flow regime with flow regime model of Barnea (1987) at $\theta = 30^0$

At pipe inclination $\theta = 30^0$ (refer to figure (3.10)), prediction of transition line from slug to dispersed-bubble for present model agrees with that of Barnea (1987). The figure further shows that contrary to model results of Barnea (1987), stratified flow in present model exists at inclination angle above 20^0. Transition from stratified to annular flow matches the prediction of Barnea (1987).

Comparison of present unified flow regime with flow regime model of Barnea (1987) at $\theta = 80^0$

Figure (3.11) compares present unified flow regime model's prediction with the model of Barnea (1987) at pipe inclination $\theta = 80^0$. At $V_{SG} \leq 2.9$ m/s, present model's transition from intermittent to dispersed-bubble flow is approximately constant at $V_{SL} \simeq 2.9$ m/s; this value approximately matches the prediction of Barnea

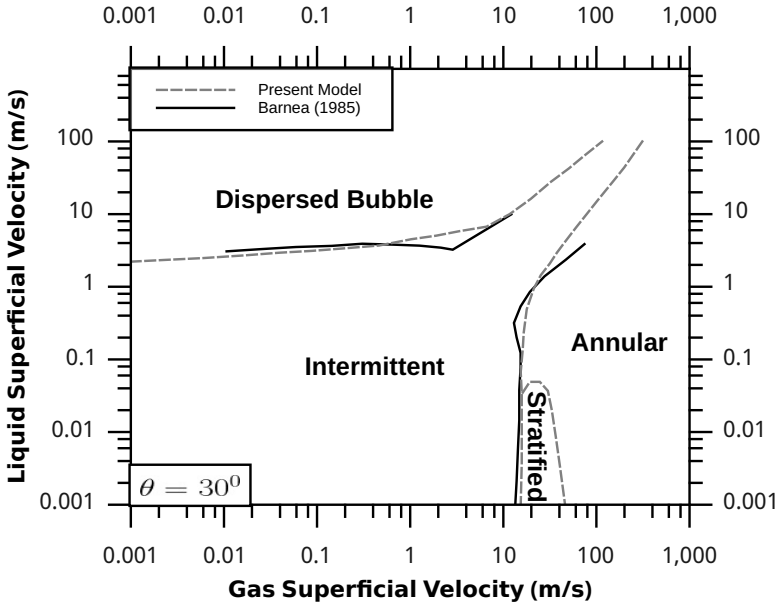

Figure 3.10 – Comparison of present model with Barnea (1987) model for air-water, 30^0 inclined flow, and at standard temperature and pressure

(1987). At $V_{SG} > 2.9\ m/s$, however, slug to dispersed-bubble transition line shows positive increase in V_{SL} with respect to V_{SG}: from $[(V_{SG}, V_{SL}) = (2.9, 2.9)]\ m/s$ to $[(V_{SG}, V_{SL}) = (106.0, 99.0)]\ m/s$. At $V_{SL} < 0.74\ m/s$, present model predictions for stratified to annular transition match Barnea's predictions.

3.4.3 Flow regime map for vertical two-phase flow

Comparison of present unified flow regime with flow regime model of Barnea (1987) at $\theta = 90^0$

At pipe inclination $\theta = 90^0$, present unified flow regime model predictions are compared with Barnea (1987) flow regime map for air-water two-phase at standard temperature and pressure (figure (3.12)). Similar results are obtained as for $\theta = 80^0$. At $V_{SG} \leq 2.9\ m/s$, present unified flow regime model's line of transition from intermittent to dispersed-bubble occurs at constant value: $V_{SL} \approx 2.9\ m/s$. At higher values of V_{SG}, transition line shows positive increase in V_{SL} with respect to V_{SG}: from $[(V_{SG}, V_{SL}) \approx (2.9, 2.9)]\ m/s$ to $[(V_{SG}, V_{SL}) = (106.1, 99.2)]\ m/s$.

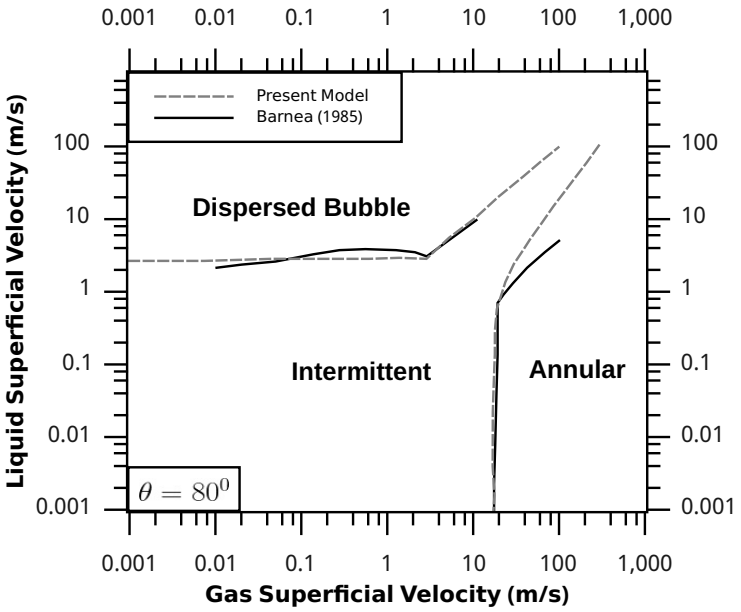

Figure 3.11 – Comparison of present model with Barnea (1987) model for air-water, 80^0 inclined flow, and at standard temperature and pressure

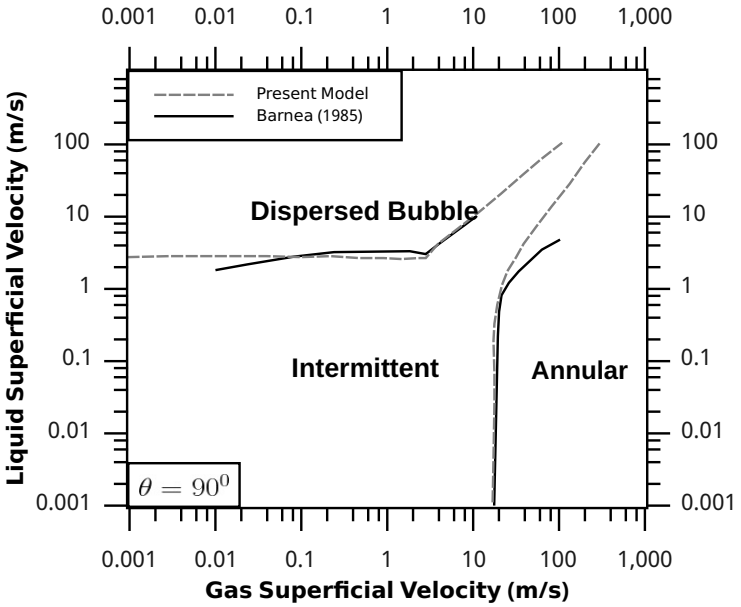

Figure 3.12 – Comparison of present model with Barnea (1987) model for air-water, 90^0 inclined flow, and at standard temperature and pressure

Comparison of present unified flow regime with the flow regime map of Weisman and Kang (1981)

Present unified flow regime transition model is also compared with the data of Weisman and Kang (1981) in figure (3.13). Transition from intermittent to dispersed-

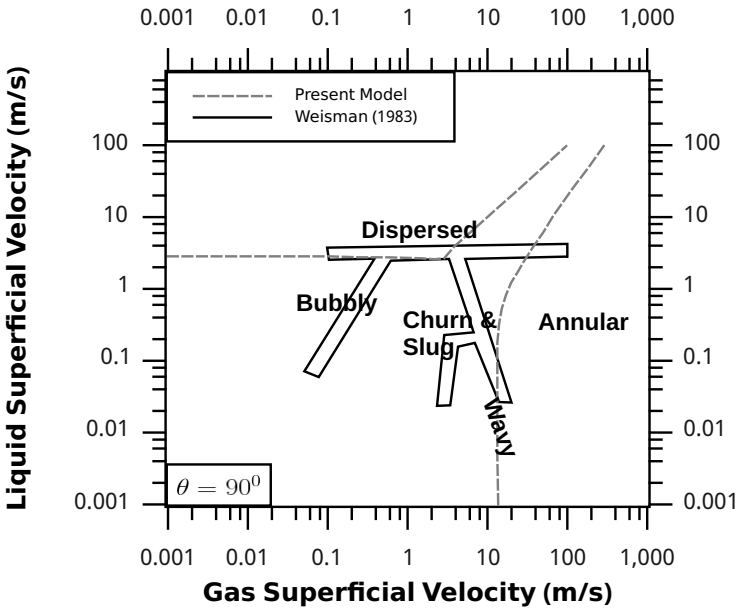

Figure 3.13 – Comparison of present model with Weisman and Kang (1981) model for air-water vertical flow, at standard temperature and pressure

bubble flow for this data occur in the range: $2.54 < V_{SL} < 4.23\ m/s$, while the corresponding transition line for present model occurs at value of $V_{SL} \approx 2.9\ m/s$.

3.4.4 Comparison of present model with experimental data

Comparison of present unified flow regime with data of França and Lahey (1992)

Figure (3.14) compares present model with the experimental data of França and Lahey (1992). In comparison with the original Taitel and Dukler (1976b) model, at higher gas flow rates present model's transition from stratified to annular occur at higher V_{SG}; present model's transition line matches França and Lahey (1992)'s transition line (dash gray line). The model of Taitel and Dukler (1976b) on the other hand underpredicts the transition from stratified to annular since it only identified 92% of the data of França and Lahey (1992).

The first plug model identified 50% of experimental data points, the remaining data points were identified as slug. The second plug model however identified approximately 100% of same experimental data.

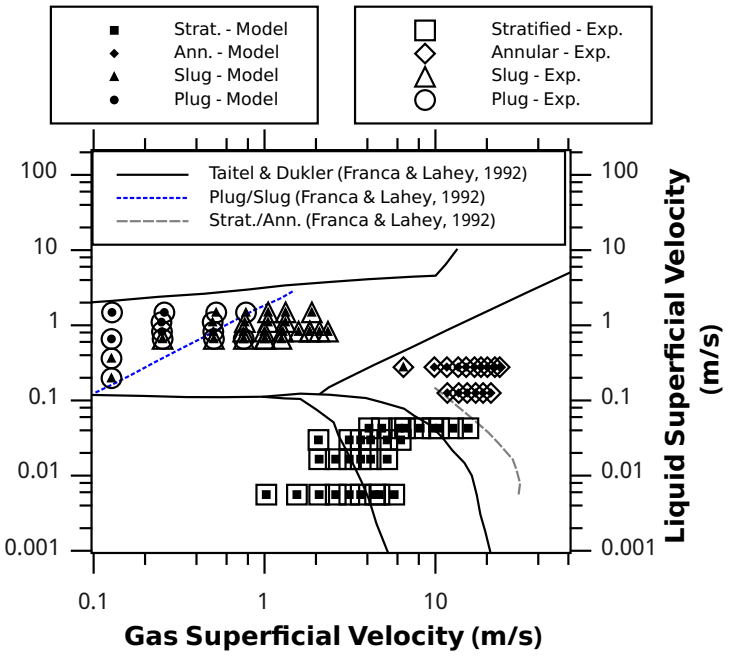

Figure 3.14 – Comparison of present model with data of França and Lahey (1992)

Comparison of present unified flow regime with data of Asante (2000)

Figure (3.15) compares present model's predictions and Mandhane et al. (1974) flow regime map with experimental data of Asante (2000). The experimental data are classified as shown in table (3.2). Predictions' results show that about 57% and

Table 3.2 – Classification of the experimental data of Asante (2000)

Flow regime identifier	Flow regime description
IC_Stratified	Stratified data from Imperial College London
UC_Stratified	Stratified data from University of Calgary
IC_Mist	Mist data from Imperial College London
UC_Mist	Mist data from University of Calgary

36% of IC_Stratified data were accurately predicted by present model and Mandhane et al. (1974) flow regime map respectivley. Similar assesment of UC_Stratified data show 88% and 50% accurate prediction for present model and Mandhane et al. (1974) flow regime map respectivley. Since mist flow is not identified by Mandhane et al. (1974), results are obtained only for present model. Present model accurately predict 75% and 88% of IC_Mist and UC_Mist data respectively.

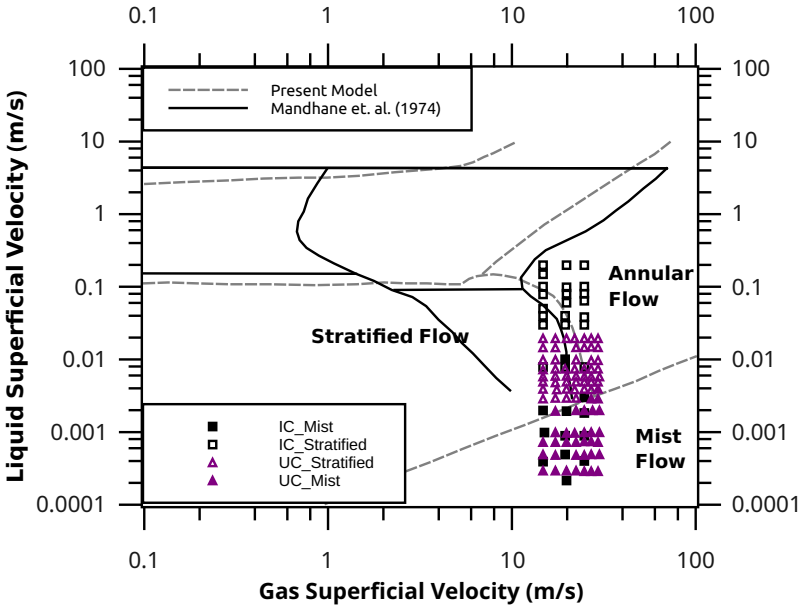

Figure 3.15 – Comparison of present model with data of Asante (2000)

3.5 Discussion

3.5.1 Flow regime map for horizontal two-phase flow

Based on observations in subsection (3.4.1), at $V_{SG} \leq 10m/s$, present model's transition from intermittent to dispersed-bubble flow match Taitel and Dukler's prediction, since the contribution of equation (3.19) to equation (3.20) becomes zero at zero pipe inclination. Thus transition criterion is based on stability of buoyancy and turbulence forces acting on gas pocket (Taitel and Dukler, 1976b). However, at higher values of V_{SG}, additional transition criterion based on 0.52 maximum void fraction, proposed by Barnea (1987), results in transition to dispersed-bubble flow regime at much lower gas flow rate when compared with Taitel and Dukler (1976b). These predictions are significantly different for Mandhane et al. (1974).

Transition from stratified to annular flow regime occurs at higher gas superficial velocities for present model when compared with Taitel and Dukler model (Minami and Shoham, 1994). This difference is due to the fact that present model replaces nondimensional film height $\widetilde{h}_L$ in the original Taitel and Dukler model with liquid holdup H_L. Thus, at high gas flow rate, $(1 - H_L) > (1 - \widetilde{h}_L)$, leading to higher gas superficial velocity at transition boundary, but approaches Taitel and Dukler (1976b) criterion as $U_{SL} \rightarrow 0$. Based on the same analogy, at low gas flow rates, $(1 - H_L) < (1 - \widetilde{h}_L)$, resulting in transition of stratified to intermittent flow at lower liquid superficial velocities when compared with Taitel and Dukler (1976b), but approaches Taitel and Dukler (1976b) criterion as $U_{SG} \rightarrow 0$. Therefore, the point of intersection of present model and the original Taitel and Dukler (1976b) model occurs at $\widetilde{h}_L = H_L$. The significance of this phenomena is that present stratified to annular transition model improves the underprediction identified in the original Taitel and Dukler (1976b) model by shifting transition line to the right. The predictions of the flow regime model of Mandhane et al. (1974), at transition completion from stratified to annular, underpredicts transition line of present flow regime model.

3.5.2 Flow regime map for inclined two-phase flow

Although similar observations and explanations are obtained, in inclined flow as well as horizontal flow, for the case of transition from intermittent to dispersed-bubble flow. However, contrary to model results and experimental observations of Shoham (2005) and Taitel et al. (1980), stratified flow in present model exists at inclination angle above 20^0. The existence of stratified flow regime can be attributed to the replacement of $(1 - \widetilde{h}_L)$ with $(1 - H_L)$ in the original Taitel and Dukler (1976b) model; thus moving stratified to annular transition line further into annular region.

This discrepancy can be resolved by noting that annular flow profile for horizontal and inclined flows is typically eccentric (Ullmann and Brauner (2006); Rovinsky et al. (1997); Asante (2000); Gorelik and Brauner (1999); Brauner et al. (1998); Ng et al. (2001); Hamersma and Hart (1987)). At transition from annular to stratified flow, film thickness at top of pipe cross-section approaches zero; the resulting stratified flow profile is typically concave (or convex depending on fluid properties and pipe geometry).

3.5.3 Flow regime map for vertical two-phase flow

Transition from intermittent to dispersed-bubble was observed to occur at constant value of $V_{SL} = 2.9m/s$ provided $(0 \leq \alpha < 0.52)$. This value compares reasonably (within 3.33%) with minimum $V_{SL}(= 3m/s)$ transition proposed by Taitel et al. (1980), and falls within transition range for the flow regime map of Weisman and Kang (1981). This shows that present flow regime model predicts, within reasonable accuracy, transition from intermittent to dispersed-bubble flow.

Transition to annular flow is similar for present unified model, as for the model of Barnea (1987), since both are based on the Kutateladze transition criterion (Shoham, 2005; Brill, 1987). As observed in the results, flow regime map of Weisman and Kang (1981) however gives different classification at high values of V_{SL}, that is: part of annular region was identified as intermittent. This region can be better classified as churn flow, or transition zone from slug to annular flow (Shoham, 2005).

Therefore, present unified flow regime transition model is applicable to vertical two-phase flows, and predicts transition from intermittent to dispersed-bubble flow within reasonable accuracy of existing vertical flow regime models and maps.

3.5.4 Comparison of present model with experimental data

Based on explanations provided in section (3.5.1) (i.e. replacement of $\widetilde{h}_L$ with H_L), present unified flow regime model gives better stratified to annular transition when compared with the model of Taitel and Dukler (1976b). It is further demonstrated that present unified flow regime model gives better stratified to annular transition predictions than the flow regime map of Mandhane et al. (1974). Also, present unified flow regime is capable of identifying plug model, and prediction accuracy can be further improved by varying the value of critical void fraction for transition to plug/bubble flow as explained in subsection (3.1.4).

3.5.5 Implications of proposed unified flow regime model

The unified flow regime model proposed in this study are limited as follows:

Stratified to annular transition criterion Although the transition criterion gives improved predictions (in comparison with existing models and maps) for the data of França and Lahey (1992) and Asante (2000), however, the rationale behind the changing of h_L/D to H_L in proposed model may not necessarily apply for data outside experimental system domain of the study of França and Lahey (1992) and Asante (2000). In particular, variation of pipe diameter affects observed flow regime, owing to complex nature of phases interactions (Smith et al., 2012; Schlegel et al., 2012; Ali and Yeung, 2014). Also, flow regime predictions vary with dynamic viscosities of liquid and gas (Matsubara and Naito, 2011; Zhao et al., 2013). Hence, the proposed stratified to annular transition criterion should be compared with expanded domain of experimental data.

Mist empirical criterion The mist empirical criterion proposed in this study identifies mist data of Asante (2000), the data from which it was derived. Therefore, care must be observed in applying mist empirical criterion to system domain (fluid properties and pipe geometry of Asante (2000)) different from that for which it was derived.

Intermittent to dispersed-bubble transition Proposed transition criterion from intermittent to dispersed-bubble has been compared with existing models and maps, but limited to air-water pipe flow system, 25mm – 78mm pipe diameter, and standard temperature and pressure. Application of the proposed intermittent to dispersed-bubble transition model outside this system domain must be done with caution.

Plug empirical criterion Proposed plug transition criteria is based on the data of França and Lahey (1992). Therefore, caution must be observed in the application of these plug criteria to other system flow conditions outside that of França and Lahey (1992).

Chapter 4

Mechanistic model

This chapter presents development of the Single Equation Two-phase Mechanistic (SETM) model, as well as improvements to exiting pressure gradient and liquid holdup models, carried out in this study. The first section (4.1), detailed the theory and model development of SETM. The second section (4.2), outlined algorithm for SETM. The third section (4.3), provides SETM's performance evaluation. Section (4.4) details proposed improvement to homogeneous two-phase pressure gradient model for pipe flow. Section (4.5) provides correction factor to improve overprediction observed in liquid holdup model proposed by Choi et al. (2012). Section (4.6) provides validation results. The last section (4.7), presents discussion.

4.1 Theory: SETM

Based on existing mechanistic or phenomenological pressure gradient in a liquid-gas pipe flow, prior-knowledge of flow regime is required, followed by application of flow-regime-specific pressure gradient model. The Single Equation Two-Phase Mechanistic (SETM) model is proposed to implicitly determine flow regime and pressure gradient in liquid-gas pipe flow. A major requirement is the transition of flat liquid-gas interface, to curve stratified-wavy, to annular flow (refer to figure (4.2)). In order to achieve seamless transition (described in subsection (4.1.3)) between these liquid-gas interfaces, a transition zone and criteria are required. This requirement is dealt with presently. The Single Equation Two-phase Mechanistic (SETM) model is developed based on steady state momentum equation, Taitel and Dukler flow regime transition mechanisms, and the Kutateladze criterion for transition to annular flow. For simplicity, the Single Equation Two-phase Mechanistic (SETM) model is referred to as present model. Several modifications and observations are made to obtain present model, these include:

1. Contrary to conventional methods in existing two-phase mechanistic pressure

gradient models, flow regimes are not determined prior to calculating pressure gradient. Flow regimes and pressure gradient are determined implicitly.

2. Liquid entrainment is not taken into consideration for stratified and annular flows.

3. New flow regime transition boundaries and mechanisms are incorporated.

4. Prior knowledge of liquid holdup is assumed.

5. Depending on the flow rates of gas and liquid phases, pressure gradient equation adapts to appropriate form for prevailing flow regime.

Figure (4.1) shows flow regimes and transition boundaries for present model. Transition zone, ADEBCF, between annular/mist and other flow regimes' region is outlined by area bounded by curves ADE and BCF. Curves ADE and BCF are also referred to, respectively, as the *initiation* and *completion* of transition to annular flow. The other flow regimes' region is further categorised into stratified, slug, and dispersed bubble based on the value of β, where β is defined for two-phase flow slug unit as L_F/L_U. Previous studies demonstrated that the value of β determines prevalent flow regime (Minami and Shoham, 1994). However, β depends on pre-knowledge of H_L. For slug flow to exist, $0 < \beta < 1$, whereas criteria for the existence of stratified and dispersed bubble flows are $\beta \geq 1$ and $\beta \leq 0$ respectively. Figure (4.2) illustrates changes in cross sectional geometry of flow between initiation and completion of transition to annular flow.

For a given liquid superficial velocity, U_{SL}, a unique gas superficial velocity, U_{SG}, is determined for each of curves ADE and BCF as U^1_{SG} and U^2_{SG} respectively. U^1_{SG} is calculated in equation (4.1) as the maximum of three possible values of U_{SG} at the *initiation* of transition to annular flow. U^2_{SG} is calculated, using equation (4.2), as the maximum of three possible values of U_{SG} at the *completion* of transition to annular flow. Gas superficial velocities U^a_{SG}, U^b_{SG}, U^c_{SG}, U^d_{SG}, U^e_{SG}, and U^f_{SG} are determined next.

$$U^1_{SG} = max\big(U^a_{SG}, U^d_{SG}, U^e_{SG}\big) \tag{4.1}$$

$$U^2_{SG} = max\Big(U^b_{SG}, U^c_{SG}, U^f_{SG}\Big) \tag{4.2}$$

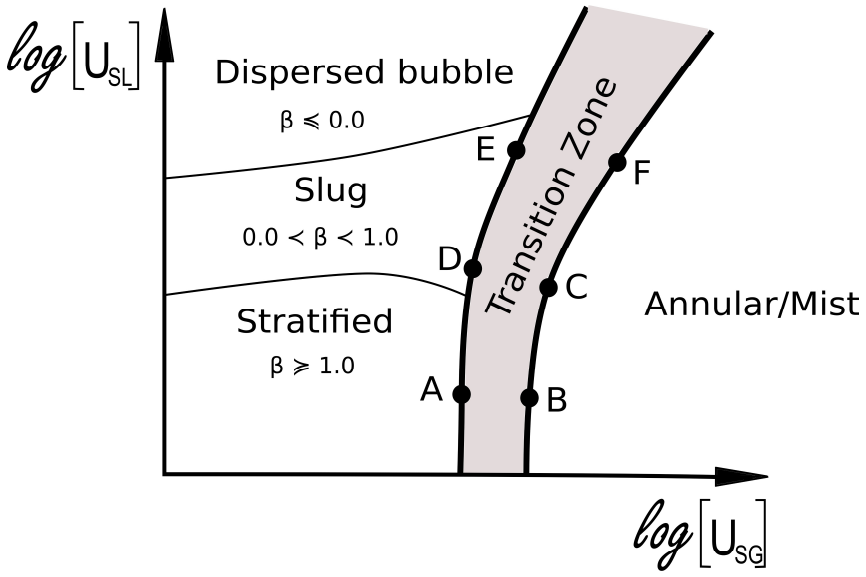

Figure 4.1 – Flow regimes and transition boundaries of SETM model

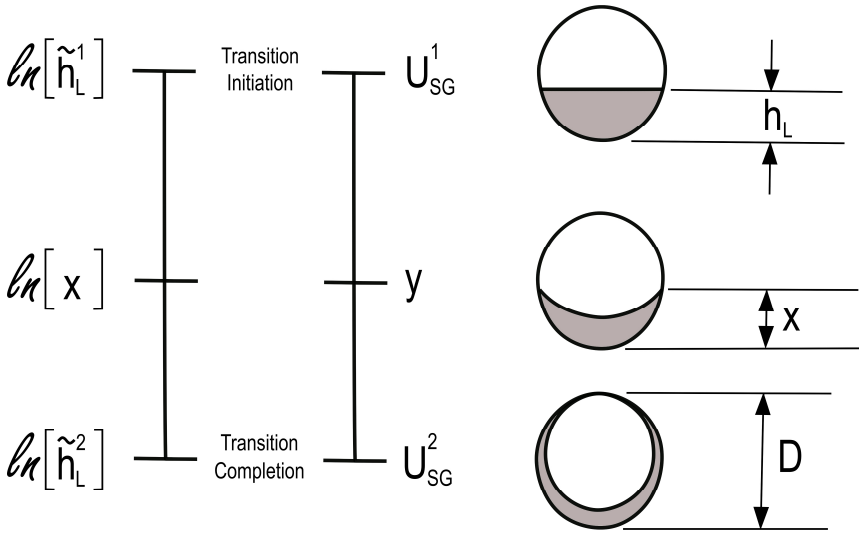

Figure 4.2 – Changes in flow cross sectional geometry between initiation and completion of transition to annular flow

4.1.1 Gas velocities at the initiation of transition to annular

U^a_{SG} is determined from the criterion (equation (4.3)) of Taitel and Dukler (1976b) for transition from smooth to wavy stratified flow.

$$U^a_G = \left[\frac{4\mu_L(\rho_L - \rho_G)g\cos\theta}{s\rho_L\rho_G U_L}\right]^{0.5} \tag{4.3}$$

where, U_G^a = gas velocity (for smooth to wavy stratified) $[m/s]$, U_L = liquid velocity $[m/s]$, ρ_G = gas density $[kg/m^3]$, ρ_L = liquid density $[kg/m^3]$, s = arbitrary constant taken as 0.01 (Shoham, 2005), g = acceleration due to gravity $[m/s^2]$. Superficial velocities of gas and liquid are related to liquid holdup by equation (4.4). Substituting equation (4.4) into equation (4.3), taking $H_L \approx \lambda_L$, and simplifying gives equation (4.5), where λ_L is no-slip liquid holdup, generally defined as $U_{SL}/(U_{SG}^a + U_{SL})$. f^a is a calibration factor based on experimental data in tables (4.1 - 4.4), defined as $f^a = 10/(1-\lambda_L)^2$.

$$U_L = \frac{U_{SL}}{H_L} \ , \ U_G^a = \frac{U_{SG}^a}{1-H_L} \tag{4.4}$$

$$U_{SG}^a = (1-\lambda_L)\sqrt{\lambda_L}\left[\frac{4\mu_L(\rho_L-\rho_G)g\cos\theta}{s\rho_L\rho_G U_{SL}}\right]^{0.5} \cdot f^a \tag{4.5}$$

Expression for finding U_{SG}^d is derived from the classical Kutateladze criterion for transition to annular flow in upward inclined flow. In order to account for the initiation of transition to annular flow, instead of the Kutateladze number of 3.1, an arbitrary constant value lower than 3.1 is required. In this study, a value of 1.0 is used as shown in equation (4.6). It should be noted that an optimised constant or variable is not considered in this study.

$$U_{SG}^d = 1.0\left[\frac{g\sigma\sin\theta(\rho_L-\rho_G)}{\rho_G}\right]^{0.5} \tag{4.6}$$

U_{SG}^e is calculated from stratified model of Taitel and Dukler (1976b) using annular profile with negligible liquid entrainment (details of the model has been provided in subsection (2.2.2)) , taking liquid holdup $H_L^e = 0.35$ at the initiation of transition to annular.

4.1.2 Gas velocities at the completion of transition to annular

Expression for finding U_{SG}^b is derived from the criterion (equation (4.7)) of Taitel and Dukler (1976b) for transition from stratified to non-stratified flow. $\widetilde{h}_L$ is a dimensionless term defined as h_L/D, where h_L = liquid film height, D = internal diameter of pipe.

$$U_G^b = \left(1-\widetilde{h}_L\right)\left[\frac{(\rho_L-\rho_G)gA_G\cos\theta}{\rho_G S_I}\right]^{0.5} \tag{4.7}$$

In this study, $\widetilde{h}_L$ is replaced with liquid holdup, H_L. Using the method of Sylvester (1987), H_L is expressed in equation (4.8) as a function of annular film thickness, δ_L. Geometric terms S_I and A_G are also expressed for annular flow (equation (4.9)). Then setting $H_L \approx \lambda_L$, gives final expression in equation (4.10).Similar to f^a, f^b is a calibration factor from experimental data in tables (4.1 - 4.4), defined as $f^b = 10$.

$$\delta_L = \frac{D}{2}\left[1 - \sqrt{1 - H_L}\right] \tag{4.8}$$

$$S_I = \pi(D - 2\delta_L)\ ,\ A_G = \frac{\pi}{4}(D - 2\delta_L)^2 \tag{4.9}$$

$$U_{SG}^b = (1 - \lambda_L)^2\left[\frac{(\rho_L - \rho_G)g\cos\theta}{\rho_G}\cdot\frac{(D - 2\delta)}{4}\right]^{0.5}\cdot f^b \tag{4.10}$$

U_{SG}^b is determined from the classical Kutateladze criterion for transition to annular flow in upward inclined flow (equation (4.11)).

$$U_{SG}^c = 3.1\left[\frac{g\sigma\sin\theta(\rho_L - \rho_G)}{\rho_G}\right]^{0.5} \tag{4.11}$$

Based on previous studies (Shoham, 2005), slug flow collapses into annular or stratified flow at $H_L \leq 0.24$. Therefore, U_{SG}^f is calculated from Taitel and Dukler (1976b) stratified model using annular profile with negligible liquid entrainment, taking $H_L^f = 0.24$ at the completion of transition to annular.

4.1.3 Gas liquid interface of Single Equation Two-Phase Mechanistic model

Gas-liquid interface, S_I, of present model is determined in equations (4.12) through (4.15), by linear interpolation between $S_{I,f}$ and S_F (figure (4.3)). It is assumed that the liquid cross sectional area corresponding to $S_{I,f}$, S_I, and S_F are $A_{F,f}$, A_F, and 0 respectively.

First, apparent liquid height X (refer to figure (4.2)) is estimated (equation (4.12)) from $\tilde{h}_L^1$, $\tilde{h}_L^2$, U_{SG}^1, and U_{SG}^2 by linear interpolation, and noting that $y = U_{SG}$. A_F and A_G are calculated from liquid holdup in film region, H_{LTB} (equation (4.13)). Once X is known, S_F is calculated using equation (4.14). S_I is calculated in equation (4.15), using the method of Zhang et al. (2003).

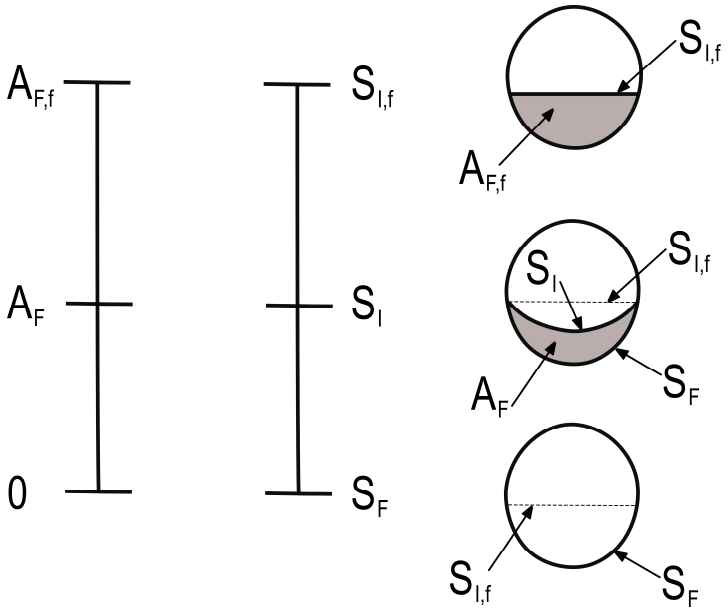

Figure 4.3 – Gas-liquid interface of SETM model

$$X = D \exp\left\{ \left(U_{SG}^2 - y\right) \left[\frac{\ln\left(\tilde{h}_L^1\right)}{U_{SG}^2 - U_{SG}^1} \right] \right\} \tag{4.12}$$

$$A_F = A \cdot H_{LTB} \ , \ A_G = A - A_F \tag{4.13}$$

$$S_F = D\left[\pi - \cos^{-1}\left(2\frac{X}{D} - 1\right)\right] \ , \ S_G = \pi D - S_F \tag{4.14}$$

$$S_I = S_F - (S_F - S_{I,f})\frac{A_F}{A_{F,f}} \tag{4.15}$$

4.1.4 Pressure gradient of Single Equation Two-Phase Mechanistic model

Slug model of Taitel and Barnea is solved (refer to appendix (C.1.3) for details) for L_F, L_s, L_u, β, and H_{LTB}^*, where $\beta = L_F/L_u$. In this study maximum and minimum values for β are set as 1.0 and 0.0 respectively. H_L is determined using the method of Choi et al. (2012). For low λ_L, flow regime typically approaches annular/mist flow, thus H_L is calculated using the method of Hart et al. (1989). Details for calculating H_L is given in subsection (4.1.5). Intermediate value for liquid holdup in slug body, H_{LLS}^*, is estimated using equation (4.16). H_{LLS}^H represents value of H_{LLS} for horizontal flow (Gregory et al., 1978) as shown in equation (4.19), and H_{LLS}^V is the value of H_{LLS} for vertical flow (Fernandes et al., 1983) as described in equation (4.20). The final expression for liquid holdup in slug body, H_{LLS}, is a linear interpolation between H_{LLS}^* and H_L (equation (4.17)). The final form of H_{LTB} is

also calculated by linear interpolation of between H^*_{LTB} and H_L (equation (4.18)).

$$H^*_{LLS} = H^H_{LLS}\cos^2\theta + H^V_{LLS}\sin^2\theta \tag{4.16}$$

$$H_{LLS} = H^*_{LLS}\beta + H_L\,(1-\beta) \tag{4.17}$$

$$H_{LTB} = H^*_{LTB}\,(1-\beta) + H_L\beta \tag{4.18}$$

$$H^H_{LLS} = \frac{1}{1+\left(\dfrac{U_M}{8.66}\right)^{1.39}} \tag{4.19}$$

$$H^V_{LLS} = 1 - \frac{U_{SG}}{0.425 + 2.65U_M} \tag{4.20}$$

A major contribution made by SETM to the computation of pressure gradient in two-phase pipe flow is the adaptation of the model to prevalent flow regime based on flow conditions (figure (4.4), equation (4.21)). Figure (4.4)(a) illustrates that at $\beta = 0.0$, $H_{LLS} = H_L$, which is typical for dispersed bubble flow, thus classical homogeneous model can be easily obtained. At $\beta = 1.0$, figure (4.4)(b) shows that $H_{LTB} = H_L$, this is a typical observation for stratified and annular flows when liquid entrainment is ignored, thus any separated flow model can be applied. However, at $0.0 < \beta < 1.0$, contributions are received from both homogeneous and separated models based on the value of β, and generally defines slug model.

Therefore, the derivation of pressure gradient for present model follows similar approach as for two-phase slug flow, where steady state two-phase momentum equations are simplified to obtain a combination of pressure gradients in slug body and liquid film as expressed in equation (4.21) (Shoham, 2005).

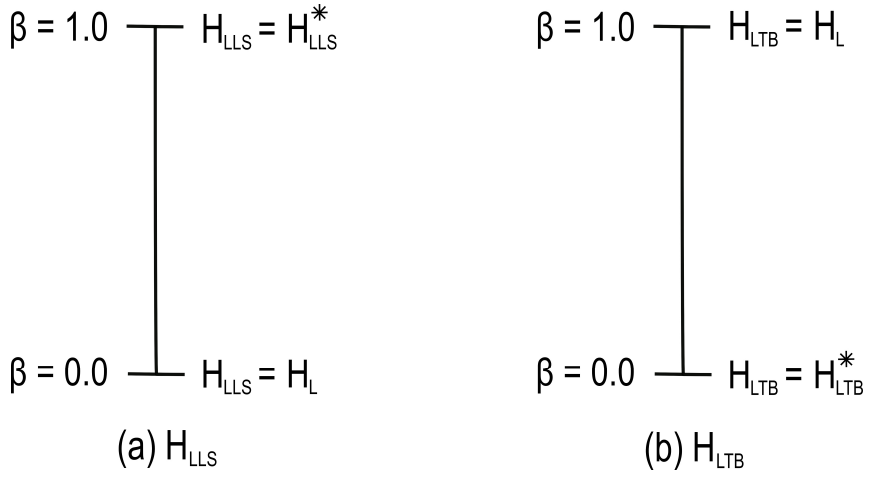

Figure 4.4 – Liquid holdup in slug body and film region

$$-\frac{dP}{dL} = \left(g\rho_S \sin\theta + \frac{\tau_S \pi D}{A}\right)(1-\beta) + \left(g\rho_F \sin\theta + \frac{\tau_F S_F}{A} + \frac{\tau_G S_G}{A}\right)\beta \tag{4.21}$$

where, ρ_S = density of slug body $[kg/m^3]$, ρ_F = density of liquid film zone $[kg/m^3]$, τ_S = shear stress at slug-wall interface $[N/m^2]$, τ_F = shear stress at liquid-wall interface $[N/m^2]$, τ_G = shear stress at gas-wall interface $[N/m^2]$. τ_G, τ_F, and τ_S take the forms employed by Shoham (2005), defined in equations (4.22), (4.23), and (4.24) respectively. Subscripts S and F represent slug body and slug film zone respectively. It should be noted that fluid properties in slug film zone and slug body are estimated as follows: $\rho_F = \rho_L H_{LTB} + \rho_G(1 - H_{LTB})$, $\rho_S = \rho_L H_{LLS} + \rho_G(1 - H_{LLS})$, and $\mu_S = \mu_L H_{LLS} + \mu_G(1 - H_{LLS})$. Pipe cross-sectional area is given as $A = \pi D^2/4$. Mixture velocity is $U_S = U_{SG} + U_{SL}$.

$$\tau_G = f_G \frac{\rho_G |\, U_{GTB}\, | U_{GTB}}{2} \tag{4.22}$$

$$\tau_F = f_F \frac{\rho_L |\, U_{LTB}\, | U_{LTB}}{2} \tag{4.23}$$

$$\tau_S = f_S \frac{\rho_S {U_S}^2}{2} \tag{4.24}$$

$$f_S = 0.001375\left[1 + \left(2{\times}10^4 \frac{\varepsilon}{D} + \frac{10^6}{Re_S}\right)^{\frac{1}{3}}\right] \tag{4.25}$$

Friction factors for wall interface with gas and liquid are defined respectively as $f_G = C_G {Re_G}^{-m}$ and $f_F = C_F {Re_F}^{-n}$. Friction factor f_S is obtained using Fanny

friction factor (refer to equation (4.25)). $C_G = C_F = 16$ and $m = n = 1$ for laminar flow, and $C_G = C_F = 0.046$ and $m = n = 0.2$ for turbulent flow. Reynold's numbers for film region and gas pocket are given respectively as: $Re_F = (\rho_L d_F \mid U_{LTB} \mid / \mu_L)$ and $Re_G = (\rho_G d_G \mid U_{GTB} \mid / \mu_G)$. Slug unit's hydraulic diameters are obtained for gas pocket and liquid film as $d_G = 4A_G/(S_G + S_I)$ and $d_F = 4A_F/S_F$ respectively. Friction factor at slug-wall interface is calculated from Fanny's equation, using slug Reynold's number $Re_S = (\rho_S D \mid U_S \mid / \mu_S)$. Phase velocities in the liquid film region and slug body are calculated in equations (4.26) and (4.27) respectively.

$$U_{LTB} = \frac{U_{SL}}{H_{LTB}} \ , \ U_{GTB} = \frac{U_{SG}}{1 - H_{LTB}} \tag{4.26}$$

$$U_{LLS} = \frac{U_{SL}}{H_{LLS}} \ , \ U_{GLS} = \frac{U_{SL}}{1 - H_{LLS}} \tag{4.27}$$

4.1.5 Liquid holdup model for SETM

Experimental data in tables (4.1-4.4) is plotted in figure (4.5), with no-slip liquid holdup on the vertical axis and number of data points on the horizontal axis. Two divisions of experimental flow data is obtained as slug (i.e. if $\lambda_L \geq 0.005$) and stratified/annular/mist (i.e. if $\lambda_L < 0.005$). Thereafter, a liquid holdup model for SETM is obtained as shown in algorithm (1).

The liquid holdup model of Choi et al. (2012) was derived using drift-flux closure relationship (refer to appendix (C.2.1)), and prediction accuracy was demonstrated to be 9.6% mean absolute error.

The liquid holdup model of Choi et al. (2012) is valid for $D = 0.051$ $[m]$, $0 < H_L < 0.06$, horizontal flow, air-water system, with mean absolute error of 10%. Refer to appendix (C.2.2) for details of Hart et al. (1989) liquid holdup model.

Algorithm 1 Liquid holdup sub-algorithm for SETM

procedure

Calculate no-slip liquid holdup:

$\lambda_L \leftarrow \dfrac{U_{SL}}{U_{SG} + U_{SL}}$

Determine liquid holdup model to implement in SETM:

if $(\lambda_L \geq 0.005)$ **then**

$H_L \leftarrow$ *liquid holdup model of* Choi et al. (2012)

else if $(\lambda_L < 0.005)$ **then**

$H_L \leftarrow$ *liquid holdup model of* Hart et al. (1989)

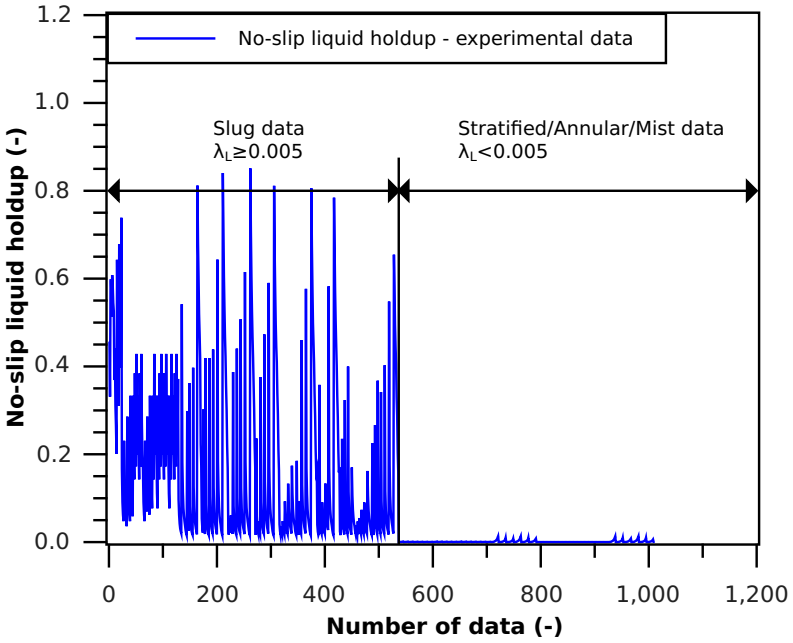

Figure 4.5 – Algorithm for Single Equation Two-Phase Mechanistic (SETM) model; data from tables (4.1 - 4.4)

4.2 SETM algorithm

Algorithm for the Single Equation Two-phase Mechanistic model is presented in this section (refer to figure (4.6)). Given a set of input data, the SETM algorithm implements the previously described equations in subsection (4.1) to implicitly obtain pressure gradient and flow regime solutions. Input data include: gas and liquid superficial velocities (i.e. $U_{SG},\ U_{SL}$), physical properties of the two fluids (i.e. $\rho_G,\ \rho_L,\ \mu_G,\ \mu_L,\ \sigma$), and geometric variables of pipe ($D,\ \theta,\ \varepsilon,\ L$).

No-slip liquid holdup (λ_L) is given in equation (4.28)

$$\lambda_L = \frac{U_{SL}}{U_{SL} + U_{SG}} \tag{4.28}$$

Liquid holdup at U^e_{SG} (i.e. possible U_{SG} at initiation of transition from stratified to annular flow) is given as H^e_L (refer to subsection (4.1.1)). Liquid holdup at U^f_{SG} (i.e. possible U_{SG} at completion of transition from stratified to annular flow) is given as H^f_L (refer to subsection (4.1.2)). It should be noted that H^e_L and H^f_L are only required to estimate U^e_{SG} and U^f_{SG} respectively.

Flowregime is determined using criteria given in figures (4.1) and (4.2); outline for determining flowregime is given in algorithm (2).

Algorithm 2 SETM Flow regime sub-algorithm

procedure

Enter input data:

  $input \leftarrow (U_{SG},\ U^1_{SG},\ U^2_{SG},\ \beta)$

Determine prevalent flow regime; based on figures 4.1 and 4.2:

  if $(U_{SG} \geq U^2_{SG})$ **then**

    $Flowregime \leftarrow Annular$

  else if $(U^1_{SG} < U_{SG} < U^2_{SG})$ **then**

    $Flowregime \leftarrow TransitionZone$

  else if $(U_{SG} \leq U^1_{SG})$ **then**

    if $\beta \leq 1$ **then**

      $Flow\ regime \leftarrow Dispersed\ bubble$

    else if $\beta \geq 1$ **then**

      $Flow\ regime \leftarrow Stratified$

    else if $0 < \beta < 1$ **then**

      $Flow\ regime \leftarrow Slug$

4.3 Validation of SETM

The Single Equation Two-phase mechanistic model developed in this study is validated against experimental pressure gradient data available in literature. Summary of experimental data for the validation exercise is given in tables (4.1-4.4). SETM is also compared with existing flow regime specific pressure gradient models, namely: slug model of Taitel and Barnea (1990), stratified model of Taitel and Dukler (1976b), and two-phase homogeneous model (Shoham, 2005).

Table 4.1 – Range of experimental data for validating SETM model: Asante (2000)

Source	No. of data [−]	Flow regime [−]	θ $[deg]$	D $[m]$
Asante (2000)	255	Stratified	0	$0.0254 - 0.0762$
Asante (2000)	243	Annular/Mist	0	$0.0254 - 0.0762$
Pressure: 101,325 Pa				
Temperature: 15 ^0C				
Fluid: oil/water/air				
U_{SG}: $5 - 30\ m{\cdot}s^{-1}$				
U_{SL}: $0.02 - 20\ m{\cdot}s^{-1}$				
ρ_G: $1.2\ m{\cdot}s^{-1}$				
ρ_L: $oil = 860\ Kg{\cdot}m^{-3}$				
ρ_L: $water = 999\ Kg{\cdot}m^{-3}$				
μ_G: $1.8e-5\ Pa{\cdot}s$				
μ_L: $oil = 0.001\ Pa{\cdot}s$				
μ_L: $water = 0.0065\ Pa{\cdot}s$				
Total	498			

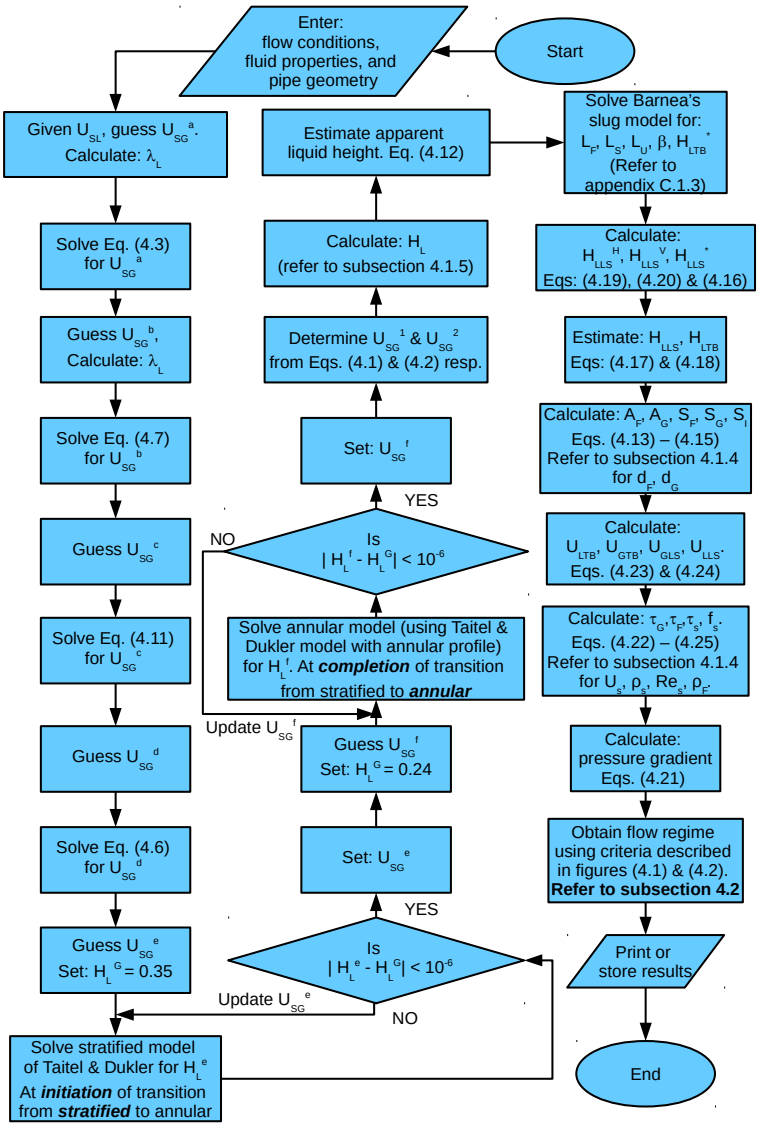

Figure 4.6 – Algorithm for Single Equation Two-Phase Mechanistic (SETM) model

Table 4.2 – Range of experimental data for validating SETM model: Marruaz et al. (2001)

Source	No. of data [–]	Flow regime [–]	θ [*degrees*]	D [m]
Marruaz et al. (2001)	15	Slug	0	0.150
Pressure: Up to 1,961,330 Pa				
Temperature: atmospheric				
Fluid: oil/water/gas				
U_{SG}: $0.45 - 1.6\ m{\cdot}s^{-1}$				
U_{SL}: $0.38 - 1.5\ m{\cdot}s^{-1}$				
Total	15			

Table 4.3 – Range of experimental data for validating SETM model: Hernandez (2007)

Source	No. of data [−]	Flow regime [−]	θ [deg]	D [m]
Hernandez (2007) Pressure: Up to $3,700,000\ Pa$ Temperature: 20 ^0C Fluid: water/air U_{SG}: $0.15 - 12.32\ m{\cdot}s^{-1}$ U_{SL}: $0.04 - 0.73\ m{\cdot}s^{-1}$ ρ_G: $1.224\ m{\cdot}s^{-1}$ ρ_L: $1000\ Kg{\cdot}m^{-3}$ μ_G: $1.8e-5\ Pa{\cdot}s$ μ_L: $0.001\ Pa{\cdot}s$	430	Slug	$0 - 90$	0.038
Total	430			

Table 4.4 – Range of experimental data for validating SETM model: Tullius (2000)

Source	No. of data [−]	Flow regime [−]	θ [$degrees$]	D [m]
Tullius (2000) Pressure: atmospheric Temperature: atmospheric Fluid: oil/water/air U_{SG}: $0 - 17\ m{\cdot}s^{-1}$ U_{SL}: $0.1 - 2.0\ m{\cdot}s^{-1}$	91	Slug	0	0.101
Total	91			

4.3.1 Criteria for evaluating performance of Single Equation Two-phase Mechanistic model

Criteria for evaluating present model is based on the following statistical parameters:

Average percentage error, ε_{ave}

$$\varepsilon_{ave} = \left(\frac{1}{n}\sum_{i=1}^{n}\epsilon_R\right)\times 100\% \tag{4.29}$$

where,

$$\epsilon_R = \frac{\left(-\frac{dP}{dL}\right)_C - \left(-\frac{dP}{dL}\right)_M}{\left(-\frac{dP}{dL}\right)_M} \tag{4.30}$$

Absolute average percentage error, ε_{abs}

$$\varepsilon_{abs} = \left(\frac{1}{n} \sum_{i=1}^{n} \mid \epsilon_R \mid \right) \times 100\% \tag{4.31}$$

Standard deviation of error, SD

$$SD = \sqrt{\frac{1}{n-1} \sum_{i=1}^{n} (100(\epsilon_R)_i - \varepsilon_{ave})^2} \tag{4.32}$$

4.4 Homogeneous model

Improved homogeneous two-phase pressure gradient model is provided in this section. First, description is given for the general homogeneous model (Wallis, 1969; Shoham, 2005). Thereafter, two modifications to homogeneous model developed in this study is presented. These two modifications are referred to as HM1 and HM2, and described in subsections (4.4.2) and (4.4.3) respectively.

4.4.1 General homogeneous pressure gradient model

Homogeneous two-phase pressure gradient model is generally described as:

$$-\frac{dP}{dL} = \frac{2 f_M U_M^2 \rho_M}{D} + \rho_M g \sin\theta \tag{4.33}$$

where mixture velocity is given in equation (4.34)

$$U_M = U_{SG} + U_{SL} \tag{4.34}$$

Mixture values of density (ρ_M) and viscosity (μ_M) are given as functions of liquid holdup (H_L) or no-slip liquid holdup (λ_L).

Unmodified homogeneous model: ρ_M and μ_M as functions of H_L

$$\rho_M = \rho_L H_L + \rho_G (1 - H_L) \tag{4.35}$$

$$\mu_M = \mu_L H_L + \mu_G (1 - H_L) \tag{4.36}$$

H_L is calculated using the method proposed by Choi et al. (2012), since it applies to a wide range of flow conditions.

Homogeneous no-slip model: ρ_M and μ_M as functions of λ_L

$$\rho_M = \rho_L \lambda_L + \rho_G (1 - \lambda_L) \tag{4.37}$$

$$\mu_M = \mu_L \lambda_L + \mu_G (1 - \lambda_L) \tag{4.38}$$

λ_L is no-slip liquid holdup, previously defined in equation (3.22).

Friction factor of mixture flow

Friction factor of mixture flow (f_M) is defined as Fanny fraction, and expressed in equation (4.39).

$$f_M = 0.001375 \left[1 + \left(2 \times 10^4 \frac{\varepsilon}{D} + \frac{10^6}{Re_M} \right)^{\frac{1}{3}} \right] \tag{4.39}$$

Reynold's number (Re_M) of mixture flow is given as:

$$Re_M = \frac{D \rho_M U_M}{\mu_M} \tag{4.40}$$

4.4.2 Modified homogeneous pressure gradient model: HM1

In order to obtain the first modification to general homogeneous two-phase pressure gradient model (HM1), equation (4.33) is modified using a correction factor as shown in equation (4.41). ε_{ave} is the average percentage error between predictions of equation (4.33) and experimental data. ε_{ave} is evaluated using a new model proposed in this study as shown in equation (4.42). Figure (4.7) shows distribution of computed data used in the derivation of correction factor given in equation (4.42).

$$-\frac{dP}{dL} = \left(\frac{100}{100 - \varepsilon_{ave}} \right) \left\{ \frac{2 f_M U_M^2 \rho_M}{D} \right\} + \rho_M g \sin\theta \tag{4.41}$$

$$\varepsilon_{ave} = \begin{cases} a_1 \exp(b_1 \lambda_L) & \cdots 0.10 \leq \lambda_L \leq 1.00 \\ \dfrac{a_2 + b_2 \lambda_L}{1 + c_2 \lambda_L + d_2 \lambda_L^2} & \cdots 0.00 \leq \lambda_L < 0.10 \end{cases} \tag{4.42}$$

The coefficients in equation (4.42) are provided in table (4.5), while table (4.6) shows values of correlation coefficient (R) and standard error. Equation (4.41) is further simplified to redefine friction factor and pressure gradient equations as shown in equations (4.43) and (4.44) respectively.

$$f_M^{mod} = \left(\frac{100}{100 - \varepsilon_{ave}} \right) 0.001375 \left[1 + \left(2 \times 10^4 \frac{\varepsilon}{D} + \frac{10^6}{Re_M} \right)^{\frac{1}{3}} \right] \tag{4.43}$$

$$-\frac{dP}{dL} = \frac{2 f_M^{mod} U_M^2 \rho_M}{D} + \rho_M g \sin\theta \tag{4.44}$$

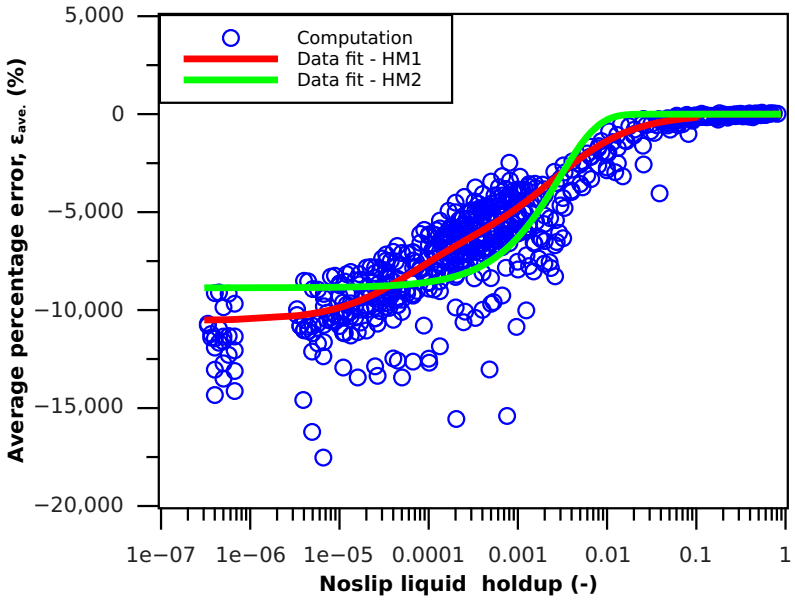

Figure 4.7 – Correction factor for homogeneous two-phase pressure gradient model. ε_{ave} is evaluated using data provided in table (4.5). Data fit model is given in equation (4.42)

Table 4.5 – Correction coefficients for modified homogeneous two-phase pressure gradient model (HM1)

Coefficient	Value
a_1	$-2.778243685916880E+02$
b_1	$-6.551397211784187E+00$
a_2	$-1.053000285683825E+04$
b_2	$-1.064005350210554E+08$
c_2	$+1.741049411519915E+04$
d_2	$+6.124170410581708E+06$

4.4.3 Modified homogeneous pressure gradient model: HM2

The second modification to general homogeneous two-phase pressure gradient model follows similar description given in subsection (4.4.2). Expression for ε_{ave} is given in equation (4.45). The coefficients in equation (4.45) are provided in table (4.7). Table (4.8) shows values of correlation coefficient (R) and standard error.

$$\varepsilon_{ave} = \begin{cases} a_1 \exp(b_1 \lambda_L) & \cdots 0.03 \leq \lambda_L \leq 1.00 \\ a_2 + b_2 \ln(\lambda_L) & \cdots 0.00 \leq \lambda_L < 0.03 \end{cases} \tag{4.45}$$

Table 4.6 – Modified homogeneous two-phase pressure gradient model (HM1): Correlation Coefficient (R) and Standard Error

ε_{ave}	R	Standard error
$a_1 \exp(b_1 \lambda_L)$	$9.581384190719511E-01$	$+1.48836755666E+01$
$\frac{a_2 + b_2 \lambda_L}{1 + c_2 \lambda_L + d_2 \lambda_L^2}$	$9.992737984288211E-01$	$+1.28701739059E+02$

Table 4.7 – Correction coefficients for modified homogeneous two-phase pressure gradient model (HM2)

Coefficient	Value
a_1	$-2.778243685916880E+02$
b_1	$-6.551397211784187E+00$
a_2	$+4.831787523606268E+03$
b_2	$+1.502663705145991E+03$

4.4.4 Validation of modified homogeneous pressure gradient model

The modified homogeneous two-phase pressure gradient model is validated against experimental data available in literature. Summary of experimental data for the validation exercise is provided in Table (4.9). Criteria for assessing the performance of the modified homogeneous two-phase model is based on descriptions provided in subsection (4.3.1); ϵ_R is replaced with $-\epsilon_R$ (this is for convenience only as ϵ_R can be applied in its original form).

Table 4.8 – Modified homogeneous two-phase pressure gradient model (HM2): Correlation Coefficient (R) and Standard Error

ε_{ave}	R	Standard error
$a_1 \exp(b_1 \lambda_L)$	$9.581384190719511E-01$	$+1.48836755666E+01$
$a_2 + b_2 \ln(\lambda_L)$	$9.661565471275946E-01$	$+8.74745455576E+02$

Table 4.9 – Range of experimental data for validating modified homogeneous pressure gradient model: Badie et al. (2000). Details of other data sources have been provided in previous tables.

Source	No. of data [−]	Flow regime [−]	θ [*degrees*]	D [*m*]
Badie et al. (2000) Pressure: atmospheric Temperature: 23.5 ^0C Fluid: water/air U_{SG}: $15-25\ m{\cdot}s^{-1}$ U_{SL}: $0.001-0.049\ m{\cdot}s^{-1}$	66	Stratified	0	0.078
Asante (2000)	255	Stratified	0	$0.0254-0.0762$
Asante (2000)	243	Annular/Mist	0	$0.0254-0.0762$
Hernandez (2007)	744	Slug	$0-90$	0.038
Marruaz et al. (2001)	15	Slug	0	0.150
Tullius (2000)	91	Slug	0	0.101
Total	1414			

4.5 Liquid holdup model

4.5.1 Modified liquid holdup model of Choi et al. (2012)

In this study, liquid holdup model (H_L^C) of Choi et al. (2012) is corrected for low liquid gas-liquid flow by using empirical correction as shown in equation (4.46); detailed description for determining H_L^C is given in appendix (C.2.1). The empirical correction factor is obtained by calculating prediction error of (H_L^C) compared with experimental data of Asante (2000). Solve equations (4.47) and (4.48) for ε_{ave} and λ_L respectively, for given experimental data (table (4.12)). ε_{ave} is correlated to λ_L as shown in equation (4.49). The coefficients in equation (4.49) are provided in table (4.10). Table (4.11) shows values of correlation coefficient (R) and standard error.

$$H_L = \left\{\frac{100}{100-\varepsilon_{ave}}\right\} H_L^C \tag{4.46}$$

$$\varepsilon_{ave} = \frac{H_L^C - H_L^{exp}}{H_L^{exp}} \times 100\% \tag{4.47}$$

$$\lambda_L = \frac{U_{SL}}{U_{SG}+U_{SL}} \tag{4.48}$$

$$\varepsilon_{ave} = \begin{cases} a_1 \exp\left(b_1 \lambda_L\right) & \cdots 2.0E-03 \leq \lambda_L \leq 1.0E+00 \\ \dfrac{a_2 + b_2 \lambda_L}{1 + c_2 \lambda_L + d_2 \lambda_L^2} & \cdots 7.0E-06 \leq \lambda_L < 2.0E-03 \\ a_3 \exp\left(b_3 \lambda_L\right) & \cdots 0.0E+00 \leq \lambda_L < 7.0E-06 \end{cases} \tag{4.49}$$

Table 4.10 – Correction coefficients for modified liquid holdup model of Choi et al. (2012)

Coefficient	Value
a_1	$-3.055467297247716E+02$
b_1	$-3.075717820024515E+02$
a_2	$-2.052325484821895E+04$
b_2	$-3.470903678437467E+08$
c_2	$+2.314348951146245E+05$
d_2	$+1.100855995240999E+09$

Application of empirical correction factor (given in equation (4.46)), to flow domain (i.e. flow rates, fluid properties, and pipe geometry) outside those of Asante (2000), must however be utilised with caution. Different flow domains would probably result in different liquid holdup predictions (Schlegel et al., 2012). In particular, the data of Asante is obtained for horizontal pipe flow and gas. Therefore, application of empirical correction factor to inclined or vertical pipe flow may result in erroneous predictions, due to different liquid-gas interactions.

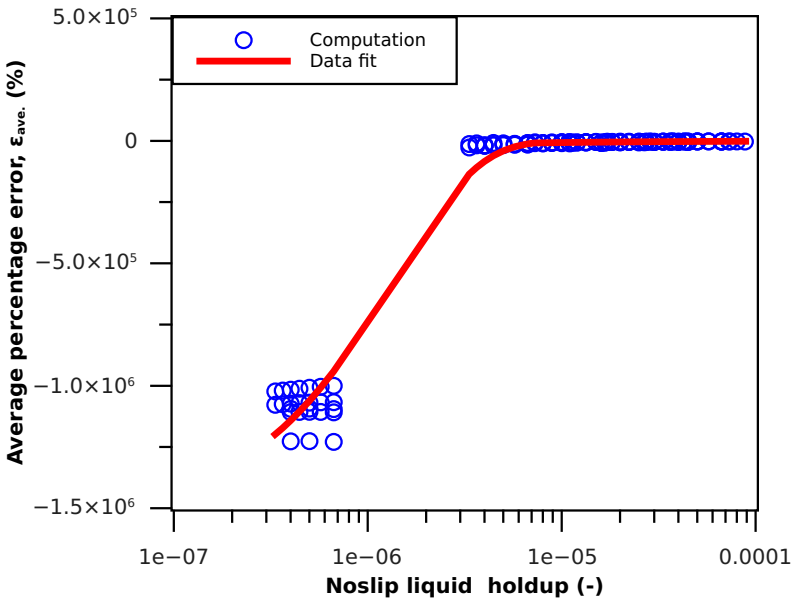

Figure 4.8 – Correction factor for homogeneous two-phase pressure gradient model. $\varepsilon_{ave.}$ is computed using data provided in table (4.10). Data fit model is given in equation (4.49)

Table 4.11 – Modified liquid holdup model of Choi et al. (2012): Correlation Coefficient (R) and Standard Error

ε_{ave}	R	Standard error
$a_1 \exp(b_1 \lambda_L)$	$8.795711532069198E-01$	$2.456391703471360E+01$
$\frac{a_2 + b_2 \lambda_L}{1 + c_2 \lambda_L + d_2 \lambda_L^2}$	$9.467168144650400E-01$	$5.948002306191545E+02$
$a_3 \exp(b_3 \lambda_L)$	$9.885666834839786E-01$	$8.104745391881585E+04$

4.5.2 Validation of modified liquid holdup model of Choi et al. (2012)

The modified H_L model of Choi et al. (2012) is validated against experimental data available in literature. Summary of experimental data for the validation exercise is provided in table (4.12). Criteria for assessing the performance of the modified homogeneous two-phase model is based on descriptions provided in subsection (4.4.4).

Table 4.12 – Range of experimental data for validating modified H_L model of Choi et al. (2012). Details of other data sources have been provided in previous tables.

Source	No. of data [−]	Flow regime [−]	θ [*degrees*]	D [m]
Asante (2000)	255	Stratified	0	0.0254 − 0.0762
Asante (2000)	243	Annular/Mist	0	0.0254 − 0.0762
Total	498			

4.6 Results

Results, obtained from the implementation of SETM and improved homogeneous models, are presented in this section. Subsection (4.6.1) compares results of SETM model with slug experimental data and slug model of Taitel and Barnea (1990). In subsection (4.6.2), SETM model is compared with stratified experimental data and stratified model of Taitel and Dukler (1976a). Subsection (4.6.3) compares SETM model with annular/mist experimental data and dispersed-bubble flow presented by Shoham (2005). Subsection (4.6.4) presents SETM's flow regime predictions at various inclination angles. Subsection (4.6.5) presents validation of the improved homogeneous two-phase pressure gradient. The last subsection (4.6.6) provides validation of the improved liquid holdup model of Choi et al. (2012).

4.6.1 Validation of SETM: slug flow data

Pressure gradient

Figure (4.9) shows a plot of pressure gradient predictions compared against slug flow experimental data. The predictions are obtained for present model and slug model of Taitel and Barnea (1990). For brevity, slug model of Taitel and Barnea (1990) is represented as TBS. Performance evaluation of present model shows average percentage error of 8.44%, absolute average percentage error of 16.51%, and standard deviation of error as 0.8. In comparison with present model, the magnitude (21.09%) of the average percentage error (−21.09%) of TBS is higher than the corresponding value (8.44%) for present model. Further, TBS shows higher values for absolute average percentage error and standard deviation of error at 24.63% and 0.9 respectively.

Figure (4.10) gives the plot of average percentage error of the predictions present

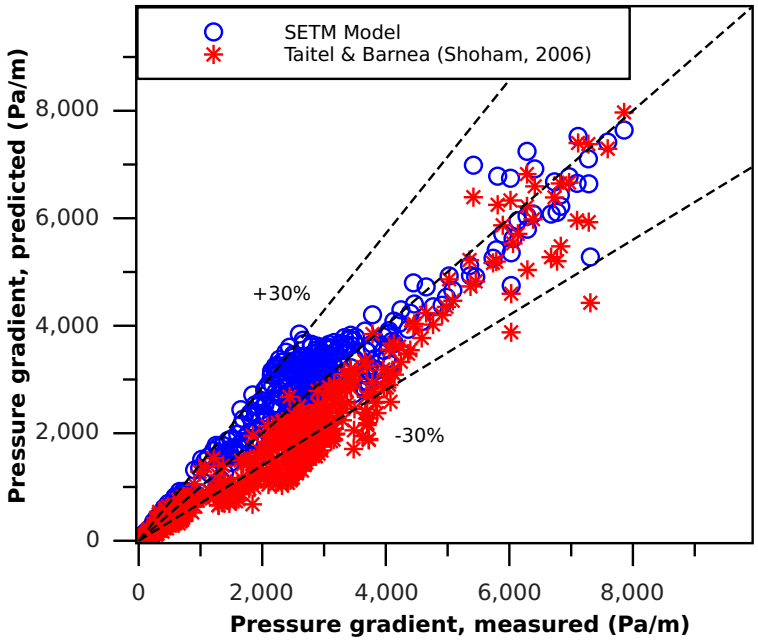

Figure 4.9 – Validation of SETM for slug flow

model and TBS, versus pipe inclination. The plot of ε_{ave} for TBS is a negative trend. The plot of ε_{ave} for present model is, however, a positive trend. Figure (4.11) shows the plot of absolute average percentage error of the predictions of present model and TBS, versus pipe inclination. Corresponding plots for standard deviation are given in figure (4.12). It is evident that the predictions of present model are better, than those of TBS, for all pipe inclination angles except at 0^0 and 90^0.

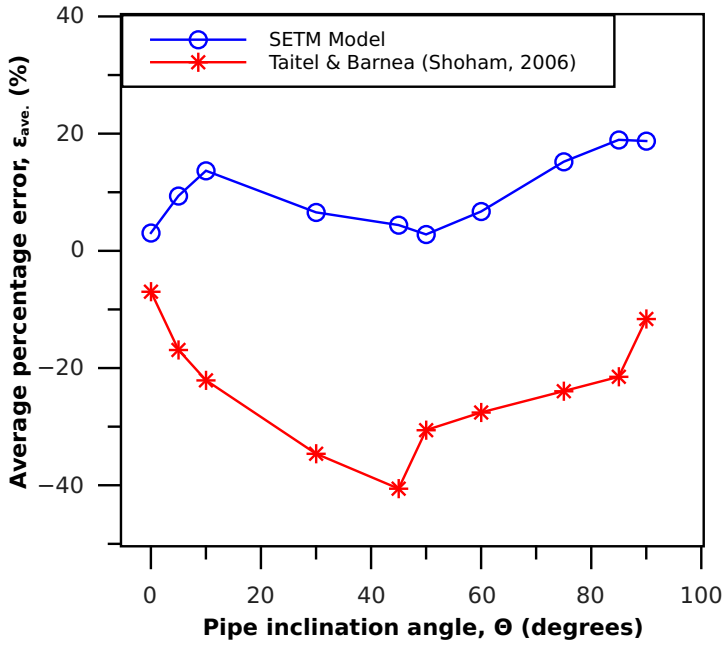

Figure 4.10 – Validation of SETM for slug flow: average percentage error, ε_{ave}

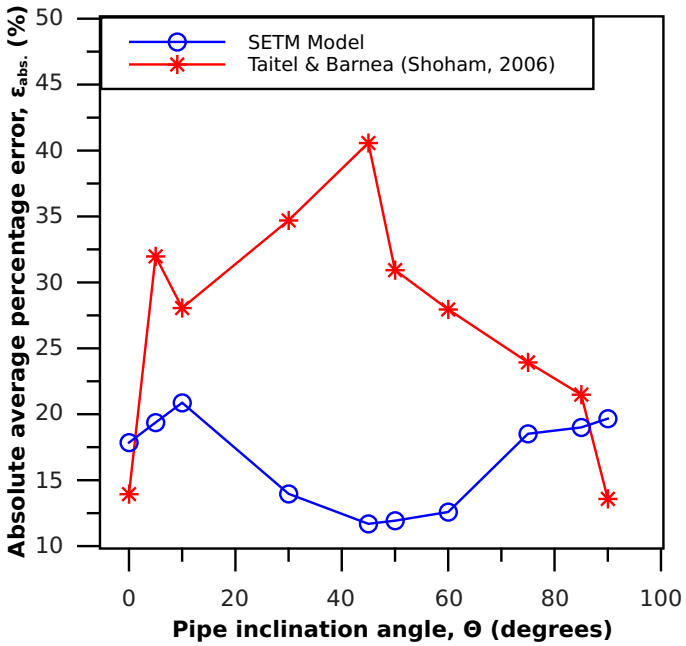

Figure 4.11 – Validation of SETM for slug flow: absolute average percentage error, ε_{abs}

Flow regime

SETM's flow regime predictions for slug data are presented in figure (4.13). The results show that 471 out of 536 data points are identified as slug, the remaining

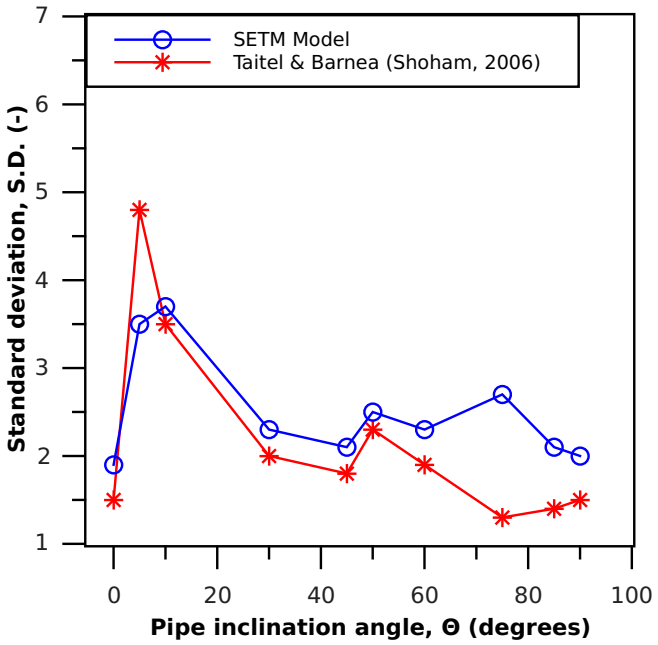

Figure 4.12 – Validation of SETM for slug flow: standard deviation, SD

2, 51 and 12 data points are identified as stratified, dispersed-bubble and transition flow respectively.

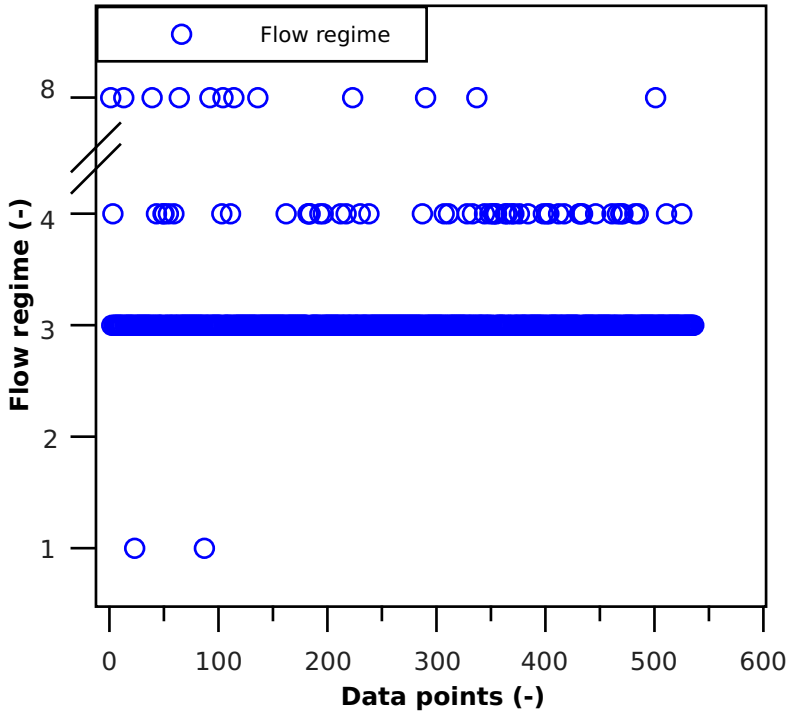

Figure 4.13 – SETM Flow regime for Slug. Flow regime designation: 1 = Stratified, 2 = Annular, 3 = Slug, 4 = Dispersed-bubble, 8 = Transition.

Liquid holdup in film region

Figure (4.14) shows SETM's predictions for liquid holdup in film region of slug unit. The results show that for the total 536 slug data points, the ratio of film zone liquid holdup (H_{LTB}) to slug unit liquid holdup (H_L) is less than unity.

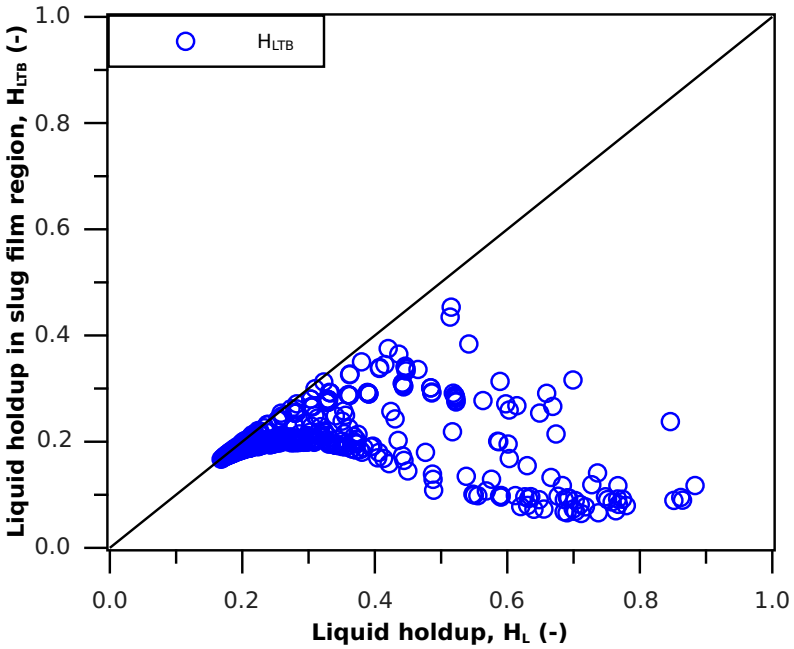

Figure 4.14 – SETM Slug: H_{LTB} against H_L

Apparent liquid height

Figure (4.15) provides SETM's predictions for dimensionless apparent liquid height. The figure shows that the ratio of dimensionless apparent liquid height (X/D) to dimensionless liquid height (h_L/D) is approximately unity for all 536 slug data examined.

Ratio of slug regions

SETM's predictions for length ratio of slug regions (β) are presented in figure (4.16). The results show that β is a scatter distribution within $0<\beta<1$.

4.6.2 Validation of SETM: stratified flow data

Pressure gradient

In tables (4.1-4.4), flow regime data classified as annular/mist flow are categorised as dispersed mist flow in the original work of Asante (2000). Therefore, homogeneous

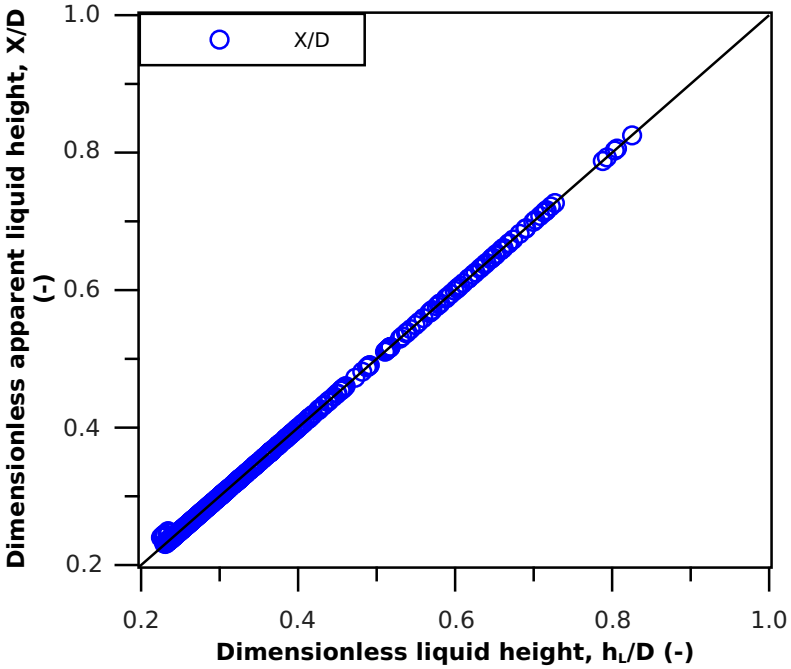

Figure 4.15 – SETM Slug: X/D against h_L/D

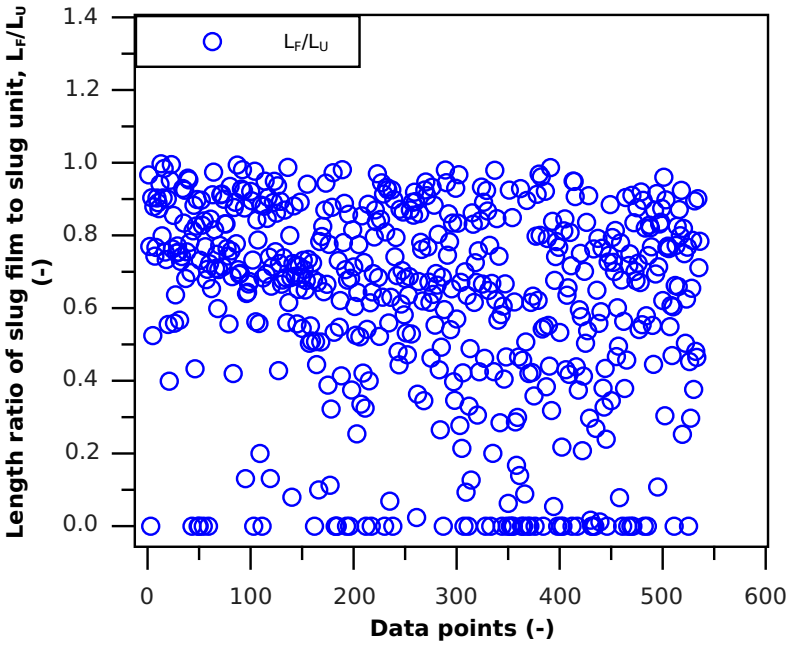

Figure 4.16 – SETM Slug: $\beta = L_F/L_U$

pressure gradient model, based on the study of Wallis (1969), is used for comparing SETM model. For brevity, homogeneous pressure gradient model is referred to as HPG.

Figure (4.17) shows a plot of present model's pressure gradient prediction compared against stratified flow experimental data. The figure also compares stratified pressure gradient model of Taitel and Dukler (1976b) with present model. For brevity, stratified pressure gradient model of Taitel and Dukler is referred to as SPG. Performance evaluation of present model shows average percentage error of -25.30%, absolute average percentage error of 26.00%, and standard deviation of error as 1.2. In comparison with present model, SPG gives higher values for average percentage error, absolute average percentage error, and standard deviation of error at 34.71%, 44.46%, and 2.3 respectively; the results show that the average value SPG predictions is higher than corresponding value for stratified experimental data, demonstrated by $\varepsilon_{ave} = 34.71\%$. The scatter ($\pm$ error values) distribution of SPG results in $\varepsilon_{abs} > \varepsilon_{ave}$, with SPG standard deviation 2.3. At $H_L < 0.05$, mean value of ε_{ave} is -21.333%, while at invalid range, $H_L > 0.05$, mean value of ε_{ave} is -47.24%.

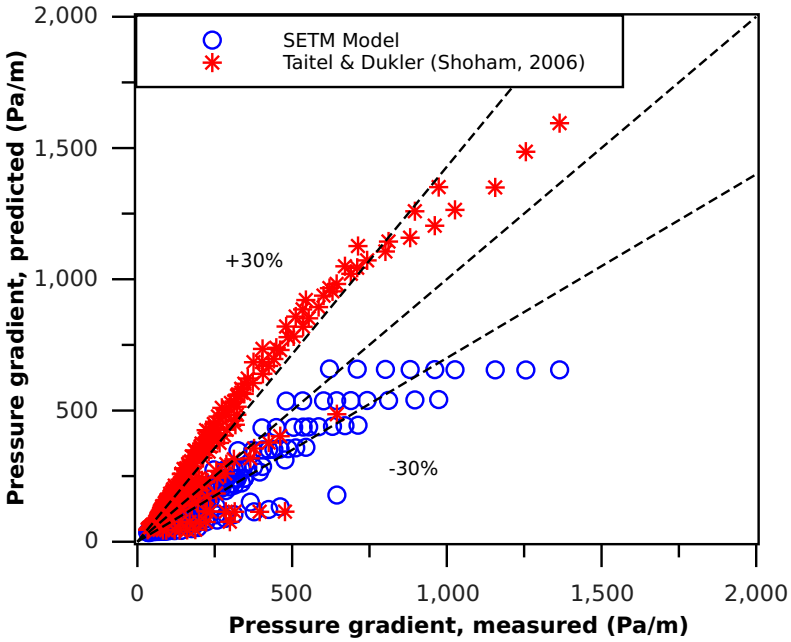

Figure 4.17 – Validation of SETM for stratified flow

Flow regime

SETM's flow regime predictions for stratified data are shown in figure (4.18). The figure shows that all 255 stratified data points are identified as transition flow.

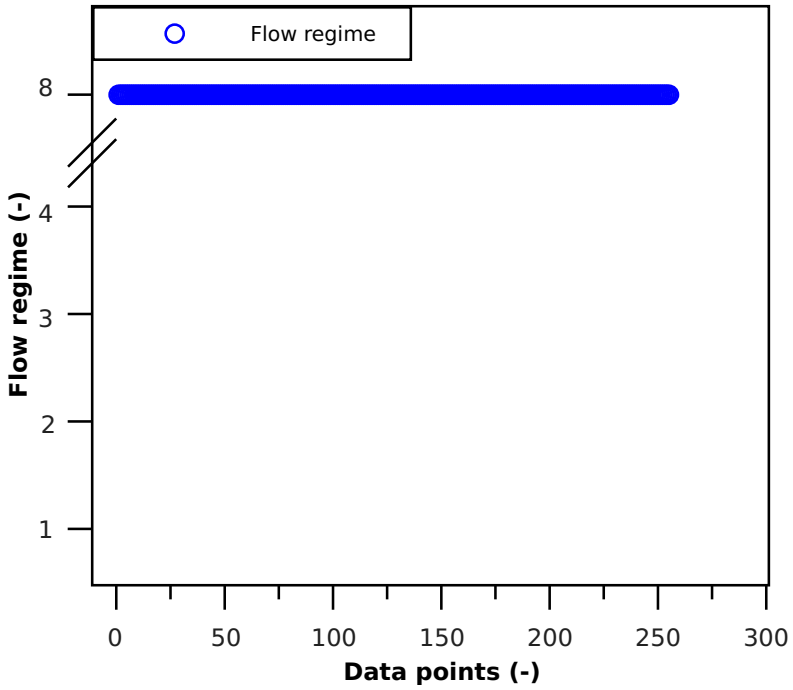

Figure 4.18 – SETM Flow regime for Stratified. Flow regime designation: 1 = Stratified, 2 = Annular, 3 = Slug, 4 = Dispersed-bubble, 8 = Transition.

Liquid holdup in film region

Figure (4.19) gives SETM's predictions for liquid holdup in film region of slug unit. The results show that for the total 255 stratified data points, the ratio of film zone liquid holdup (H_{LTB}) to slug unit liquid holdup (H_L) is approximately unity.

Apparent liquid height

Figure (4.20) shows SETM's predictions for dimensionless apparent liquid height. The results show that the ratio of dimensionless apparent liquid height (X/D) to dimensionless liquid height (h_L/D) is greater than unity for all 255 stratified data.

Ratio of slug regions

SETM's predictions for length ratio of slug regions (β) are presented in figure (4.21). The figure shows that β is approximately unity for all 255 stratified data points.

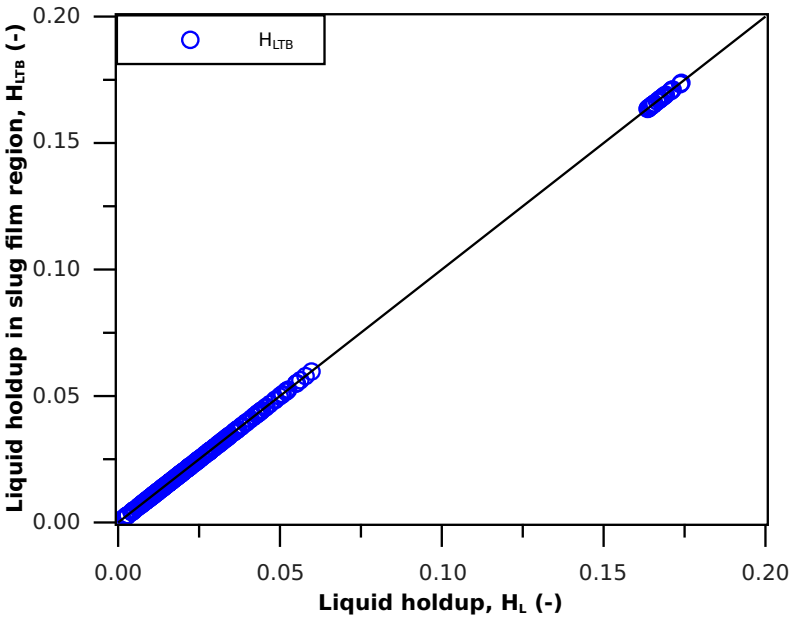

Figure 4.19 – SETM Stratified: H_{LTB} against H_L

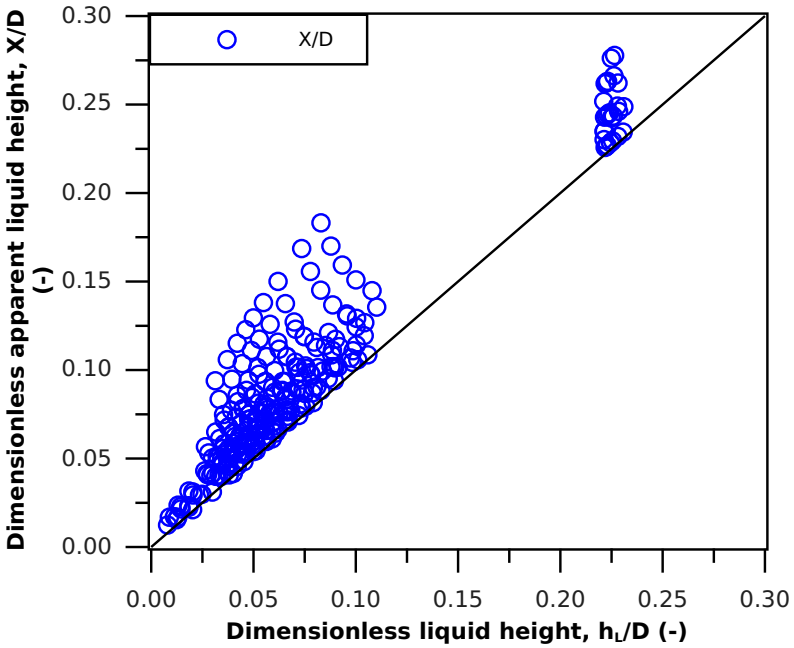

Figure 4.20 – SETM Stratified: X/D against h_L/D

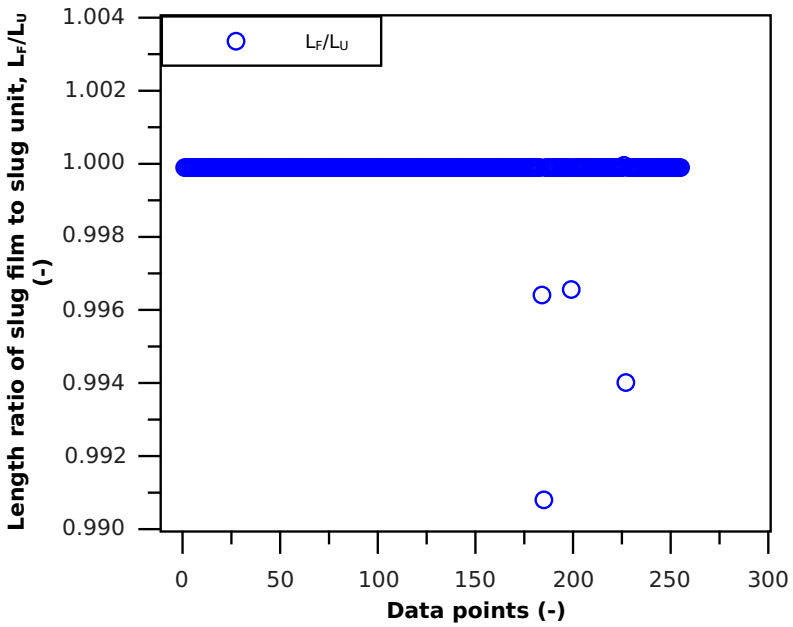

Figure 4.21 – SETM Stratified: $\beta = L_F/L_U$

4.6.3 Validation of SETM: annular/mist flow data

Pressure gradient

Figure (4.22) presents a plot of pressure gradient predictions compared against annular/mist flow experimental data. The predictions are obtained for present model and HPG. Performance evaluation of present model shows average percentage error of -1.63%, absolute average percentage error of 24.60%, and standard deviation of error as 2.0. When compared with present model, HPG gives approximately same value for ε_{ave} $(= -1.62\%)$, but lower values for ε_{abs} $(= 15.37\%)$ and SD $(= 1.4)$. There are two distributions in the scatter plot. The first distribution $(D1)$ occurs when $\varepsilon_{ave} > -30\%$ and $H_L < 0.05$; the observed H_L is within valid range specified by Hart et al. (1989). The second distribution $(D2)$, however, exists when $\varepsilon_{ave} < -30\%$, and for invalid liquid holdup range $H_L > 0.05$. It is further observed that mean values of ε_{ave} for $D1$ and $D2$ are 5.47% and -54.04% respectively. Thus the higher values of ε_{abs} and SD for present model.

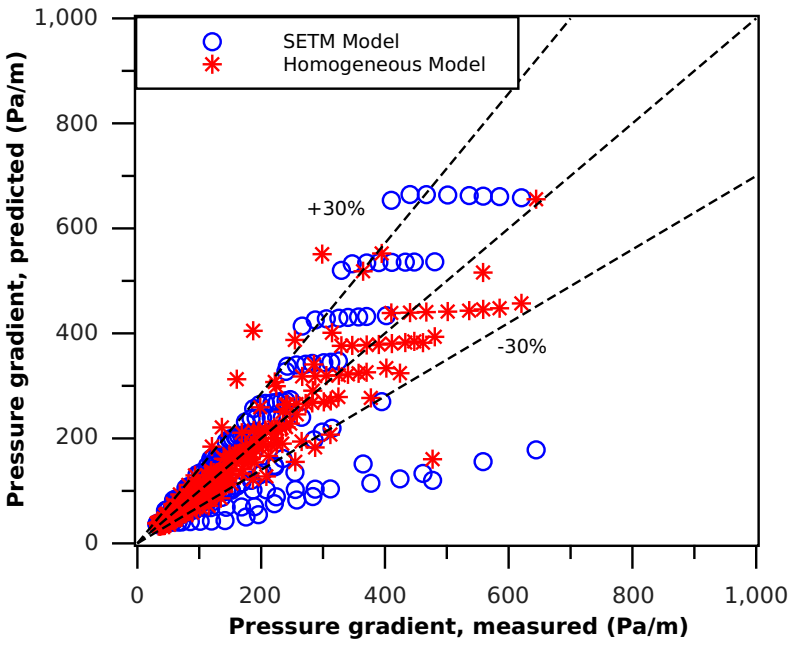

Figure 4.22 – Validation of SETM for annular/mist flow

Flow regime

Figure (4.23) shows SETM's flow regime predictions for annular/mist data. The results show that 240 out of 243 data points are identified as transition flow. The remaining 3 data points are identified as stratified.

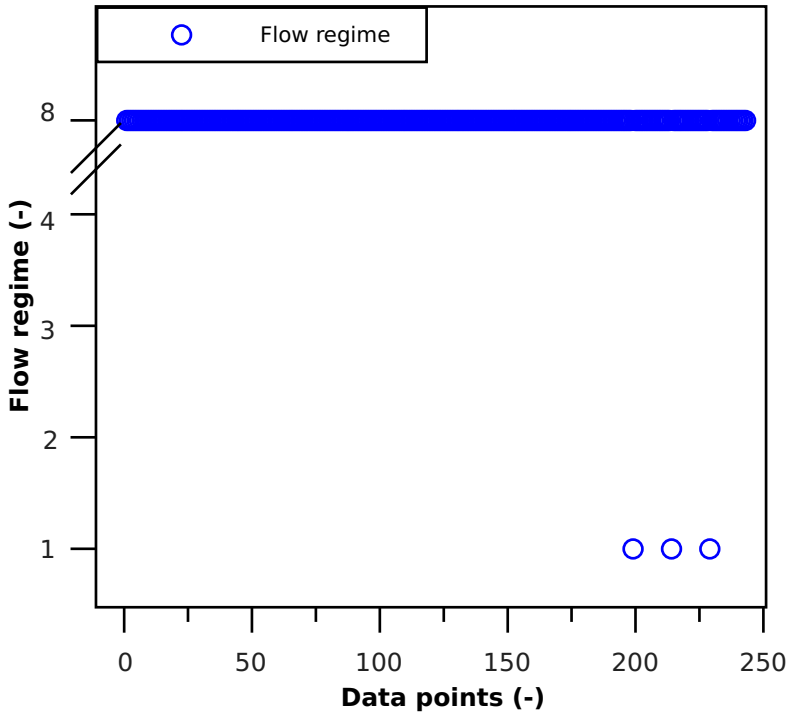

Figure 4.23 – SETM Flow regime for Annular/Mist data. Flow regime designation: 1 = Stratified, 2 = Annular, 3 = Slug, 4 = Dispersed-bubble, 8 = Transition.

Liquid holdup in film region

In figure (4.24), SETM's predictions for liquid holdup in film region of slug unit are presented. The figure shows that for the total 243 annular/mist data points, the ratio of film zone liquid holdup (H_{LTB}) to slug unit liquid holdup (H_L) is approximately unity.

Apparent liquid height

Figure (4.25) presents SETM's predictions for dimensionless apparent liquid height. The figure shows that the ratio of dimensionless apparent liquid height (X/D) to dimensionless liquid height (h_L/D) is greater than unity for all 243 annular/mist data.

Ratio of slug regions

Figure (4.26) gives SETM's predictions for length ratio of slug regions (β). The results show that β is approximately unity for all 243 annular/mist data points.

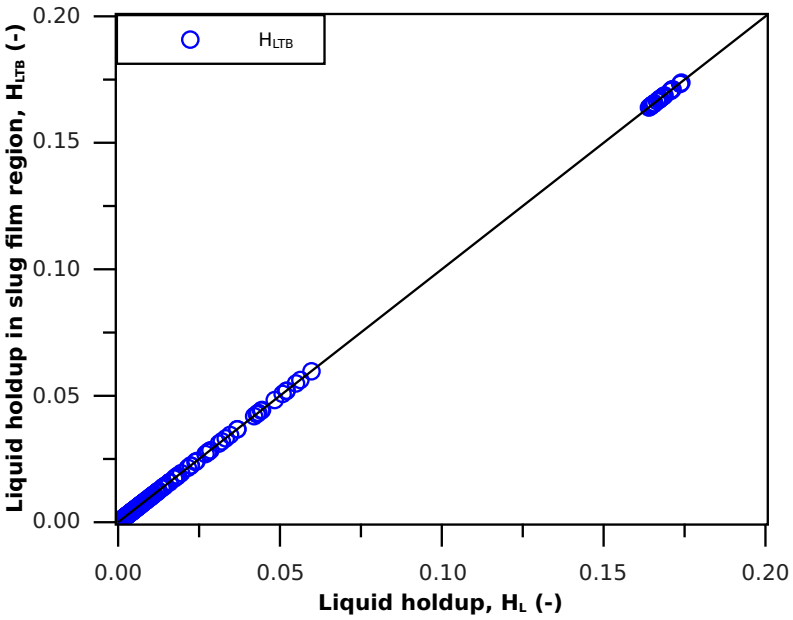

Figure 4.24 – SETM Annular/Mist: H_{LTB} against H_L

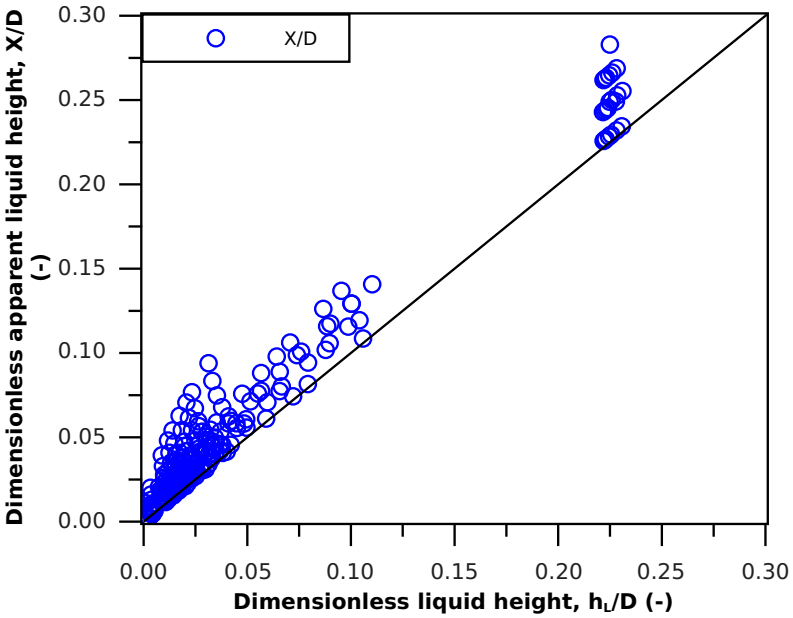

Figure 4.25 – SETM Annular/Mist: X/D against h_L/D

4.6.4 SETM flow regime predictions

Flow regime predictions by the Single Equation Two-Phase Mechanistic (SETM) model is presented in this subsection. The effect of pipe inclination angle on SETM's flow regime map is provided.

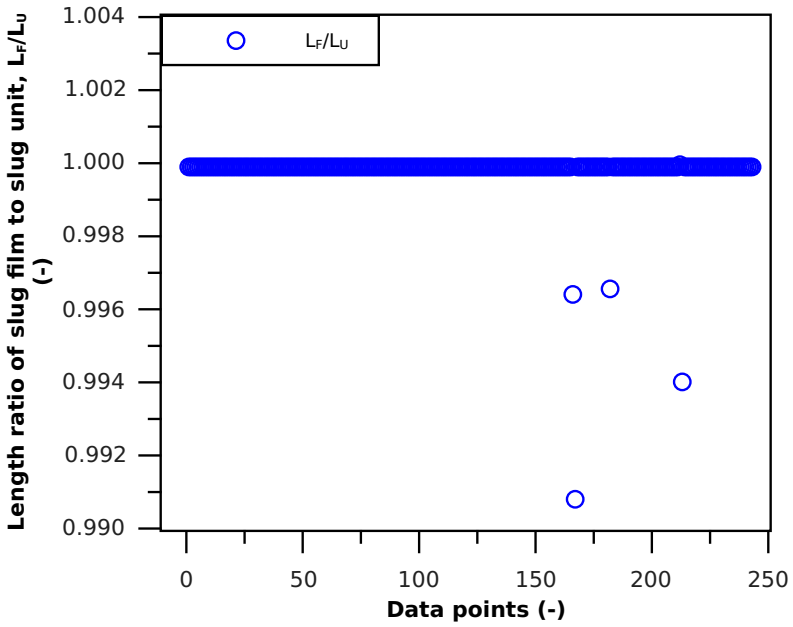

Figure 4.26 – SETM Annular/Mist: $\beta = L_F/L_U$

Effect of inclination angle on SETM's Flow regime predictions

SETM flow regime is evaluated for air-water flow system (refer to table (4.14) for summary of test set-up). SETM flow regime results are presented in figure (4.27).

The results show that at θ=0^0, five flow regimes are identified, namely: stratified, annular, slug, dispersed-bubble, and transition. Stratified flow is observed to occur in the range: $0.0 \leq U_{SG} \leq 9.2$ $[m/s]$, but below $U_{SL} = 0.15$ $[m/s]$. At $U_{SL} < 0.9$ $[m/s]$, annular flow occurs approximately at $U_{SG} \geq 125.2$ $[m/s]$; while transition zone occurs within the range: $9.2 \leq U_{SG} \leq 125.2$ $[m/s]$. At $U_{SL} \geq 0.9$ $[m/s]$, transition zone progressively decrease to a thin strip with $slope = 0.488$. At $U_{SL} > 21.0$ $[m/s]$, line of complete transition to annular also has a $slope = 0.488$. Line of transition from slug to dispersed-bubble starts at $(U_{SG}, U_{SL}) = (0.0017, 0.001)$ $[m/s]$ and ends at $(U_{SG}, U_{SL}) = (76.9, 103.3)$ $[m/s]$.

Figure (4.27) further shows that at $\theta > 0^0$, stratified zone does not exist. At $\theta > 0^0$, line of complete transition to annular flow (at $U_{SL} < 21.0$), occurs at progressively lower U_{SG} (refer to table (4.13)) when compared with $\theta = 0^0$. Examination of transition zone at $\theta > 0^0$ shows that the zone's range (in $log_{10}U_{SG}$) decrease from $(125.2 - 9.1 = 116.2)$ to $(91.9 - 26.4 = 65.5)$, corresponding to increase in θ from 0^0 to 90^0. At $U_{SL} > 21.0$ $[m/s]$, transition zone reduces to a strip at $\theta > 0^0$ as for $\theta = 0^0$. However, the *slope* reduces from 0.488 to 0.326 corresponding to increase

Table 4.13 – Effect of θ on SETM's Flow regime. Superscript: S = Start, E = End

Inclination angle $[deg]$	Transition to annular $[m/s]$	Transition zone $[m/s]$	*slope* $[-]$	Transition to dispersed-bubble $[m/s]$
0	125.2	$9.0 \leq U_{SG} \leq 125.2$	0.488	U_{SG}^S : 0.0017 U_{SG}^E : 76.9 U_{SL}^S : 0.001 U_{SL}^E : 100.0
5	121.2	$9.1 \leq U_{SG} \leq 121.2$	0.439	U_{SG}^S : 0.014 U_{SG}^E : 82.1 U_{SL}^S : 0.001 U_{SL}^E : 100.0
10	106.7	$12.8 \leq U_{SG} \leq 106.7$	0.376	U_{SG}^S : 0.03 U_{SG}^E : 87.8 U_{SL}^S : 0.001 U_{SL}^E : 100.0
45	105.9	$21.6 \leq U_{SG} \leq 105.9$	0.326	U_{SG}^S : 0.154 U_{SG}^E : 119.1 U_{SL}^S : 0.001 U_{SL}^E : 100.0
60	91.9	$26.0 \leq U_{SG} \leq 91.9$	0.367	U_{SG}^S : 0.183 U_{SG}^E : 142.0 U_{SL}^S : 0.001 U_{SL}^E : 100.0
90	76.7	$26.4 \leq U_{SG} \leq 76.7$	0.370	U_{SG}^S : 0.183 U_{SG}^E : 142.0 U_{SL}^S : 0.001 U_{SL}^E : 100.0

in θ from 0^0 to 45^0. Further increase in θ shows that the *slope* increases to a final value of 0.370 at $\theta = 90^0$. Line of transition from slug to dispersed-bubble moves from $[(U_{SG}^S, U_{SG}^E) = (0.0017, 76.9)]$ to $[(U_{SG}^S, U_{SG}^E) = (0.216, 142.0)]$ for a corresponding increase in θ from 0^0 to 90^0.

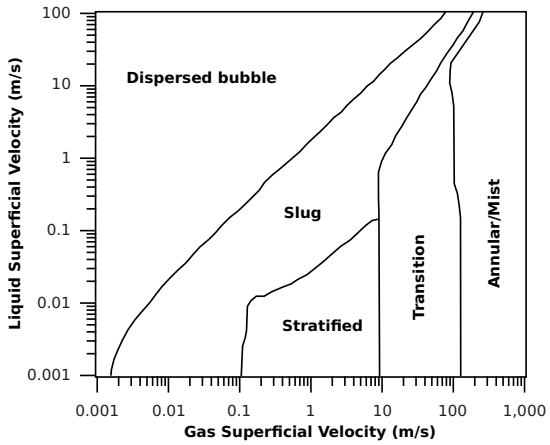

(a) $\theta = 0^0$

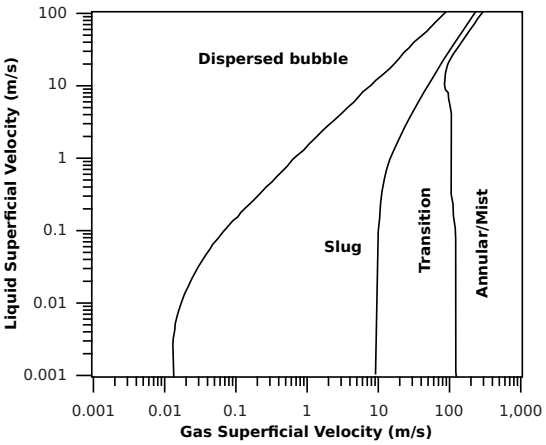

(b) $\theta = 5^0$

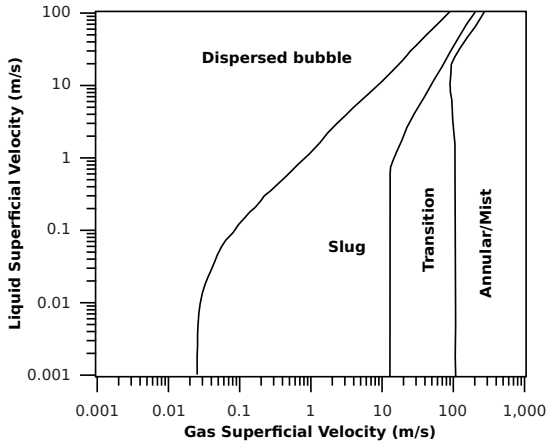

(c) $\theta = 10^0$

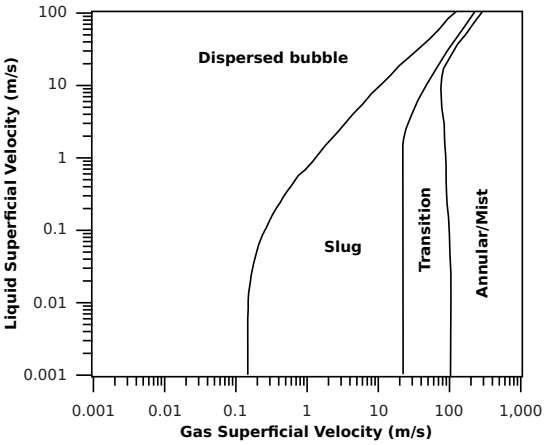

(d) $\theta = 45^0$

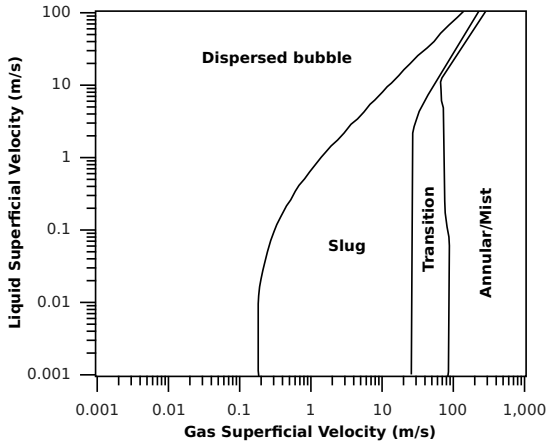

(e) $\theta = 60^0$

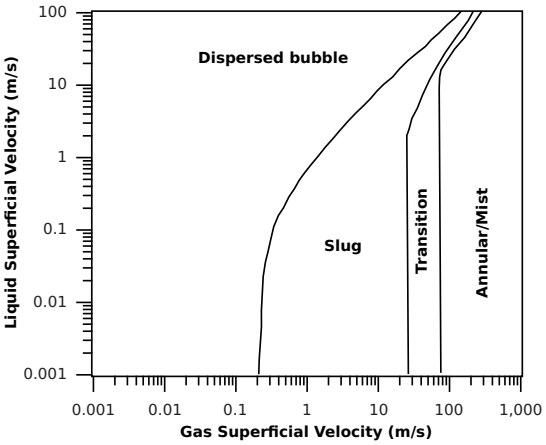

(f) $\theta = 90^0$

Figure 4.27 – Effect of inclination angle on SETM's Flow regime predictions

Table 4.14 – Effect of inclination angle on SETM's Flow regime

Fluid system	Air-Water
Pressure $[Pa]$	$1.01325E+05$
Temperature $[K]$	298.15
Diameter $[m]$	0.0779

4.6.5 Validation of the modified homogeneous pressure gradient model

Slug data

Figures (4.28), (4.29), (4.30), and (4.31), in respective order, show plots of pressure gradient by unmodified homogeneous, homogeneous noslip, HM1 and HM2 models, compared with slug flow experimental data. Analysis of the results gives average percentage error for unmodified homogeneous and homogeneous models as 206.98% and -44.42% respectively, the corresponding values of absolute average percentage error are 217.18% and 62.35% respectively. Standard deviation of error for unmodified homogeneous and homogeneous no-slip models are 18.5% and 2.43% respectively. In comparison with the unmodified homogeneous and homogeneous no-slip models, the average percentage error of HM1 and HM2 models are 5.83% and 6.07% respectively. Corresponding values of absolute average percentage error for HM1 and HM2 models are lower at 33.99% and 35.13% respectively. Similar comparison shows that standard deviation of error for HM1 and HM2 models are 3.3 and 3.6 respectively.

Stratified data

Scatter plots of stratified flow experimental data compared with predictions of unmodified homogeneous, homogeneous no-slip, HM1 and HM2 models are presented in figures (4.32), (4.33), (4.34), and (4.35) respectively. Analysis of the results shows average percentage error for unmodified homogeneous and homogeneous models are $6,552.79\%$ and 367.56% respectively, while values of absolute average percentage errors are $6,522.79\%$ and 375.28% respectively. Standard deviation of error for unmodified homogeneous and homogeneous no-slip models are 142.7 and 40.57 respectively. When compared with the unmodified homogeneous and homogeneous no-slip models, the average percentage error of HM1 and HM2 models are 15.22% and -4.03% respectively. Corresponding evaluations of absolute average percentage error for HM1 and HM2 models give 26.37% and 21.68% respectively. Similar comparison gives standard deviation of error for HM1 and HM2 models as 2.0 and 1.6

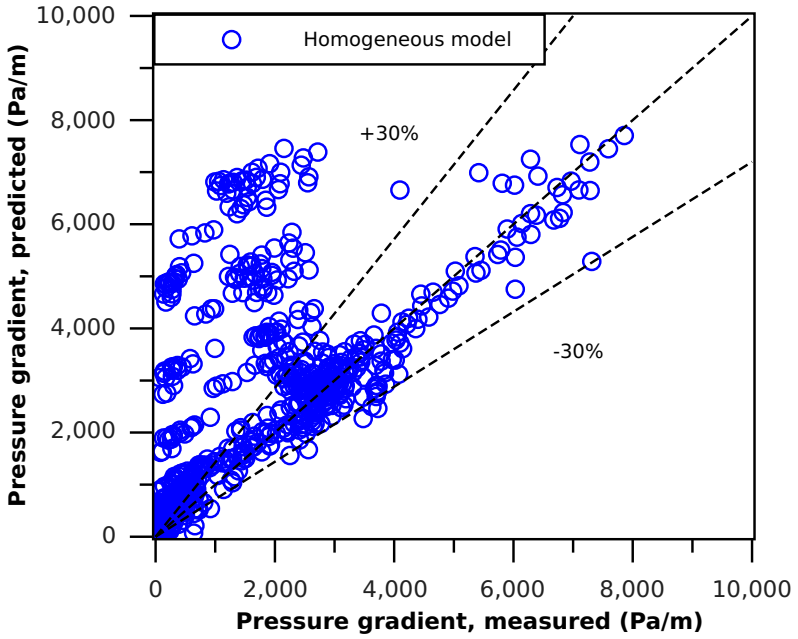

Figure 4.28 – Homogeneous pressure gradient model: Slug data

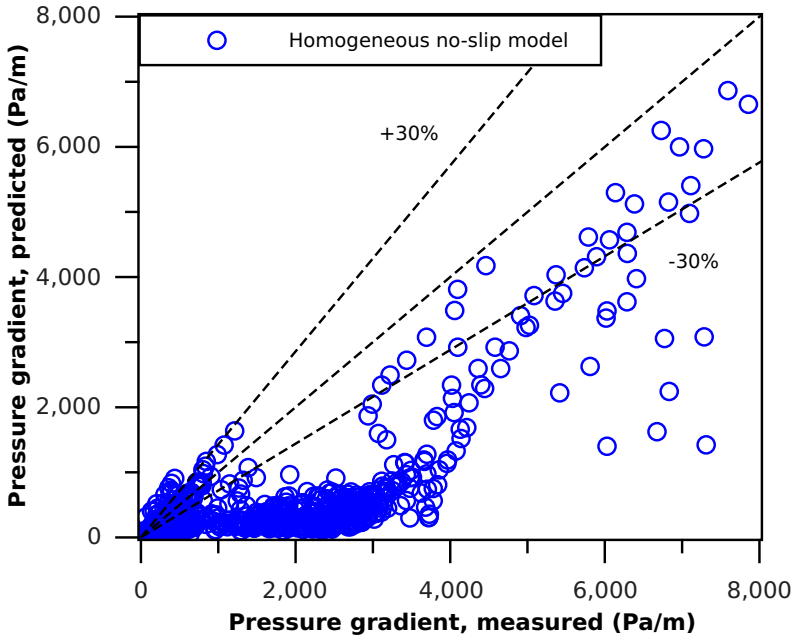

Figure 4.29 – Homogeneous no-slip pressure gradient model: Slug data

respectively.

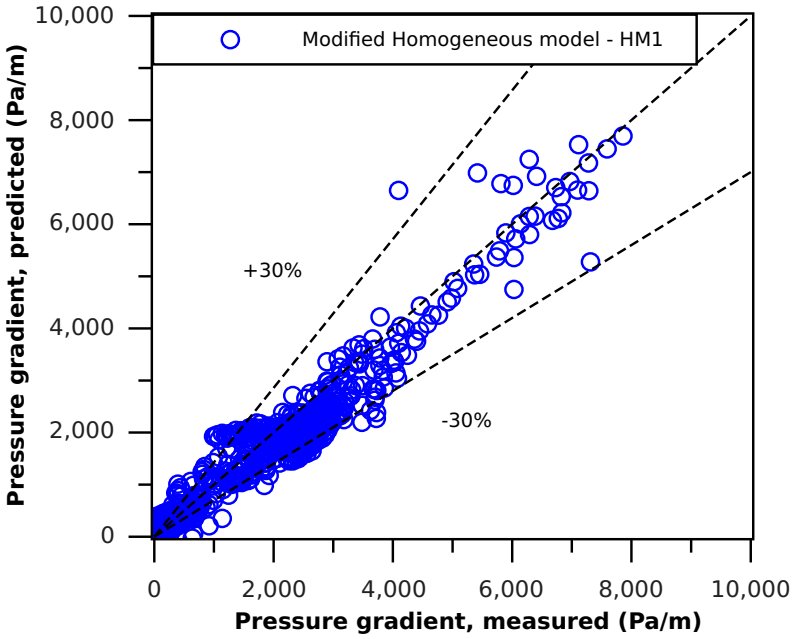

Figure 4.30 – Modified homogeneous pressure gradient model HM1: Slug data

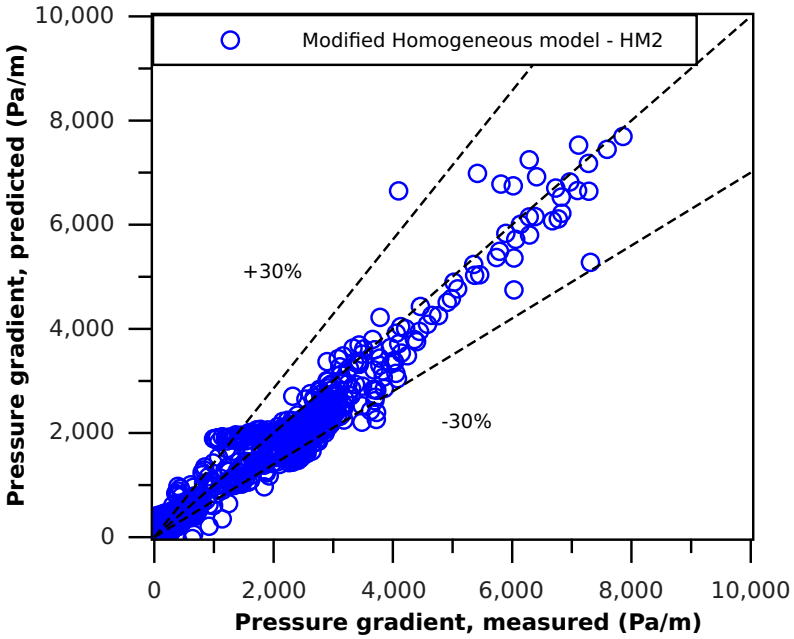

Figure 4.31 – Modified homogeneous pressure gradient model HM2: Slug data

Annular/Mist data

Figures (4.36), (4.37), (4.38), and (4.39) show scatter pressure gradient plots of annular/mist flow experimental data compared with the predictions of unmodified homogeneous, homogeneous no-slip, HM1 and HM2 models respectively. Analy-

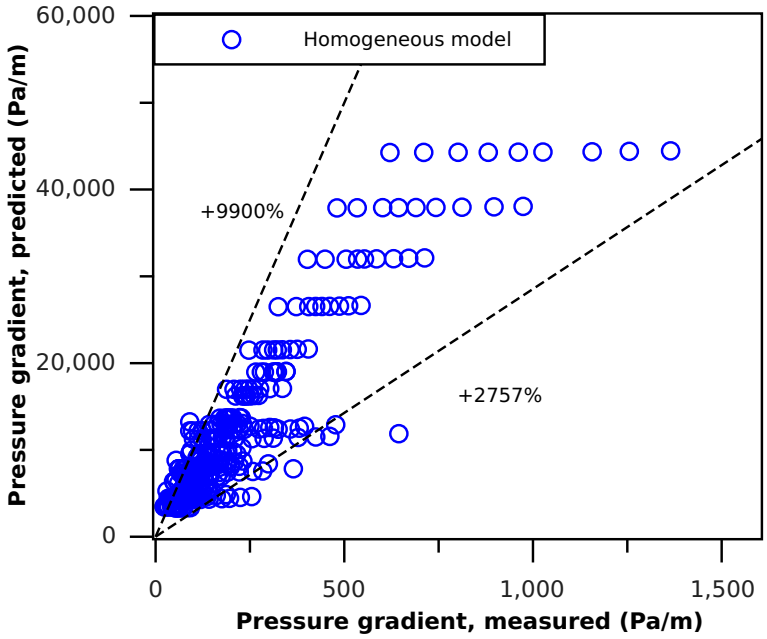

Figure 4.32 – Homogeneous pressure gradient model: Stratified data

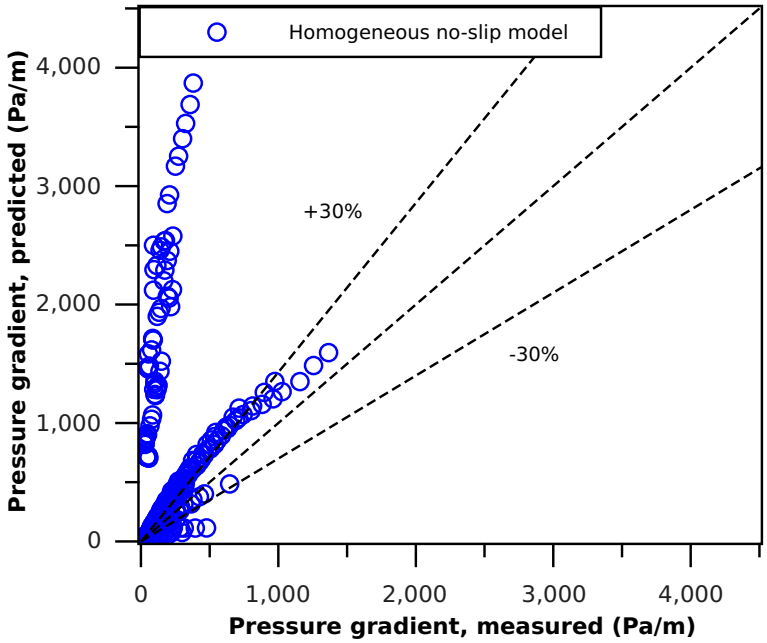

Figure 4.33 – Homogeneous no-slip pressure gradient model: Stratified data

sis of the results shows that average percentage error for unmodified homogeneous and homogeneous no-slip models are $8,422.91\%$ and -1.62% respectively, with corresponding values of absolute average percentage error are $8,422.91\%$ and 15.37% respectively. Standard deviation of error for unmodified homogeneous and homogeneous no-slip models are 177.7 and 1.36 respectively. In comparison with the

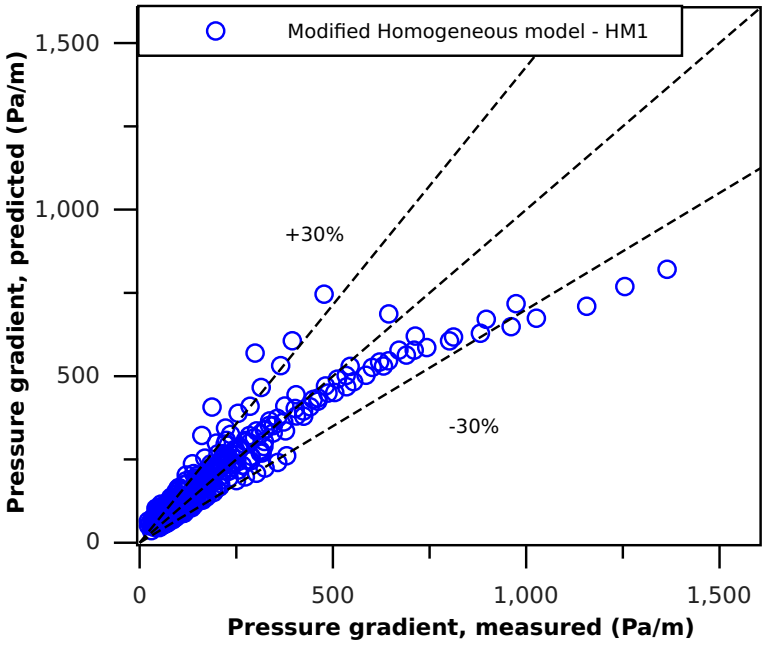

Figure 4.34 – Modified homogeneous pressure gradient model HM1: Stratified data

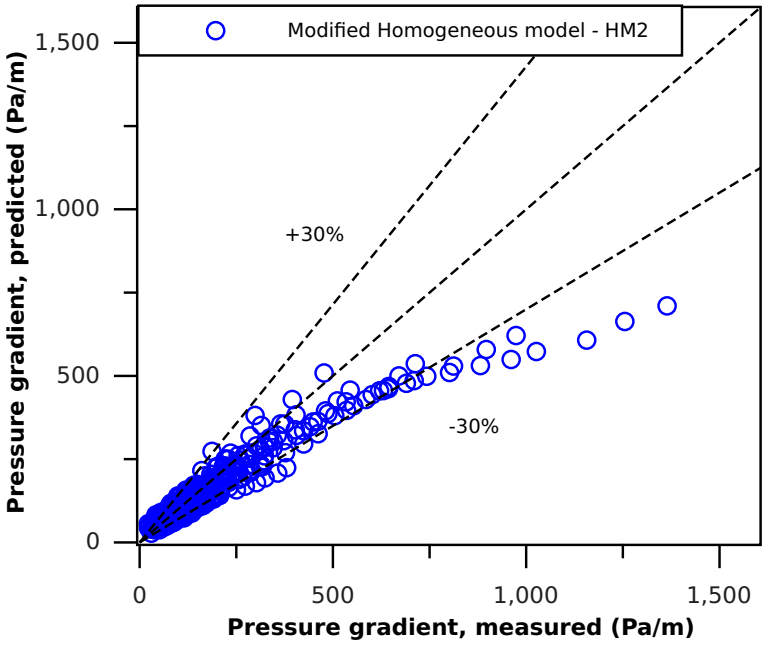

Figure 4.35 – Modified homogeneous pressure gradient model HM2: Stratified data

unmodified homogeneous and homogeneous no-slip models, the average percentage error of HM1 and HM2 models are 11.63% and −11.91% respectively. Values of absolute average percentage error for HM1 and HM2 models are 18.41% and 20.87% respectively. Also, standard deviation of error for HM1 and HM2 models are 1.6 and 1.3 respectively

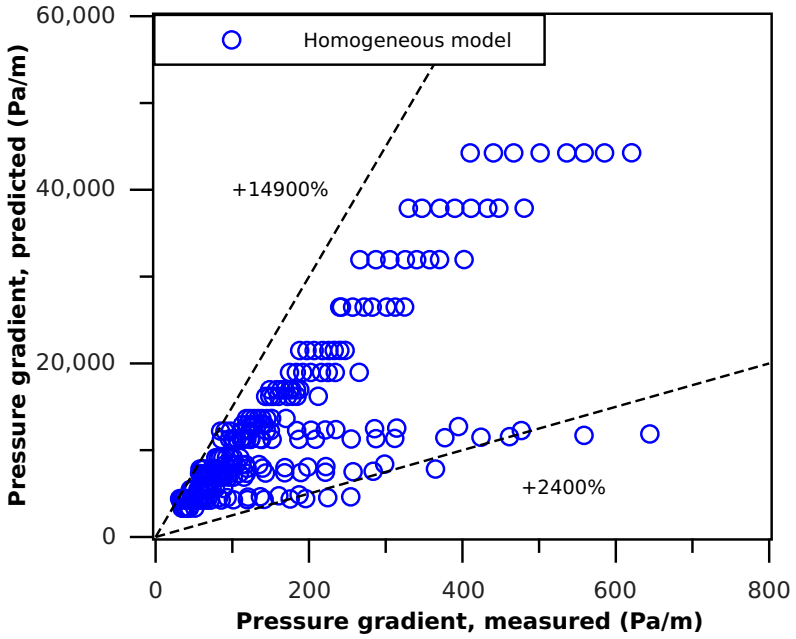

Figure 4.36 – Homogeneous pressure gradient model: Annular/Mist data

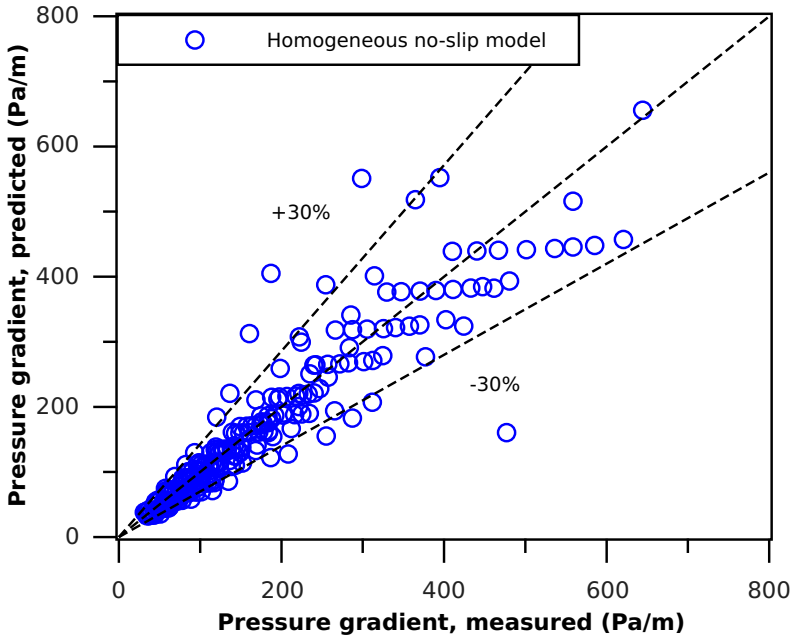

Figure 4.37 – Homogeneous no-slip pressure gradient model: Annular/Mist data

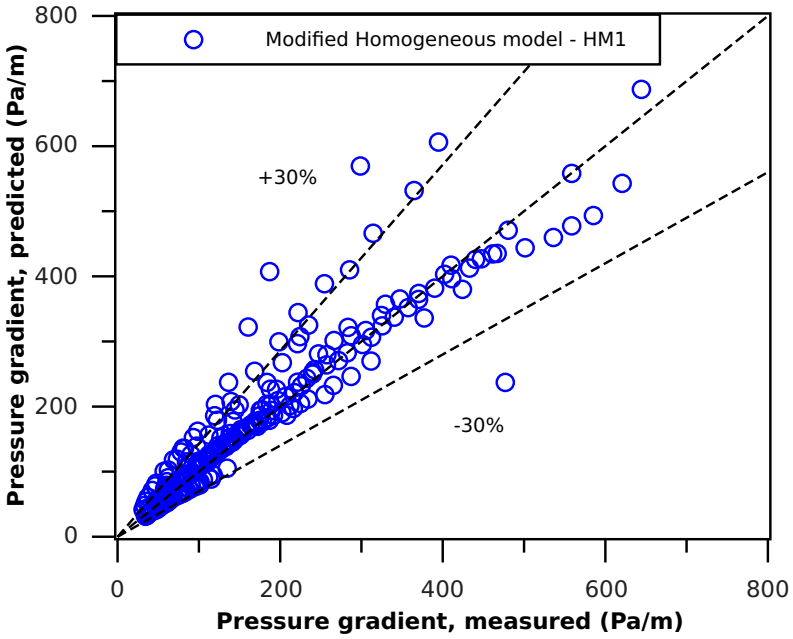

Figure 4.38 – Modified homogeneous pressure gradient model HM1: Annular/Mist data

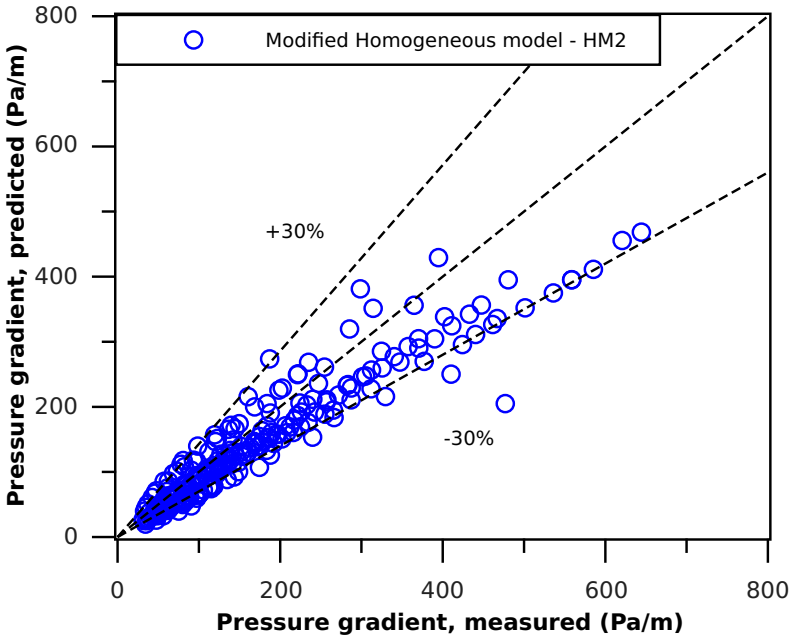

Figure 4.39 – Modified homogeneous pressure gradient model HM2: Annular/Mist data

4.6.6 Validation of the modified liquid holdup model of Choi et al. (2012)

Figures (4.40) and (4.41) compares experimental liquid holdup with two-phase liquid holdup model of Choi et al. (2012) and modified model respectively. Analysis of the results gives average percentage error for original liquid holdup model of Choi et al. (2012) as $56,489.54\%$, the values of absolute average percentage error and standard deviation of error are $56,489.68\%$ and $10,605.5$ respectively. In comparison with the unmodified model of Choi et al., the average percentage error of modified model is higher at 1.35%. Corresponding value of absolute average percentage error for modified model is lower at 15.60%, while the standard deviation of error for modified model is lower at 1.0.

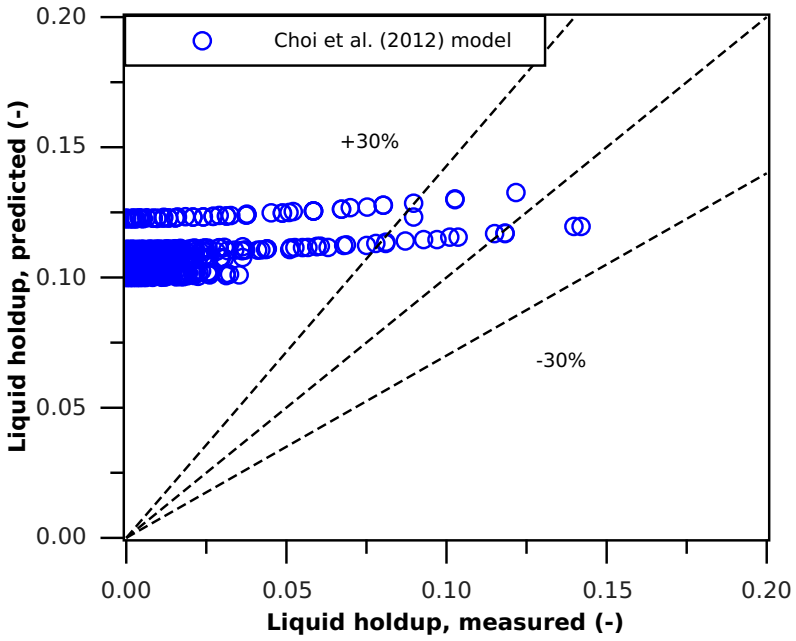

Figure 4.40 – Original liquid holdup model of Choi et al. (2012)

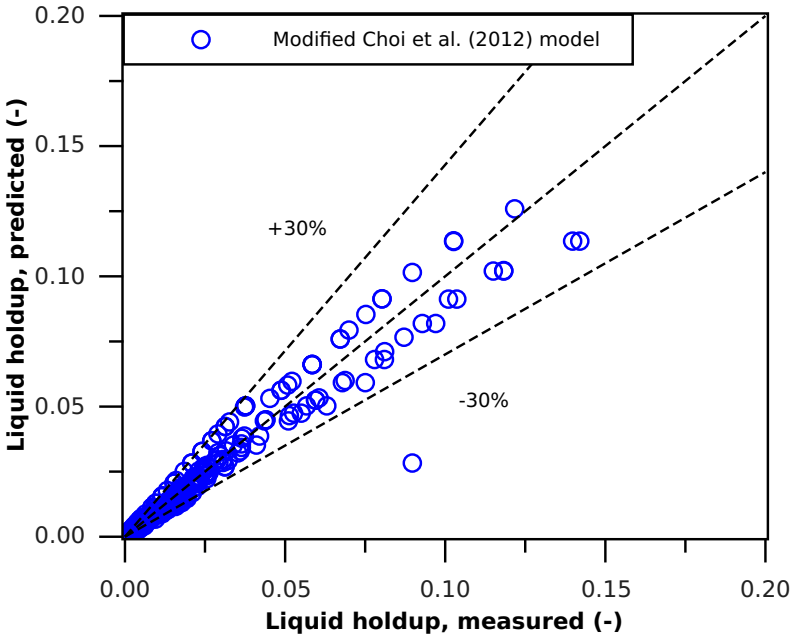

Figure 4.41 – Modified liquid holdup model of Choi et al. (2012)

4.7 Discussion

4.7.1 Validation of SETM

Pressure gradient

As observed in subsection (4.6.1), the plot of ε_{ave} for slug model of Taitel and Barnea (1990) is a negative trend, this agrees with observations made by Marruaz et al. (2001) for oil and gas flow, due to limitations of this model. However, a positive trend observed for SETM can be attributed to the fact that some data points are predicted as dispersed bubble flow, for which pressure gradient is typically higher in comparison with slug flow Mccready (1998). Also, another significant reason is that H_{LTB} used in SETM is theoretically higher than H^*_{LTB} used in the model of Taitel and Barnea (1990), thus resulting in higher pressure gradient for SETM and the observed positive ε_{ave} trend. It is evident that the predictions of present model are better than those of Taitel and Barnea (1990), for all pipe inclination angles except at 0^0 and 90^0. This can be attributed to the fact that correlating factors used in the Taitel and Barnea (1990) model, such as friction factors, are obtained for horizontal and vertical flows. Therefore, in order to improve the performance of SETM, relevant correlating factors can be optimised for improved prediction performance.

Although SETM gives better pressure gradient average predictions for stratified data, however, examination of the results demonstrated that limitations in the H_L model of Hart et al. (1989) resulted in the two categories of results (subsection (4.6.2)) with extreme error values. For example, at $H_L > 0.05$, the predictions of SETM show that the magnitude of average percentage error is larger (at 47.2%) than average value of 34.7% observed for stratified model of Taitel and Dukler. This can be attributed to the fact that liquid holdup model is valid for $H_L < 0.06$. Although similar H_L limitations and categorisation of results are observed for annular/mist flow as for stratified. However, better predictions by homogeneous pressure gradient model over SETM can be attributed in part to: (a) limitations of H_L model of Hart et al. (1989), and (b) absence of liquid entrainment in the SETM model.

In order to improve the prediction of SETM for stratified and annular/mist flows, liquid holdup model of Choi et al. (2012) and Hart et al. (1989) can be further improved. Also, further experimental and numerical studies can be carried out to determine the effect of liquid film entrainment on the performance of SETM, especially for predicting pressure gradient for annular/mist flows.

Implications of SETM Pressure gradient predictions

Implementation of the assumptions made in the development of SETM may limit prediction accuracy of SETM. This is dealt with presently.

Negligible liquid entrainment. Liquid entrainment is generally observed in slug flow (e.g. churn flow or when flow approaches annular), stratified (e.g. flow moving from stratified smooth to stratified wavy), and annular (flow moving towards mist). Therefore, different distribution of phase fractions in three-phase flow (including: liquid, gas, and entrained liquid droplets) would result in different pressure gradient contributions (i.e. from the three phases) to the total pressure gradient, which would be most probably be different with total pressure gradient from liquid-gas two-phase prediction (refer to figures (4.9), (4.17), and (4.22)).

Liquid holdup algorithm. The liquid model algorithm implemented in SETM combines liquid holdup models of Choi et al. (2012) and Hart et al. (1989) based on no-slip liquid holdup distribution of data in tables (4.1-4.4). Therefore, application SETM to other flow domains (flow rates, fluid properties, and pipe geometry), different from those presented in tables (4.1-4.4), must be carried out with caution. For instance, liquid holdup of Hart et al. (1989) are derived for horizontal flow. Similar to this, modified liquid holdup of Choi et al. (2012) proposed in this study is valid for horizontal flow.

Pipe inclination. Pressure gradient predictions in inclined and vertical flow (refer to figures (4.9), (4.10), and (4.11)) have only been validated for slug flow. The limitations of negligible liquid entrainment and liquid holdup algorithm (limited to horizontal flow) has not been examined, but could affect the accuracy of SETM. Therefore, application of SETM to inclined flow has to be carried out with caution.

Other results: flow regime, H_{LTB}, X/D, β

Flow regime. Flow regime predictions by SETM for slug data identify majority of the data as slug, and the remaining data as dispersed-bubble and transition (refer to figure (4.13)). The transition zone predictions can be identified as churn flow, which is generally a transition zone between slug and annular flow (Shoham, 2005). Alternatively, fundamental assumptions made in SETM (i.e. no liquid entrainment, and liquid holdup algorithm). The dispersed-bubble predictions can also be attributed to same assumptions.

Flow regime predictions by SETM for stratified data identify the data as transition

zone (refer to figure (4.18)). The stratified data are sourced from Asante (2000) and were identified as stratified-wavy, with curved liquid-gas interface. Thus these data, by definition of apparent liquid height (X/D), fall within transition zone. Flow regime predictions by SETM for annular data identify the data as transition zone (refer to figure (4.23)). Non-prediction of annular flow regime may be attributed to limitations of liquid holdup algorithm employed and the non-inclusion of liquid entrainment in the SETM model. Further studies need to be carried out to improve predictions.

Liquid holdup in slug film zone, H_{LTB}. H_{LTB} predictions by SETM for slug data show that $H_{LTB} \geq H_L$ (refer to figure (4.14)), since H_L receives contributions from both H_{LTB} and H_{LLS} in slug film zone and slug body respectively. H_{LTB} predictions for stratified and annular data show that $H_{LTB} \approx H_L$ (refer to figures (4.19) and (4.24)). These predictions follow similar observations in previous studies (Brill, 1987; Shoham, 2005).

Apparent liquid height, X/D. X/D predictions by SETM for slug data show that $X/D \approx h_L/D$ (refer to figure (4.15)), since majority of the predictions fall to the left of transition zone. However, annular cross-sectional profile of slug film zone, which typically observed in vertical flow (Shoham, 2005; Van Der Meulen, 2012), was not taken into account in SETM, hence this phenomenon is not detected. X/D predictions by SETM for stratified and annular data show that $X/D > h_L/D$ (refer to figures (4.20) and (4.25)), since majority of the predictions fall in the transition zone. These predictions follow similar observations in previous studies (Ullmann and Brauner, 2006).

Length ratio of slug film to slug unit, β. Figure (4.16) shows that $0 < \beta < 1$ for slug data, since slug flow receives contributions from both slug film zone and slug body. Figures (4.21) and (4.26) show that $\beta \approx 1$ for stratified and annular data respectively, since stratified and annular receives contributions from slug film zone only. Similar trends are observed in previous studies (Minami and Shoham, 1994; Di Salvo, 2014).

4.7.2 SETM flow regime predictions

Existence of stratified flow in the prediction of SETM for horizontal flows follows observations by previous studies (Taitel and Dukler, 1976b; Barnea, 1987; Shoham, 2005). However, at low values of U_{SG} and U_{SL}, slug and dispersed-bubble flows are identified instead of stratified flow. This is due to limitations in H_L model of Choi et al. (2012), which gives $H_L \to 1.0$ at low flow rates. This limitation is

illustrated using equation (4.50): H_L approaches unity for two conditions, namely: (a) $U_{SG} \rightarrow 0$, and (b) $(C_o V_M + U_D) \gg U_{SG}$.

$$H_L = 1 - \frac{U_{SG}}{C_o V_M + U_D} \tag{4.50}$$

Parts of transition zone at low U_{SL} are general identified as stratified wavy flow (Taitel and Dukler, 1976a), while transition at high U_{SL} is typically slug or annular (Shoham, 2005).

At inclined flows, flow regime transition follows similar trends as for Barnea (1987), since same Kutateladze criterion is applied. The transition zone for inclined (especially as $\theta \rightarrow 90^0$) flow can be technically referred to as churn zone/flow (experimetally identified by previous studies (Shoham, 2005)). Although different transition mechanisms apply, slug to dispersed-bubble flow predictions by present unified flow regime model and the model of Barnea (1987) are similar for inclined flow.

4.7.3 Validation of the modified homogeneous pressure gradient model

The over-prediction of pressure gradient by the unmodified homogeneous two-phase model can be attributed to two factors, namely: (a) non-homogeneous nature of two-phase flows, and (b) in-accurate liquid holdup model. The non-homogeneous nature of two-phase flows, especially separated flows (i.e. stratified and annular flows), leads to in-accurate estimation of mixture fluid properties and eventually pressure gradient (Shoham, 2005). Also, liquid holdup model has been demonstrated (refer to subsection (4.7.2)) to be limited in over predicting H_L at low flow rates. This limitation is particularly severe for stratified and annular/mist flows. Therefore, mixture properties (e.g. ρ_M) receive greater contribution from liquid phase than necessary. Thus resulting in higher average percentage error values of 206.98%, 6,552.79%, and 8,422.91% for slug, stratified, and annular experimental data respectively. The work of Thome (2006) also demonstrated that homogeneous pressure gradient applies to high flow rates.

Homogeneous no-slip liquid-gas pipe flow pressure gradient model gives low prediction error for annular/mist data since the model was developed for dispersed-bubble or dispersed-droplet flow. In this case, mist flow is a dispersed-droplet flow: gas is the main fluid flow, and liquid dispersed as droplets in the gas. Inaccurate prediction of the homogeneous no-slip pressure gradient model for stratified and slug data follows previously identified non-homogeneous nature of two-phase flow. Also,

no-slip homogeneous pressure gradient neglects pressure gradient contribution due to slip between liquid and gas interface, thus contributing to under-prediction (i.e. $\varepsilon_{ave} = -44.42\%$) of slug experimental data (figure (4.29)). In the case of stratified data, higher order of error ($\varepsilon_{ave} = 56,489.54\%$) in the prediction of H_L (shown in figures (4.40)) results in pressure gradient over-prediction at $\varepsilon_{ave} = 367.56\%$ (refer to figure (4.33)).

Poor predictions of homogeneous pressure gradient model slug and stratified flow experimental data agrees with observations of Jerez-Carrizales et al. (2015). Although, the modifications to general homogeneous model did not specifically correct H_L of Choi et al. (2012), application of empirical correction factors however improve pressure gradient prediction accuracy; $\varepsilon_{abs} < 6.1\%$ for slug data, $\varepsilon_{abs} < 27\%$ for stratified data, and $\varepsilon_{abs} < 21\%$ for annular/mist data. However, application of modified homogeneous pressure gradient to other data must be carried with caution, due to empirical nature of correction factors in the modified models. Thome further demonstrated that frictional pressure gradient is mostly affected by limitations of original homogeneous model, therefore, the correction factor can be applied to friction factor (in effect, frictional pressure gradient part of the homogeneous model).

4.7.4 Validation of the modified liquid holdup model of Choi et al. (2012)

H_L model of Choi et al. over-predicts experimental data at low liquid flow rates, including: stratified and annular/mist flows. Based on results presented in figure (4.40), experimental liquid holdup data in the range ($0 \leq H_L^{exp} \leq 0.15$) is predicted by liquid holdup model of Choi et al. (2012) in the range ($0 \leq H_L^{exp} \leq 0.15$). Therefore, as H_L^{exp} approaches zero (i.e. $H_L^{exp} \rightarrow 0$), H_L^C is approximately constant at values greater than 0.10, ε_{ave} approaches higher order values (refer to equation (4.47)). Empirical correction factor applied to liquid holdup of Choi et al. (2012) is derived from Asante (2000), the same data used for validation. Therefore, application of proposed H_L model of Choi et al. to other experimental or field data must be carried out with caution.

Chapter 5

Transient model

This chapter presents simplified transient two-phase pipe flow model, developed in this study. The first section (5.1) gives detailed theory and model development, numerical solution (at large time step and spatial discretiastion) based on upwind finite volume scheme and explicit time discretisation. The second section (5.2) provides algorithm for the simplified transient model. The third section (5.3) outlines experimental data for validation of the simplified transient model, and comparison with OLGA predictions. Section (5.4) presents results. The last section (5.5) gives discussion.

5.1 Theory: Transient model

5.1.1 One dimensional Navier-Stokes equations for two-phase flow

One dimensional two-fluid Navier-Stokes equations, with negligible mass transfer between the fluids and zero contribution from energy equation, is considered. The resulting continuity and momentum equations are given in equations (5.1 - 5.4)

Continuity equations

$$\frac{\partial}{\partial t}(\rho_G \alpha_G) + \frac{\partial}{\partial x}(\rho_G \alpha_G U_G) = 0 \tag{5.1}$$

$$\frac{\partial}{\partial t}(\rho_L \alpha_L) + \frac{\partial}{\partial x}(\rho_L \alpha_L U_L) = 0 \tag{5.2}$$

Momentum equations

$$\frac{\partial}{\partial t}(\rho_G \alpha_G U_G) + \frac{\partial}{\partial x}\left(\rho_G \alpha_G U_G^2\right) = -\alpha_G \frac{\partial P_G}{\partial x} - \tau_{WG} - \tau_{LG} - \alpha_G \rho_G g \sin\theta \tag{5.3}$$

$$\frac{\partial}{\partial t}(\rho_L \alpha_L U_L) + \frac{\partial}{\partial x}\left(\rho_L \alpha_L U_L^2\right) = -\alpha_L \frac{\partial P_L}{\partial x} - \tau_{WL} + \tau_{LG} - \alpha_L \rho_L g \sin\theta \tag{5.4}$$

5.1.2 Simplification of one dimensional two-fluid Navier-Stokes equations

Simplification of the one dimensional two-fluid Navier-Stokes equations is carried out by implementing the following modifications:

1. The two fluids are considered to be incompressible

2. Superficial velocities are defined as:

$$U_{SG} = \alpha_G U_G,\ U_{SL} = \alpha_L U_L \tag{5.5}$$

3. Steady-state pressure gradient applies as shown in equations (5.6) and (5.7). The treatment of steady state pressure gradient for the two-fluid pipe flow is provided in section (5.1.4).

$$0 = -\alpha_G \frac{\partial P_G}{\partial x} - \tau_{WG} - \tau_{LG} - \alpha_G \rho_G g \sin\theta \tag{5.6}$$

$$0 = -\alpha_L \frac{\partial P_L}{\partial x} - \tau_{WL} + \tau_{LG} - \alpha_L \rho_L g \sin\theta \tag{5.7}$$

4. Single pressure model applies for the two fluids:

$$P_G = P_L = P \tag{5.8}$$

5. The phase fraction of the lighter phase (typically gas) is expressed as a function of the phase fraction of the heavier phase:

$$\alpha_G = 1 - \alpha_L \tag{5.9}$$

6. Two dimensionless terms are introduced into the combined two-fluid continuity equation (refer to equation (5.11)). The first dimensionless term is the ratio of transient liquid holdup to steady-state liquid holdup (refer to first part of equation (5.10)). The second dimensionless term is the ratio of transient gas fraction to steady-state gas fraction (refer to second part of equation (5.10)). Theoretically, the two dimensionless terms in equation (5.10) should converge to unity after transient simulations stabilise to steady-state conditions.

$$\frac{\alpha_L}{H_L},\ \frac{1-\alpha_L}{1-H_L} \tag{5.10}$$

Continuity equations By using modifications 1, 2, 5, and 6, and further simplifications, the combined two-fluid continuity equations is now expressed as shown in equations (5.11).

$$\frac{\partial}{\partial t}(\alpha_L) - \frac{1}{2\rho_G}\frac{\partial}{\partial x}\left\{\left(\frac{1-\alpha_L}{1-H_L}\right)\rho_G U_{SG}\right\} + \frac{1}{2\rho_L}\frac{\partial}{\partial x}\left\{\left(\frac{\alpha_L}{H_L}\right)\rho_L U_{SL}\right\} = 0 \tag{5.11}$$

Momentum equations Application of modifications 1, 2, 3, and 5, transforms the two-fluid momentum equations into:

$$\frac{\partial}{\partial t}(U_{SG}) + \frac{1}{\rho_G}\frac{\partial}{\partial x}\left\{\left(\frac{\rho_G}{1-\alpha_L}\right)U_{SG}^2\right\} = 0 \tag{5.12}$$

$$\frac{\partial}{\partial t}(U_{SL}) + \frac{1}{\rho_L}\frac{\partial}{\partial x}\left\{\left(\frac{\rho_L}{\alpha_L}\right)U_{SL}^2\right\} = 0 \tag{5.13}$$

The simplified transient two-phase model, proposed in this study, consists of equations (5.11), (5.12), and (5.13), combined with steady-state pressure gradient (i.e. equations (5.6) and (5.7) for gas and liquid respectively).

5.1.3 Model analysis

The governing equation of any given model can be algebraically expressed as:

$$\mathbf{M}_1\frac{\partial}{\partial t}(\mathbf{U}) + \mathbf{M}_2\frac{\partial}{\partial x}(\mathbf{U}) = \mathbf{S}(\mathbf{U}) \tag{5.14}$$

where $\mathbf{M}_1$ and $\mathbf{M}_2$ are non-singular square matrices, and their coefficients are functions of flow variables. $\mathbf{U}$ is the vector of conservative variables. $\mathbf{S}$ represents vector of source terms. The study of model characteristics results in the evaluation of the equation:

$$det(\mathbf{M}_2 - \lambda\mathbf{M}_1) = det\big(\mathbf{M}^{det}\big) = 0 \tag{5.15}$$

where λ is a characteristic value.

If conservative vector $\mathbf{U}$ is defined as:

$$\mathbf{U} = \begin{pmatrix} \alpha_L \\ U_{SG} \\ U_{SL} \end{pmatrix} \tag{5.16}$$

Therefore, matrices $\mathbf{M}_1$ and $\mathbf{M}_2$ are expressed as:

$$\mathbf{M}_1 = \mathbf{I} = \begin{pmatrix} 1 & 0 & 0 \\ 0 & 1 & 0 \\ 0 & 0 & 1 \end{pmatrix} \tag{5.17}$$

and

$$\mathbf{M}_2 = \begin{pmatrix} \frac{1}{2}\left(\frac{H_L U_{SG} + (1-H_L)U_{SL}}{H_L(1-H_L)}\right) & -\frac{1}{2}\left(\frac{1-\alpha_L}{1-H_L}\right) & \frac{1}{2}\left(\frac{\alpha_L}{H_L}\right) \\ \\ \frac{U_{SG}}{(1-\alpha_L)^{3/2}} & 2\left(\frac{U_{SG}}{1-H_L}\right) & 0 \\ \\ -\frac{U_{SL}}{(\alpha_L)^{3/2}} & 0 & 2\left(\frac{U_{SL}}{H_L}\right) \end{pmatrix} \tag{5.18}$$

Since incompressible flow is assumed, vector $\mathbf{S}$ of source terms reduces to:

$$\mathbf{S} = \begin{pmatrix} 0 \\ 0 \\ 0 \end{pmatrix} \tag{5.19}$$

For simplicity, the elements of matrix $\mathbf{M}_2$ can be symbolically represented as shown in equation (5.20).

$$\mathbf{M}_2 = \begin{pmatrix} m(1,1) & m(1,2) & m(1,3) \\ \\ m(2,1) & m(2,2) & m(2,3) \\ \\ m(3,1) & m(3,2) & m(3,3) \end{pmatrix} \tag{5.20}$$

Therefore, $\mathbf{M}^{det} = (\mathbf{M}_2 - \lambda\mathbf{M}_1)$ is expressed as:

$$\mathbf{M}^{det} = \begin{pmatrix} m(1,1)-\lambda & m(1,2) & m(1,3) \\ \\ m(2,1) & m(2,2)-\lambda & m(2,3) \\ \\ m(3,1) & m(3,2) & m(3,3)-\lambda \end{pmatrix} \tag{5.21}$$

Hence, evaluating equation (5.15) yields a polynomial:

$$\lambda^3 + a_1\lambda^2 + a_2\lambda + a_3 = 0 \tag{5.22}$$

where,
$a_1 = -m(1,1) - m(2,2) - m(3,3)$
$a_2 = m(1,1)m(2,2) + m(1,1)m(3,3) + m(2,2)m(3,3) - m(1,2)m(2,1) + m(1,3)m(3,1)$
$a_3 = -m(1,1)m(2,2)m(3,3) + m(1,2)m(2,1)m(3,3) + m(1,3)m(3,1)m(2,2)$

The three characteristics of the model are:

$$\lambda_1 = S + T - \frac{1}{3}a_1 \tag{5.23}$$

$$\lambda_2 = -\frac{1}{2}(S+T) - \frac{1}{3}a_1 + \frac{1}{2}i\sqrt{3}(S-T) \tag{5.24}$$

$$\lambda_3 = -\frac{1}{2}(S+T) - \frac{1}{3}a_1 - \frac{1}{2}i\sqrt{3}(S-T) \tag{5.25}$$

where,

$$S = \sqrt[3]{R + \sqrt{\triangle}} \tag{5.26}$$

$$T = \sqrt[3]{R - \sqrt{\triangle}} \tag{5.27}$$

and

$$\triangle = Q^3 + R^2 \tag{5.28}$$

$$Q = \frac{3a_2 - {a_1}^2}{9} \tag{5.29}$$

$$R = \frac{9a_1a_2 - 27a_3 - 2{a_1}^3}{54} \tag{5.30}$$

The discriminant $\triangle$ must be less than or equal to zero to ensure the roots ($\lambda_1,\ \lambda_2,\ \lambda_3$) of the polynomial are all real.

Fluid properties Pressure generally depends on fluid temperature and density, mathematically expressed by equation of state. For negligible temperature variation, pressure only depends on fluid density. Therefore, a linear thermodynamic relation is assumed for gas and liquid densities as shown in equations (5.32) and (5.31) respectively.

$$\rho_L = \rho_{L,0} + \frac{P_L - P_{L,0}}{c_L^2} \tag{5.31}$$

$$\rho_G = \frac{P_G}{c_G^2} \tag{5.32}$$

5.1.4 Steady-state pressure gradient

Mathematical model for predicting pressure gradient in the present simplified transient two-phase fluid flow in pipe is selected and validated using experimental data.

For simplicity, the pressure gradient model proposed by García et al. (2003) is selected for horizontal flows. The model of Garcia et al. was developed for horizontal flows. For two-phase flow with complex pipe geometry, unified pressure gradient model employed is the method presented by Shoham (2005). Pressure gradient models of García et al. and Shoham are presented in appendices (D.1) and (C.1) respectively.

Validation of pressure gradient model The pressure gradient models of García et al. (2003) and Shoham (2005) are validated using experimental data detailed in table (5.1), and the validation results are given in figures (5.1) and (5.2) respectively. The results show that the models of García et al. (2003) and Shoham (2005) predict 83% and 65% of experimental data (in respective order) within $-30\% < \varepsilon_{ave} < +30\%$.

Table 5.1 – Experimental data for validating pressure gradient models of García et al. (2003) and Shoham (2005).

Source	No. of data [−]	Flow regime [−]	θ [*degrees*]	D [*m*]
Asante (2000)	255	Stratified	0	0.0254 − 0.0762
Asante (2000)	243	Annular/Mist	0	0.0254 − 0.0762
Hernandez (2007)	38	Slug	0	0.038
Marruaz et al. (2001)	23	Slug	0	0.150
Tullius (2000)	101	Slug	0	0.101
Total	660			

5.1.5 Numerical discretisation of simplified transient two-phase model

Finite volume scheme, with scattered grid arrangement in spatial domain, is applied to the simplified transient two-phase model. The combined continuity equation (5.11) is explicitly discretised by the upwind method as shown in equation (5.33). Simplified momentum equations of gas and liquid are approximated as presented in equations (5.34) and (5.35) respectively. Finally, steady-state pressure gradient model is estimated as shown in equations (5.36) and (5.37).

Combined continuity equations

$$\frac{(\alpha_L)_i^{n+1} - (\alpha_L)_i^n}{\triangle t} = A_1 \left((U_{SG})_{i-\frac{1}{2}}^n \left[1 - (\alpha_L)_{i-1}^n \right] \right) + A_2 \left((U_{SG})_{i+\frac{1}{2}}^n [1 - (\alpha_L)_i^n] \right) + A_3 \left((U_{SL})_{i-\frac{1}{2}}^n (\alpha_L)_{i-1}^n \right) + A_4 \left((U_{SL})_{i+\frac{1}{2}}^n (\alpha_L)_i^n \right) \tag{5.33}$$

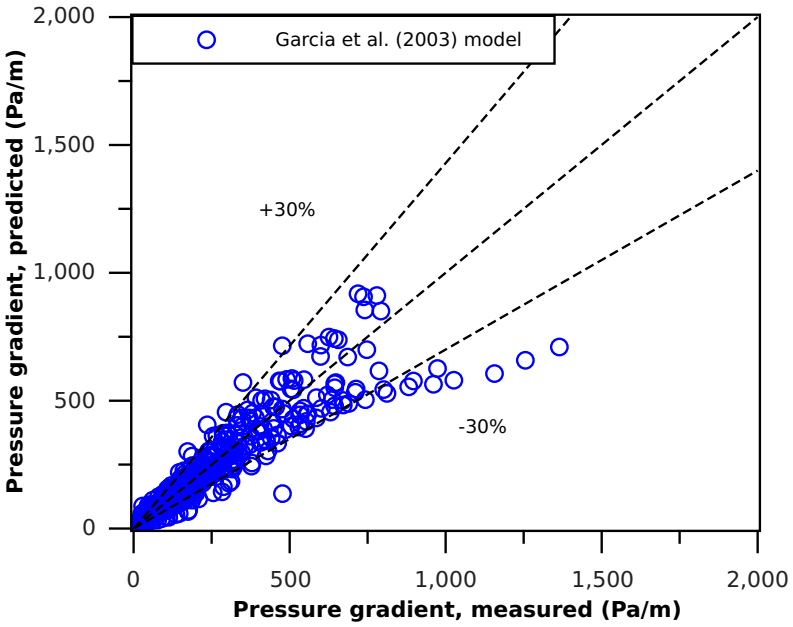

Figure 5.1 – Validation of the steady state pressure gradient model of García et al. (2003)

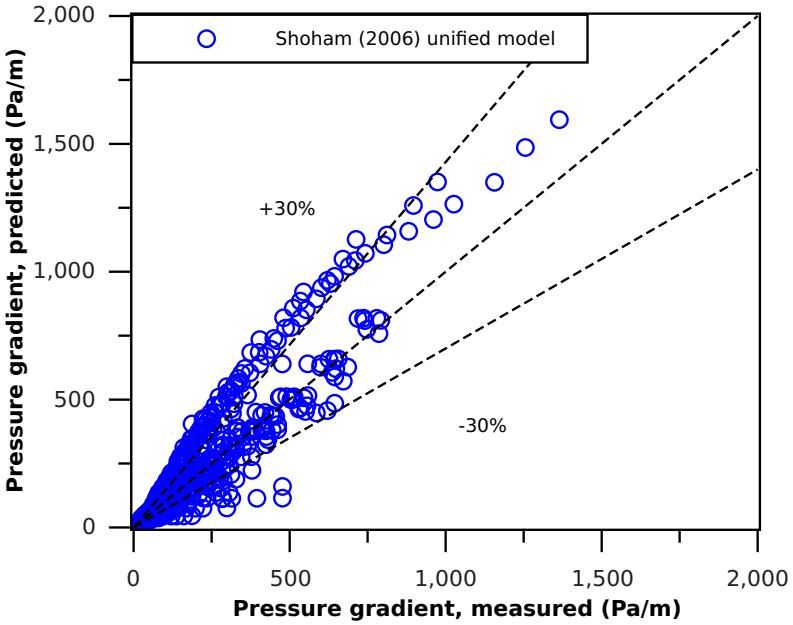

Figure 5.2 – Validation of the steady state pressure gradient model of Shoham (2005)

where,

$$A_1 = \left(\frac{1}{2\rho_G}\right)_i^n \left(\frac{-1}{\triangle x}\right)_i \left\{\left(\frac{1+\beta_{i-\frac{1}{2}}^G}{2}\right)\left(\frac{\rho_G}{1-H_L}\right)_{i-1} + \left(\frac{1-\beta_{i-\frac{1}{2}}^G}{2}\right)\left(\frac{\rho_G}{1-H_L}\right)_i\right\}^n$$

$$A_2 = \left(\frac{1}{2\rho_G}\right)_i^n \left(\frac{1}{\triangle x}\right)_i \left\{\left(\frac{1+\beta^G_{i+\frac{1}{2}}}{2}\right)\left(\frac{\rho_G}{1-H_L}\right)_i + \left(\frac{1-\beta^G_{i+\frac{1}{2}}}{2}\right)\left(\frac{\rho_G}{1-H_L}\right)_{i+1}\right\}^n$$

$$A_3 = \left(\frac{1}{2\rho_L}\right)_i^n \left(\frac{1}{\triangle x}\right)_i \left\{\left(\frac{1+\beta^L_{i-\frac{1}{2}}}{2}\right)\left(\frac{\rho_L}{H_L}\right)_{i-1} + \left(\frac{1-\beta^L_{i-\frac{1}{2}}}{2}\right)\left(\frac{\rho_L}{H_L}\right)_i\right\}^n$$

$$A_4 = \left(\frac{1}{2\rho_L}\right)_i^n \left(\frac{-1}{\triangle x}\right)_i \left\{\left(\frac{1+\beta^L_{i+\frac{1}{2}}}{2}\right)\left(\frac{\rho_L}{H_L}\right)_i + \left(\frac{1-\beta^L_{i+\frac{1}{2}}}{2}\right)\left(\frac{\rho_L}{H_L}\right)_{i+1}\right\}^n$$

Simplified momentum equations of gas and liquid

Gas:

$$\frac{(U_{SG})^{n+1}_{i+\frac{1}{2}} - (U_{SG})^n_{i+\frac{1}{2}}}{\triangle t} = B_1\left(\frac{\left[(U_{SG})^n_{i-\frac{1}{2}}\right]^2}{1-(\alpha_L)^n_{i-\frac{1}{2}}}\right) + B_2\left(\frac{\left[(U_{SG})^n_{i+\frac{1}{2}}\right]^2}{1-(\alpha_L)^n_{i+\frac{1}{2}}}\right) + B_3\left(\frac{\left[(U_{SG})^n_{i+\frac{3}{2}}\right]^2}{1-(\alpha_L)^n_{i+\frac{3}{2}}}\right) \tag{5.34}$$

where,

$$B_1 = \left(\frac{1}{\rho_G}\right)^n_{i+\frac{1}{2}} \left(\frac{1}{\triangle x}\right)_{i+\frac{1}{2}} \left\{\left(\frac{1+\beta^G_{i+\frac{1}{2}}}{2}\right)(\rho_G)_{i-\frac{1}{2}}\right\}^n$$

$$B_2 = \left(\frac{1}{\rho_G}\right)^n_{i+\frac{1}{2}} \left(\frac{-1}{\triangle x}\right)_{i+\frac{1}{2}} \left\{\beta^G_{i+\frac{1}{2}}(\rho_G)_{i+\frac{1}{2}}\right\}^n$$

$$B_3 = \left(\frac{1}{\rho_G}\right)^n_{i+\frac{1}{2}} \left(\frac{-1}{\triangle x}\right)_{i+\frac{1}{2}} \left\{\left(\frac{1-\beta^G_{i+\frac{1}{2}}}{2}\right)(\rho_G)_{i+\frac{3}{2}}\right\}^n$$

Liquid:

$$\frac{(U_{SL})^{n+1}_{i+\frac{1}{2}} - (U_{SL})^n_{i+\frac{1}{2}}}{\triangle t} = C_1\left(\frac{\left[(U_{SL})^n_{i-\frac{1}{2}}\right]^2}{(\alpha_L)^n_{i-\frac{1}{2}}}\right) + C_2\left(\frac{\left[(U_{SL})^n_{i+\frac{1}{2}}\right]^2}{(\alpha_L)^n_{i+\frac{1}{2}}}\right) + C_3\left(\frac{\left[(U_{SL})^n_{i+\frac{3}{2}}\right]^2}{(\alpha_L)^n_{i+\frac{3}{2}}}\right) \tag{5.35}$$

where,

$$C_1 = \left(\frac{1}{\rho_L}\right)^n_{i+\frac{1}{2}} \left(\frac{1}{\triangle x}\right)_{i+\frac{1}{2}} \left\{\left(\frac{1+\beta^L_{i+\frac{1}{2}}}{2}\right)(\rho_L)_{i-\frac{1}{2}}\right\}^n$$

$$C_2 = \left(\frac{1}{\rho_L}\right)^n_{i+\frac{1}{2}} \left(\frac{-1}{\triangle x}\right)_{i+\frac{1}{2}} \left\{\beta^L_{i+\frac{1}{2}}(\rho_L)_{i+\frac{1}{2}}\right\}^n$$

$$C_3 = \left(\frac{1}{\rho_L}\right)^n_{i+\frac{1}{2}} \left(\frac{-1}{\triangle x}\right)_{i+\frac{1}{2}} \left\{\left(\frac{1-\beta^L_{i+\frac{1}{2}}}{2}\right)(\rho_L)_{i+\frac{3}{2}}\right\}^n$$

Pressure gradient: Discretised pressure gradient models of García et al. (2003) and Shoham (2005) are given in equations (5.36) and (5.37) respectively. Descriptions of *friction* and *gravity* terms in equation (5.37) are provided in appendix (C.1).

$$-\frac{P^{n+1}_{i+1} - P^{n+1}_i}{(\triangle x)_{i+\frac{1}{2}}} = \left(\frac{2f_M U^2_M \rho_M}{D}\right)_{i+\frac{1}{2}} + (\rho_M g \sin\theta)_{i+\frac{1}{2}} \tag{5.36}$$

$$-\frac{P^{n+1}_{i+1} - P^{n+1}_i}{(\triangle x)_{i+\frac{1}{2}}} = \left[\left(\frac{dP}{dL}\right)_{friction}\right]_{i+\frac{1}{2}} + \left[\left(\frac{dP}{dL}\right)_{gravity}\right]_{i+\frac{1}{2}} \tag{5.37}$$

Size of time step

Explicit discretisation of the simplified transient two-phase model is constrained with the general Courant-Friedrichs-Levy (CFL) number. CFL is defined as:

$$\triangle t = CFL \frac{\triangle x}{\lambda^n_{max}} \tag{5.38}$$

where $CFL \leq 1$ for stability of the scheme. The higher the value of CFL, the higher the efficiency of the scheme.

The term λ^n_{max} in equation (5.38) is generally taken as the largest wave speed throughout the computational domain at time level n. λ^n_{max} is defined in equation (5.39) for a system of N_{eq} differential equations in a computational domain with N elements:

$$\lambda^n_{max} = \max_j \max_k \mid \lambda^k_j \mid \quad for\ j = 1, ..., N\ and\ k = 1, ..., N_{eq} \tag{5.39}$$

Boundary conditions

A one-dimensional fluid flow system is solved in spatial domain: $0 \leq x \leq L$, where the inlet and outlet boundaries are $x = 0$ and $x = L$ respectively (refer to figure (5.3)). In order to determine numerical values of conservation variables at the boundaries, ghost cells are defined (Prosperetti and Tryggvason, 2007). In this study, conservative values at ghost cells are defined as shown in equations (5.40) and (5.41) for inlet and outlet boundaries respectively.

$$(\alpha_L)_{j=0} = (\alpha_L)_{j=1}\ ,\ (U_{SG})_{j=0} = (U_{SG})_{j=1}\ ,\ (U_{SL})_{j=0} = (U_{SL})_{j=1} \tag{5.40}$$

$$P_{j=N+1} = P_{j=N} \tag{5.41}$$

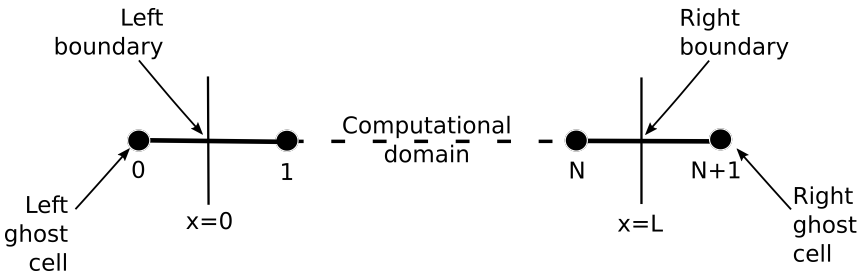

Figure 5.3 – Boundary conditions transient thesis

5.1.6 Pipe geometry and discretisation

Pipe profile is provided as pipe segments (or sub-regions) based on inclination angle (refer to figure (5.4)). Number of elements per segment is also provided such that the ratio of element size for adjacent segments approaches unity inorder to obtain a uniform grid. For example, for segments j and $j+1$, the ratio of element size is defined as:

$$\frac{\triangle x_j}{\triangle x_{j+1}} \rightarrow 1.0 \tag{5.42}$$

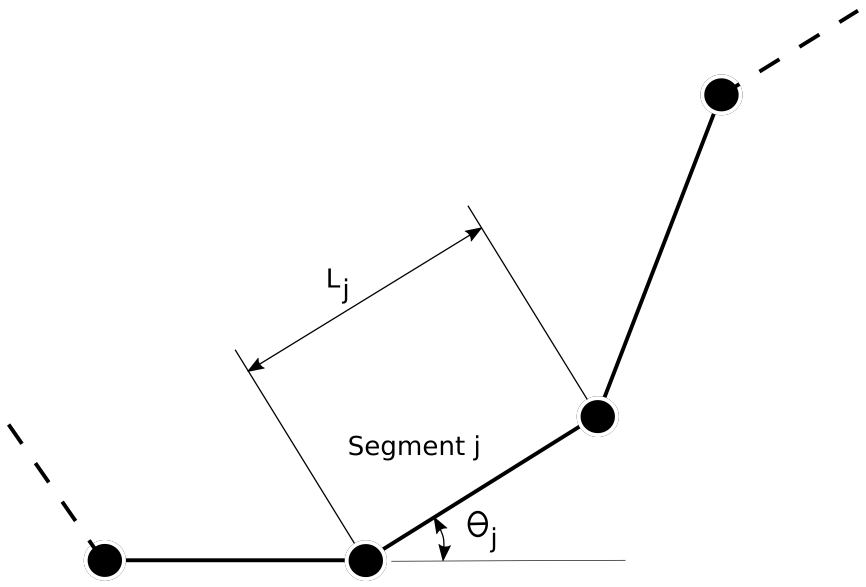

Figure 5.4 – Pipe profile divided into segments: L_j = Length of segment j $[m]$, θ_j = inclination angle of segment j $[degree]$

5.1.7 Sensitivity analysis

Sensitivity analysis is carried estimating pressure gradient, using flow data of Vigneron et al. (1995), at different number of nodes $N+1$, namely: $N+1 = 42$, 82, 124, 164, 328, 656, 1312 and 2624.

Spatial sensitivity analysis

Spatial sensitivity analysis is carried out, using pressure gradient as reference, as shown in equation (5.43). Figure (5.5) gives results of spatial sensitivity analysis. The results show that $\varepsilon_{ave} = -5.9\%$ at $N+1 = 42$ and increases logarithmically to $\varepsilon_{ave} = 0\%$ at $N+1 = 2624$. The curve traced in figure (5.5) shows that estimating pressure gradient at $N+1 > 2624$ would lead to the curve reaching a limiting value (i.e. $\varepsilon_{ave} \approx 0\%$) that is asymptotic to $\varepsilon_{ave} = 0\%$.

$$\varepsilon_{ave} = \frac{\left(-\frac{dP}{dL}\right)_{2624} - \left(-\frac{dP}{dL}\right)_{N+1}}{\left(-\frac{dP}{dL}\right)_{2624}} \times 100\% \tag{5.43}$$

Temporal sensitivity analysis

Since time step $\triangle t$ is calculated from element size $\triangle x$, separate sensiivity analysis is not carried out. However, computation time is examined for different sizes of spatial discretistion and shown in equation (5.44) and figure (5.6). The figure shows that computational time increases, exponentially with increase in spatial disretisaiton, from $t_{ratio} = 1$ at $N+1 = 42$ to $t_{ratio} = 2438$ at $N+1 = 2624$.

Discussion: implication of sensitivity analysis

Spatial sensitivity analysis, for proposed simplified transient liquid-gas pipe flow, shows that at coarse discretisation ($N+1 = 42$), pressure gradient predictions error fall within -6% of predictions for very fine discretisation ($N+1 = 2624$). Furthermore, temporal sensitivity analysis shows that solution is faster at coarse discretisation scheme $t_{ratio} = 1$ at $N+1 = 42$ compared to solution time at fine discretisation scheme $t_{ratio} = 2438$ at $N+1 = 2624$. Therefore, from the point of view of low demand on computation resources and time, and prediction accuracy, coarse spatial discretisation scheme at $N+1 = 42$ is chosen.

$$t_{ratio} = \frac{t_{N+1}}{t_{42}} \tag{5.44}$$

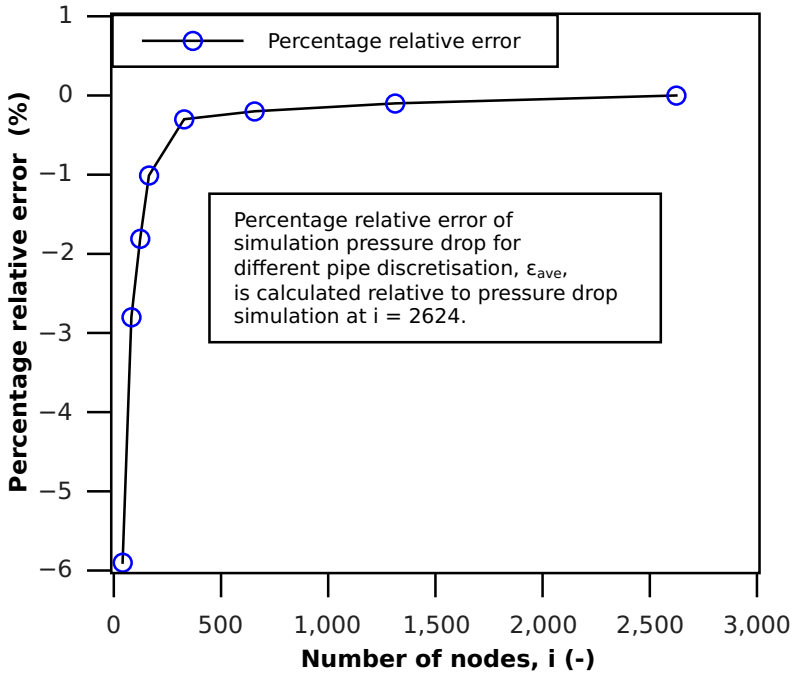

Figure 5.5 – Sensitivity analysis for spatial steady-state error

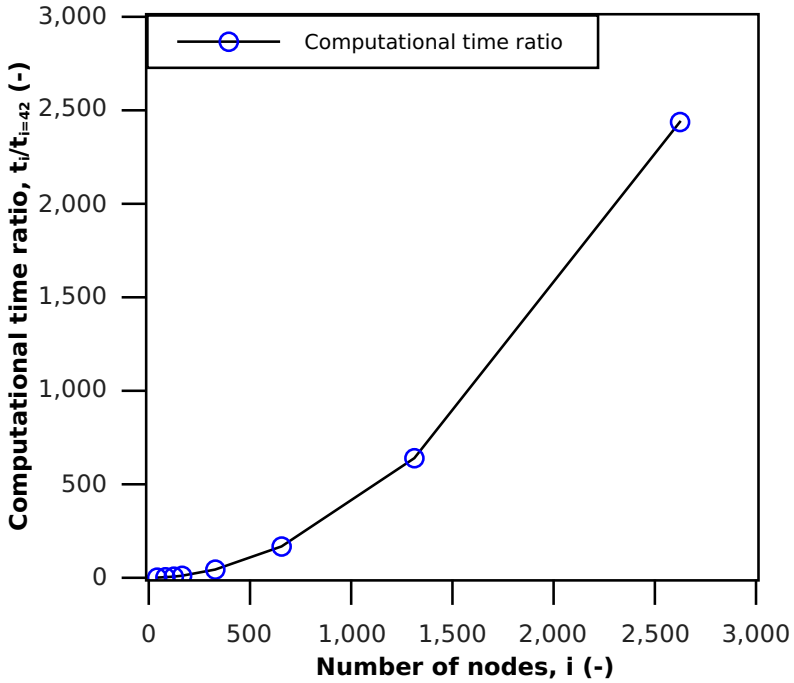

Figure 5.6 – Sensitivity analysis for time

5.2 Transient algorithm

Algorithm for the simplified transient two-phase model is presented in this section (refer to figure (5.7)). For a given set of input data, the transient algorithm implements equations described in subsection (5.1) in order to determine dynamic responses of flow variables. Input data include: gas and liquid superficial velocities (i.e. $U_{SG},\ U_{SL}$), physical properties of the two fluids (i.e. $\rho_G,\ \rho_L,\ \mu_G,\ \mu_L,\ \sigma$), and geometric variables of pipe ($D,\ \theta,\ \varepsilon,\ L$).

Steady state pressure gradient sub-algorithm implemented in proposed transient liquid-gas pipe flow model is given in algorithm (3).

Algorithm 3 Simplified transient model: Steady state pressure gradient sub-algorithm

procedure

Enter input data:
    input (*control volume boundary*) $\leftarrow$ ($flow\ rates$)
    input (*control volume centre*) $\leftarrow$ ($fluid\ properties\ and\ pipe\ geometry$)

Determine pressure gradient equation:
    if ($\theta == 0$) **then**
        Pressure gradient equation $\leftarrow$ *equation*(5.36)
    else
        Pressure gradient equation $\leftarrow$ *equation*(5.37)

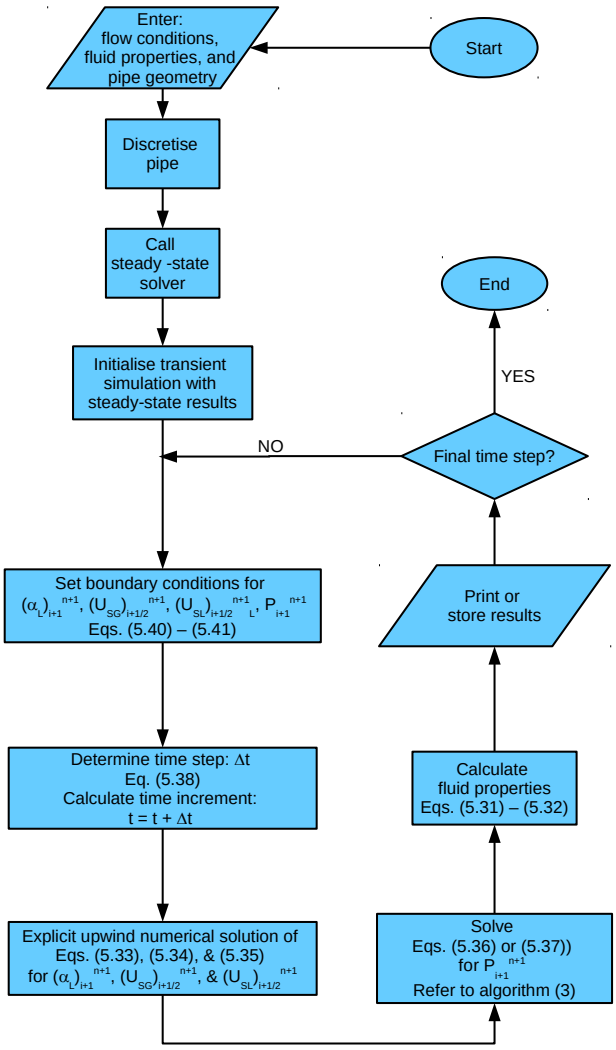

Figure 5.7 – Algorithm for transient two-phase flow model

Table 5.2 – Test facility of Bendiksen et al. (1991)

			Recording
Pipeline profile	Horizontal:	$[0-400]\ m$	
	Vertical:	$[400-457]\ m$	
Length of pipeline	$457\ m$		
Diameter	$0.19\ m$		
Test stations	Station 1:	$10\ m$	Absolute pressure
	Station 2:	$49\ m$	Liquid holdup
	Station 3:	$178\ m$	Liquid holdup
	Station 4:	$299\ m$	Liquid holdup
	Station 5:	$407\ m$	Liquid holdup
	Station 6:	$429\ m$	Liquid holdup
	Station 7:	$[130-328]\ m$	Pressure difference
	Station 8:	$[407-457]\ m$	Pressure difference
Fluids	Fluid 1:	Nitrogen	
	Fluid 2:	Kerosene	

5.3 Validation of model

The simplified transient two-phase pipe flow model, developed in this study, is validated against experimental data available in literature. Summaries of experiments, conducted by Bendiksen et al. (1991) and Vigneron et al. (1995), are given in subsections (5.3.1) and (5.3.2) respectively.

5.3.1 Transient data of Bendiksen et al. (1991)

The test facility of Bendiksen et al. (1991) is described in table (5.2), while summary of the experiment is given in figure (5.8). One of the fluids in table (5.2) is kerosene, which is a complex mixture of hydrocarbons (Marcus, 2002). In this study, the properties of kerosene is approximated from n-Dodecane hydrocarbon (Marcus, 2002; Williams, 2009; Kislik, 2011).

For initial steady state condition, fluid properties (including: density, dynamic viscosity, surface tension, and speed of sound) are estimated using CoolProp^{TM} fluid properties library. Description and validation of this library is provided in tables (B.1) through (B.6) (refer to appendix (B)). In the case of transient simulation, fluid properties are estimated using approach provided in subsection (5.1.3).

5.3.2 Transient data of Vigneron et al. (1995)

The test facility of Vigneron et al. (1995) is summarised in table (5.3). Table (5.4) gives summary of the experiment of Vigneron et al. (1995). Fluid properties is determined following same procedure provided in subsection (5.3.1).

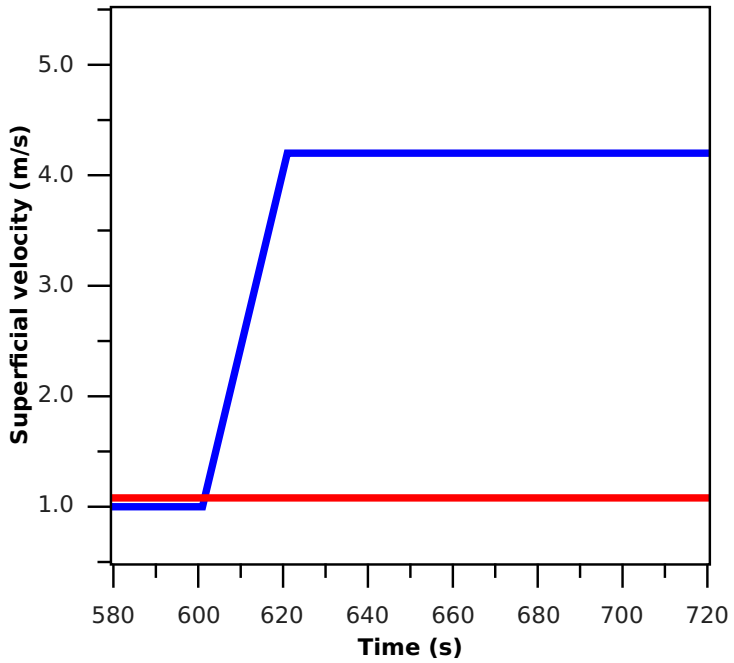

Figure 5.8 – Inlet flow variation (Bendiksen et al., 1991)

Table 5.3 – Test facility of Vigneron et al. (1995)

Pipeline profile	Horizontal: $[0 - 420]$ m	
Length of pipeline	420 m	
Diameter	0.0779 m	
Test stations	Station 1:	61.6 m
	Station 2:	396 m
Fluids	Fluid 1:	Air
	Fluid 2:	Kerosene

5.3.3 OLGA

OLGA Dynamic Multiphase Flow Simulator is the petroleum industry standard for prediction of transient multiphase hydraulics in pipes. OLGA code has been validated with large field and experimental data (including data from IFE and SINTEF flow loops) (Ali, 2009; Belt et al., 2011). Therefore, the performance of proposed simplified transient liquid-gas pipe flow is compared with OLGA, using the data of Bendiksen et al. (1991) and Vigneron et al. (1995).

Table 5.4 – Summary of experiment (Vigneron et al., 1995)

TEST No.	INITIAL (I) FINAL (F)	FLOW RATE LIQUID (m^3/d)	FLOW RATE GAS (Sm^3/d)	FLOW REGIME	Psep (Bar)
LIQUID FLOW RATE CHANGE					
1-A	I	32.5	815	Slug	1.67
	F	168.4	815	Slug	
1-B	I	8.4	400	Stratified Smooth	1.67
	F	31.8	400	Stratified Wavy	
1-C	I	8.4	4055	Stratified Wavy	1.76
	F	32	4055	Stratified Wavy	
1-D	I	340	880	Slug	1.67
	F	168	880	Slug	
1-E	I	28.1	2590	Stratified Wavy	1.67
	F	294	2590	Slug	
1-F	I	295	7620	Slug	1.74
	F	172	7620	Slug	
1-G	I	32.9	2745	Stratified Wavy	1.67
	F	8.5	2745	Stratified Smooth	
GAS FLOW RATE CHANGE					
2-A	I	8	850	Stratified Smooth	1.67
	F	8	4520	Stratified Wavy	
2-B	I	20.2	340	Stratified Smooth	1.67
	F	20.2	2530	Stratified Wavy	
2-C	I	203	870	Slug	1.76
	F	203	3690	Slug	
2-D	I	195	1875	Slug	1.67
	F	195	10840	Slug	
2-E	I	323	815	Slug	1.67
	F	323	5000	Slug	
LIQUID BLOW OUT					
3-A	I	48.8	4825	Stratified Wavy	1.69
	F	0	4825	Single Phase Gas	
3-B	I	204	5880	Slug	1.69
	F	0	5880	Single Phase Gas	
STARTUP					
4-A0	I		$H_L = 0.0$		1.68
	F	22	2650	Stratified Wavy	
4-A1	I		$H_L = 1.0$		1.68
	F	21.8	2615	Stratified Wavy	
4-B0	I		$H_L = 0.0$		1.66
	F	322	1870	Slug	
4-B1	I		$H_L = 1.0$		1.66
	F	322.5	1910	Slug	

5.4 Results

Transient model results are presented in this section. Subsection (5.4.1) compares present simplified transient model results with transient experimental data of Bendiksen et al. (1991). In subsection (5.4.2), the simplified transient model is compared with experimental data of Vigneron et al. (1995).

5.4.1 Simplified model results: data of Bendiksen et al.

Definitions of stations $1-8$ are given in table (5.2). Number of nodes is 46.

Liquid hoildup at stations 2 and 3

Figure (5.9) shows experimental data and model predictions of liquid holdup at station 2. The results show that experimental liquid holdup decreases from 0.597 to 0.297, while from the simplified transient model, liquid holdup decreases from 0.633 to 0.237. Olga prediction decreases from 0.594 to 0.244.

Figure (5.10) shows experimental data and model predictions of liquid holdup at station 3. The results show that experimental liquid holdup decreases from 0.569 to 0.303, while from the predictions of simplified transient model, liquid holdup decreases from 0.634 to 0.237. Olga prediction decreases from 0.627 to 0.258.

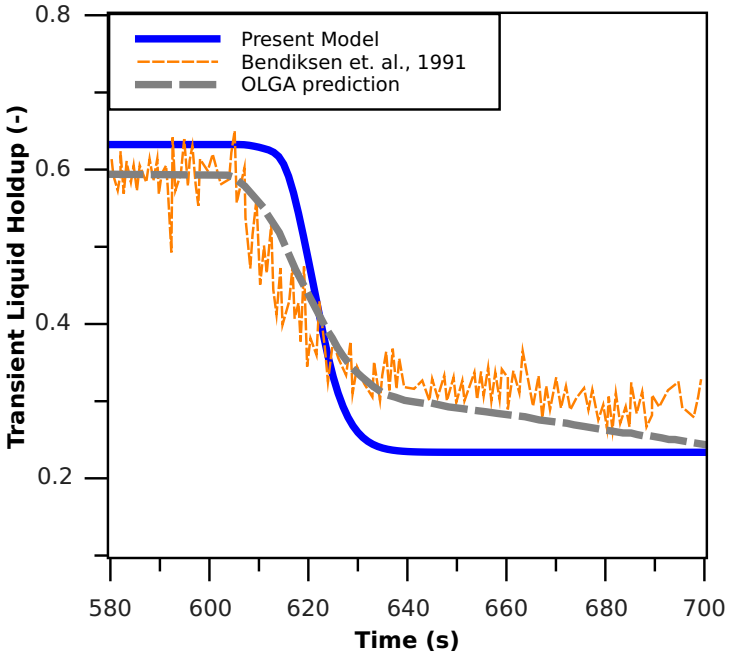

Figure 5.9 – Simplified transient model compared with experimental data of Bendiksen et al. (1991). Liquid holdup at station 2.

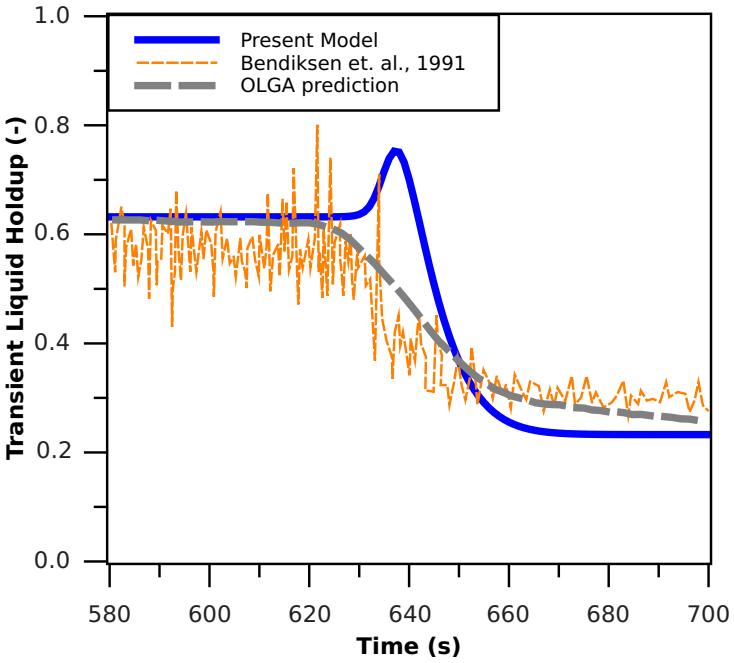

Figure 5.10 – Simplified transient model compared with experimental data of Bendiksen et al. (1991). Liquid holdup at station 3.

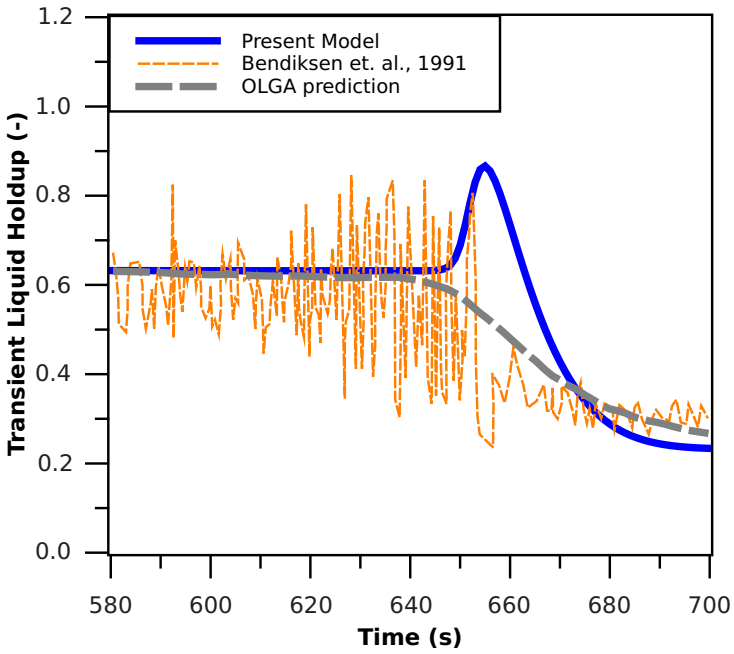

Figure 5.11 – Simplified transient model compared with experimental data of Bendiksen et al. (1991). Liquid holdup at station 4.

Liquid hoildup at stations 4, 5 and 6

Figure (5.11) shows experimental data and model predictions of liquid holdup at station 4. The results show that experimental liquid holdup decreases from 0.576 to 0.321, while from the simplified transient model, liquid holdup decreases from 0.633 to 0.244. Olga prediction decreases from 0.630 to 0.270.

Figure (5.12) shows experimental data and model predictions of liquid holdup at station 5. The results show that experimental liquid holdup decreases from 0.529 to 0.214, while from the simplified transient model, liquid holdup decreases from 0.613 to 0.391. Olga prediction decreases from 0.534 to 0.269.

Figure (5.13) shows experimental data and model predictions of liquid holdup at station 6. The results show that experimental liquid holdup decreases from 0.515 to 0.197, while from the simplified transient model, liquid holdup decreases from 0.612 to 0.428. Olga prediction decreases from 0.525 to 0.284.

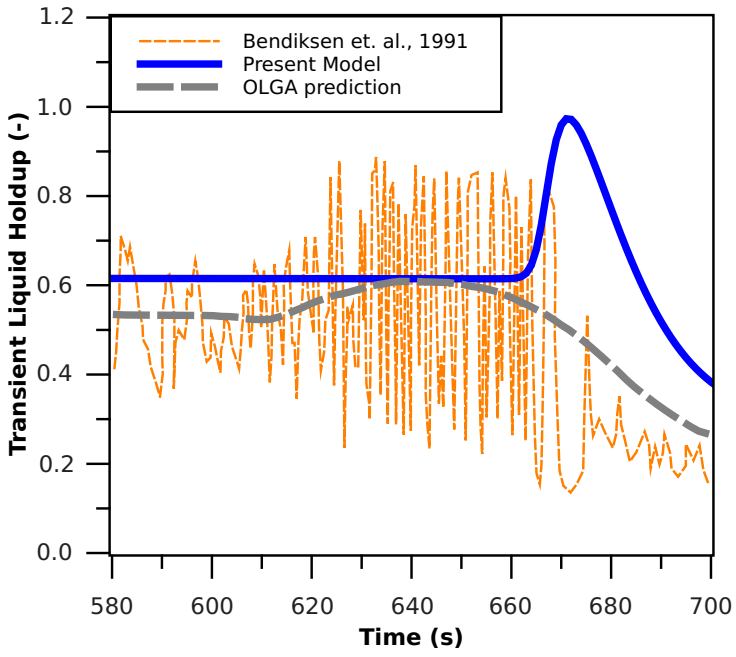

Figure 5.12 – Simplified transient model compared with experimental data of Bendiksen et al. (1991). Liquid holdup at station 5.

Pressure at stations 1, 7 and 8

Figure (5.14) shows experimental data and model predictions of absolute pressure at station 1. The figure shows that experimental absolute pressure decreases from 64.50 *bar* to 64.14 *bar*, while from the simplified transient model, absolute pressure

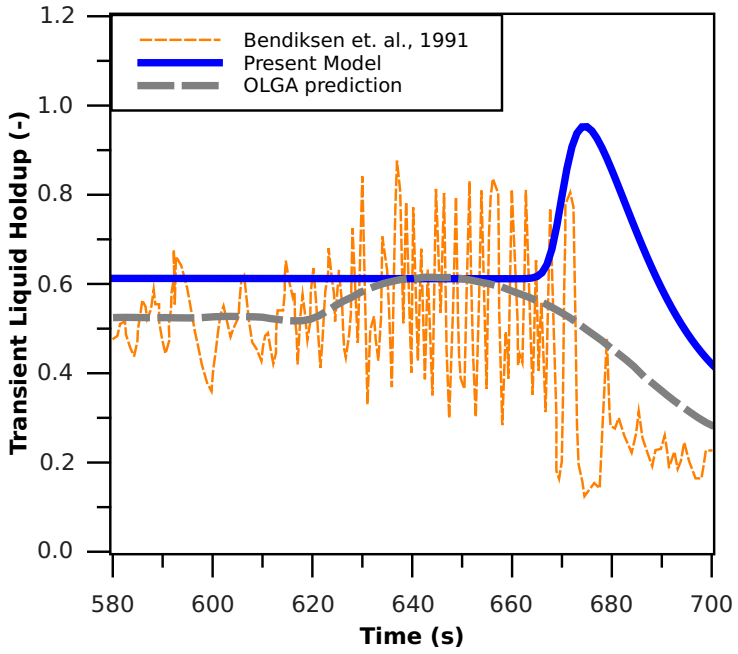

Figure 5.13 – Simplified transient model compared with experimental data of Bendiksen et al. (1991). Liquid holdup at station 6.

decreases from 64.42 *bar* to 64.00 *bar*. Olga prediction decreases from 64.41 *bar* to 64.14 *bar*.

Figure (5.15) shows experimental data and model predictions of pressure difference at station 7. The results show that experimental pressure difference decreases from -0.053 *bar* to -0.377 *bar*, while from the simplified transient model, pressure difference decreases from -0.071 *bar* to -0.263 *bar*. Olga prediction decreases from -0.097 *bar* to -0.454 *bar*.

Figure (5.16) shows experimental data and model predictions of pressure difference at station 8. The figure shows that experimental pressure difference decreases from 28.860 m to 16.126 m, while from the simplified transient model, pressure difference decreases from 29.646 m to 20.803 m. Olga prediction decreases from 28.51 m to 14.60 m.

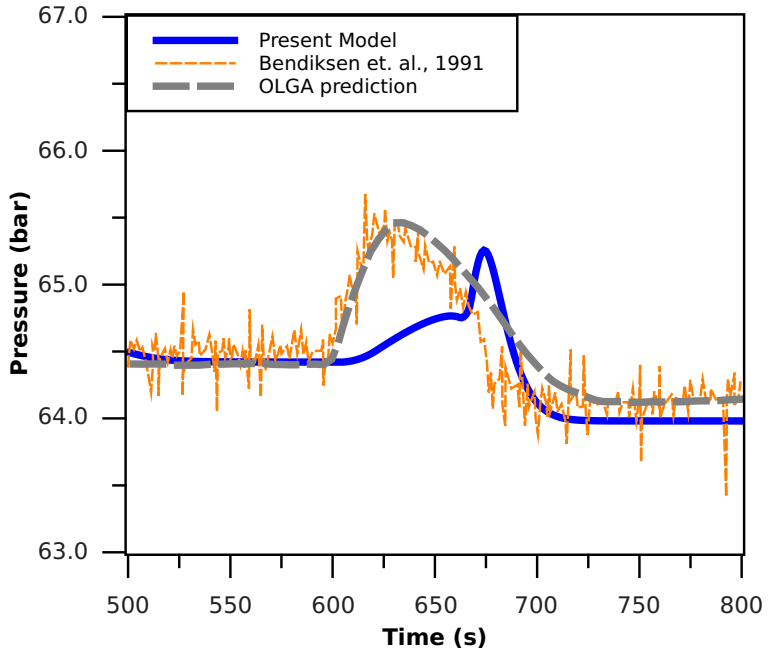

Figure 5.14 – Simplified transient model compared with experimental data of Bendiksen et al. (1991). Absolute pressure at station 1.

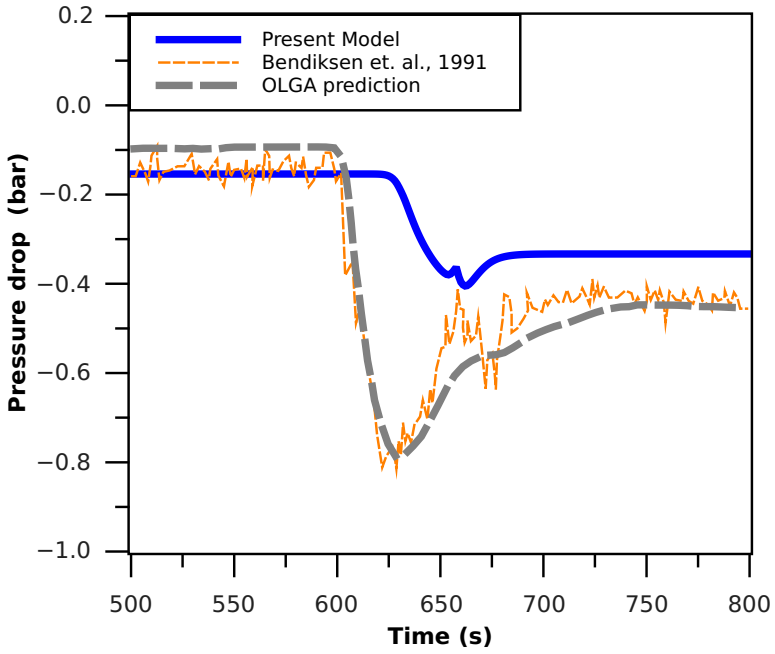

Figure 5.15 – Simplified transient model compared with experimental data of Bendiksen et al. (1991). Pressure difference at station 7.

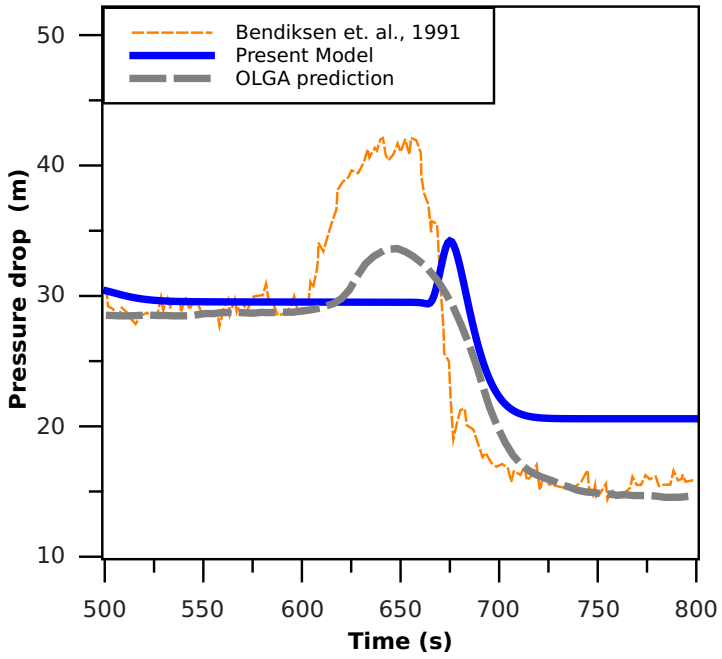

Figure 5.16 – Simplified transient model compared with experimental data of Bendiksen et al. (1991). Pressure difference at station 8.

5.4.2 Simplified model results: data of Vigneron et al.

Definitions of stations 1 and 2 are given in table (5.3). Number of nodes is 42.

Pressure results for tests 1-A, 1-D, and 2-D

Figure (5.17) shows experimental data and simplified transient model predictions of pressure at station 1 for test 1-A. The figure shows that experimental pressure increases from $161,733.33\ Pa$ to $181,517.39\ Pa$, while from the simplified transient model, pressure increases from $175,289.91\ Pa$ to $212,924.25\ Pa$. Olga prediction increases from $169,898\ Pa$ to $192,991\ Pa$.

Figure (5.18) shows experimental data and model predictions of pressure difference at station 1 for test 1-D. The figure shows that experimental pressure decreases from $219,643.89\ Pa$ to $191,430.08\ Pa$, while from the simplified transient model, pressure difference decreases from $263,282.79\ Pa$ to $208,317.36\ Pa$. Olga prediction decreases from $230,887\ Pa$ to $192,977\ Pa$.

Figure (5.19) shows experimental data and model predictions of pressure at station 1 for test 2-D. The results show that experimental pressure increases from $212,735.00\ Pa$ to $324,077.10\ Pa$, while from the simplified transient model, pressure difference increases from $254,500.15\ Pa$ to $608,677.14\ Pa$. Olga prediction increases from $220,235.49\ Pa$ to $388,679.39\ Pa$.

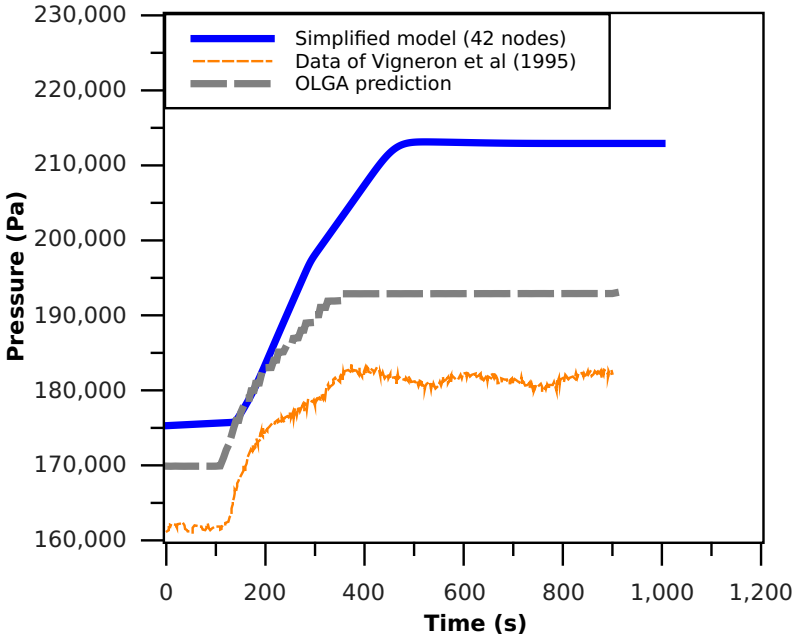

Figure 5.17 – Simplified transient model compared with experimental data of Vigneron et al. (1995). Pressure result for Test 1-A.

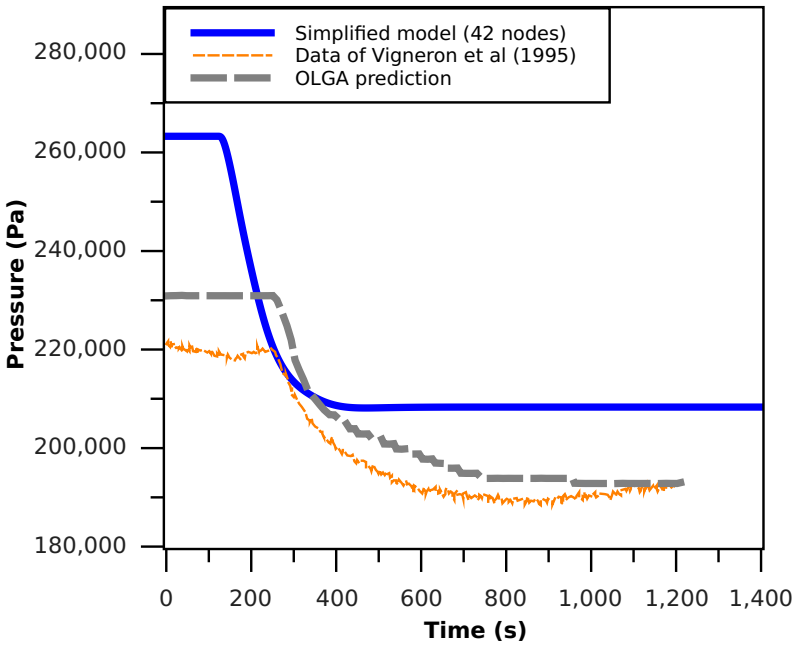

Figure 5.18 – Simplified transient model compared with experimental data of Vigneron et al. (1995). Pressure result for Test 1-D.

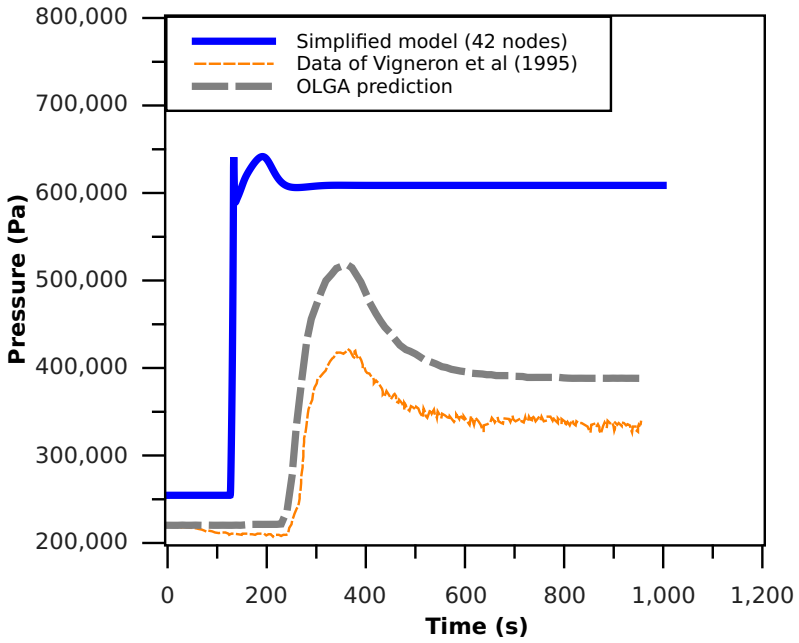

Figure 5.19 – Simplified transient model compared with experimental data of Vigneron et al. (1995). Pressure result for Test 2-D.

Liquid holdup results for tests 1-A, 1-D, and 2-D

Figure (5.20) shows experimental data and model predictions of liquid holdup at station 1 for test 1-A. The results show that experimental liquid holdup increases from 0.40 to 0.60, while from the simplified transient model, liquid holdup increases from 0.23 to 0.39. Olga prediction increases from 0.335 to 0.474.

Figure (5.21) shows experimental data and model predictions of liquid holdup at station 1 for test 1-D. The results show that experimental liquid holdup decreases from 0.60 to 0.45, while from the simplified transient model, liquid holdup decreases from 0.47 to 0.40. Olga prediction decreases from 0.590 to 0.454.

Figure (5.22) shows experimental data and model predictions of liquid holdup at station 1 for test 2-D. The results show that experimental liquid holdup decreases from 0.40 to 0.20, while from the simplified transient model, liquid holdup decreases from 0.32 to 0.15. Olga prediction decreases from 0.327 to 0.131.

Predictions of proposed simplified transient liquid-gas pipe flow model for the complete data of Vigneron et al. are given in figures (D.1 - D.16) (refer to appendix (D.2)).

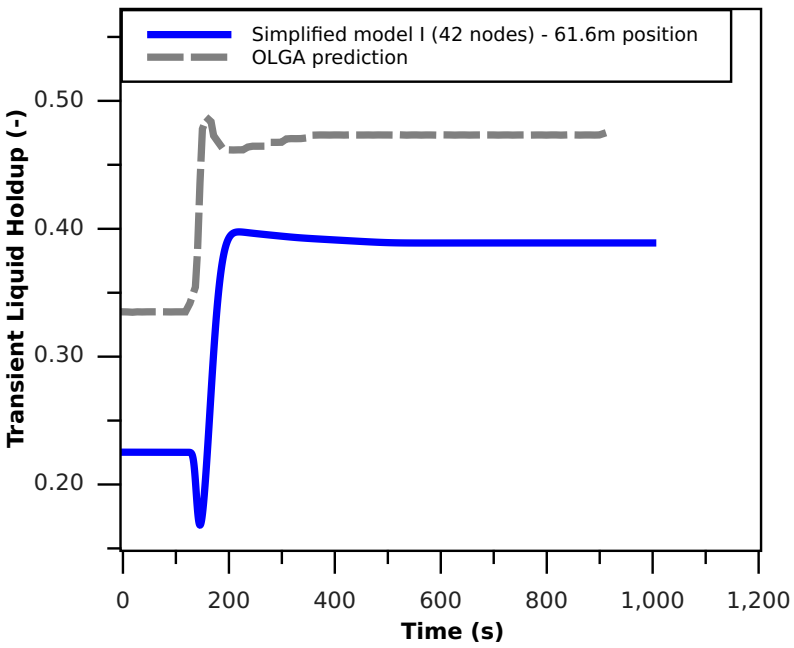

Figure 5.20 – Simplified transient model. Liquid holdup result for Test 1-A.

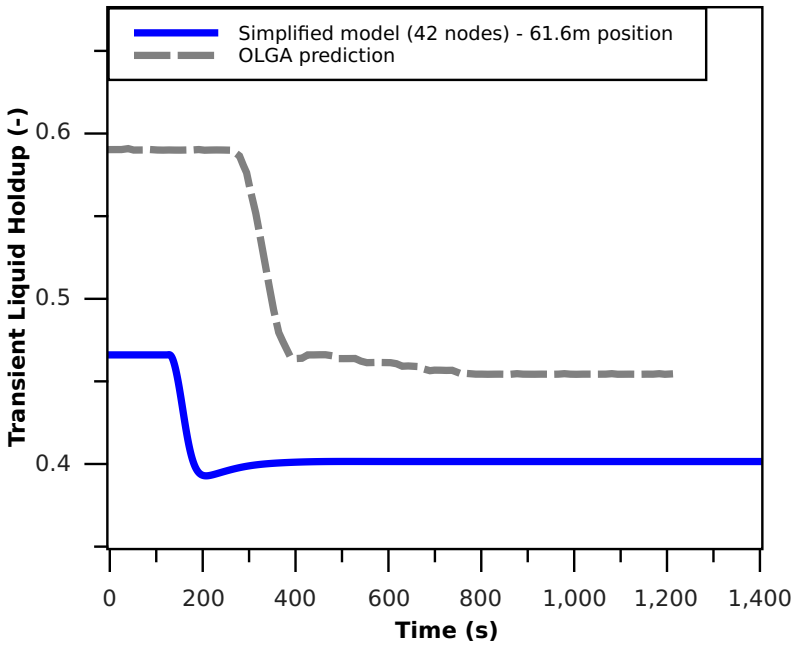

Figure 5.21 – Simplified transient model. Liquid holdup result for Test 1-D.

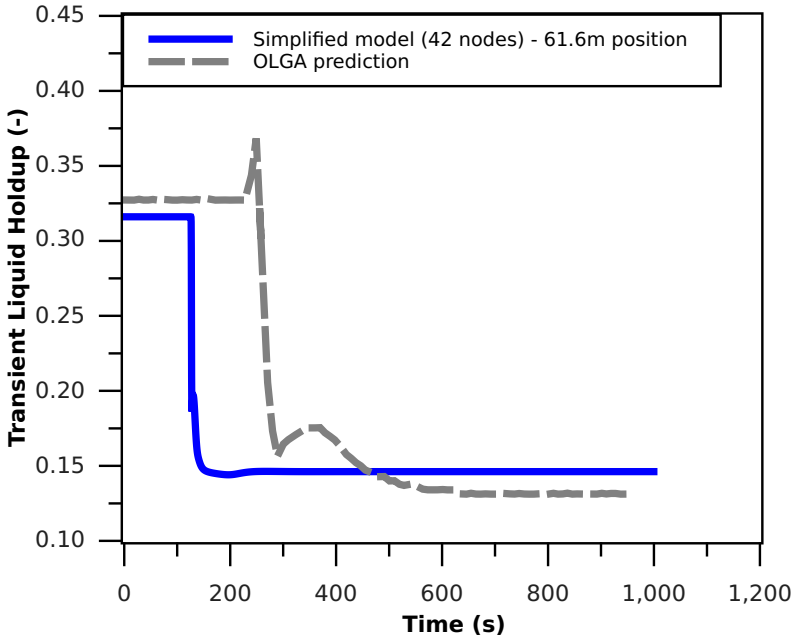

Figure 5.22 – Simplified transient model. Liquid holdup result for Test 2-D.

5.5 Discussion

Validation of steady state pressure gradient models of García et al. (2003) and Shoham (2005) shows

5.5.1 Transient data of Bendiksen et al. (1991)

Although the simplified transient two-phase model, proposed in this study, predicts liquid holdup and pressure profile with similar trends as the experimental data of Bendiksen et al. (1991), however, the responses of proposed model is slower than experimental observation. This can be explained by considering: (a) rate of flow change, and (b) coupling of the two phases. These two conditions are inter-linked. Gradual flow rate change as well as uncoupled two-phase flow leads to delayed responses. Nevertheless, proposed transient model gives approximate result to the experimental observations; with maximum absolute error of 0.22% (in figure (5.14)) and 81% (in figure (5.13)) for pressure and liquid holdup predictions respectively. Olga, on the other hand, gives better pressure gradient and liquid holdup predictions of transient experimental data (Bendiksen et al., 1991) compared with proposed simplified transient liquid-gas pipe flow model; with lower maximum absolute error of 0.14% (in figure (5.14)) and 44% (in figure (5.13)) for pressure and liquid holdup predictions respectively. This can be attributed to Olga utilising coupled interactions between liquid-gas flow rates and pressure in the conservation equations.

5.5.2 Transient data of Vigneron et al. (1995)

Similar to the experimental data of Bendiksen et al. (1991), the proposed simplified transient two-phase model gives similar trends as experimental data of Vigneron et al. (1995); with maximum absolute error of 73.22% (figure (5.19)) and 44.3% (figure (5.20)) for pressure and liquid holdup predictions respectively. However, the responses are different for the following reasons. Since the assumptions made in the proposed model neglect two-phase coupling, in addition to fast flow variation in the experiment of Vigneron et al. (1995), responses are: (a) faster for large flow variations, and (b) similar for moderate for flow variations. Detailed evaluation of the effect of flow variation on flow responses has not been taken into account in this study. Similar to subsection (5.5.1), Olga gives better pressure gradient and liquid holdup predictions of transient experimental data (Vigneron et al., 1995) compared with proposed simplified transient liquid-gas pipe flow model; with maximum absolute error of 19.94% (figure (5.19)) and 34.5% (figure (5.22)) for pressure and liquid holdup predictions respectively.

Chapter 6

Conclusions

Multiphase flow is a complex flow occurrence in engineering application found in major industrial fields, such as petroleum, chemical, geothermal, and space industries. The complex nature of multiphase flow makes the design of multiphase-flow-dependent engineering applications challenging; analytical solutions are generally not available. Nevertheless, several pioneering research studies led to the development of methods for predicting critical multiphase pipe flow variables, namely: pressure profile, and liquid holdup. These pioneering methods are however limited in accuracy Shoham (2005). Requirements for improved prediction methods led to the development of flow-regime-dependent mechanistic models.

Although flow-regime-dependent mechanistic models give better predictions than the pioneering multiphase prediction methods (Govier and Aziz, 1972; Brill, 1987; Shoham, 2005), however, mechanistic models are limited because of their subjective solution procedure which requires: (a) to first determine the prevalent flow regime, (b) then apply flow-regime-dependent mechanistic model to find pressure gradient and/or liquid holdup.

Transient analysis is also a major requirement, particularly for the design of multiphase separator, slug catcher, and pipeline fatigue design. However, analytical solution to conservation equations (i.e. Navier-Stokes equations) of multiphase flow are difficult and practically non-existence for most flow scenarios (such as non-homogeneous two-phase flow in flowlines with complex configurations). Instead, numerical solutions are often sort with significant success records. But numerical methods are generally computationally intensive. This limitation motivated the development of simplified transient two-phase models (Li, 2011; Shoham, 2005). However, these simplified transient models assume complete quasi-steady state condition for momentum equations of the phases.

Based on the limitations identified in: (a) existing flow-regime-dependent two-phase mechanistic pressure gradient model, and (b) simplified transient two-phase model with complete quasi-steady-state condition for momentum equations of the phases, the aim of this study is to develop steady-state and transient models for accurate prediction of multiphase/two-phase flow in flowlines. The objectives of this study have been given in subsection (1.3).

6.1 Flow regime

In order to achieve the first objective, a unified flow regime model is proposed. The proposed model is a combination of new flow regime transition criteria, and modifications of existing flow regime transition criteria. The new flow regime transition criteria include transition to/flow: (a) intermittent from/to dispersed-bubble flow, and (b) mist from/to annular or stratified flow. Improvement is made to existing stratified to annular (or non-stratified) transition criterion of Taitel and Dukler (1976b); this is accomplished by replacing $\widetilde{h}_L$ with H_L.

Application of new unified flow regime model shows that:

- improved predictions are achieved by modified stratified to annular criteria when compared with the original criteria of Taitel and Dukler (1976b). This improvement has been validated using previously published flow regime maps, models and experimental data
- the proposed unified flow regime model predicts flow regime transitions with pipe inclination angle, without discontinuities
- proposed plug identification criteria predict the existence of plug flow, with the possibility of varying prediction accuracy by changing the value of critical void fraction which is the threshold for the existence of plug flow
- proposed mist identification criterion have been validated using experimental data

However, application of proposed unified flow regime model to flow domains (flow rates, fluid properties, and pipe geometry) different from those of Asante (2000) and França and Lahey (1992) should be carried out with caution.

6.2 SETM model

The second objective is achieved by modifications and subsequent application of two-phase steady-state momentum equations, Taitel and Dukler flow regime transition

mechanism, and Kutateladze criterion for existence of annular flow, to achieve the Single Equation Two-Phase Mechanistic (SETM) model. SETM has the following features:

- Contrary to conventional methods in existing two-phase mechanistic pressure gradient models, flow regimes are not calculated prior to calculating pressure gradient. Flow regimes and pressure gradient are determined implicitly,
- Liquid entrainment is not taken into consideration for stratified and annular flows,
- New flow regime transition boundaries and mechanisms are incorporated,
- prior knowledge of liquid holdup is assumed, and
- Depending on the flow rates of gas and liquid phases, pressure gradient equation adapts to appropriate form for prevailing flow regime

Application of SETM shows that:

- pressure gradient predictions can be achieved for slug, stratified, annular/mist flow, with reasonable degree of accuracy when compared with experimental data and flow-regime-specific mechanistic model
- pressure gradient and flow regime of two-phase pipe flow can be simultaneously determined

However, the assumptions (namely: negligible liquid entrainment, simple liquid holdup algorithm for different flow regimes, and liquid holdup algorithm is limited to horizontal flow) made in the development of SETM may limit prediction accuracy of the model. Hence, application of SETM should be done with caution.

6.3 Modified homogeneous model

The first half of the third objective is achieved by applying two correction factors to the general homogeneous two-phase pressure gradient model. Previous studies show that homogeneous pressure gradient model is limited in predicting pressure gradient due to non-homogeneity of two-phase flows, and in-accurate liquid holdup model. The liquid holdup model of Choi et al. (2012) is applied in the study. Although H_L model of Choi et al. (2012) is applicable to all flow regimes, this model erroneously give $H_L \to 1$ at low gas flow rates irrespective the value of liquid flow rate. The modifications made to general homogeneous model did not specifically correct H_L of Choi et al. (2012), however, application of correction factors aims at improving

pressure gradient prediction accuracy.

Application of the two correction factors to the general homogeneous pressure gradient liquid-gas pipe flow model, gives two modified homogeneous pressure gradient models (referred to as HM1 and HM2). Validation of HM1 and HM2, using experimental data, shows that the two modified models can predict, with reasonable degree accuracy, pressure gradient for slug, stratified, and annular/mist flows.

Proposed homogeneous pressure gradient liquid-gas pipe flow models may give erroneous predictions if applied to flow domains (flow rates, fluid properties, and pipe geometry) outside those from which the models are derived.

6.4 Modified H_L model

The second half of the third objective is accomplished by applying a correction factor to H_L model of Choi et al. (2012). The original H_L model of Choi et al. (2012) over-predicts experimental data. Therefore, a correction factor is derived aimed at correcting this limitation, thus achieving a modified H_L model of Choi et al. (2012). This modified model is validated using experimental data, particularly for stratified and annular/mist flows.

However, prediction error may result in the application of modified liquid holdup of Choi et al. (2012), if applied to flow domain or conditions outside those of Asante (2000).

6.5 Transient model

The fourth objective is achieved by simplifying two-phase conservations (i.e. Navier-Stokes equations). This simplification include the following modifications:

- The two fluids are considered to be incompressible
- Flow rates are defined in terms of superficial velocities
- Steady-state pressure gradient is applied
- Single pressure model applies for the two fluids
- The phase fraction of the lighter phase (typically gas) is expressed as a function of the phase fraction of the heavier phase

- Two dimensionless terms are introduced into combined two-fluid continuity equation (refer to equation (5.11)). The first dimensionless term is the ratio of transient liquid holdup to steady-state liquid holdup (refer to first part of equation (5.10)). The second dimensionless term is the ratio of transient gas fraction to steady-state gas fraction (refer to second part of equation (5.10)). Theoretically, the two dimensionless terms in equation (5.10) should converge to unity after transient simulations stabilise to steady-state conditions

Therefore, the final form of the proposed simplified transient two-phase model consists of:

- combined continuity equation of gas and liquid
- simplified gas momentum - only convective term is taken into account
- simplified liquid momentum - only convective term is considered

These three equations are consequently solved numerically for transient liquid holdup (α_L), gas superficial velocity (U_{SG}), and liquid superficial velocity (U_{SL}). Thereafter, U_{SG} and U_{SL} are used to solve steady-state pressure gradient models.

The proposed simplified transient two-phase model is compared with experimental data. The results show that the proposed model follows similar trend as experimental data. However, the response of proposed transient model to flow changes vary, depending on rate of flow changes; this effect is particularly observed at high rate of gas flow changes. Although this observation can be attributed to uncoupled nature in the simplified model, however, the significance or effect of proposed simplified transient two-phase model on flow responses has not been taken into account.

Olga shows better predictions of experimental data of Bendiksen et al. (1991) and Vigneron et al. (1995), compared with proposed simplified transient liquid-gas pipe flow model. This can be attributed to Olga utilising coupled interactions between liquid-gas flow rates and pressure in the conservation equations.

Recommendations for future work

Unified flow regime model

- Further studies is required to account for the effect of diameter variation on the performance on unified flow regime model proposed in this study.
- Also, proposed unified flow regime model should be validated for downward inclined flow.
- Further experimental validation for the existence of (a) dispersed-bubble flow, and (b) mist flow is also required.
- expand experimental data used for deriving criteria for identifying mist and plug flows.

Mechanistic model

SETM model

- In order to improve prediction accuracy and application to wider flow systems, optimisation of calibration factors f^a and f^b, from equations (4.5) and (4.10) respectively, is required.
- Contribution of liquid entrainment to SETM model is required, especially for stratified-wavy and annular/mist flows.
- Furthermore, modified or improved H_L model is required, especially for wavy-stratified and annular/mist flows. The modified H_L model of Choi et al. (2012), developed in this study, can be applied to SETM model.
- improved SETM's flow regime predictions is required for stratified flow conditions: (a) $U_{SG} \to 0$, and (b) $(C_o V_M + U_D) \gg U_{SG}$.
- expand experimental data used for obtaining liquid holdup algorithm.

Modified homogeneous pressure gradient model

- Correction factors applied to general homogeneous two-phase pressure gradient model, as suggetsed in subsection (4.4), can be applied to mixture friction factor, f_M, to obtain f_M^{mod}. However, further studies is required to compare f_M^{mod} with experimental data.
- Further validation of SETM model is required for low-liquid flows (i.e. stratified-wavy and annular/mist flows) and dispersed-bubble flows.
- expand experimental data used for deriving correction factors for modified homogeneous pressure gradient liquid-gas pipe flow models.
- develop correction factors applicable to inclined flow.

Modified H_L model of Choi et al. (2012)

- The modified H_L model of Choi et al., proposed in this study, has only been validated for small diameter flow systems of air-water and air-oil. Further validation of the modified H_L model of Choi et al. is required for:
  - large pipe diameter flows, and
  - gas-oil-water flow system.
- expand experimental data used for deriving correction factors for modified liquid holdup model of Choi et al. (2012).
- develop correction factors applicable to inclined flow.

Transient model

- Improved coupling of simplified transient two-phase model is required in order to achieve accurate flow variation responses when compared with experimental data.
- Furthermore, detailed evaluation of the effect of flow variation on flow responses needs to be taken into account.
- Further studies is required to account for the effect of modification factors (equation (5.10)), introduced in combined continuity equation (5.11), on prediction accuarcy of proposed simplified transient two-phase pipe flow model.

Bibliography

Ahn, T.-H., Yun, B.-J., and Jeong, J.-J. (2015). Void fraction prediction for separated flows in the nearly horizontal tubes. *Nuclear Engineering and Technology*, 47(6):669–677.

AI-Sheikh, J. N., Saunder, D. E., and Brodkey, R. S. (1970). Prediction of Flow Patterns in Horizontal Two-Phase Pipe Flow. *Can. J. of Chemical Eng.*, 48:21–29.

Ali, S. F. (2009). *Two Phase Flow In Large Diameter Vertical Riser*. PhD thesis, Cranfield University.

Ali, S. F. and Yeung, H. (2014). Two-phase flow patterns in large diameter vertical pipes. *Asia-Pacific Journal of Chemical Engineering*, 9(1):105–116.

Alves, I., Caetano, E., K., M., and Shoham, O. (1991). Modelling Annular Flow Behaviour for Gas Wells. In *1988 ASME Annual Meeting*, page 435, Chicago. SPEPE.

Asante, B. (2000). *Multiphase Transport of gas and Low Loads of Liquids in Pipelines*. Phd thesis, University of Calgary.

Azevedo, G. R., Baliño, J. L., and Burr, K. P. (2017). Influence of pipeline modeling in stability analysis for severe slugging. *Chemical Engineering Science*, 161:1–13.

Aziz, K., Govier, G., and Fogarasi, M. (1972). Pressure Drop in Wells Producing Oil and Gas. *Journal of Canadian Petroleum Technology*, 38.

Badie, S., Hale, C., Lawrence, C., and Hewitt, G. (2000). Pressure gradient and holdup in horizontal two-phase gas–liquid flows with low liquid loading. *International Journal of Multiphase Flow*, 26(9):1525–1543.

Baker, O. (1954). Design for Simultaneous Flow of Oil and Gas. *The Oil and Gas Journal*, 53:185–192.

Banafi, A. and Talaie, M. b. (2015). A new mechanistic model to predict gas-liquid interface shape of gas-liquid flow through pipes with low liquid loading. *AIChE Journal*, 61(3):1043–1053.

Barnea, D. (1987). A Unified Model for Predicting Flow-Pattern Trasitions for the Whole Range of Pipe Inclinations. *Int. J. Multiphase Flow*, 13(1):1–12.

Barnea, D., Shoham, O., Taitel, Y., and a.E. Dukler (1980). Flow pattern transition for gas-liquid flow in horizontal and inclined pipes. Comparison of experimental data with theory. *International Journal of Multiphase Flow*, 6(3):217–225.

Barnea, D., Shoham, O., Taitel, Y., and Dukler, A. E. (1985). Gas-liquid flow in inclined tubes: Flow pattern transitions for upward flow. *Chemical Engineering Science*, 40(1):131–136.

Bassani, C., Barbuto, F., Sum, A., and Morales, R. (2017). Modeling the effects of hydrate wall deposition on slug flow hydrodynamics and heat transfer. *Applied Thermal Engineering*, 114:245–254.

Beggs, D. and Brill, J. (1973). A Study of Two-Phase Flow in Inclined Pipes. *Journal of Petroleum Technology*, 25(5):607–617.

Bell, I. H., Wronski, J., Quoilin, S., and Lemort, V. (2014). Pure and pseudo-pure fluid thermophysical property evaluation and the open-source thermophysical property library coolprop. *Industrial and Engineering Chemistry Research*, 53(6):2498–2508.

Belt, R., Djoric, B., Kalali, S., Duret, E., and Larrey, D. (2011). Comparison of commercial multiphase flow simulators with experimental and field databases. *15th International Conference on Multiphase Production Technology*, pages 413–427.

Bendiksen, K., Brandt, I., Fuchs, P., Linga, H., D., M., and Moe, R. (1986). Two-Phase Flow Research at SINTEF and IFE: Some Experimental Results and a Demonstration of the Dynamic Two-Phase Flow Simulator OLGA. In *1986 Offshore Northern Seas Conference*, Stavanger.

Bendiksen, K., Maines, D., Moe, R., and Nuland, S. (1991). The Dynamic Two-Fluid Model OLGA: Theory and Application. *SPE Production Engineering*, 6(May):171 – 180.

Bergelin, O. and Gazley, C. J. (1949). Co-Current Gas-Liquid Flow 1. Flow in Horizontal Tubes. *Proc. Heat Transfer Fluid Mech. Inst.*, pages 5–18.

Black, P., Daniels, L., Hoyle, N., and Jepson, W. (1990). Studying transient multiphase flow using the Pipeline Analysis Code (PLAC). *Journal of Energy Resources Technology*, 112:25–29.

Bonnecaze, R., Eriskine, W. J., and Greskovich, E. (1971). Holdup and Pressure Drop for Two-Phase Slug Flow in Inclined Pipes. *AIChE Journal*, 17:1109.

Bratland, O. (2010). Pipe Flow 2: Multiphase Flow Assurance. Bratland.

Brauner, N., Moalem Maron, D., and Rovinsky, J. (1998). A two-fluid model for stratified flows with curved interfaces. *International Journal of Multiphase Flow*, 24(6):975–1004.

Brill, J. P. (1987). *Multiphase Flow in Wells*, volume 39. Henry L. Doherty Memorial Fund of AIME, Society of Petroleum Engineers Incorporated.

Brooks, C. S., Hibiki, T., and Ishii, M. (2012). Interfacial drag force in one-dimensional two-fluid model. *Progress in Nuclear Energy*, 61:57–68.

Cazarez-Candia, O. d., Benítez-Centeno, O., and Espinosa-Paredes, G. (2011). Two-fluid model for transient analysis of slug flow in oil wells. *International Journal of Heat and Fluid Flow*, 32(3):762–770.

Chen, X. T., Cai, X. D., and Brill, J. B. (1997). Gas-Liquid Stratified-Wavy Flow in Horizontal Pipelines. *Journal of Energy Resources Technology*, 119:209–216.

Cheng, L., Ribatski, G., and Thome, J. R. (2008). Two-Phase Flow Patterns and Flow-Pattern Maps: Fundamentals and Applications. *Applied Mechanics Reviews*, 61(September 2008):050802.

Choi, J., Pereyra, E., Sarica, C., Lee, H., Jang, I. S., and Kang, J. (2013). Development of a fast transient simulator for gas-liquid two-phase flow in pipes. *Journal of Petroleum Science and Engineering*, 102:27–35.

Choi, J., Pereyra, E., Sarica, C., Park, C., and Kang, J. M. (2012). An efficient drift-flux closure relationship to estimate liquid holdups of gas-liquid two-phase flow in pipes. *Energies*, 5(12):5284–5306.

Collier, J. and Thome, J. (1994). *Convective boiling and condensation*. Oxford University Press, third edit edition.

Crowley, C. and Rothe, P. (1986). State-of-the-Art report on Multiphase Methods for Gas and Oil pipelines.

Cunliffe, R. (1978). Prediction of Condensate Flow Rate in Large Diameter High-Pressure Wet-Gas Pipelines. *APEA Journal*, 18:171.

Delhaye, J., Giot, M., and Riethmuller, M. (1981). *Thermal-hydraulics of two-phase systems for industrial design and nuclear engineering*. Hemisphere McGraw-Hill Press, New York.

Di Salvo, R. F. (2014). *Mechanistic Models to Simulate Slug Flow in Horizontal and Vertical Pipes Supervised by Dr Raad Issa*. PhD thesis, Imperial College London.

Dinh, T. N., Nourgaliev, R. R., and Theofanous, T. G. (2003). Understanding the ill-posed two-fluid model. In *10th international topical meeting on nuclear reactor thermal-hydraulics*, number 1971, pages 1–37.

Dukler, A. (1960). Fluid Mechanics and Heat Transfer in Vertical Falling-Film Systems. *Chemical Engineering Progress Symposium Series*, 56(30):1.

Dukler, A. E. and Hubbard, M. G. (1975). A Model for Gas-Liquid Slug Flow in Horizontal and Near Horizontal Tubes. *Industrial & Engineering Chemistry Fundamentals*, 14(4):337–347.

Dukler, E., Wicks, M. I., and Cleveland, R. (1964). Frictional Pressure Drop in Two-Phase Flow: An Approach Through Similarity Analysis. *AlChE Journal*, 10(1):44.

Duns, H. and Ros, N. (1963). Vertical Flow of Gas and Liquid Mixtures in Wells. In *Sixth World Petroleum Congress*, pages 451–465, Frankfurt, Germany.

Eaton, B., Andrews, D., Knowles, C., Silberberg, I., and Brown, K. (1967). The Prediction of Flow Patterns, Liquid Holdup and Pressure Losses Occurring During Continuous Two-Phase Flow in Horizontal Pipelines. *Journal of Petroleum Technology*, 815:240.

Felizola, H. and Shoham, O. (1995). A Unified Model for Slug Flow in Upward Inclined Pipes. *ASME. J. Energy Resour. Technol.*, 117(1):7–12.

Fernandes, R. C., Semiat, R., and Dukler, A. E. (1983). Hydrodynamic model for gas-liquid slug flow in vertical tubes. *Aiche Journal*, 29(6):981–989.

Flanigan, O. (1958). Effect of Uphill Flow on Pressure Drop in Design of Two-Phase gathering Systems. *Oil & Gas Journal*, 56:132.

França, F. and Lahey, R. T. (1992). The use of drift-flux techniques for the analysis of horizontal two-phase flows. *International Journal of Multiphase Flow*, 18(6):787–801.

García, F., García, R., Padrino, J. C., Mata, C., Trallero, J. L., and Joseph, D. D. (2003). Power law and composite power law friction factor correlations for laminar and turbulent gas-liquid flow in horizontal pipelines. *International Journal of Multiphase Flow*, 29(10):1605–1624.

Gorelik, D. and Brauner, N. (1999). The interface configuration in two-phase stratified pipe flows. *International Journal of Multiphase Flow*, 25(6-7):977–1007.

Gould, T. (1974). Vertical Two-Phase Stream Water Flow in Geothermal Wells. *Journal of Petroleum Technology*, page 883.

Gould, T., Tek, M., and Katz, D. (1974). Two-Phase Flow Through Vertical, Inclined or Curved Pipes. *Journal of Petroleum Technology*, 915:Trans., AIME 257.

Govier, G. W. and Aziz, K. (1972). *The Flow of Complex Mixtures in Pipes.* Van Nostrand Reinhold Co.

Govier, G. W. and Omer, M. M. (1962). The horizontal pipeline flow of air-water mixtures. *The Canadian Journal of Chemical Engineering*, 40(3):93–104.

Gregory, G. A., Nicholson, M. K., and Aziz, K. (1978). Correlation of the liquid volume fraction in the slug for horizontal gas-liquid slug flow. *International Journal of Multiphase Flow*, 4(1):33–39.

Hagedorn, A. and Brown, K. (1965). Experimental Study of Pressure Gradients occurring During Continuous Two-Phase Flow in Small-Diameter Vertical Conduits. *Journal of Petroleum Technology*, page 475.

Hamersma, P. J. and Hart, J. (1987). A pressure drop correlation for gas/liquid pipe flow with a small liquid holdup. *Chemical Engineering Science*, 42(5):1187–1196.

Harmathy, T. (1960). Velocity of Large Drops and Bubbles in Media of Infinite or Restricted Extent. *AIChE Journal*, 6:281.

Hart, J., Hamersma, P. J., and Fortuin, J. M. H. (1989). Correlations predicting frictional pressure drop and liquid holdup during horizontal gas-liquid pipe flow with a small liquid holdup. *International Journal of Multiphase Flow*, 15(6):947–964.

Hasan, A. and Kabir, C. (1988). A study of multiphase flow behavior in vertical wells. *SPE Production Engineering*, 3(May):263 – 272.

Hernandez, V. (2007). *Gas-liquid two-phase flow in inclined pipes.* PhD thesis, University of Nottingham.

Hewitt, G. (1961). Analysis of Annular Two-Phase Flow: Application of the Dukler Analysis to Vertical Upward Flow in a Tube. Technical report, UKAEA, Harwell, Oxon.

Hewitt, G. (1982). Flow regimes. In *Handbook of multiphase systems*. Hemisphere Publication Corporation, New York, hetsroni edition.

Hinze, J. (1955). Fundamentals of the Hydrodynamic Mechanism of Splitting in Dispersion Processes. *AlChE Journal*, 1:289.

Hoogendoorn, C. J. (1959). Gas-Liquid Flow in Horizontal Pipes. *Chemical Engineering Science*, 9:205–217.

Ishii, M. and Hibiki, T. (2014). *Thermo-Fluid Dynamics of Two-Phase Flow*. Springer New York.

Ishii, M. and Mishima, K. (1984). Two-fluid model and hydrodynamic constitutive relations. *Nuclear Engineering and Design*, 82(2-3):107–126.

Jepson, W. P. and Taylor, R. E. (1993). Slug Flow and its Transitions in Large Diameter Horizontal Pipes. *International Journal of Multiphase Flow*, 19(3):5–18.

Jerez-Carrizales, M., Jaramillo, J. E., and Fuentes, D. (2015). Prediction of Multiphase Flow in Pipelines: Literature Review. *Ingeniería y Ciencia*, 11(22):213–233.

Kadambi, V. (1982). Stability of annular flow in horizontal tubes. *International Journal of Multiphase Flow*, 8(4):311–328.

Kaichiro, M. and Ishii, M. (1984). Flow regime transition criteria for upward two-phase flow in vertical tubes. *International Journal of Heat and Mass Transfer*, 27(5):723–737.

Kelessidis, V. C. and Dukler, A. E. (1989). Modeling flow pattern transitions for upward gas-liquid flow in vertical concentric and eccentric annuli. *International Journal of Multiphase Flow*, 15(2):173–191.

Kislik, V. S. (2011). *Solvent Extraction: Classical and Novel Approaches*. Elsevier Science.

Kohda, K., Suzukawa, Y., and Furukawa, H. (1987). Analysis of Transient Gas-Liquid Two-Phase Flow in Pipelines. In *1987 ASME Pipeline Engineering Symposium, Annual ETCE*, Dallas.

Li, M. (2011). Transient Two-Phase Flow Modeling. In *Tulsa University Fluid Flow Projects, Seventy Sixth Semi-Annual Advisory Board Meeting Brochure and Presentation*, pages 241–340.

Lin, P. Y. and Hanratty, T. J. (1986). Prediction of the initiation of slugs with linear stability theory. *International Journal of Multiphase Flow*, 12(1):79–98.

Liu, Y., Difoggio, R., Sanderlin, K., Perez, L., and Zhao, J. (2011). Measurement of density and viscosity of dodecane and decane with a piezoelectric tuning fork over 298-448 K and 0.1-137.9 MPa. *Sensors and Actuators, A: Physical*, 167(2):347–353.

Loilier, P. (2006). *Numerical Simulation of Two-Phase Gas-Liquid Flows in Inclined and Vertical Pipelines*. PhD thesis, Cranfield University.

Lyons, W., Gary J Plisga, B. S., and Lorenz, M. (2015). *Standard Handbook of Petroleum and Natural Gas Engineering*. Elsevier Science.

Ma, Z. H., Qian, L., Causon, D. M., and Mingham, C. G. (2011). Simulation of solitary breaking waves using a two-fluid hybrid turbulence approach. In *Proceedings of the International Offshore and Polar Engineering Conference*, pages 231–237.

Mandhane, J. M., Gregory, G. A., and Aziz, K. (1974). A flow pattern map for gas-liquid flow in horizontal pipes. *Int. J. Multiphase Flow*, 1(4):537–553.

Mao, D. and Harvey, A. (2011). Transient Nonisothermal Multiphase Wellbore Model Development with Phase Change and its application to Insitu Producer Wells. Society of Petroleum Engineers.

Marcus, Y. (2002). *Solvent Mixtures: Properties and Selective Solvation*. Taylor & Francis.

Marruaz, K. S., Gonçalves, M. a. L., Ribeiro, G. S., França, F. a., and Rosa, E. S. (2001). Horizontal Slug Flow in a Large-Size Pipeline: Experimentation and Modeling. *Journal of the Brazilian Society of Mechanical Sciences*, 23(4):481–490.

Masella, J. M., Tran, Q., Ferre, D., and Pauchon, C. (1998). Transient simulation of two-phase flows in pipes. *Revue de L'Institut Français du Pétrole*, 53(6):801–811.

Matovu, F., Preisig, H., and Morud, J. (2014). DRIFT-FLUX MODELS. Technical report, NORWEGIAN UNIVERSITY OF SCIENCE AND TECHNOLOGY.

Matsubara, H. and Naito, K. (2011). Effect of liquid viscosity on flow patterns of gas-liquid two-phase flow in a horizontal pipe. *International Journal of Multiphase Flow*, 37(10):1277–1281.

Mccready, M. J. (1998). Demonstration of the effect of flow regime on pressure drop.

McQuillan, F., Culham, J., and Yovanovich, M. (1984a). Properties of Some Gases and Liquids at One Atmosphere (Ar, CO2,He, N2,H2 O(l)). Technical Report July, Microelectronics Heat Transfer Lab, University of Waterloo.

McQuillan, F. J., Culham, J. R., and Yovanovich, M. M. (1984b). Properties of Dry Air at One Atmosphere. Technical Report June, lectronics Heat Transfer Lab, University of Waterloo.

McQuillan, K. W. and Whalley, P. B. (1985). Flow patterns in vertical two-phase flow. *International Journal of Multiphase Flow*, 11(2):161–175.

Minami, K. and Shoham, O. (1994). Transient two-phase flow behavior in pipelines-experiment and modeling. *International Journal of Multiphase Flow*, 20(4):739–752.

Morales-Ruiz, S., Rigola, J., Rodriguez, I., and Oliva, A. (2012). Numerical resolution of the liquid–vapour two-phase flow by means of the two-fluid model and a pressure based method. *International Journal of Multiphase Flow*, 43:118–130.

Mukherjee, H. and Brill, J. P. (1985). Empirical equations to predict flow patterns in two-phase inclined flow. *International Journal of Multiphase Flow*, 11(3):299–315.

Ng, T. S., Lawrence, C. J., and Hewitt, G. F. (2001). Interface shapes for two-phase laminar stratified flow in a circular pipe. *International Journal of Multiphase Flow*, 27(7):1301–1311.

Nicholson, M. K., Aziz, K., and Gregory, G. A. (1978). Intermittent two phase flow in horizontal pipes: Predictive models. *The Canadian Journal of Chemical Engineering*, 56(6):653–663.

Oliemans, R., Pots, B., and Trompe, N. (1986). Modelling of Annular Dispersed Two-Phase Flow in Vertical Pipes. *International Journal of Multiphase Flow*, 12(5):711.

Orkiszewski, J. (1967). Predicting Two-Phase Pressure Drops in Vertical Pipes. *Journal of Petroleum Technology*, page 829.

Pauchon, C. and Banerjee, S. (1986). Interphase momentum interaction effects in the averaged multifield model. *International Journal of Multiphase Flow*, 12(4):559–573.

Pauchon, C., Dhulesia, H., Binh-Cirlot, G., and Fabre, J. (1994). TACITE: A transient tool for multiphase pipeline and well simulation. In *SPE Annual Technical Conference*, pages 25–28, New Orleans, LA, USA.

Pauchon, C., Dhulesia, H., Lopez, D., and Fabre, J. (1993). TACITE: A comprehensive mechanistic model for two-phase flow. In *6th International Conference on Multiphase Production*, Cannes, France.

Pompilio, R. (2013). *Experimental analysis of air-water two-phase flow in vertical large pipes and development of drift-flux models*. PhD thesis, Politecnico di Milano.

Prosperetti, A. and Tryggvason, G. (2007). *Computational Methods for Multiphase Flow*. Cambridge books online. Cambridge University Press.

Ransom, V. and Hicks, D. (1984). Hyperbolic two-pressure models for two-phase flow. *Journal of Computational Physics*, 53(1):124–151.

Rovinsky, J., Brauner, N., and Maron, D. M. (1997). Analytical solution for laminar two-phase flow in a fully eccentric core-annular configuration. *International Journal of Multiphase Flow*, 23(3):523–543.

Saurel, R. and Abgrall, R. (1999). A multiphase godunov method for compressible multifluid and multiphase flows. *Journal of Computational Physics*, 150:425–467.

Schlegel, J. P., Miwa, S., Chen, S., Hibiki, T., and Ishii, M. (2012). Experimental study of two-phase flow structure in large diameter pipes. *Experimental Thermal and Fluid Science*, 41:12–22.

Scoggins, M. J. (1977). *A Numerical Simulation Model for Transient Two-Phase Flow in a Pipeline*. PhD thesis, University of Tulsa.

Shirdel, M. and Sepehrnoori, K. (2012). Development of a transient mechanistic two-phase flow model for wellbores. *SPE Journal*, 17(3):942–955.

Shoham, O. (2005). *Mechanistic modeling og gas-liquid two-phase flow in pipes*. Society of Petroleum.

Singh, G. and Griffith, P. (1970). Determination of the Pressure Drop and Optimum Pipe Size for a Two-Phase Slug Flow in an Inclined Pipe. *Journal of Industrial Engineering*, pages Trans., ASME, 92, 717.

Smith, T. R., Schlegel, J. P., Hibiki, T., and Ishii, M. (2012). Two-phase flow structure in large diameter pipes. *International Journal of Heat and Fluid Flow*, 33(1):156–167.

Spedding, P. L. and Nguyen, V. T. (1976). Regime maps for air-water two-phase flow. *Chemical Engineering Science*, 35:779–793.

Stanislav, J., Kiokal, S., and Nicholson, M. (1986). Intermittent Gas-Liquid Flow in Upward inclined Pipes. *International Journal of Multiphase Flow*, 12:325.

Stuhmiller, J. (1977). The influence of interfacial pressure forces on the character of two-phase flow model equations. *International Journal of Multiphase Flow*, 3(6):551–560.

Sylvester, N. D. (1987). A Mechanistic Model for Two-Phase Vertical Slug Flow in Pipes. *Journal of Energy Resources Technology*, 109(4):206.

Taitel, Y. and Barnea, D. (1990). Two-Phase Slug Flow. *Advances in Heat Transfer*, 20(C):83–132.

Taitel, Y., Bornea, D., and Dukler, A. (1980). Modelling flow pattern transitions for steady upward gas-liquid flow in vertical tubes.

Taitel, Y. and Dukler, A. (1976a). A theoretical approach to the Lockhart-Martinelli correlation for stratified flow. *International Journal of Multiphase Flow*, 2(5-6):591–595.

Taitel, Y. and Dukler, A. E. (1976b). A model for predicting flow regime transitions in horizontal and near horizontal gas liquid flow. *AIChE Journal*, 22(1):47–55.

Taitel, Y., Shoham.O., and Brill, J. (1989). Simplified Transient Solution and Simulation of Two-Phase Flow in Pipelines. *Chemical Engineering Science*, 44(6):1353.

Talley, J., Kim, S., Mahaffy, J., Bajorek, S., and Tien, K. (2011). Implementation and evaluation of one-group interfacial area transport equation in TRACE. *Nuclear Engineering and Design*, 241(3):865–873.

Thome, J. R. (2006). Two-Phase Pressure Drops. In *Engineering Data Book III*. Wolverine Tube, Inc.

Thome, J. R. (2015). *Encyclopedia of Two-Phase Heat Transfer and Flow I: Fundamentals and Methods (A 4-Volume Set)*. World Scientific Publishing Company.

Tullius, L. (2000). *A Study Of Drag Reducing Agents in Multiphase Flow in Large Diameter Horizontal Pipelines*. PhD thesis, Ohio University.

Ullmann, A. and Brauner, N. (2006). Closure relations for two-fluid models for two-phase stratified smooth and stratified wavy flow. *International Journal of Multiphase Flow*, 32(1):82–105.

Van Der Meulen, G. P. (2012). *Churn-Annular Gas-Liquid Flows In Large Diameter Vertical Pipes*. PhD thesis, University of Nottingham.

Vigneron, F., Sarica, C., and Brill, J. (1995). Experimental analysis of imposed two-phase flow transients in horizontal pipelines. In *7th International Conference*, pages 199–217, Cannes, France.

Vo, D. and Shoham, O. (1989). A Note on the Existence of a Solution for Two-Phase Slug Flow in Vertical Pipes. *ASME. J. Energy Resour. Technol.*, 111(2):64–65.

Wallis, G. B. (1969). *One-dimensional Two-phase Flow*. McGraw-Hill.

Watson, M. (1990). Non-linear waves in pipeline two-phase flows. In *3rd Conference on Hyperbolic Problems*.

Weisman, J. and Kang, S. Y. (1981). Flow pattern transitions in vertical and upwardly inclined lines. *International Journal of Multiphase Flow*, 7(3):271–291.

Williams, M. C. (2009). *Fuel Cell Seminar 2008*. Number 1 in ECS transactions. Electrochemical Society.

Yao, S. and Sylvester, N. (1987). A Mechanistic Model for Two-Phase Annular Mist Flow in Verical pipes. *AlChE Journal*, 33:1008.

Zangana, M. H. S. (2011). *Film Behaviour of Vertical Gas-Liquid Flow in a Large Diameter Pipe*. PhD thesis, University of Nottingham.

Zhang, H.-Q., Wang, Q., Sarica, C., and Brill, J. P. (2003). Unified Model for Gas-Liquid Pipe Flow via Slug Dynamics—Part 2: Model Validation. *Journal of Energy Resources Technology*, 125(4):274.

Zhao, X. (2005). *Mechanistic-based models for slug flow in vertical pipes*. PhD thesis, Texas Tech University.

Zhao, Y., Yeung, H., Zorgani, E. E., Archibong, A. E., and Lao, L. (2013). High viscosity effects on characteristics of oil and gas two-phase flow in horizontal pipes. *Chemical Engineering Science*, 95:343–352.

Appendix A

Flow regime

A.1 Liquid holdup model

Stratified model of Taitel and Dukler (Taitel and Dukler, 1976a; Ahn et al., 2015) for liquid-gas pipe flow is expressed as liquid and gas momentum equations in equations (A.1) and (A.2) respectively.

$$-A_L\left(\frac{dP}{dL}\right)_L - \tau_{WL}S_L + \tau_I S_I - \rho_L A_L g\sin\theta = 0 \tag{A.1}$$

$$-A_G\left(\frac{dP}{dL}\right)_G - \tau_{WG}S_G - \tau_I S_I - \rho_G A_G g\sin\theta = 0 \tag{A.2}$$

Equations (A.1) and (A.2) are combined to give equation (A.3), which is subsequently solved for liquid film height (h_L). Thereafter, liquid holdup is calculated using equation (A.14).

$$\tau_{WG}\frac{S_G}{A_G} - \tau_{WL}\frac{S_L}{A_L} + \tau_I S_I\left(\frac{1}{A_L}+\frac{1}{A_G}\right) - (\rho_L-\rho_G)g\sin\theta = 0 \tag{A.3}$$

Geometric terms are defined as:

$$A_L = \frac{1}{4}D^2\left\{\pi - \cos^{-1}\left(2\frac{h_L}{D}-1\right) + \left(2\frac{h_L}{D}-1\right)\sqrt{1-\left(2\frac{h_L}{D}-1\right)^2}\right\} \tag{A.4}$$

$$A_G = \frac{1}{4}D^2\left\{\cos^{-1}\left(2\frac{h_L}{D}-1\right) - \left(2\frac{h_L}{D}-1\right)\sqrt{1-\left(2\frac{h_L}{D}-1\right)^2}\right\} \tag{A.5}$$

$$S_L = D\left\{\pi - \cos^{-1}\left(2\frac{h_L}{D}-1\right)\right\} \tag{A.6}$$

$$S_G = \pi D - S_L \tag{A.7}$$

$$S_I = D\sqrt{1 - \left(2\frac{h_L}{D} - 1\right)^2} \tag{A.8}$$

$$d_L = \frac{4A_L}{S_L} \tag{A.9}$$

$$d_G = \frac{4A_G}{(S_G + S_I)} \tag{A.10}$$

Additional terms are defined as:

$$\tau_{WL} = f_L \frac{\rho_L {U_L}^2}{2} \tag{A.11}$$

$$\tau_{WG} = f_G \frac{\rho_G {U_G}^2}{2} \tag{A.12}$$

$$\tau_I = f_I \frac{\rho_G (U_G - U_L)^2}{2} \tag{A.13}$$

$$H_L = \frac{A_L}{A} \tag{A.14}$$

Cross-sectional area of pipe is defined as:

$$A = \pi \frac{D^2}{4} \tag{A.15}$$

Appendix B

CoolProp^{TM} library

"CoolProp is a C++ library that implements:

- *Pure and pseudo-pure fluid equations of state and transport properties for 122 components*
- *Mixture properties using high-accuracy Helmholtz energy formulations*
- *Correlations of properties of incompressible fluids and brines*
- *Highest accuracy psychrometric routines*
- *User-friendly interface around the full capabilities of NIST REFPROP*
- *Cubic equations of state (SRK, PR)"*

Bell et al. (2014)

Procedure for using CoolProp C++ library

- Implementation of CoolProp in a C++ program only requires including header file **"CoolProp.h"**
- Add **"using namespace CoolProp"** before declaration of C++ **"Class"**
- Declare variables for fluid names (e.g. Density (D), Dynamic Viscosity (V), etc.) as **float** data type
- Declare variables for fluid properties (e.g. Air) as **string** data type
- Declare variables for fluid temperature (T) and pressure (P) as **float** data type, and initialise
- Call function **PropsSI(**"D","T",T,"P",P,Air**)** to get density (D) of Air at temperature (T) and pressure (P)

B.1 Validation of CoolProp

B.1.1 Validation of CoolProp for physical properties of Air

CoolProp^{TM} library is validated against the data of McQuillan et al. (1984b).

Table B.1 – Density of Air: CoolProp^{TM} compared with prediction models presented by McQuillan et al. (1984b)

Pressure $[Mpa]$	Temperature $[K]$	Density McQuillan et al. $[Kg/m^3]$	Density CoolProp^{TM} $[Kg/m^3]$	Relative Error [%]
0.101325	200.00	1.7686	1.7692	-0.03
0.101325	205.00	1.7252	1.7257	-0.02
0.101325	210.00	1.6840	1.6843	-0.02
0.101325	215.00	1.6446	1.6448	-0.01
0.101325	220.00	1.6071	1.6072	-0.01
0.101325	225.00	1.5712	1.5712	0.00
0.101325	230.00	1.5369	1.5369	0.00
0.101325	235.00	1.5041	1.5040	0.01
0.101325	240.00	1.4726	1.4725	0.01
0.101325	245.00	1.4424	1.4423	0.01
0.101325	250.00	1.4135	1.4133	0.01
0.101325	255.00	1.3857	1.3855	0.01
0.101325	260.00	1.3589	1.3587	0.01
0.101325	265.00	1.3332	1.3330	0.01
0.101325	270.00	1.3084	1.3082	0.01
0.101325	275.00	1.2845	1.2843	0.01
0.101325	280.00	1.2615	1.2613	0.01
0.101325	285.00	1.2393	1.2391	0.01
0.101325	290.00	1.2179	1.2177	0.01
0.101325	295.00	1.1971	1.1970	0.01
0.101325	300.00	1.1771	1.1770	0.01
0.101325	310.00	1.1390	1.1389	0.01
0.101325	320.00	1.1033	1.1033	0.01
0.101325	330.00	1.0698	1.0698	0.00
0.101325	340.00	1.0382	1.0382	0.00
0.101325	350.00	1.0085	1.0085	0.00
0.101325	360.00	0.9804	0.9805	-0.01
0.101325	370.00	0.9538	0.9539	-0.01
0.101325	380.00	0.9287	0.9288	-0.01
0.101325	390.00	0.9048	0.9050	-0.02
0.101325	400.00	0.8821	0.8823	-0.02

Table B.2 – Viscosity of Air: CoolProp^{TM} compared with prediction models presented by McQuillan et al. (1984b)

Pressure $[Mpa]$	Temperature $[K]$	Viscosity McQuillan et al. $[Pa.s]$	Viscosity CoolProp^{TM} $[Pa.s]$	Relative Error [%]
0.101325	200.00	13.352	13.334	0.14
0.101325	205.00	13.636	13.615	0.16
0.101325	210.00	13.916	13.893	0.17
0.101325	215.00	14.194	14.169	0.17
0.101325	220.00	14.468	14.443	0.18
0.101325	225.00	14.740	14.714	0.18
0.101325	230.00	15.010	14.983	0.18
0.101325	235.00	15.277	15.250	0.17
0.101325	240.00	15.541	15.515	0.17
0.101325	245.00	15.803	15.778	0.16
0.101325	250.00	16.062	16.038	0.15
0.101325	255.00	16.319	16.297	0.14
0.101325	260.00	16.574	16.553	0.13
0.101325	265.00	16.827	16.808	0.11
0.101325	270.00	17.077	17.060	0.10
0.101325	275.00	17.325	17.311	0.08
0.101325	280.00	17.571	17.560	0.06
0.101325	285.00	17.815	17.807	0.04
0.101325	290.00	18.056	18.052	0.02
0.101325	295.00	18.296	18.296	0.00
0.101325	300.00	18.534	18.537	-0.02
0.101325	310.00	19.004	19.016	-0.06
0.101325	320.00	19.466	19.488	-0.11
0.101325	330.00	19.922	19.954	-0.16
0.101325	340.00	20.370	20.413	-0.21
0.101325	350.00	20.812	20.867	-0.27
0.101325	360.00	21.247	21.315	-0.32
0.101325	370.00	21.677	21.758	-0.38
0.101325	380.00	22.100	22.196	-0.43
0.101325	390.00	22.518	22.628	-0.49
0.101325	400.00	22.930	23.055	-0.55

B.1.2 Validation of CoolProp for physical properties of Nitrogen

CoolProp^{TM} library is validated against the data of McQuillan et al. (1984a).

Table B.3 – Density of Nitrogen: CoolProp^{TM} compared with prediction models presented by McQuillan et al. (1984a)

Pressure $[Mpa]$	Temperature $[K]$	Density McQuillan et al. $[Kg/m^3]$	Density CoolProp^{TM} $[Kg/m^3]$	Relative Error [%]
0.101325	200.00	1.71021	1.71066	-0.03
0.101325	210.00	1.62841	1.62858	-0.01
0.101325	220.00	1.55408	1.55406	0.00
0.101325	230.00	1.48624	1.48609	0.01
0.101325	240.00	1.42408	1.42385	0.02
0.101325	250.00	1.36691	1.36664	0.02
0.101325	260.00	1.31415	1.31386	0.02
0.101325	270.00	1.26531	1.26502	0.02
0.101325	280.00	1.21997	1.21970	0.02
0.101325	290.00	1.17777	1.17752	0.02
0.101325	300.00	1.13839	1.13816	0.02
0.101325	310.00	1.10156	1.10136	0.02
0.101325	320.00	1.06704	1.06687	0.02
0.101325	330.00	1.03461	1.03448	0.01
0.101325	340.00	1.00410	1.00400	0.01
0.101325	350.00	0.97534	0.97527	0.01
0.101325	360.00	0.94817	0.94815	0.00
0.101325	370.00	0.92248	0.92249	0.00
0.101325	380.00	0.89815	0.89818	0.00
0.101325	390.00	0.87507	0.87513	-0.01
0.101325	400.00	0.85314	0.85323	-0.01

Table B.4 – Viscosity of Nitrogen: CoolProp^{TM} compared with prediction models presented by McQuillan et al. (1984a)

Pressure $[Mpa]$	Temperature $[K]$	Viscosity McQuillan et al. $[Pa.s]$	Viscosity CoolProp^{TM} $[Pa.s]$	Relative Error [%]
0.101325	200.00	12.8464	12.9110	0.99
0.101325	210.00	13.3921	13.4465	0.82
0.101325	220.00	13.9269	13.9728	-1.13
0.101325	230.00	14.4514	14.4902	0.10
0.101325	240.00	14.9659	14.9990	-0.70
0.101325	250.00	15.4710	15.4996	0.06
0.101325	260.00	15.9669	15.9923	4.38
0.101325	270.00	16.4541	16.4774	1.65
0.101325	280.00	16.9329	16.9552	-2.52
0.101325	290.00	17.4037	17.4260	4.95
0.101325	300.00	17.8667	17.8901	4.12
0.101325	310.00	18.3223	18.3476	0.48
0.101325	320.00	18.7708	18.7989	0.15
0.101325	330.00	19.2124	19.2442	-0.55
0.101325	340.00	19.6473	19.6836	2.52
0.101325	350.00	20.0759	20.1174	0.91
0.101325	360.00	20.4984	20.5457	0.99
0.101325	370.00	20.9149	20.9689	0.60
0.101325	380.00	21.3257	21.3869	0.91
0.101325	390.00	21.7310	21.8001	2.50
0.101325	400.00	22.1309	22.2085	7.46

B.1.3 Validation of CoolProp for physical properties of n-Dodecane

CoolProp^{TM} library is validated against the data of Liu et al. (2011).

Table B.5 – Density of n-Dodecane: CoolProp^{TM} compared with prediction models presented by Liu et al. (2011)

Pressure $[Mpa]$	Temperature $[K]$	Density Liu et al. $[Kg/m^3]$	Density CoolProp^{TM} $[Kg/m^3]$	Relative Error [%]
13.58	298.15	757.81	755.10	0.36
27.87	298.15	764.06	763.92	0.02
41.44	298.15	768.75	771.48	-0.36
55.02	298.15	775.00	778.42	-0.44
69.31	298.15	778.13	785.16	-0.90
82.88	298.15	781.25	791.12	-1.26
96.46	298.15	784.38	796.72	-1.57
110.03	298.15	789.06	802.01	-1.64
124.32	298.15	792.19	807.27	-1.90
137.90	298.15	793.75	812.01	-2.30
0.71	348.15	712.50	709.35	0.44
14.29	348.15	725.00	721.64	0.46
27.87	348.15	731.25	732.18	-0.13
41.44	348.15	737.50	741.47	-0.54
55.02	348.15	743.75	749.82	-0.82
69.31	348.15	750.00	757.82	-1.04
82.88	348.15	754.69	764.80	-1.34
96.46	348.15	757.81	771.29	-1.78
110.03	348.15	762.50	777.36	-1.95
123.61	348.15	767.19	783.36	-2.11
137.90	348.15	770.31	788.73	-2.39
13.58	398.15	690.63	687.28	0.48
27.87	398.15	701.56	701.36	0.03
41.44	398.15	709.38	712.72	-0.47
55.02	398.15	717.19	722.70	-0.77
69.31	398.15	725.00	732.10	-0.98
82.88	398.15	728.13	740.19	-1.66
96.46	398.15	734.38	747.62	-1.80
110.03	398.15	739.06	754.52	-2.09
124.32	398.15	743.75	761.28	-2.36
137.90	398.15	746.88	767.30	-2.73
14.29	448.15	654.69	654.09	0.09
27.87	448.15	668.75	670.96	-0.33
41.44	448.15	678.13	684.80	-0.98
55.02	448.15	689.06	696.64	-1.10
69.31	448.15	695.31	707.57	-1.76
82.88	448.15	703.13	716.85	-1.95
96.46	448.15	709.38	725.29	-2.24
110.03	448.15	714.06	733.05	-2.66
124.32	448.15	720.31	740.59	-2.82
137.90	448.15	723.44	747.27	-3.29

Table B.6 – Viscosity of n-Dodecane: CoolProp^{TM} compared with prediction models presented by McQuillan et al. (1984a)

Pressure $[Mpa]$	Temperature $[K]$	Viscosity Liu et al. $[Pa.s]$	Viscosity CoolProp^{TM} $[Pa.s]$	Relative Error [%]
13.58	298.15	1.61585	1.59978	0.99
27.87	298.15	1.89024	1.87477	0.82
41.44	298.15	2.13415	2.15824	-1.13
55.02	298.15	2.46951	2.46714	0.10
69.31	298.15	2.80488	2.82438	-0.70
82.88	298.15	3.20122	3.19929	0.06
96.46	298.15	3.78049	3.61473	4.38
110.03	298.15	4.14634	4.07773	1.65
123.61	298.15	4.51220	4.62602	-2.52
137.19	298.15	5.48780	5.21614	4.95
14.29	348.15	0.82317	0.78927	4.12
27.87	348.15	0.91463	0.91022	0.48
41.44	348.15	1.03659	1.03508	0.15
55.02	348.15	1.15854	1.16486	-0.55
69.31	348.15	1.34146	1.30771	2.52
82.88	348.15	1.46341	1.45015	0.91
96.46	348.15	1.61585	1.59990	0.99
110.03	348.15	1.76829	1.75773	0.60
124.32	348.15	1.95122	1.93349	0.91
137.90	348.15	2.16463	2.11052	2.50
13.58	398.15	0.51829	0.47962	7.46
27.87	398.15	0.54878	0.56040	-2.12
41.44	398.15	0.64024	0.63706	0.50
55.02	398.15	0.70122	0.71453	-1.90
69.31	398.15	0.82317	0.79757	3.11
82.88	398.15	0.91463	0.87831	3.97
96.46	398.15	0.97561	0.96117	1.48
110.03	398.15	1.06707	1.04644	1.93
123.61	398.15	1.15854	1.13905	1.68
137.90	398.15	1.28049	1.23000	3.94
14.29	448.15	0.27439	0.33107	-20.66
27.87	448.15	0.33537	0.38859	-15.87
41.44	448.15	0.39634	0.44431	-12.10
55.02	448.15	0.45732	0.49931	-9.18
69.31	448.15	0.51829	0.55709	-7.48
82.88	448.15	0.54878	0.61226	-11.57
96.46	448.15	0.60976	0.66798	-9.55
110.03	448.15	0.70122	0.72444	-3.31
124.32	448.15	0.76220	0.78484	-2.97
137.90	448.15	0.79268	0.84328	-6.38

Appendix C

Mechanistic model

C.1 Unified model

The unified two-phase pressure gradient model of Shoham (2005) is presented in this section. Four pressure gradient models are implemented, each for: stratified, annular, slug, and dispersed-bubble flow regime. Transition criteria for each flow regime has been provided by Shoham (2005).

The unified pressure gradient model takes a general form as shown in equation (C.1).

$$-\frac{dP}{dL} = \left(\frac{dP}{dL}\right)_{friction} + \left(\frac{dP}{dL}\right)_{gravity} \tag{C.1}$$

C.1.1 Stratified model

$$\tau_{WG}\frac{S_G}{A_G} - \tau_{WL}\frac{S_L}{A_L} + \tau_I S_I\left(\frac{1}{A_L} + \frac{1}{A_G}\right) - (\rho_L - \rho_G)g\sin\theta = 0 \tag{C.2}$$

$$-A_L\left(\frac{dP}{dL}\right)_L - \tau_{WL}S_L + \tau_I S_I - \rho_L A_L g\sin\theta = 0 \tag{C.3}$$

$$-A_G\left(\frac{dP}{dL}\right)_G - \tau_{WG}S_G - \tau_I S_I - \rho_G A_G g\sin\theta = 0 \tag{C.4}$$

Symbols: τ = shear stress, S = perimeter, A = cross-section area, ρ = density. Subscripts: W_G = gas-pipe wall interface, W_L = liquid-pipe wall interface, I = gas-liquid interface.

C.1.2 Annular model

$$-\tau_{WL}\frac{S_L}{A_F} + \tau_I S_I\left(\frac{1}{A_F} + \frac{1}{A_C}\right) - (\rho_L - \rho_C)g\sin\theta = 0 \tag{C.5}$$

$$-A_F\left(\frac{dP}{dL}\right)_F - \tau_{WL}S_L + \tau_I S_I - \rho_L A_F g\sin\theta = 0 \tag{C.6}$$

$$- A_C \left(\frac{dP}{dL}\right)_C - \tau_I S_I - \rho_G A_C g \sin\theta = 0 \tag{C.7}$$

Subscript: C = gas core which consist of gas phase and entrained liquid droplets.

C.1.3 Slug model

$$\tau_F \frac{S_F}{A_F} - \tau_G \frac{S_G}{A_G} - \tau_I S_I \left(\frac{1}{A_F} + \frac{1}{A_G}\right) + (\rho_L - \rho_G) g \sin\theta = 0 \tag{C.8}$$

$$- \left(\frac{dP}{dL}\right)_U = \left(\rho_S g \sin\theta + \frac{\tau_S \pi d}{A_P}\right)\frac{L_S}{L_U} + \left(\rho_F g \sin\theta + \frac{\tau_F S_F d}{A_P} + \frac{\tau_G S_G d}{A_P}\right)\frac{L_F}{L_U} \tag{C.9}$$

Symbol: L = length. Subscripts: S = slug body, F = liquid film region, U = slug unit, P = pipe cross-section.

C.1.4 Dispersed-bubble model

$$\lambda_L = \frac{U_{SL}}{U_{SG} + U_{SL}} \tag{C.10}$$

$$1.53\left[\frac{g(\rho_L - \rho_G)\sigma}{\rho_L^2}\right]^{0.25} (1-\alpha)^{0.5} sin\theta = \frac{U_{SG}}{\alpha} - 1.2\,(U_{SG} + U_{SL}) \tag{C.11}$$

$$-\frac{dP}{dL} = \rho_M g \sin\theta + \frac{\pi D}{A}\tau_{WM} \tag{C.12}$$

where,

$$\tau_{WM} = \frac{1}{2} f_M \rho_M {U_M}^2 \tag{C.13}$$

Mixture friction is calculated using Fanny friction equation:

$$f_M = 0.001375\left[1 + \left(2{\times}10^4 \frac{\varepsilon}{D} + \frac{10^6}{Re_M}\right)^{\frac{1}{3}}\right] \tag{C.14}$$

where,

$$Re_M = \frac{\rho_M U_M D}{\mu_M} \tag{C.15}$$

For λ_L:

$$\rho_M = \rho_L \lambda_L + \rho_G (1 - \lambda_L) \tag{C.16}$$

$$\mu_M = \mu_L \lambda_L + \mu_G (1 - \lambda_L) \tag{C.17}$$

For H_L:

$$\rho_M = \rho_L H_L + \rho_G (1 - H_L) \tag{C.18}$$

$$\mu_M = \mu_L H_L + \mu_G (1 - H_L) \tag{C.19}$$

C.2 Liquid holdup

C.2.1 Liquid holdup model of Choi et al. (2012)

Liquid holdup model of Choi et al. (2012), H_L^C, is given as:

$$H_L^C = 1 - \frac{U_{SG}}{C_0(U_{SG} + U_{SL}) + U_D} \tag{C.20}$$

Distribution parameter, C_0, is defined as:

$$C_0 = \frac{2}{1 + \left(\frac{Re}{1000}\right)^2} + \frac{1.2 - 0.2\sqrt{\frac{\rho_G}{\rho_L}}(1 - \exp(-18\alpha_G))}{1 + \left(\frac{1000}{Re}\right)^2} \tag{C.21}$$

Drift velocity, U_D, is defined as:

$$U_D = A\cos\theta + B\left(\frac{g\sigma(\rho_L - \rho_G)}{\rho_L^2}\right)^{1/4}\sin\theta \tag{C.22}$$

where coefficients A and B are defined as 0.0246 and 1.606 respectively. α_G is guessed, and equation (C.20) is solved iteratively for H_L^C; with α_G updated at each iteration step as: $\alpha_G = 1 - H_L^C$.

C.2.2 Liquid holdup model of Hart et al. (1989)

Hart et al. (1989) applied steady state force balance (in liquid-gas pipe flow) to extend the liquid holdup empirical correlation previously developed by Butterworth (Badie et al., 2000; Banafi and Talaie, 2015)

$$\frac{H_L}{1 - H_L} = \frac{U_{SL}}{U_{SG}}\left[1 + \left(\frac{f_L\rho_L}{f_i\rho_G}\right)^{\frac{1}{2}}\right] \cdots valid\ for\ H_L \leq 0.06 \tag{C.23}$$

Hamersma and Hart (1987) simplified equation (C.23) by expressing the ratio of liquid friction factor to interface friction factor as a function of superficial gas Reynolds number; refer to equation (C.24).

$$\frac{f_L}{f_i} = 108 Re_{SL}^{-0.726} \tag{C.24}$$

Appendix D

Transient model

D.1 Pressure gradient model of García et al. (2003)

Pressure gradient model of García et al. (2003) is given in equation

$$-\frac{dP}{dL} = \frac{2 f_M \rho_M U_M^2}{D} \tag{D.1}$$

where,

$$f_M = F_2 + \frac{F_1 - F_2}{\left[1 + \left(\frac{Re}{t}\right)^c\right]^d} \tag{D.2}$$

F_1 and F_2 are power laws defined as:

$$F_1 = a_1 Re^{b_1} \tag{D.3}$$

$$F_2 = a_2 Re^{b_2} \tag{D.4}$$

Mixture density and Reynold's number are expressed, respectively, as:

$$\rho_M = \rho_L \lambda_L + \rho_G (1 - \lambda_L) \tag{D.5}$$

$$Re = \frac{U_M D}{\nu_L} \tag{D.6}$$

Kinematic viscosity of liquid, ν_L, is defined as:

$$\nu_L = \frac{\mu_L}{\rho_L} \tag{D.7}$$

García et al. defined coefficients a_1, b_1, a_2, b_2, c, d, and t as 13.98, -0.9501, 0.0925, -0.2534, 4.864, 0.1972, and 293 respectively.

D.2 Results

Figures (D.1-D.16) show predictions of the data of Vigneron et al. (1995) using proposed simplified transient liquid-gas pipe flow model. For each figure, sub-figures (a), (b), (c), (d), and (e) represent pressure profile, transient liquid holdup, steady state liquid holdup, liquid superficial velocity, and gas superficial velocity. respectively.

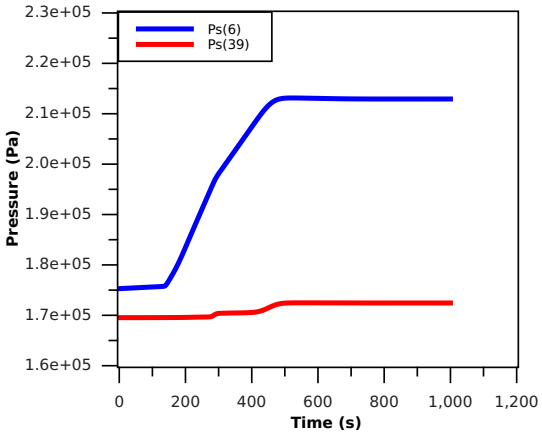

(a) Pressure

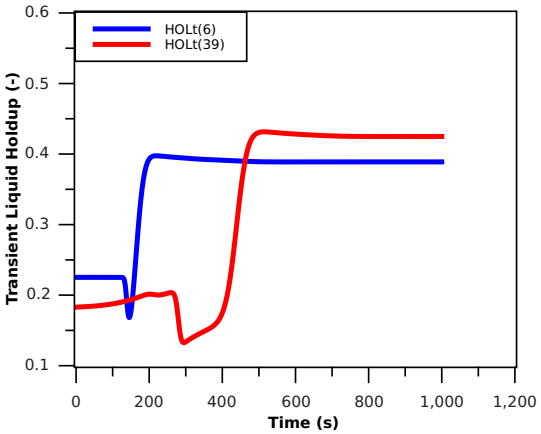

(b) Transient Liquid Holdup

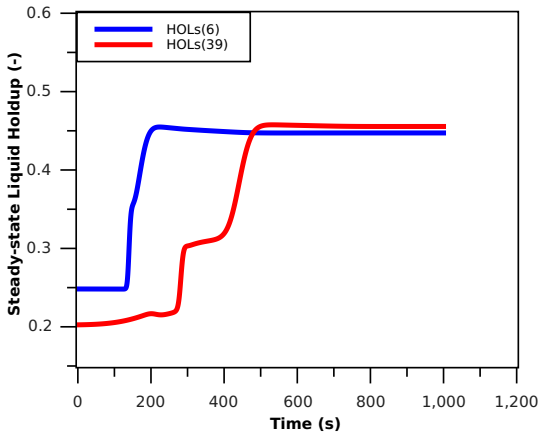

(c) Steady-State Liquid Holdup

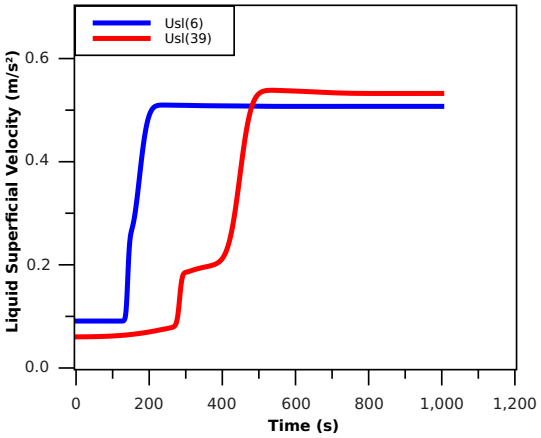

(d) Liquid Superficial Velocity

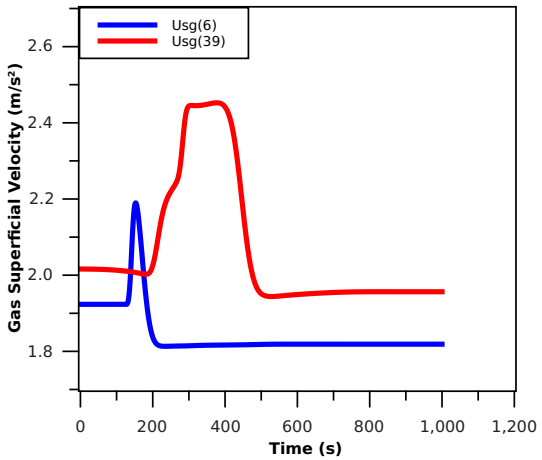

(e) Gas Superficial Velocity

Figure D.1 – Simplified two-phase transient model predictions: Experiment 1-A (Vigneron et al., 1995)

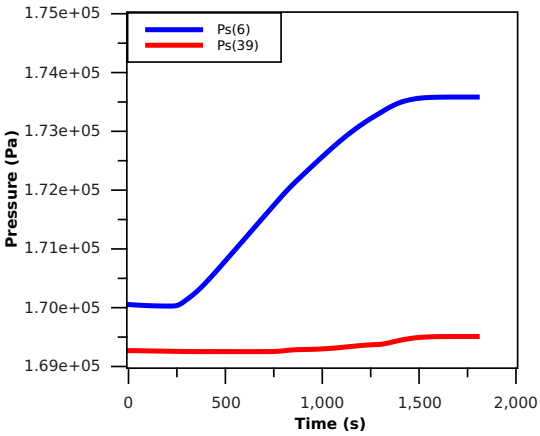

(a) Pressure

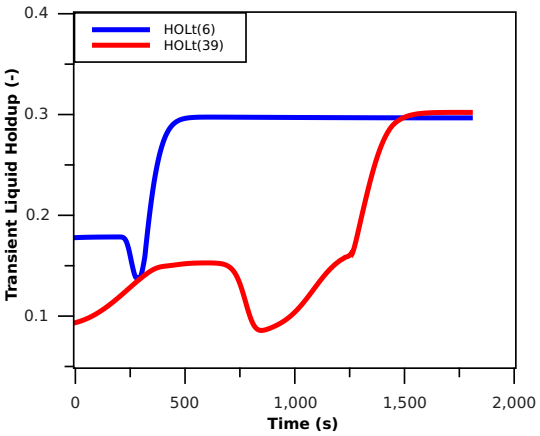

(b) Transient Liquid Holdup

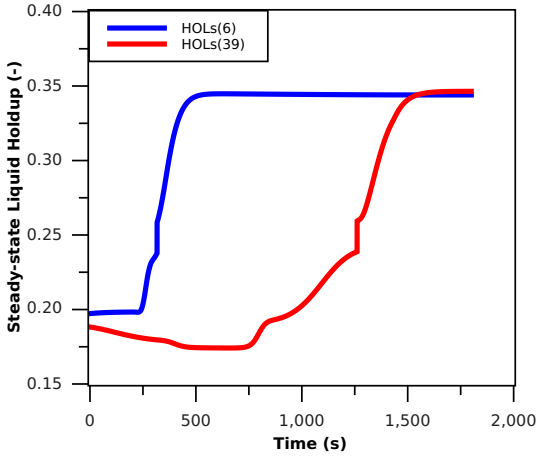

(c) Steady-State Liquid Holdup

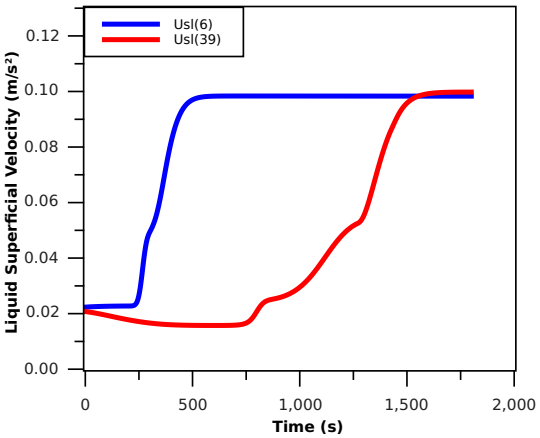

(d) Liquid Superficial Velocity

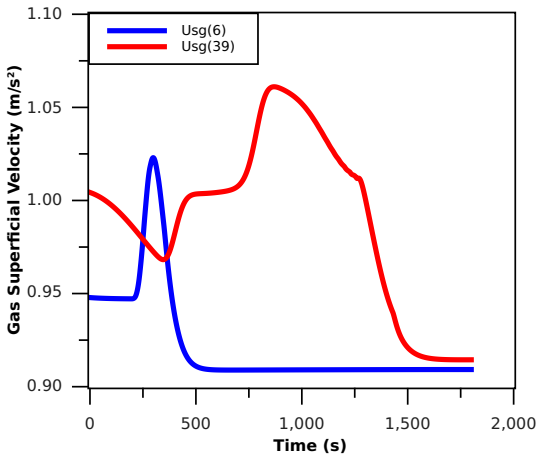

(e) Gas Superficial Velocity

Figure D.2 – Simplified two-phase transient model predictions: Experiment 1-B (Vigneron et al., 1995)

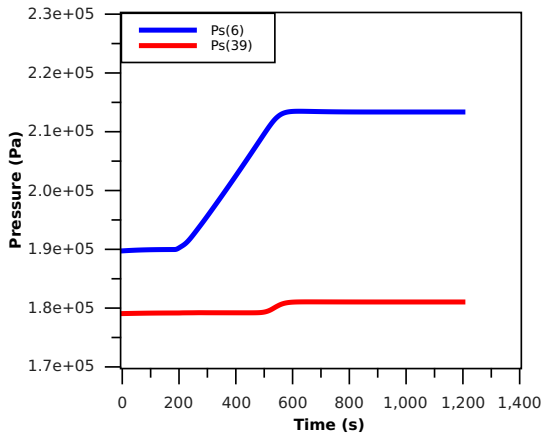

(a) Pressure

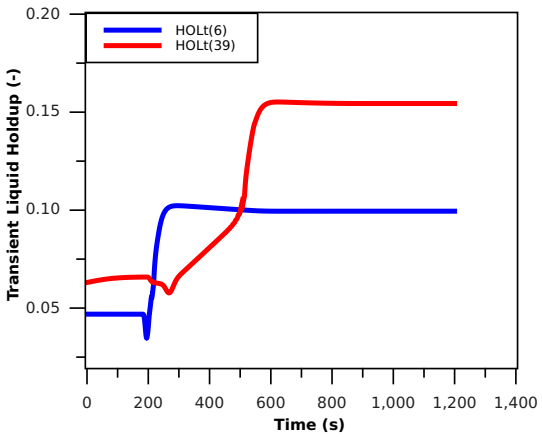

(b) Transient Liquid Holdup

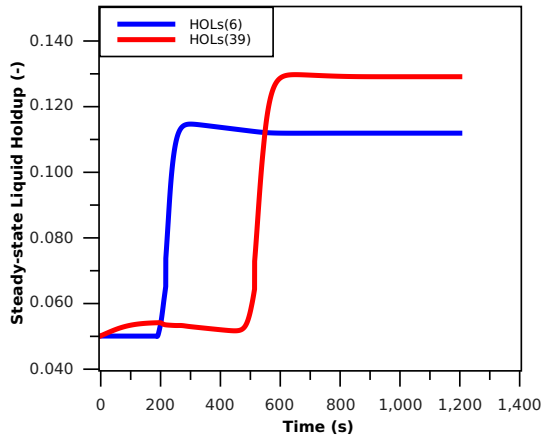

(c) Steady-State Liquid Holdup

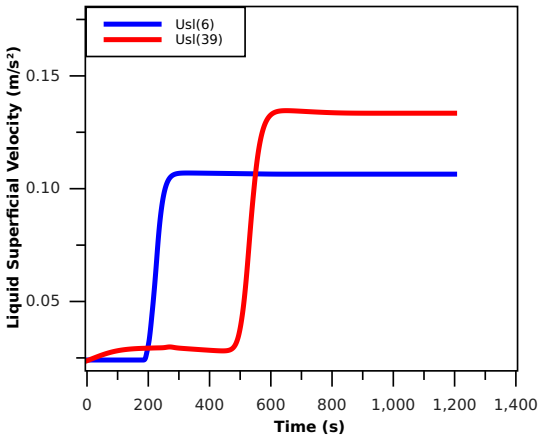

(d) Liquid Superficial Velocity

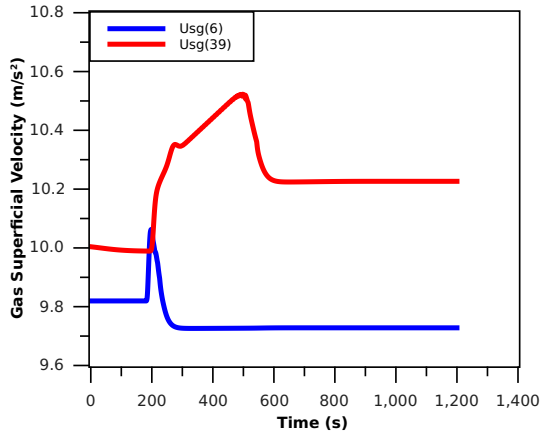

(e) Gas Superficial Velocity

Figure D.3 – Simplified two-phase transient model predictions: Experiment 1-C (Vigneron et al., 1995)

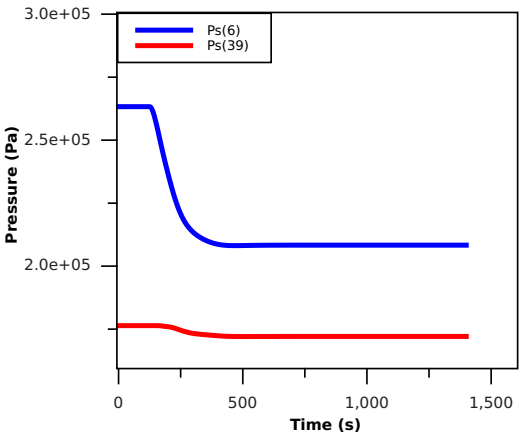

(a) Pressure

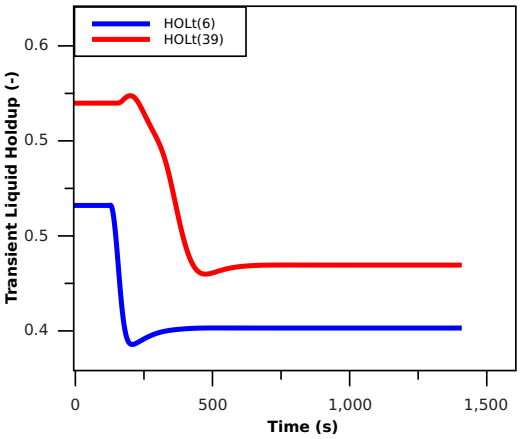

(b) Transient Liquid Holdup

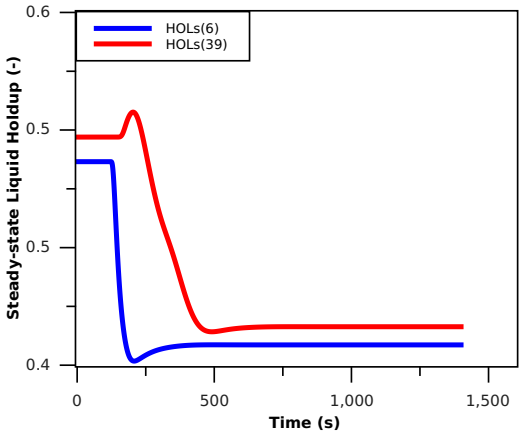

(c) Steady-State Liquid Holdup

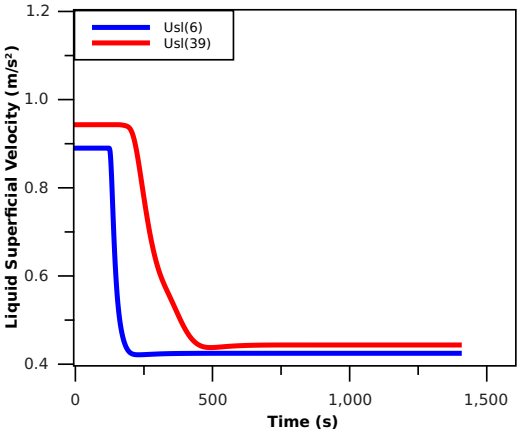

(d) Liquid Superficial Velocity

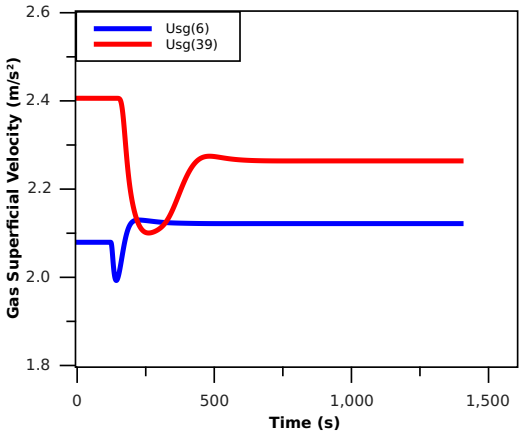

(e) Gas Superficial Velocity

Figure D.4 – Simplified two-phase transient model predictions: Experiment 1-D (Vigneron et al., 1995)

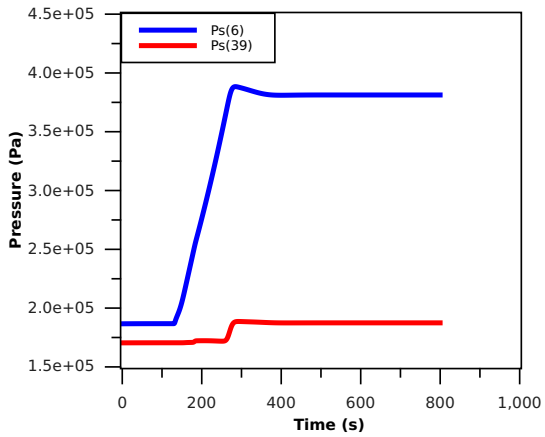

(a) Pressure

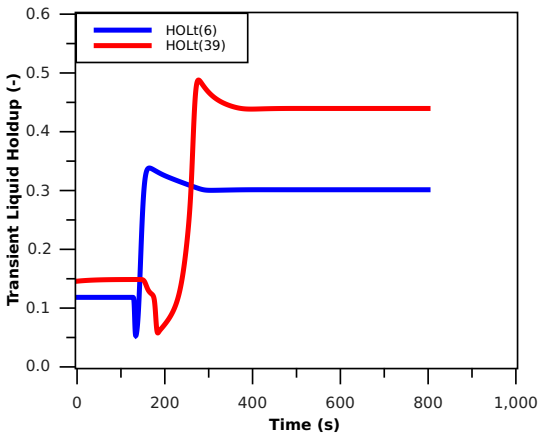

(b) Transient Liquid Holdup

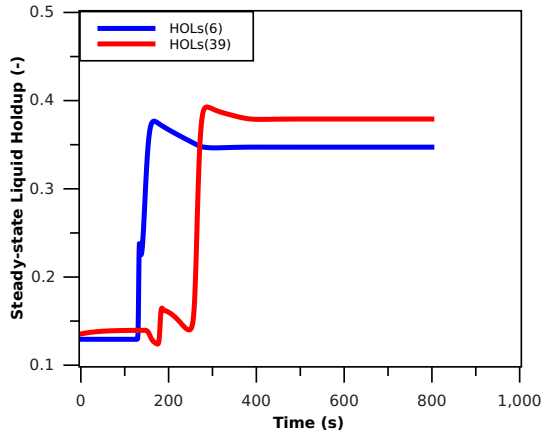

(c) Steady-State Liquid Holdup

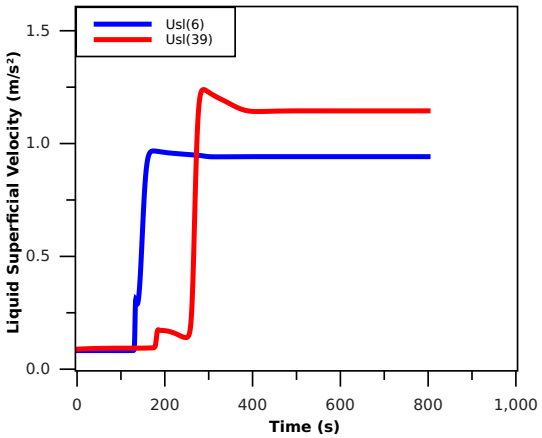

(d) Liquid Superficial Velocity

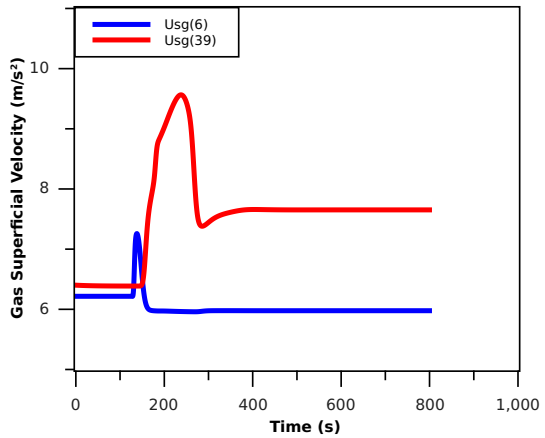

(e) Gas Superficial Velocity

Figure D.5 – Simplified two-phase transient model predictions: Experiment 1-E (Vigneron et al., 1995)

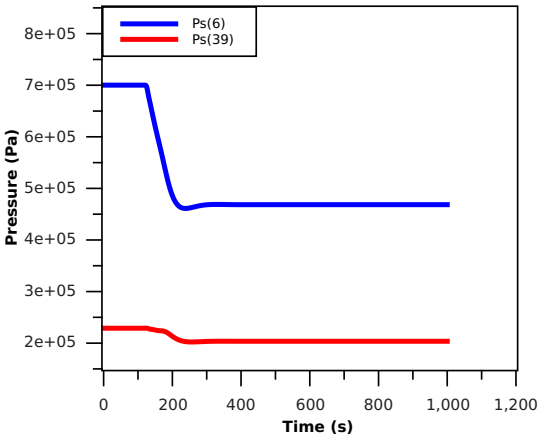

(a) Pressure

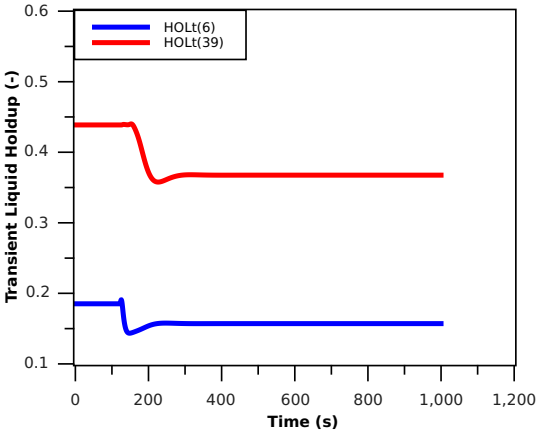

(b) Transient Liquid Holdup

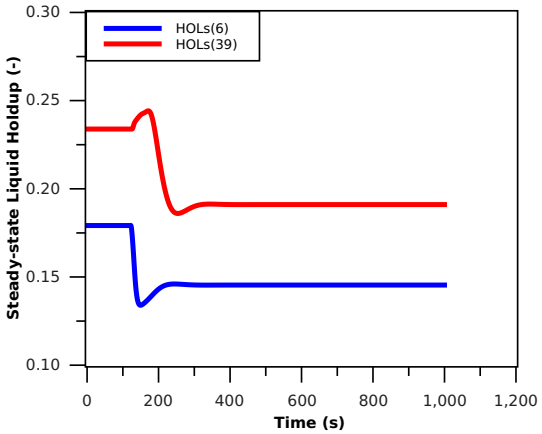

(c) Steady-State Liquid Holdup

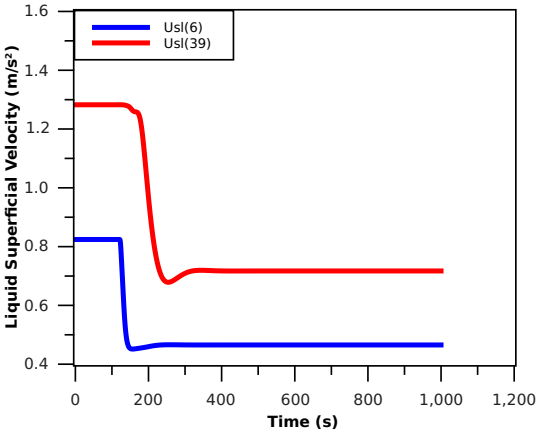

(d) Liquid Superficial Velocity

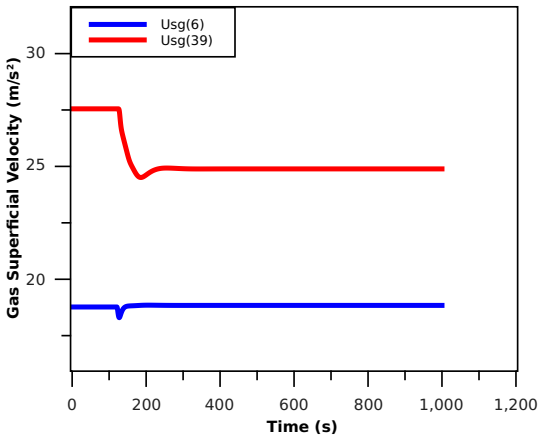

(e) Gas Superficial Velocity

Figure D.6 – Simplified two-phase transient model predictions: Experiment 1-F (Vigneron et al., 1995)

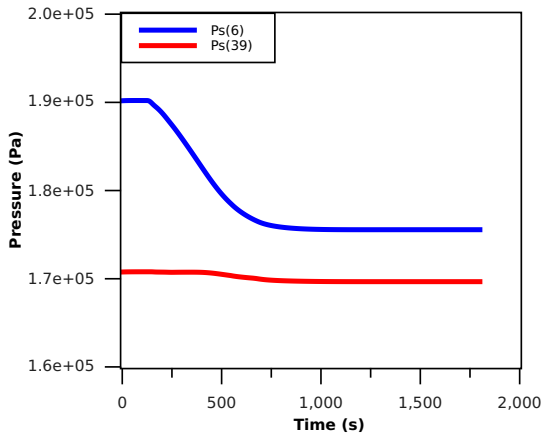

(a) Pressure

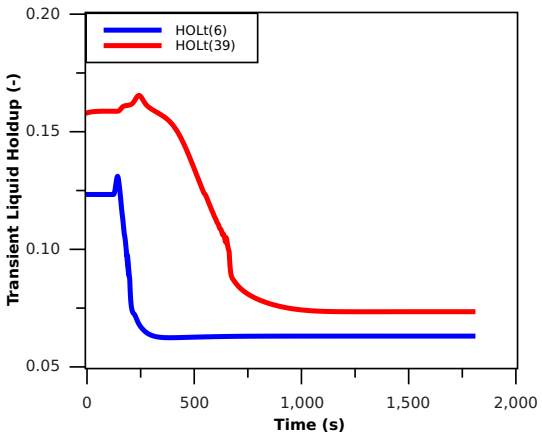

(b) Transient Liquid Holdup

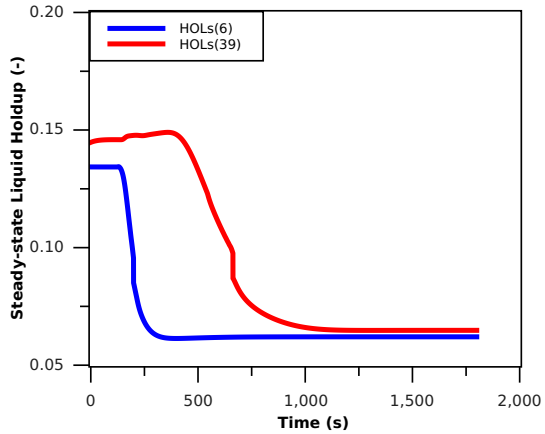

(c) Steady-State Liquid Holdup

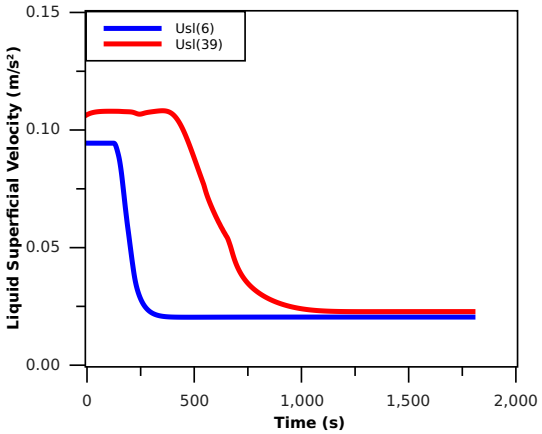

(d) Liquid Superficial Velocity

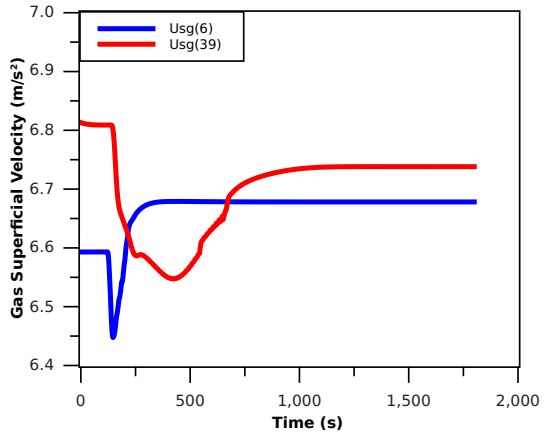

(e) Gas Superficial Velocity

Figure D.7 – Simplified two-phase transient model predictions: Experiment 1-G (Vigneron et al., 1995)

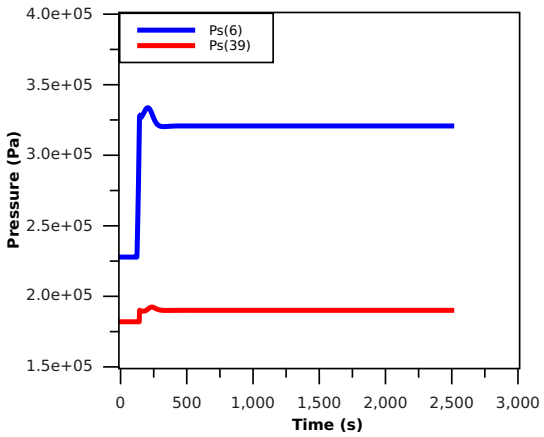

(a) Pressure

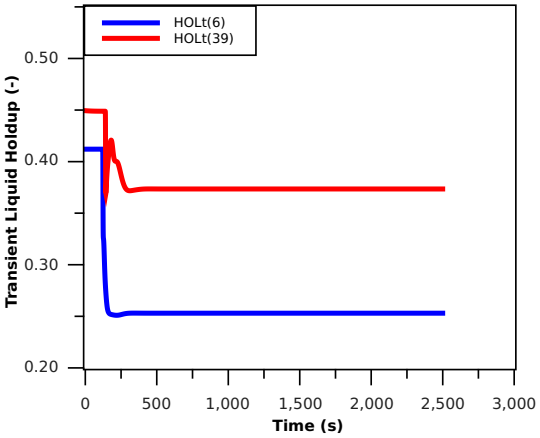

(b) Transient Liquid Holdup

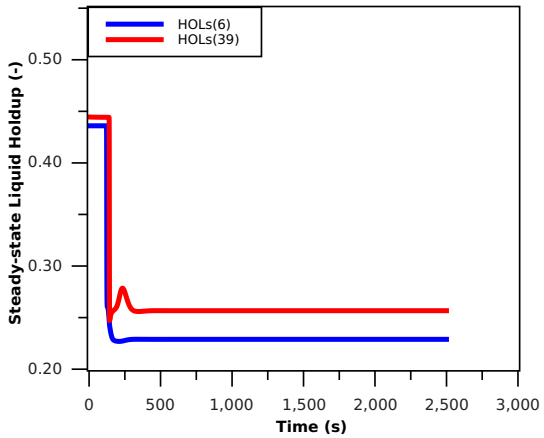

(c) Steady-State Liquid Holdup

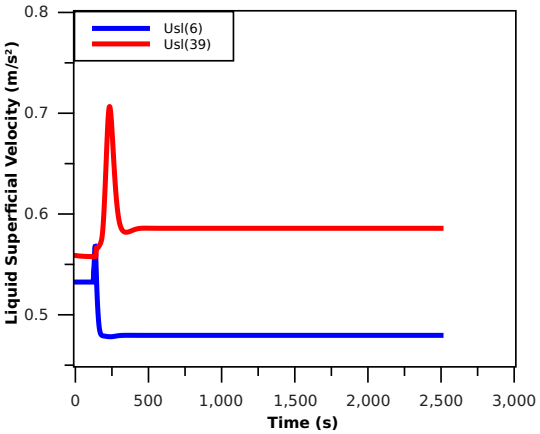

(d) Liquid Superficial Velocity

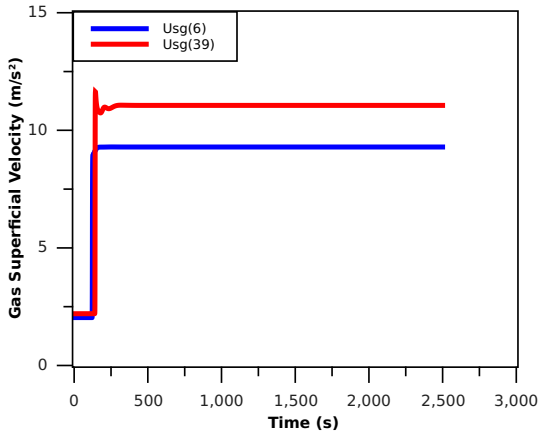

(e) Gas Superficial Velocity

Figure D.8 – Simplified two-phase transient model predictions: Experiment 2-C (Vigneron et al., 1995)

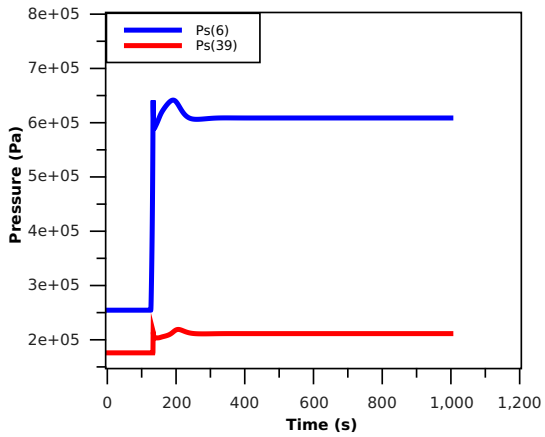

(a) Pressure

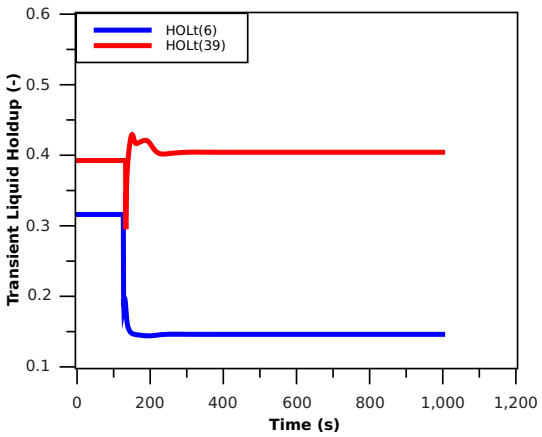

(b) Transient Liquid Holdup

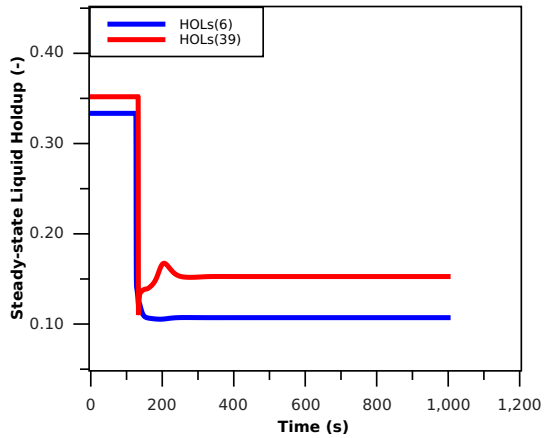

(c) Steady-State Liquid Holdup

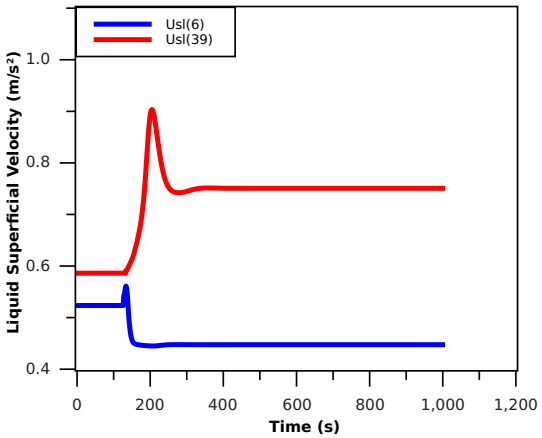

(d) Liquid Superficial Velocity

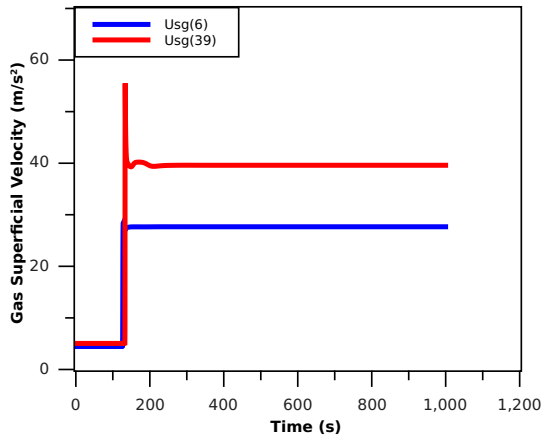

(e) Gas Superficial Velocity

Figure D.9 – Simplified two-phase transient model predictions: Experiment 2-D (Vigneron et al., 1995)

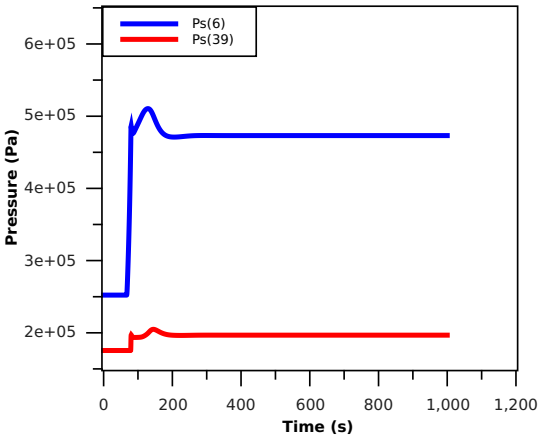

(a) Pressure

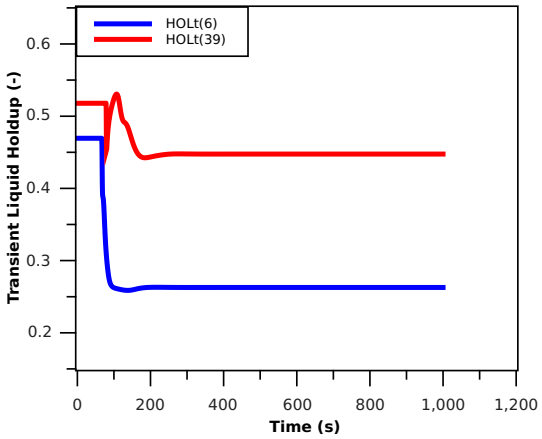

(b) Transient Liquid Holdup

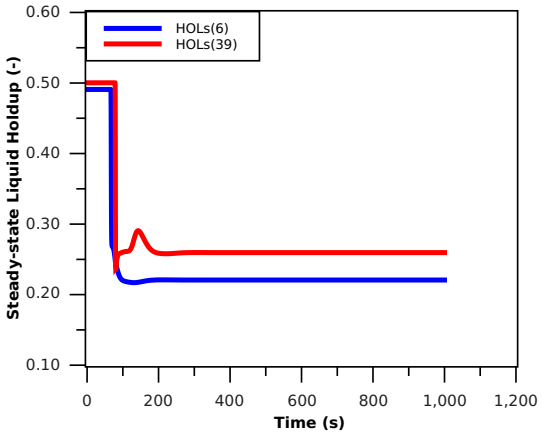

(c) Steady-State Liquid Holdup

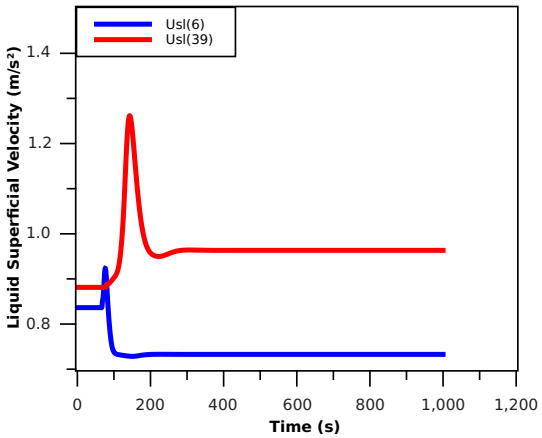

(d) Liquid Superficial Velocity

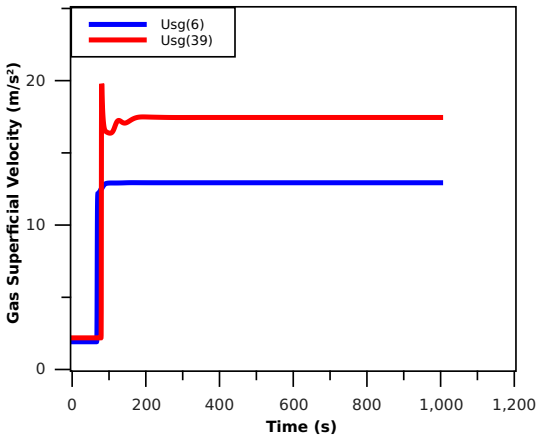

(e) Gas Superficial Velocity

Figure D.10 – Simplified two-phase transient model predictions: Experiment 2-E (Vigneron et al., 1995)

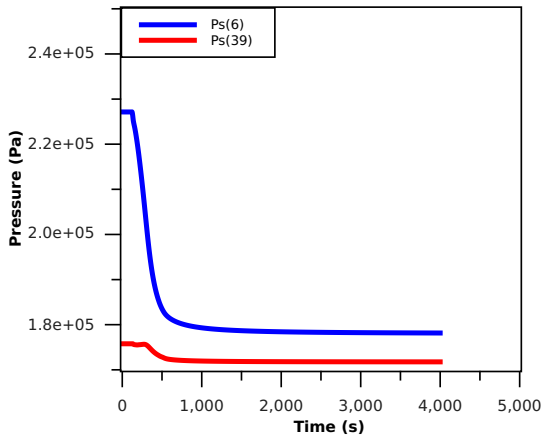

(a) Pressure

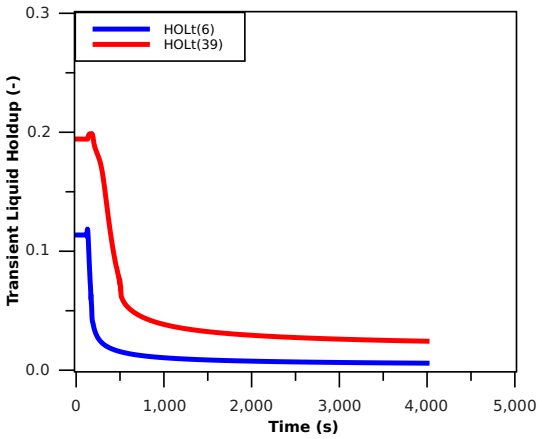

(b) Transient Liquid Holdup

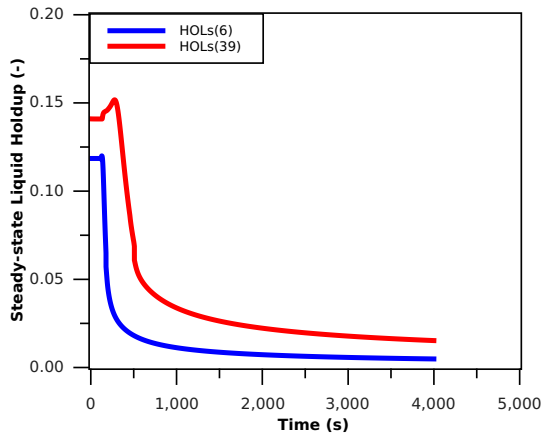

(c) Steady-State Liquid Holdup

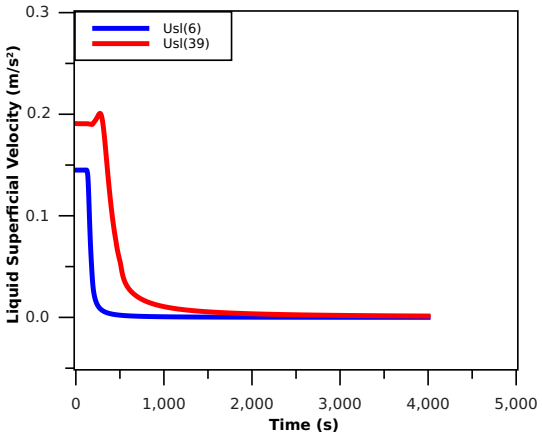

(d) Liquid Superficial Velocity

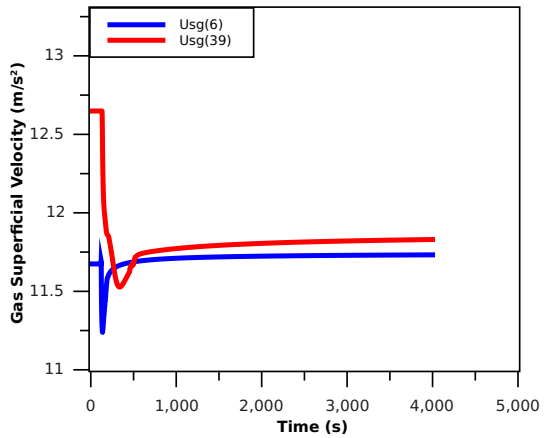

(e) Gas Superficial Velocity

Figure D.11 – Simplified two-phase transient model predictions: Experiment 3-A (Vigneron et al., 1995)

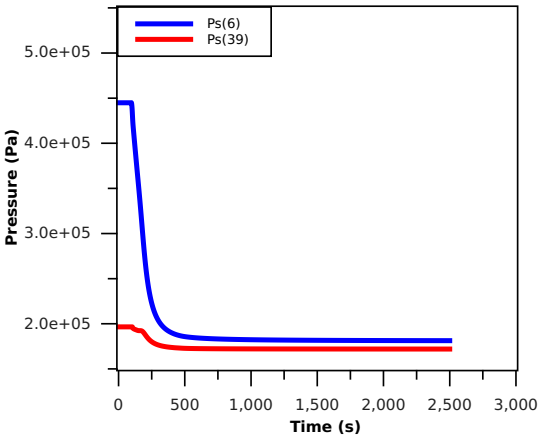

(a) Pressure

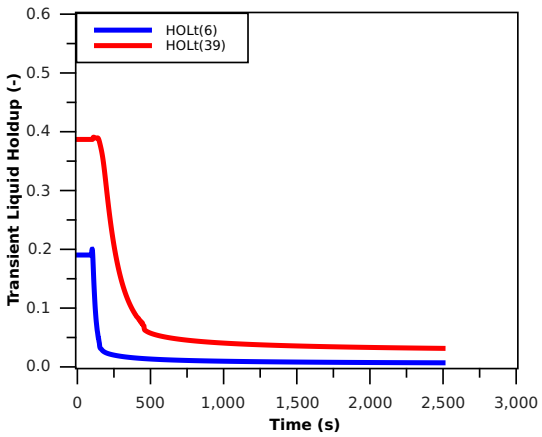

(b) Transient Liquid Holdup

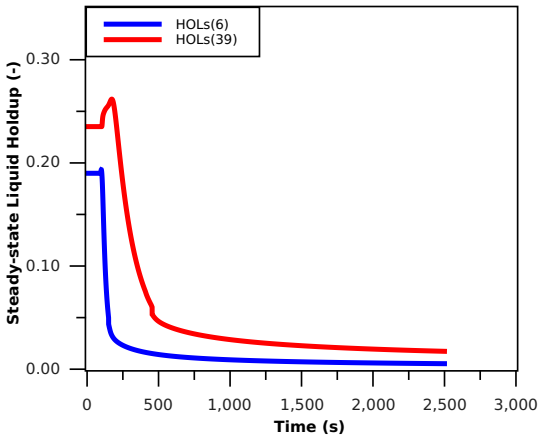

(c) Steady-State Liquid Holdup

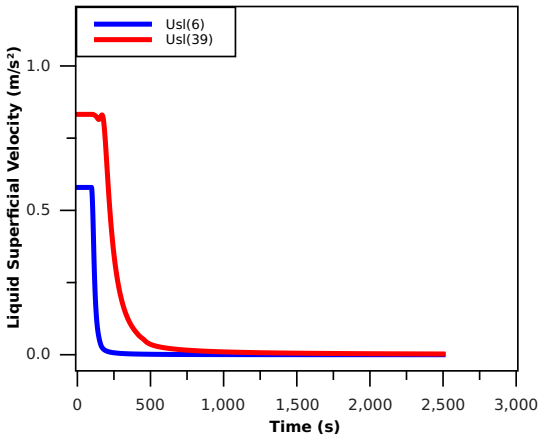

(d) Liquid Superficial Velocity

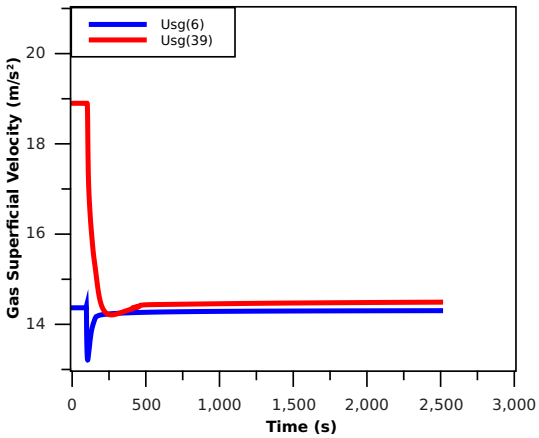

(e) Gas Superficial Velocity

Figure D.12 – Simplified two-phase transient model predictions: Experiment 3-B (Vigneron et al., 1995)

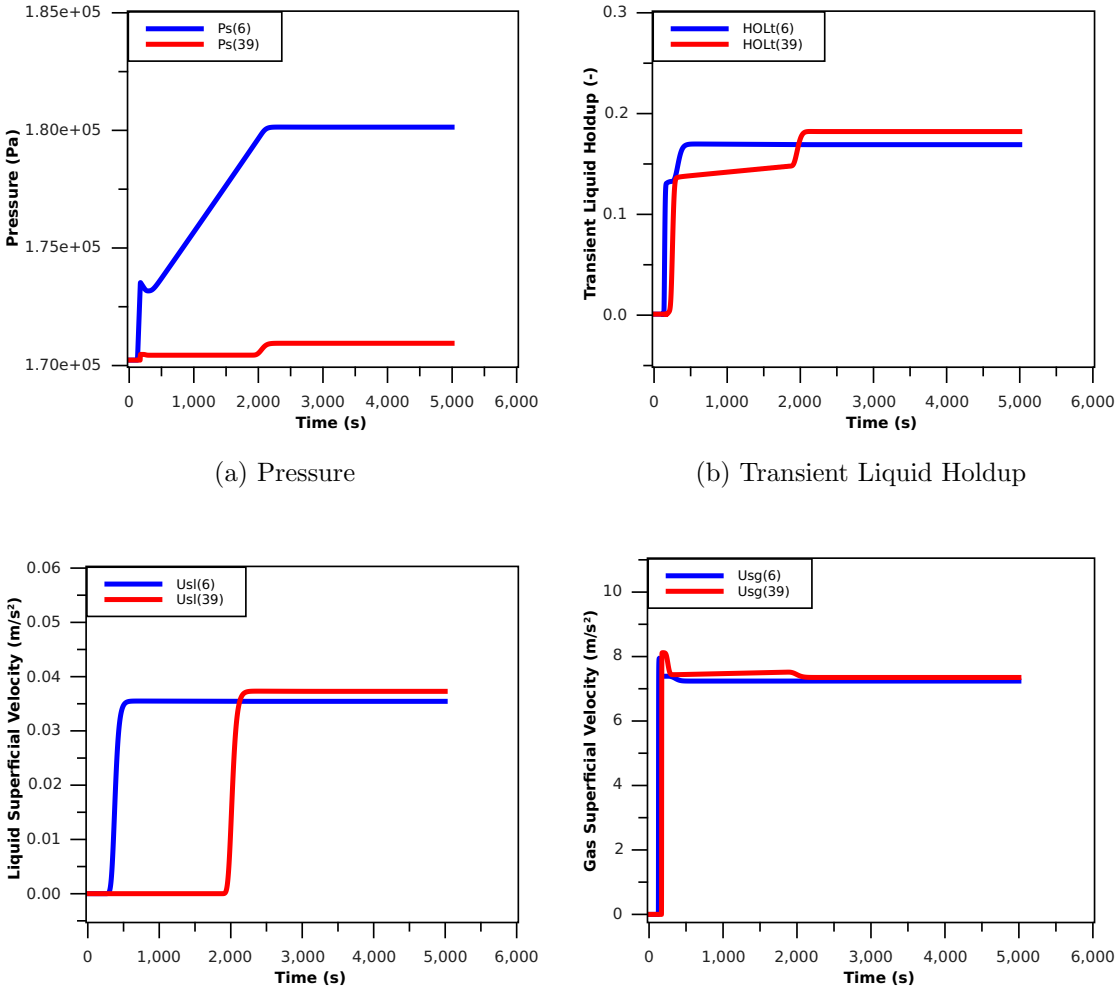

(a) Pressure

(b) Transient Liquid Holdup

(c) Liquid Superficial Velocity

(d) Gas Superficial Velocity

Figure D.13 – Simplified two-phase transient model predictions: Experiment 4-A0 (Vigneron et al., 1995)

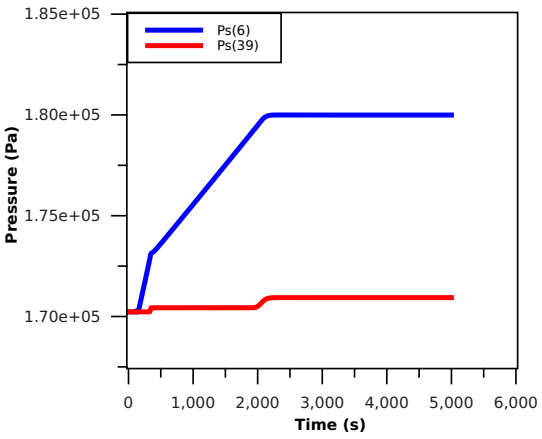

(a) Pressure

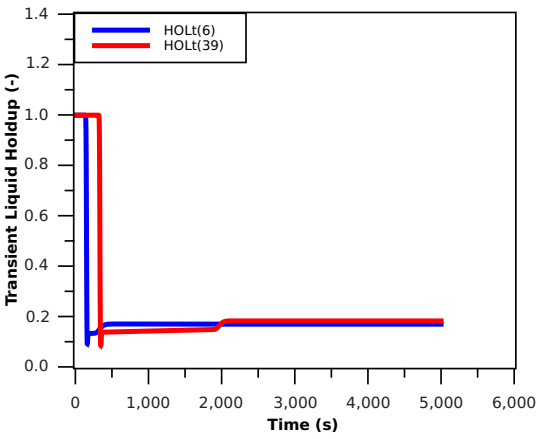

(b) Transient Liquid Holdup

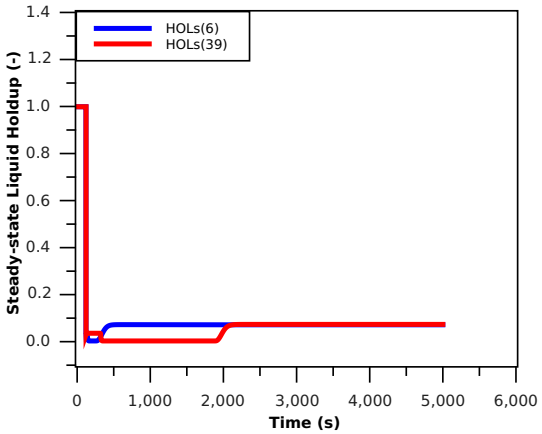

(c) Steady-State Liquid Holdup

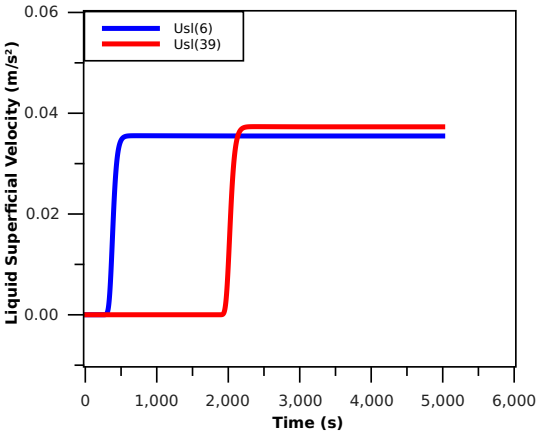

(d) Liquid Superficial Velocity

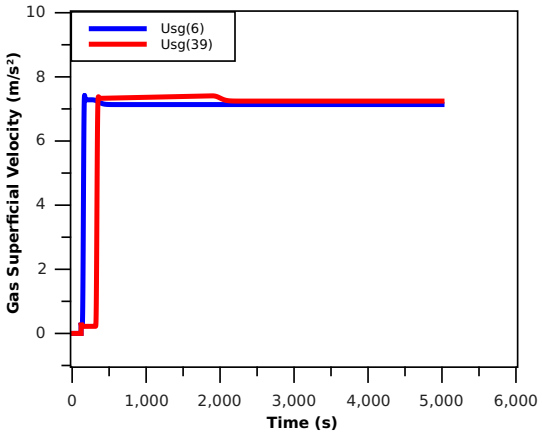

(e) Gas Superficial Velocity

Figure D.14 – Simplified two-phase transient model predictions: Experiment 4-A1 (Vigneron et al., 1995)

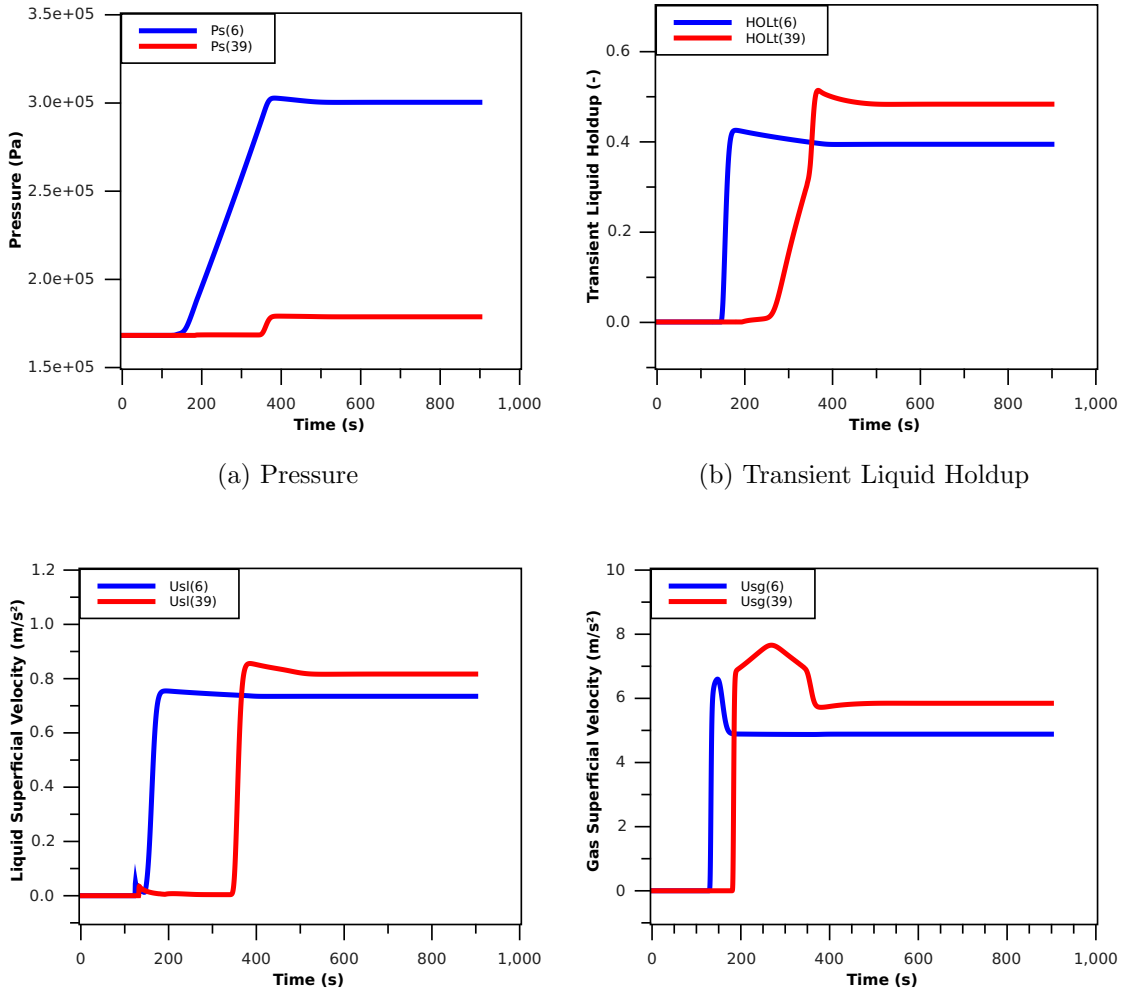

(a) Pressure

(b) Transient Liquid Holdup

(c) Liquid Superficial Velocity

(d) Gas Superficial Velocity

Figure D.15 – Simplified two-phase transient model predictions: Experiment 4-B0 (Vigneron et al., 1995)

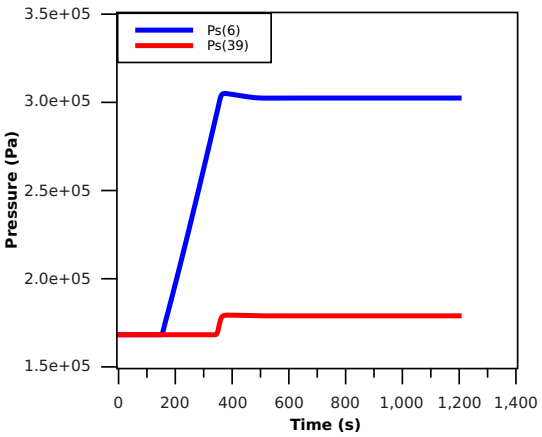

(a) Pressure

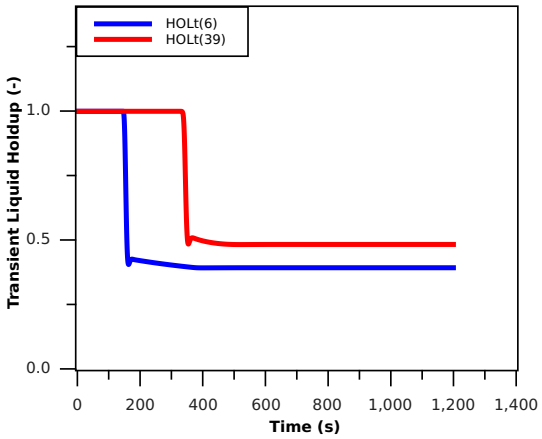

(b) Transient Liquid Holdup

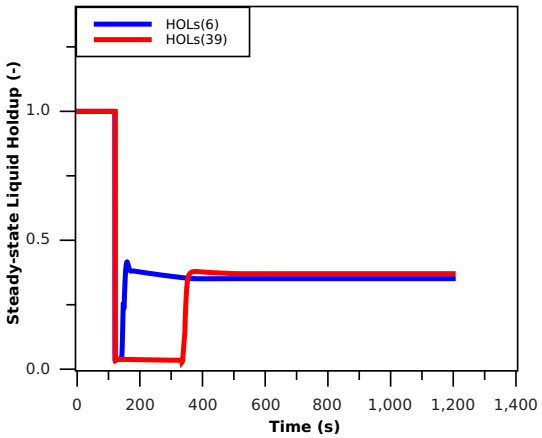

(c) Steady-State Liquid Holdup

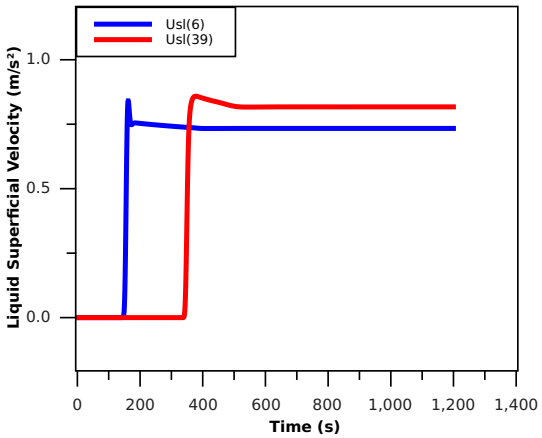

(d) Liquid Superficial Velocity

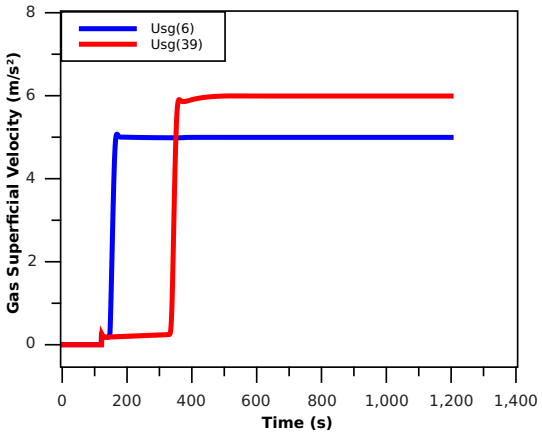

(e) Gas Superficial Velocity

Figure D.16 – Simplified two-phase transient model predictions: Experiment 4-B1 (Vigneron et al., 1995)